

Model Package Report: 100-K Scale-Appropriate Fate and Transport Model

Version 1.0

Prepared for the U.S. Department of Energy
Assistant Secretary for Environmental Management

Contractor for the U.S. Department of Energy
under Contract DE-AC06-08RL14788

CH2MHILL
Plateau Remediation Company

P.O. Box 1600
Richland, Washington 99352

Model Package Report: 100-K Scale-Appropriate Fate and Transport Model

Version 1.0

Document Type: ENV

Program/Project: EP&SP

H. Rashid
INTERA, Inc.
M. C. Weber
INTERA, Inc.

G. Ruskauff
INTERA, Inc.
R. Suribhatla
INTERA, Inc.

Date Published
August 2018

Prepared for the U.S. Department of Energy
Assistant Secretary for Environmental Management

Contractor for the U.S. Department of Energy
under Contract DE-AC06-08RL14788

CH2MHILL
Plateau Remediation Company
P.O. Box 1600
Richland, Washington 99352

APPROVED

By Mary P. Curry at 6:44 pm, Aug 20, 2018

Release Approval

Date

TRADEMARK DISCLAIMER

Reference herein to any specific commercial product, process, or service by tradename, trademark, manufacturer, or otherwise, does not necessarily constitute or imply its endorsement, recommendation, or favoring by the United States Government or any agency thereof or its contractors or subcontractors.

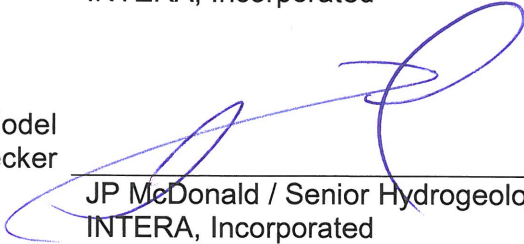
This report has been reproduced from the best available copy.

Printed in the United States of America

Signature Page

Model Preparer S.M. Hetaluro Rashid
H Rashid / Hydrologist
INTERA, Incorporated

Date 03/19/2018

Model Checker 
JP McDonald / Senior Hydrogeologist
INTERA, Incorporated

Date 3/19/2018

Model Senior Reviewer 
WE Nichols / Modeling Team Leader
CHPRC

Date 20 MAR 2018

Responsible Manager 
AH Aly / Risk Assessment and Model Integration
Manager
CHPRC *W.E. NICHOLS, ACTING*

Date 20 MAR 2018

Basis of Qualifications for MPR Roles

Preparer: Helalur Rashid

Hydrologist

MS, Civil Engineering, Washington State University, 2010

BS, Civil Engineering, Bangladesh University of Engineering & Technology, 2007

Licenses: Professional Engineer (PE), Washington State

Helalur Rashid's professional experience encompasses numerical modeling of groundwater in the saturated and unsaturated zones, model calibration, groundwater management, geostatistics analysis, sediment transport, and hydraulic characterization of watersheds. He has applied a wide variety of modeling codes and geographic information system software including MODFLOW, MODFLOW-SURFACT, MT3DMS, MODPATH, PEST, Parallel PEST, STOMP, SWAT, HEC-HMS, ArcGIS, Leapfrog Hydro, Groundwater Vistas, RETC, and TecPlot. Helal has worked primarily on environmental restoration projects for the federal government. He is also skilled in using various laboratory and field instruments such as acoustic Doppler velocimeters, laser distance meters, and viscometers.

Checker: John McDonald

Senior Hydrogeologist

BS, Geology, Eastern Washington University, 1993

AS, General Studies, Columbia Basin College, 1989

AAS, Computer Science, Columbia Basin College, 1985

John McDonald brings experience in soil and groundwater remediation under the Comprehensive Environmental Response, Compensation, and Liability Act (CERCLA) and Resource Conservation and Recovery Act (RCRA). He specializes in groundwater sampling, water-level monitoring, groundwater sample representativeness, hydraulic gradient determinations by trend-surface analyses, flow dynamics in high transmissivity aquifers, barometric corrections by multiple regression/deconvolution, analyses of automated water-level data, hydrologic testing data analysis, and statistical analyses. His experience includes implementation of remedial actions, conceptual model development, multimedia/risk assessment modeling, groundwater sample data interpretation, water level data interpretation, and reporting. He also has experience in taking hydraulic head measurements, operating continuous water-level recording equipment, generating potentiometric surface maps, conducting hydrologic tests, collecting water samples, and generating contaminant plume maps.

Senior Reviewer: Will Nichols

Principal Hydrogeologist

MS, Civil Engineering, Oregon State University, 1990

BS, Agricultural Engineering, Oregon State University, 1987

William "Will" Nichols' professional experience as water resources engineer has focused on the areas of hydrology, environmental site characterization, fate and transport modeling, pathway and exposure modeling, uncertainty and sensitivity analysis, integrated risk assessment, probabilistic modeling and simulation, and software quality assurance. He has applied his expertise in these areas to help solve problems of national importance in the areas of Resource Conservation and Recovery Act, Comprehensive Environmental Response, Compensation, and Liability Act, remedial investigations and feasibility studies, radioactive waste disposal facility licensing, National Environmental Policy Act (NEPA) reviews and environmental impact statement development. Will's expertise has been applied in support of environmental restoration, dose reconstruction for legacy radioactive waste practices, and demonstration of compliance with applicable waste disposal regulatory requirements. He has successfully led science and engineering teams in software development efforts and scientific studies to deliver high-impact products including scientific simulators used to evaluate environmental dose and total system performance assessment. Will's NEPA experience includes contributing to long-term consequences portions of environmental impact statements for nationally important facilities, including proposed and operating radioactive waste repositories.

Model Package Report

100-K Scale-Appropriate Fate and Transport Model

Version 1.0

March 2018

Prepared for:

Technical Integration

Prepared by:

*Helal Rashid, Raghavendra Suribhatla, Mary Weber, and Greg Ruskauff
(CH2M HILL Plateau Remediation Company)*

Executive Summary

This model package report describes the numerical groundwater flow and transport model of the 100-KR-4 OU area (100-K Model) developed for use by CH2M Hill Plateau Remediation Company in support of remediation activities at the Hanford Site, Washington. This model package report describes model objectives, conceptual model basis of the numerical model, model construction, flow calibration and sensitivity analysis, transport parameters, and basic testing of the model's flow and transport functions for fitness of purpose via simple representative, but not necessarily site-specific, remediation actions.

The primary purposes of this model include the following:

- Computing groundwater head and flows to the Columbia River for use in general flow system understanding as well as potential remediation system (e.g. pump and treat) design/evaluation.
- Estimating future groundwater concentrations of hexavalent chromium, trichloroethene, nitrate, carbon-14, tritium, and strontium-90 to support risk screening and evaluation of remediation options.
- Estimating contaminant discharge to the Columbia River and potential influent concentrations for extracted groundwater.

Contaminated groundwater in the 100-KR-4 OU flows toward the northwest and discharges into the Columbia River. To represent this process, the model domain encompasses the saturated Ringold Formation unit E sediment above Ringold Upper Mud and basalt near the 100-KR-4 OU – the Ringold Upper Mud and basalt are considered impermeable relative to the Ringold E sediment – and extends under the Columbia River to allow for groundwater upwelling into the river. Groundwater flow from the north side of the river is assumed to create a flow divide in the middle of the river.

Flow model calibration to the Automatic Water Level Network (47 wells) and manual (171 wells) water level measurements (13,710 total observations) from January 2013 through December 2016 were used to estimate model hydraulic properties within the OU by exploiting the correlation between river stage fluctuation and aquifer head changes occurring over about 10 to 40 days. Remediation pumping is included in the simulation. A spatially distributed parameter estimation technique was used to estimate hydraulic conductivity; specific storage, specific yield, and vertical anisotropy were represented by areas of constant properties. This resulted in aquifer hydraulic properties conditioned to large-scale hydraulic responses that are also representative of the plume migration scale.

One-dimensional models implemented in the *Subsurface Transport Over Multiple Phases* (STOMP©) (PNNL-12030, *STOMP: Subsurface Transport Over Multiple Phases Version 2.0: Theory Guide*) code were constructed for waste site locations that have been inferred from historical process knowledge and persistent groundwater contamination to be continuing sources for groundwater contamination. Constituents included tritium, nitrate, strontium-90, carbon-14, and Cr(VI). These one-dimensional (1D) models were used to generate mass input to the saturated zone that resulted in simulated groundwater concentrations similar to those observed in overall trend and magnitude; little to no soil concentration data below the depth of excavation (when a waste site had been remediated) was available to inform the model soil concentrations. Hexavalent chromium leaching at the KW and KE reactor headhouses' sodium dichromate storage tanks was modeled using a kinetic approach derived from Pacific Northwest National Laboratory analysis of sodium dichromate contaminated soil elsewhere in the river corridor. Waste sites suspected to be contributing to groundwater contamination include 183.1KE and 183.1KW Headhouse tank farms, 116-KE-1 and 116-KW-1 gas condensate cribs, 116-KE-3 and 116-KW-2 Fuel Storage Basin

cribs/reverse wells, 116-K-1 Crib, 116-K-2 Trench, and 118-K-1 Burial Ground. Significant uncertainty, judged irreducible, exists over the long-term chromium source.

The estimated residual STOMP model soil concentrations were used as the source for long-term (125 year) forecasts under a no further action scenario.

The following results were observed in the no further action scenario:

Hexavalent Chromium:

- Aquifer concentrations gradually decline over time but always stays way above the cleanup level for hexavalent chromium (48 µg/L) within 125 years of simulation period
- At no time are there any shoreline concentrations greater than the hexavalent chromium cleanup level (48 µg/L)
- Shoreline concentrations remains above aquatic benchmark (10 µg/L) within 125 years of simulation period

Strontium-90:

- Aquifer concentrations gradually decline over time but always stays way above the cleanup level for strontium-90 (8 pCi/L) within 300 years of simulation period
- At no time are there any shoreline concentrations greater than the strontium-90 aquatic benchmark (278 pCi/L)

Carbon-14:

- Aquifer concentrations gradually decline over time and eventually drops below the cleanup level for carbon-14 (2,000 pCi/L) within 16 years of simulation period
- Shoreline concentrations gradually declines over time and eventually drops below the carbon-14 aquatic benchmark (609 pCi/L) within 16 years of simulation period

Nitrate:

- Aquifer concentrations gradually decline over time and eventually drops below the cleanup level for nitrate (45 mg/L) within 10 years of simulation period
- At no time are there any shoreline concentrations greater than the nitrate aquatic benchmark (88.6 mg/L)

Tritium:

- Aquifer concentrations gradually decline over time and eventually drops below the cleanup level for tritium (20,000 pCi/L) within 10 years of simulation period
- At no time are there any shoreline concentrations greater than the tritium aquatic benchmark (2.65E+08 pCi/L)

Trichloroethene:

- Aquifer concentrations gradually decline over time and eventually drops below the cleanup level for trichloroethene (5 µg/L) within 5 years of simulation period
- At no time are there any shoreline concentrations greater than the trichloroethene aquatic benchmark (47 µg/L)

Conceptual and parameter uncertainties include the following:

- Hydraulic conductivity (and hence transmissivity and groundwater flow rate) uncertainty grows away from Automated Water Level Network wells. This uncertainty is qualitatively judged of modest importance.
- The long-term behavior of the chromium sources cannot be known with high certainty because chromium exists in several chemical states in the aquifer with greatly differing release characteristics. Due to reactor operations chromium is a ubiquitous soil contaminant that, despite extensive soil remediation, may still linger in the periodically rewetted zone in some locations that are not well understood.

Contents

1	Purpose.....	1
1.1	Need	1
1.2	Background	1
1.3	Document Organization	5
1.4	Model Objectives	5
2	Model Conceptualization.....	6
2.1	Hydrogeologic Overview	6
2.1.1	Hanford Formation.....	8
2.1.2	Ringold Formation Units	10
2.1.3	Hanford and Ringold Hydraulic Conductivity, Specific Storage, and Specific Yield ..	11
2.2	Features, Events, and Processes (FEPs)	15
2.2.1	FEP: Anthropogenic Recharge.....	15
2.2.2	FEP: Natural Recharge	16
2.2.3	FEP: Columbia River Interaction.....	22
2.2.4	FEP: Groundwater Flow	25
2.2.5	FEP: Pump and Treat System	30
2.2.6	FEP: Potential Hexavalent Chromium Sources	31
2.2.7	FEP: Potential Strontium-90 Sources	32
2.2.8	FEP: Potential Tritium, Nitrate, and Carbon-14 Sources.....	33
2.3	Nature and Extent of Contamination.....	33
2.4	Conceptual Model Summary	41
3	Model Implementation.....	42
3.1	Software	42
3.2	Discretization.....	44
3.2.1	Temporal Discretization.....	44
3.2.2	Spatial Discretization	46
3.3	Parameterization.....	50
3.3.1	Recharge Boundary Condition.....	50
3.3.2	West, South, and East Landward Boundary Conditions	53
3.3.3	River Boundary Conditions	54
3.3.4	Initial Head Condition.....	55
3.3.5	Initial Concentrations.....	55
3.3.6	Aquifer Hydraulic Property Parameterization	56
3.3.7	Effective Porosity.....	62
3.3.8	Dispersivity	62
3.3.9	Adsorption	67

3.3.10	Contaminant Treatment System (CTS).....	67
3.4	Flow Model Calibration	67
3.4.1	General Approach	67
3.4.2	Parameter Estimation Framework.....	70
3.4.3	Flow Model Calibration Results	71
3.4.4	Qualitative Flow Model Evaluation.....	74
3.4.5	Calibrated Flow Model Properties	75
3.5	Transport Model Calibration	81
3.5.1	Vadose Zone Modeling.....	81
3.5.2	Construction of Source/Sink Mixing Package	92
3.5.3	Processing Observation Data for Calibration.....	92
3.5.4	Transport Model Calibration Results.....	92
3.5.5	Predictive Transport Model	108
4	Model Sensitivity and Uncertainty Analysis.....	136
4.1	Sensitivity Analysis.....	136
4.2	Uncertainty Analysis	139
5	Model Limitations	143
6	Model Configuration Management	144
6.1	Version History	144
7	Model Recommendations	145
8	References	146

Appendices

A.	Priest Rapids to K-Gauge Correlation.....	154
B.	Observed Data and Simulated Hydrographs.....	161

Figures

Figure 1-1.	Hanford Site Map.....	2
Figure 1-2.	100-K Topography (from DOE/RL-2010-97, Draft A)	3
Figure 1-3.	100-K Reactors and Operable Units (from DOE/RL-2010-97)	4
Figure 2-1.	Stratigraphy and Hydrogeologic Units of 100-K	7
Figure 2-2.	Cross Section Base Map (from DOE/RL-2010-97)	9
Figure 2-3.	Geologic Cross Section A-A' (from DOE/RL-2010-97)	9

Figure 2-4. Geologic Cross Section E-E' (from DOE/RL-2010-97) 10

Figure 2-5. Elevation of the Top Surface of the RUM Unit (from DOE/RL-2010-97)..... 11

Figure 2-6. Ringold Hydraulic Conductivity ECDF from SGW-44022 12

Figure 2-7. Hanford Hydraulic Conductivity ECDF from SGW-44022..... 12

Figure 2-8. Natural Vegetation Recharge Scenario Applied for Preliminary Remediation Goal Calculation in 100-Area Waste Sites Subject to Historic Irrigation..... 18

Figure 2-9. Aerial Imagery of 100-K Model Domain Showing Spatial Variability of Surface Conditions that are Reflected in Natural Recharge Rates that Depend on Surface Soil Type and Vegetation Density 20

Figure 2-10. Conceptualization of Spatially and Temporally Variable Natural Recharge Rate Boundary Condition 21

Figure 2-11. Annual Trends in River Stage at One Location Illustrating Repeatable Annual Cycles (from DOE/RL-2010-97, DRAFT A) 23

Figure 2-12. Pore Water Samples from the Columbia River Bed..... 25

Figure 2-13. 100-K Water Table March 2015 (from DOE/RL-2016-09, Rev. 0)..... 27

Figure 2-14. 1989 Water Table Elevations in the 100-KR-4 OU (from DOE/RL-90-21) 28

Figure 2-15. Columbia River Stage and Selected Well Water Level Elevations..... 29

Figure 2-16. Hanford Site and Outlying Areas Water Table Map, April/May 2006 (from PNNL-16346) 30

Figure 2-17. Changes in Selected 100-KR-4 OU Plume Areas since 2003 (from DOE/RL-2016-09) 31

Figure 2-18. Observed Hexavalent Chromium Concentrations at Wells 199-K-173 and 199-K-205 32

Figure 2-19. 100-KR Cr(VI) Plume in the Unconfined Aquifer (2015 Low River Stage), KE and KW Reactor Vicinity (from DOE/RL-2016-09)..... 34

Figure 2-20. 100-KR Cr(VI) Plume in the Unconfined Aquifer (2015 Low River Stage), 116-K-2 Trench and 100-N Vicinity (from DOE/RL-2016-09) 35

Figure 2-21. 100-KR Tritium Plume in the Unconfined Aquifer (from DOE/RL-2016-09) 36

Figure 2-22. 100-KR Nitrate Plume in the Unconfined Aquifer (from DOE/RL-2016-09) 37

Figure 2-23. 100-KR Strontium-90 Plume in the Unconfined Aquifer (from DOE/RL-2016-09)..... 38

Figure 2-24. 100-KR Carbon-14 Plume in the Unconfined Aquifer (from DOE/RL-2016-09) 39

Figure 2-25. 100-KR Trichloroethene Plume in the Unconfined Aquifer (from DOE/RL-2016-09)..... 40

Figure 3-1. Comparison between Daily River Stage and Average River Stage Based on Stress Period Length at K-River Gauge for January 2013 to December 2016 45

Figure 3-2. Comparison between Daily River Stage and Average River Stage Based on Stress Period Length at K-River Gauge for the Predictive Model..... 45

Figure 3-3. 100-K Groundwater Flow and Transport Model Plan View Grid..... 47

Figure 3-4. Hydrogeological Cross Section Base Map for 100-Area GFM within 100-K GWFTM Model Domain 49

Figure 3-5. 100-Area GFM with Columbia River, MODFLOW Model Layers and 2014 Water Table through Cr(VI) Plume in KW Area..... 49

Figure 3-6. 100-Area GFM with Columbia River, MODFLOW Model Layers and 2014 Water Table through Cr(VI) Plume in KE Area..... 50

Figure 3-7. EW Cross Section at 100-Area GFM with MODFLOW Model Layers and 2014 Water Table..
 50

Figure 3-8. 2013-2016 Recharge 52

Figure 3-9. GHB Head vs. Distance Considering Stage, Gradient, Prior Levels, and Distance Correction
 for the First Eight Stress Periods of the 100-BC GWFTM..... 54

Figure 3-10. Pilot Point Locations with Hydrostratigraphic Unit Distribution in Layer 1 58

Figure 3-11. Pilot Point Locations with Hydrostratigraphic Unit Distribution in Layer 2 59

Figure 3-12. Pilot Point Locations with Hydrostratigraphic Unit Distribution in Layer 3 60

Figure 3-13. Pilot Point Locations with Hydrostratigraphic Unit Distribution in Layer 4 61

Figure 3-14. Longitudinal Dispersivity by Rock Type 63

Figure 3-15. Longitudinal Dispersivity by Reliability Level for all Rock Types with Linear and Log Fits ..
 64

Figure 3-16. Longitudinal Dispersivity by Reliability Level for Alluvial Sediments Only with Linear and
 Log Fits 65

Figure 3-17. Calibration Features 69

Figure 3-18. Observed Versus Simulated AWLN Heads 72

Figure 3-19. Observed Versus Simulated Manually Measured Heads 73

Figure 3-20. March 2015 Annual Groundwater Monitoring Report (Right) and Model Simulated (Left)
 Maps 74

Figure 3-21. March 2016 Annual Groundwater Monitoring Report (Right) and Model Simulated (Left)
 Maps 75

Figure 3-22. Layer 1 Hydraulic Conductivity..... 77

Figure 3-23. Layer 2 Hydraulic Conductivity..... 78

Figure 3-24. Layer 3 Hydraulic Conductivity..... 79

Figure 3-25. Layer 4 Hydraulic Conductivity..... 80

Figure 3-26. Potential Continuing Source Locations at KW Area..... 84

Figure 3-27. Potential Continuing Source Locations at KE Area..... 85

Figure 3-28. Representative Stratigraphic Columns for the Selected Waste Site Locations 87

Figure 3-29. Characteristic Release Rate Curves at Continuing Source Locations for Cr(VI), Carbon-14,
 Strontium-90, and Tritium (Calibration Model) 90

Figure 3-30. Characteristic Release Rate Curves for Cr(VI), Carbon-14, Strontium-90, and Tritium
 (Predictive Model) 91

Figure 3-31. Simulated (Left) and Mapped (Right) Chromium Concentrations at the end of 2016 in Layer
 1 (Top of Unconfined Aquifer)..... 94

Figure 3-32. Observed vs Simulated Chromium Concentrations at Wells near 183.1KW Headhouse..... 95

Figure 3-33. Observed vs Simulated Chromium Concentrations at Selected Wells within 100-KW Area 95

Figure 3-34. Observed vs Simulated Chromium Concentrations at Wells near 183.1KE Headhouse 96

Figure 3-35. Observed vs Simulated Chromium Concentrations at Wells near 118-K-1 Burial Ground... 96

Figure 3-36. Simulated (Left) and Mapped (Right) Strontium-90 Concentrations at the end of 2016 in
 Layer 1 (Top of Unconfined Aquifer)..... 98

Figure 3-37. Observed vs Simulated Strontium-90 Concentrations at Wells near 116-KW-2 Crib 99

Figure 3-38. Observed vs Simulated Strontium-90 Concentrations at Wells near KE FSB 99

Figure 3-39. Observed vs Simulated Strontium-90 Concentrations at Wells near 116-K-2 Trench..... 100

Figure 3-40. Evaluation of Carbon-14 Plume Definition between 2013 and 2015 in KW Area 100

Figure 3-41. Evaluation of Carbon-14 Plume Definition between 2013 and 2015 in KE Area 101

Figure 3-42. Simulated (Left) and Mapped (Right) Carbon-14 Concentrations at the end of 2016 in Layer 1 (Top of Unconfined Aquifer)..... 101

Figure 3-43. Observed vs Simulated Carbon-14 Concentrations at Wells near 116-KW-1 Gas Condensate Crib 102

Figure 3-44. Observed vs Simulated Carbon-14 Concentrations at Wells near 116-KE-1 Gas Condensate Crib 102

Figure 3-45. Evaluation of Nitrate Plume Definition between 2013 and 2015 in KW Area 103

Figure 3-46. Simulated (Left) and Mapped (Right) Nitrate Concentrations at the end of 2016 in Layer 1 (Top of Unconfined Aquifer)..... 104

Figure 3-47. Observed vs Simulated Nitrate Concentrations at Wells near 116-KW-1 Gas Condensate Crib 104

Figure 3-48. Observed vs Simulated Nitrate Concentrations at Selected Wells downstream of 116-KW-1 Gas Condensate Crib..... 105

Figure 3-49. Simulated (Left) and Mapped (Right) Tritium Concentrations at the end of 2016 in Layer 1 (Top of Unconfined Aquifer)..... 106

Figure 3-50. Observed vs Simulated Tritium Concentrations at Wells near 116-KW-1 Gas Condensate Crib 106

Figure 3-51. Observed vs Simulated Tritium Concentrations at Wells near 116-KW-2 Crib 107

Figure 3-52. Observed vs Simulated Tritium Concentrations at Wells near 116-KE-1 Gas Condensate Crib and 118-K-1 Burial Ground 107

Figure 3-53. Simulated (Left) and Mapped (Right) TCE Concentrations at the End of 2016 in Layer 1 (Top of Unconfined Aquifer)..... 108

Figure 3-54. Simulated Cr(VI) Plume in 2017 at the Top of the Unconfined Aquifer 110

Figure 3-55. Simulated Cr(VI) Plume in 2027 at the Top of the Unconfined Aquifer 111

Figure 3-56. Simulated Cr(VI) Plume in 2042 at the Top of the Unconfined Aquifer 112

Figure 3-57. Simulated Cr(VI) Plume in 2067 at the Top of the Unconfined Aquifer 113

Figure 3-58. Simulated Cr(VI) Plume in 2117 at the Top of the Unconfined Aquifer 114

Figure 3-59. Simulated Sr-90 Plume in 2017 at the Top of the Unconfined Aquifer 116

Figure 3-60. Simulated Sr-90 Plume in 2117 at the Top of the Unconfined Aquifer 117

Figure 3-61. Simulated C-14 Plume in 2017 at the Top of the Unconfined Aquifer..... 119

Figure 3-62. Simulated C-14 Plume in 2027 at the Top of the Unconfined Aquifer..... 120

Figure 3-63. Simulated Nitrate Plume in 2017 at the Top of the Unconfined Aquifer..... 122

Figure 3-64. Simulated Nitrate Plume in 2024 at the Top of the Unconfined Aquifer..... 123

Figure 3-65. Simulated Tritium Plume in 2017 at the Top of the Unconfined Aquifer..... 125

Figure 3-66. Simulated Tritium Plume in 2027 at the Top of the Unconfined Aquifer..... 126

Figure 3-67. Simulated TCE Plume in 2017 at the Top of the Unconfined Aquifer 128

Figure 3-68. Simulated TCE Plume in 2022 at the Top of the Unconfined Aquifer 129

Figure 3-69. Maximum Simulated Cr(VI) Concentration in the Aquifer over 125 Years (No Further Action) 130

Figure 3-70. Maximum Simulated Sr-90 Concentration in the Aquifer over 300 Years (No Further Action) 131

Figure 3-71. Maximum Simulated C-14 Concentration in the Aquifer over 125 Years (No Further Action) 131

Figure 3-72. Maximum Simulated Nitrate Concentration in the Aquifer over 125 Years (No Further Action) 132

Figure 3-73. Maximum Simulated Tritium Concentration in the Aquifer over 125 Years (No Further Action) 132

Figure 3-74. Maximum Simulated TCE Concentration in the Aquifer over 125 Years (No Further Action) 133

Figure 3-75. Maximum Simulated Cr(VI) Concentration at the Shoreline over 125 Years (No Further Action) 133

Figure 3-76. Maximum Simulated Sr-90 Concentration at the Shoreline over 300 Years (No Further Action) 134

Figure 3-77. Maximum Simulated C-14 Concentration at the Shoreline over 125 Years (No Further Action) 134

Figure 3-78. Maximum Simulated Nitrate Concentration at the Shoreline over 125 Years (No Further Action) 135

Figure 3-79. Maximum Simulated Tritium Concentration at the Shoreline over 125 Years (No Further Action) 135

Figure 3-80. Maximum Simulated TCE Concentration at the Shoreline over 125 Years (No Further Action) 136

Figure 4-1. Flow Model Parameter Identifiability 137

Figure 4-2. Identifiable Pilot Points (Highlighted in Yellow) with Respect to Calibration Dataset and Mapped 2013 Cr(VI) Plume 138

Figure 4-3. CDF of Calibrated Hanford and Ringold E Hydraulic Conductivity Pilot Points..... 139

Figure 4-4. Hexavalent Chromium Release Rate from Sources near 183.1KW Headhouse during the Calibration Period 141

Figure 4-5. Hexavalent Chromium Release Rate from Sources near Well 199-K-173 during the Calibration Period 141

Figure 4-6. The Estimated Lateral Extent of the Hexavalent Chromium Sources in KW Area 142

Tables

Table 2-1. Horizontal Hydraulic Conductivity Estimates for 100-K Sediments 13

Table 2-2. Native Vegetation Recharge Scenario Phases and Recharge Rates (mm/yr) 19

Table 2-3. 100-KR-4 OU Pump and Treat System Specifications	31
Table 3-1. Dispersivity-scale Relationships.....	66
Table 3-2. Recommended Dispersivity Values for 100-K.....	66
Table 3-3. Single-Value Parameter Estimates	75
Table 3-4. List of Waste Sites for Potential Continuing Sources to the Groundwater.....	82
Table 6-1. Version History of the 100-K GWFTM	144
Table A.1. Regression Equation Results and Location Information.....	159

Terms

1D	one-dimensional
2D	two-dimensional
AMSL	above mean sea level
AWLN	Automated Water Level Network
B.P.	before present
CHPRC	CH2M HILL Plateau Remediation Company
COPC	contaminant of potential concern
Cr(VI)	hexavalent chromium
CSM	conceptual site model
DOE	U.S. Department of Energy
DWS	drinking water standard
ECF	environmental calculation file
EMMA	Environmental Model Management Archive
FEP	feature, event, or process
GFM	geologic framework model
GHB	general head boundary (MODFLOW term for mixed boundary condition)
GIS	geographic information system
GWFTM	Groundwater Flow and Transport Model
HF	Hanford formation
HISI	Hanford Information System Inventory
HSU	hydro-stratigraphic unit
MODFLOW	MODular groundwater FLOW code (software)
MT3DMS	Modular 3-Dimensional Multiple Species transport code (software)
m.y.	million years
OU	Operable Unit
P&T	pump and treat
PNNL	Pacific Northwest National Laboratory
PRG	preliminary remediation goal

PRZ	periodically rewetted zone
RET	Recharge Estimation Tool
RI/FS	Remedial Investigation / Feasibility Study
RUM	Ringold Upper Mud
Rwie	Ringold E
SSL	soil screening level
SSM	source/sink mixing

1 Purpose

The groundwater flow and transport model for the 100-KR-4 Operable Unit (OU) of the U.S. Department of Energy's (DOE) Hanford Site was developed to provide the computational basis for simulation of fate and transport of groundwater contaminants. This model focuses on the hexavalent chromium, trichloroethylene, tritium, nitrate, carbon-14, and strontium-90 plumes, which are currently (2015) present at or above drinking water standards.

1.1 Need

The 100-K Groundwater Flow and Transport Model provides a consistent, mass conservative hydrogeologic framework at the scale of the OU for comparing potential remediation actions required for the Remedial Investigation/Feasibility Study (RI/FS). Model output used for this purpose could include groundwater potentials, hydraulic gradients, flow rates, future groundwater contamination concentrations, and likely influent concentrations for remedies that extract contaminated groundwater. A model that included most of the 100 Area (SGW-46269) was previously used for some of these computations.

Additionally, vadose zone source models implemented in the Subsurface Transport Over Multiple Phases (STOMP¹) code allow assessment of soil remediation decisions on groundwater quality.

1.2 Background

The U.S. government took possession of the land now known as the Hanford Site in 1943 to produce weapons-grade plutonium as a part of the Manhattan Project. The Hanford Site is divided into numerically designated areas. These areas served as the location for reactor, chemical separation, and related activities for the production and purification of special nuclear materials and other nuclear activities. The reactors and their ancillary/support facilities were located along the south shore of the Columbia River in the 100 Area, because of the need for large quantities of water to cool the reactors. The 100-K area is in the northern portion of the Hanford Site adjacent to the southern shore of the Columbia River. The 105-KE and 105-KW Reactors were the largest production reactors at Hanford. The 100-K Area is shown in Figure 1-1; the KW and KE Reactors were in this area.

¹ Battelle Memorial Institute (Battelle) retains copyright on all versions, revisions, and operational modes of the Subsurface Transport Over Multiple Phases (STOMP) software simulator, as permitted by the U.S. Department of Energy. STOMP is used here under a limited government use license.

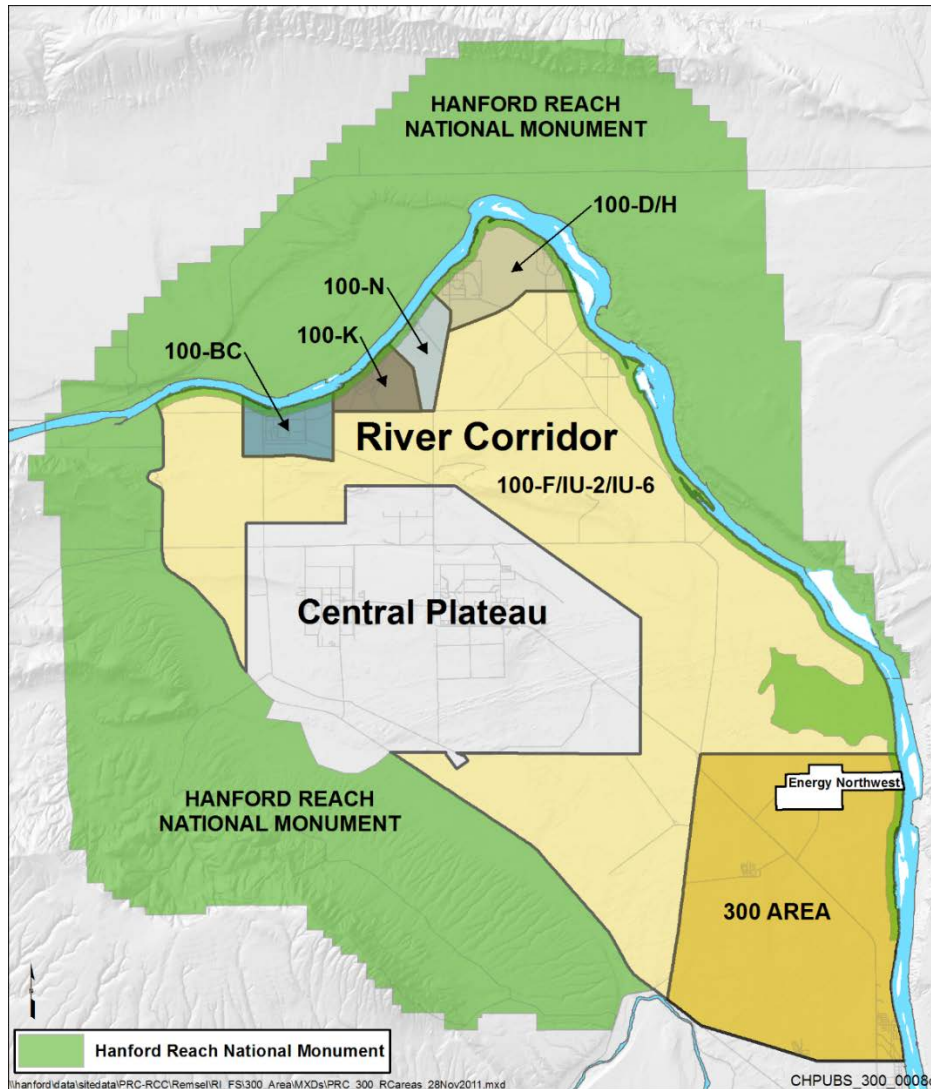


Figure 1-1. Hanford Site Map

100-K is located on the south bank of the Columbia River, upstream from all but one other Hanford Site reactor areas (100-BC is upstream of 100-K). The topography of 100-K is relatively flat inland (Figure 1-2) from the Columbia River. The area has been disturbed and graded extensively by human activity from reactor construction in the 1940s through current waste site remediation activities, including being stripped of vegetation. Surface elevations in this region range from approximately 166 m (545 ft) above mean sea level (AMSL) at the southern border to 119 m (390 ft) in the north along the river. The 100-K area had two production reactors, 105-KW and 105-KE.

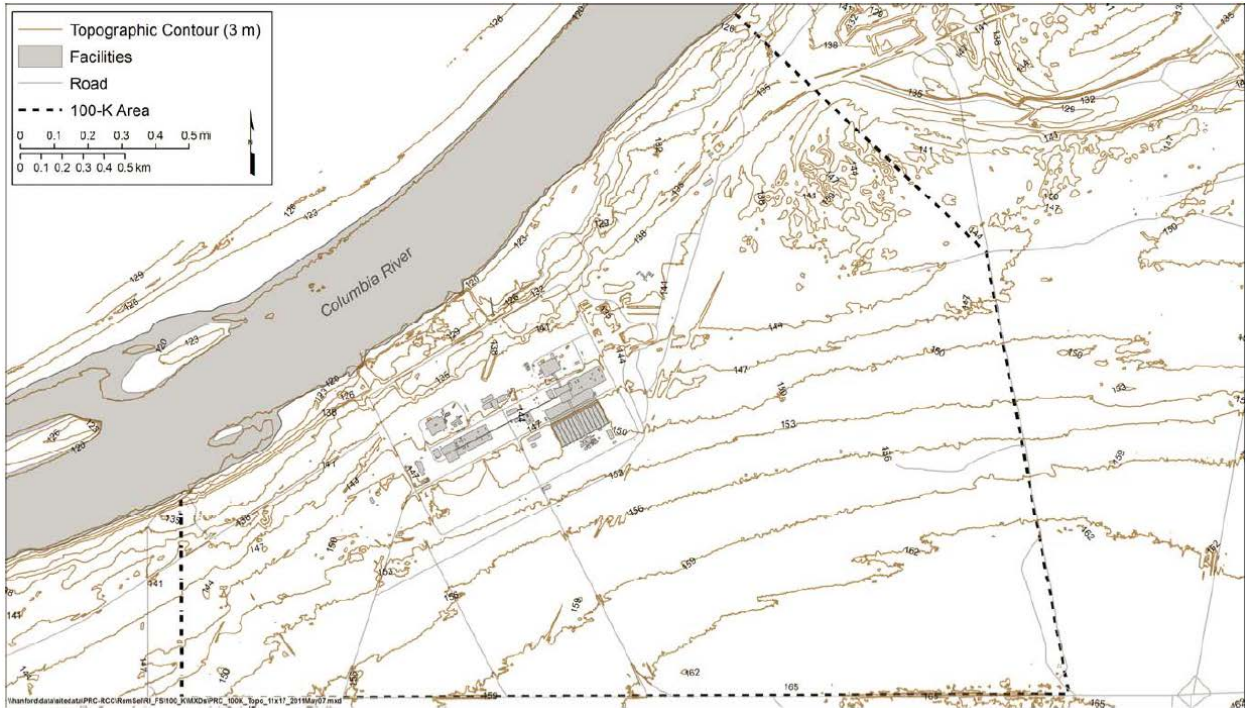


Figure 1-2. 100-K Topography (from DOE/RL-2010-97, Draft A)

The Hanford Site is characterized by a semi-arid climate and is the driest and warmest portion of the Columbia Basin. The Cascade Range, to the west, creates a rain shadow effect on the Hanford Site climate, while the Rocky Mountains and mountain ranges in southern British Columbia protect it from the more severe polar air masses from the north (*Hanford Site Climatological Summary 2004 with Historical Data* [PNNL-15160]).

The Columbia River is the only natural surface water feature near 100-K and forms the northern boundary of the model area. The Columbia River has played a major role in the depositional and erosional processes that produced the sedimentary and geologic features across the Hanford Site.

The stretch of the river that extends from Priest Rapids Dam, approximately 24 km (15 mi) upstream of 100-K, to the headwaters of Lake Wallula, is the only free flowing portion of the Columbia River in the United States. This stretch of river, named the Hanford Reach, is part of the Hanford Reach National Monument, established in June 2000 through Presidential Proclamation.

Figure 1-3 shows the OU boundaries, facilities, and reactors, both of which were shut down in 1971.

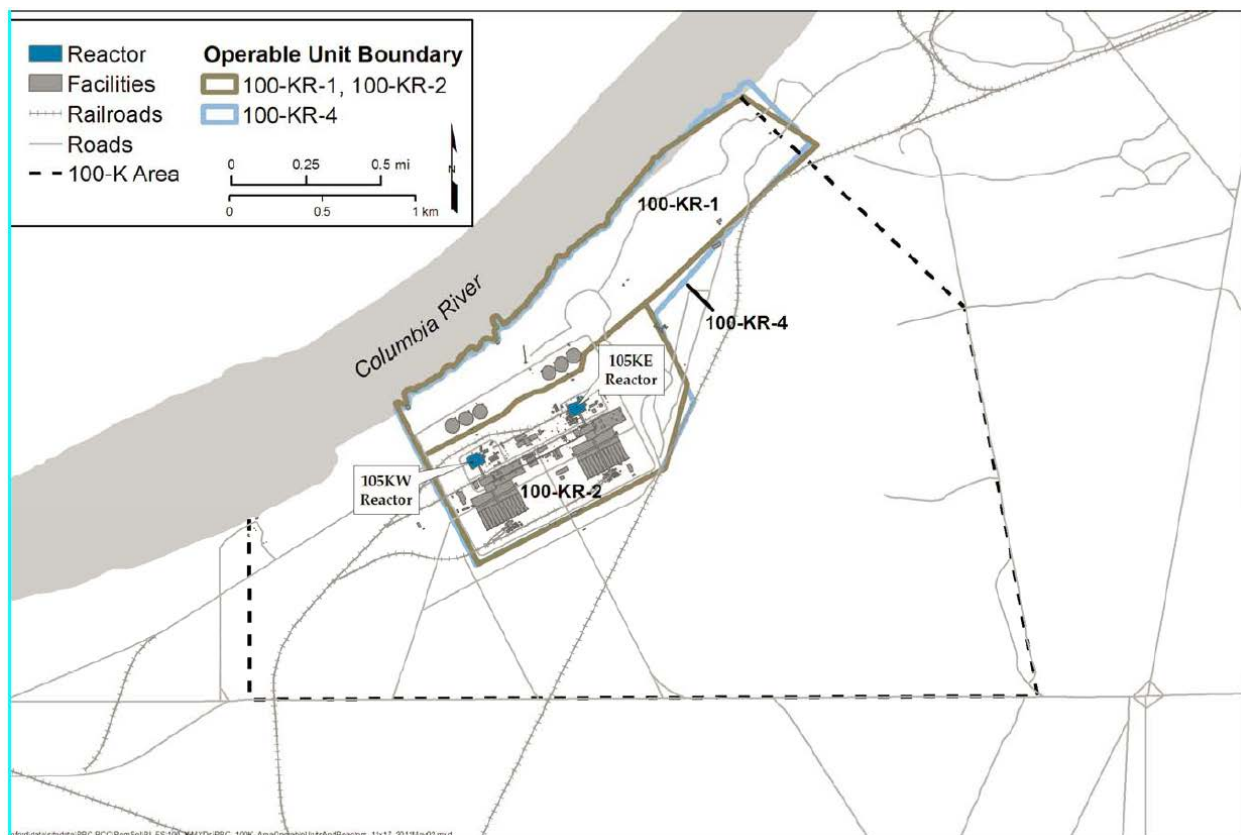


Figure 1-3. 100-K Reactors and Operable Units (from DOE/RL-2010-97)

Producing plutonium for national defense was the primary mission of the Hanford Site reactors. Materials that passed through the reactors for manufacture, or materials contacting items that passed through the reactors, were radiologically contaminated. These materials represent most of the wastes that were produced. Active physical barriers and administrative measures were in place to minimize radiological hazards throughout the Hanford Site production areas to protect plant personnel. These measures affected the placement of disposal locations and waste management procedures for various waste streams.

Waste streams from the reactor production process include the following:

- Process inputs:
 - Raw materials to be processed through the reactor
 - Process chemicals for water conditioning and inhibiting corrosion (for example, sodium dichromate) because water management was crucial to the operation of the reactors and represented a major input subsystem
 - Materials used for reactor maintenance, such as acids, solvents, and solid metal components
- Process outputs:
 - Product and waste isotopes, such as plutonium-239 and strontium-90, respectively
 - Radioactively and chemically contaminated materials (solid and liquid wastes)
 - Radioactively and chemically contaminated cooling water

Liquid wastes from reactor operations and associated facilities were released to the vadose zone and the Columbia River. Solid wastes were disposed in burial grounds associated with the facilities.

1.3 Document Organization

The organization of this model package report follows guidance set forth in a quality assurance project plan for modeling that implements the requirements of DOE O 435.1, *Quality Assurance*, in a format that follows U.S. Environmental Protection Agency guidance (EPA QA/G-5M, *Guidance for Quality Assurance Project Plans for Modeling*), as follows:

- Chapter 1 sets forth the objectives that the 100-K Model is constructed to meet.
- Chapter 2 describes the conceptualization of the system to be simulated with the numerical model, including identification of the relevant features, events, and processes (FEPs).
- Chapter 3 describes the implementation of the conceptual model as a numerical computer simulation model.
- Chapter 4 provides an overview of the sensitivity and describes sources of uncertainty for the predictions made with this model. There is some intentional redundancy in Chapters 3 to 5 to allow the report to be used as a reference document as well as a descriptive document.
- Chapter 5 enumerates the limitations of this model that result from the conceptualization, selection, and exclusion of relevant FEPs, assumptions, and numerical implementation.
- Chapter 6 describes how this model is uniquely identified, tracked, and preserved as a configuration management item.
- Chapter 7 lists recommended improvements to the model that could be made for future versions.
- Chapter 8 provides references cited in this model package report.
- Appendix A describes an assessment of the relationship between Priest Rapids Dam and K-gauge stage data.
- Appendix B shows the observed head data and simulated hydrographs for the calibration model.

1.4 Model Objectives

The overall objectives of the modeling effort are to provide a basis to assist in making informed remediation action decisions based on descriptions of current and expected future groundwater contaminant concentrations at decision points within the OU boundaries.

Problem-specific analyses will be described for each use of the model in separate environmental calculation files.

2 Model Conceptualization

The conceptual site model (CSM) is a framework for interpreting data from 100-K characterization efforts. The CSM synthesizes what is known into a framework that is pertinent for decision making. The *American Society for Testing and Materials Standard Guide for Conceptualization and Characterization of Groundwater Systems* (ASTM D5979) defines the CSM as a written, pictorial, and diagrammatic information and interpretations. The CSM results from a blending of information and expert opinion on topics that range from small-scale processes to large-scale regional constraints, honors existing data, addresses how well interpretations and parameters are known, and integrates the parts into a whole-system view of the regulatory problem that can be translated into a quantitative representation. The following section describe the data and components of the CSM. **Key conceptual points are emphasized by bold text.**

2.1 Hydrogeologic Overview

The 100-K Area lies on the northern flank of the Wahluke Syncline and is located adjacent the Columbia River. Figure 2-1 shows the generalized stratigraphy of 100-K. The area is underlain by Miocene (approximately 17 to 8.5 million years [m.y.] before present [B.P.]) basalt of the Columbia River Basalt Group and late Miocene to Pleistocene (approximately 10.5 million to 12,000 years before present) suprabasalt sediments.

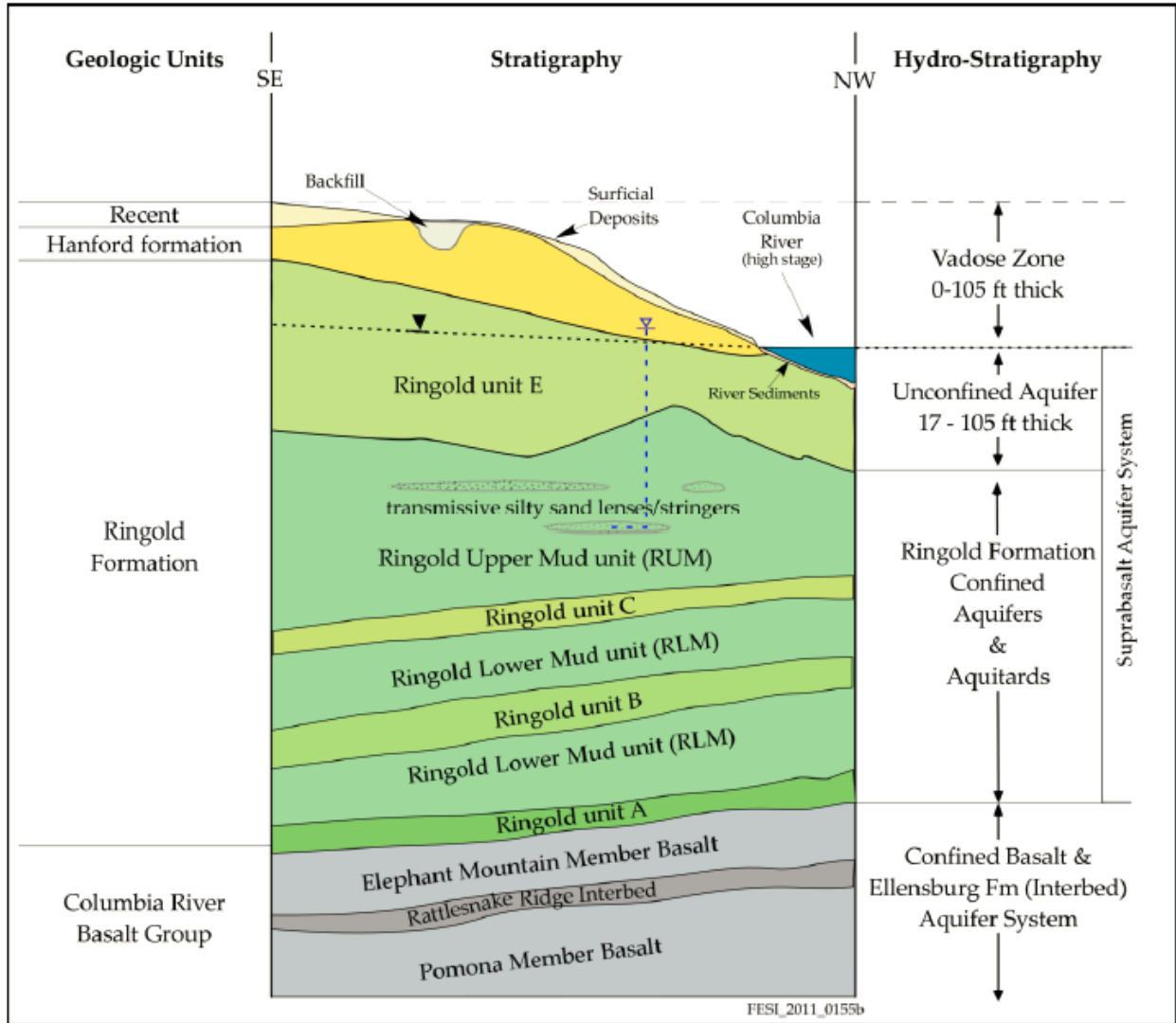


Figure 2-1. Stratigraphy and Hydrogeologic Units of 100-K

Sediments overlying the basalts are approximately 200 m (660 ft) thick at 100-K. Most of this sedimentary sequence can be divided into two main units: the Ringold Formation of late Miocene to middle Pliocene age (approximately 10.5 to 3 m.y. B.P.) and the Hanford formation of Pleistocene to Recent age (approximately 1 million to 12,000 B.P.). Holocene surficial deposits of silt, sand, and gravel form the veneer at the surface.

The sediments that overlie the basalt are divided into two primary units: the Ringold Formation (*Sedimentology and Stratigraphy of the Miocene-Pliocene Ringold Formation, Hanford Site, South-Central Washington* [WHC-SA-0740-FP]) and the informally named Hanford (*Standardized Stratigraphic Nomenclature for Post-Ringold-Formation Sediments within the Central Pasco Basin* [DOE/RL-2002-39]). Holocene surficial deposits of silt, sand, and gravel form a relatively thin veneer at the surface (*Geology and Hydrology of the Hanford Site: A Standardized Text for Use in Westinghouse Hanford Company Documents and Reports* [WHC-SD-ER-TI-003]; “Long History of Pre-Wisconsin, Ice Age Cataclysmic Floods: Evidence from Southeastern Washington State” [Bjornstad et al., 2001]).

The 100-K area is underlain by Miocene-aged (approximately 17 to 8.5 m.y. B.P.) basalt of the Columbia River Basalt Group and late Miocene- to Pleistocene-aged sediments (Ellensburg Formation, approximately 10.5 million to 12,000 B.P.) that are interbedded with basalt flows. The basalt may exceed 3,050 m (10,000 ft) in thickness, including the interbedded sediments of the Ellensburg Formation.

The physical properties of these formations influence the distribution of contamination in the subsurface. The Hanford formation, two upper units of the Ringold Formation (Ringold unit E and Ringold Upper Mud [RUM]) have been contacted by contaminated fluids. The rest of the Ringold Formation consists of a lower mud unit and Ringold units A, B, and C. **Contaminant migration units below the RUM is very unlikely in most locations because the low hydraulic conductivity of the RUM makes it an effective aquitard where it underlies the overlying Ringold unit E throughout 100-K.**

The unconfined aquifer in 100-KR ranges from 5.2 m to more than 32 m (17.1 to 105 ft) thick. This aquifer is primarily present in the Ringold unit E sand and gravel. This unit is overlain by the gravels and interbedded sand and silt of the Hanford formation, which comprise the bulk of the vadose zone. The vadose zone ranges from less than 1 m (3.3 ft) thick near the Columbia River to 32 m (105 ft) thick inland. The uneven surface of the silt- and clay-rich RUM forms the bottom of the unconfined aquifer. Contaminant concentrations are generally highest within the uppermost portion of the aquifer near the water table; however, mobile contaminants (e.g., Cr[VI]) have been detected over the entire aquifer thickness, particularly near source areas.

2.1.1 Hanford Formation

The Hanford formation is an unofficial designation for a geologic unit that consists of gravel, sand, and silt deposited by cataclysmic floodwaters that drained out of glacial Lake Missoula during the Pleistocene age (*Standardized Stratigraphic Nomenclature for Post-Ringold-Formation Sediments within the Central Pasco Basin* [DOE/RL-2002-39]). Figure 2-2 shows the locations of the eight generalized cross sections reported in DOE/RL-2010-97, DRAFT A (*Remedial Investigation/Feasibility Study for the 100-KR-1, 100-KR-2, and 100-KR-4 Operable Units*) to illustrate the hydrogeology in 100-KR-4 OU. The Hanford formation ranges in thickness from about 30 m (9 ft) near the southern boundary of 100-K to less than 1 m (3.3 ft) near the Columbia River (Figure 2-3 and Figure 2-4). Within the reactor area, the Hanford formation is no more than 20 m (65 ft) thick. **The Hanford formation is unsaturated within the 100-KR-4 OU.**

The Hanford formation is divided into three facies: gravel-dominated, sand-dominated, and silt-dominated (*Standardized Stratigraphic Nomenclature for Post-Ringold-Formation Sediments within the Central Pasco Basin* [DOE/RL-2002-39]). While the gravel-dominated facies are observed throughout 100-K, the sand-dominated facies were observed locally and cannot be correlated between boreholes.

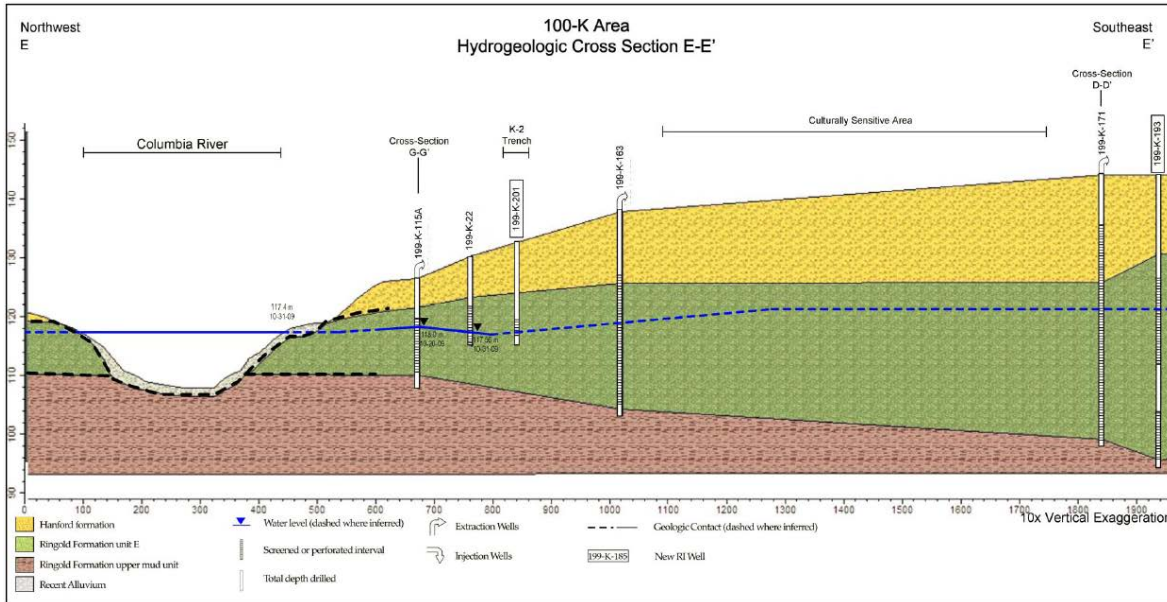


Figure 2-4. Geologic Cross Section E-E' (from DOE/RL-2010-97)

2.1.2 Ringold Formation Units

The Ringold Formation beneath 100-K contains most of the units commonly encountered elsewhere at the Hanford Site. The fluvial gravel and sand units A, B, C, and E (in ascending order) are present and interbedded with fine grained lacustrine and fluvial over bank deposits and paleosols. The uppermost unit of the Ringold Formation in 100-K is Ringold unit E, which comprises predominantly sandy gravel.

In the 100 Area, the uppermost fine grained Ringold sediments are informally termed the RUM unit. Distinguishing sandy, gravelly beds within the RUM unit from Ringold units C and B is not always possible. Similarly, silts and clays of the RUM unit may grade into deeper silt and clay units, making correlation of the units between boreholes difficult. Figure 2-5 shows the elevation of the top of the RUM, note the drop in elevation going downstream. The Ringold E is the most important Ringold unit, and comprises all the contaminated unconfined aquifer in the 100-K area.

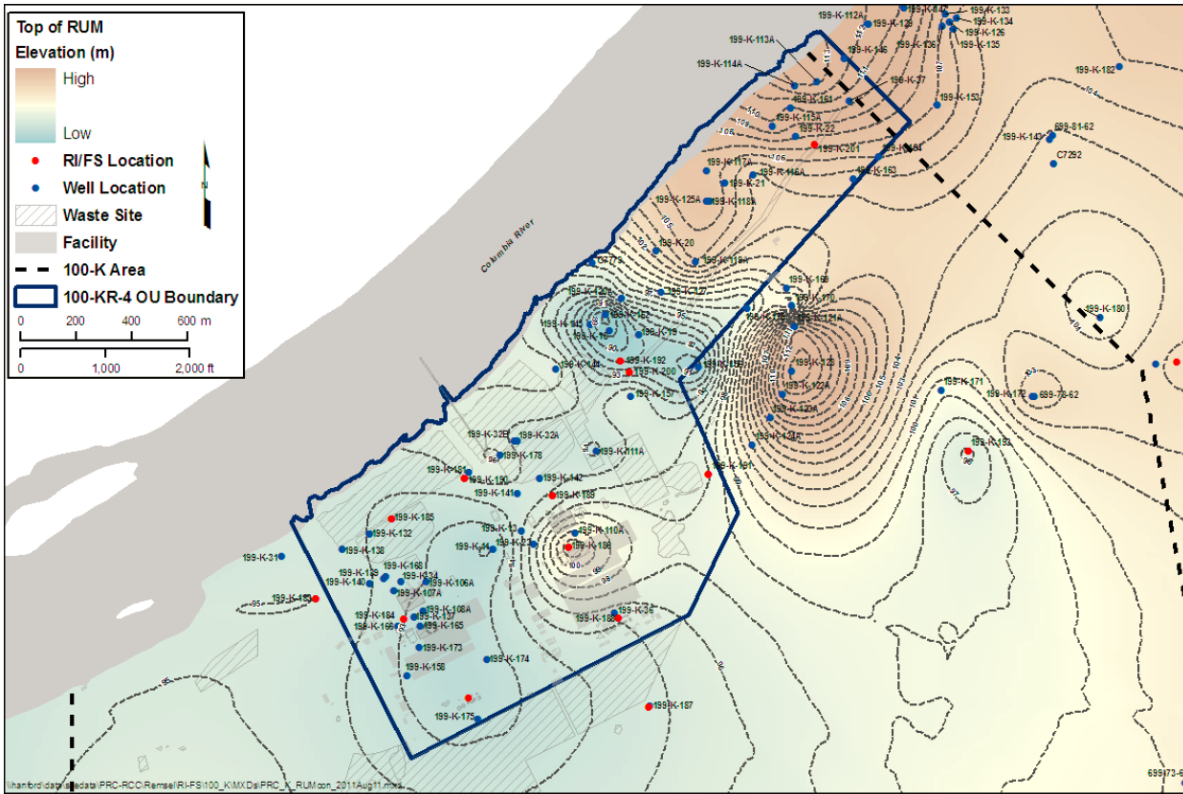


Figure 2-5. Elevation of the Top Surface of the RUM Unit (from DOE/RL-2010-97)

2.1.3 Hanford and Ringold Hydraulic Conductivity, Specific Storage, and Specific Yield

SGW-44022, *Geohydrologic Data Package in Support of 100-BC-5 Modeling*, Rev. 1, summarizes 100 Area hydraulic conductivity estimates from slug and pumping tests. Cumulative distribution plots of hydraulic conductivity by formation and test type (slug vs. pumping) are shown in Figure 2-6 and Figure 2-7. Note there is a systematic bias to higher values from pumping tests. This is because pumping tests are much less influenced by any near well residual effects from drilling compared to slug tests (Butler and Healey, 1998). Thus, the general trend of higher pumping test hydraulic conductivity holds, but cannot be more precisely identified for the Hanford or Ringold E. The 100 Area values reported in SGW-44022 for Hanford and Ringold range over more than two orders of magnitude, and thus add little to 100-K site-specific understanding. However, the **Hanford formation has systematically higher hydraulic conductivity than the Ringold E.**

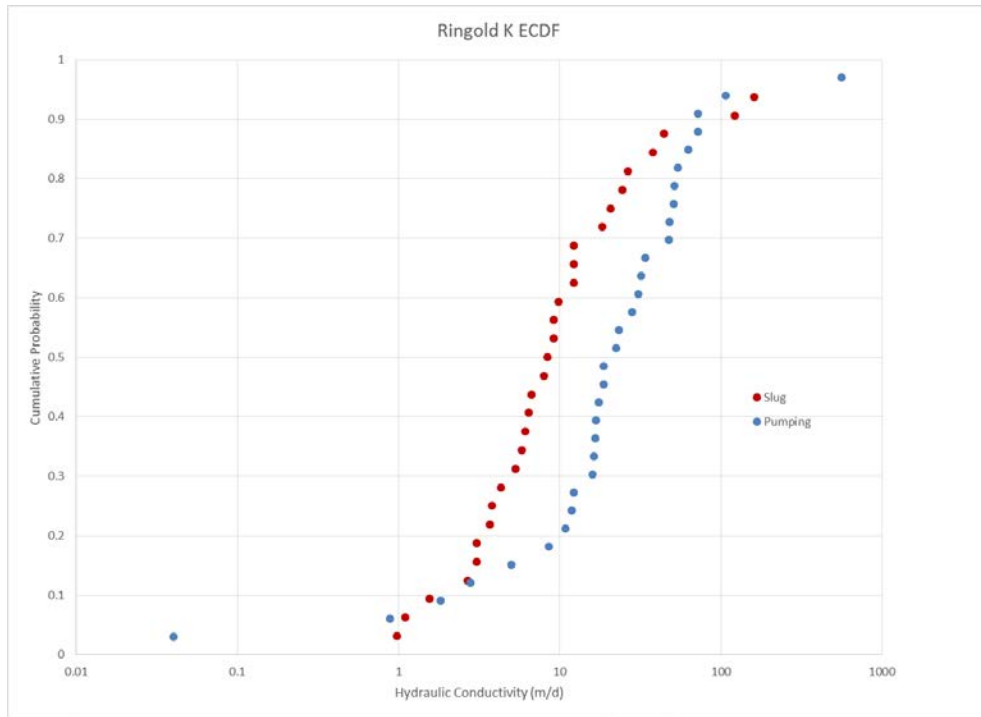


Figure 2-6. Ringold Hydraulic Conductivity ECDF from SGW-44022

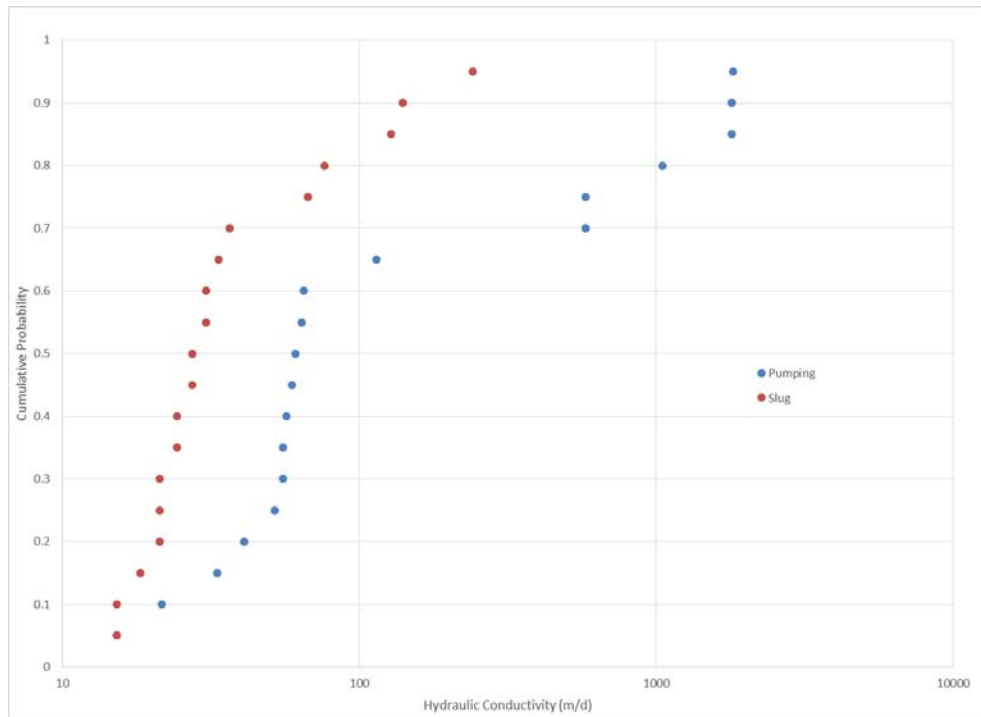


Figure 2-7. Hanford Hydraulic Conductivity ECDF from SGW-44022

Pumping and slug tests were performed at various wells in 100-KR-4 OU to estimate horizontal hydraulic conductivity (Table 2-1). The one well screened in the RUM had the lowest hydraulic conductivity, approximately 0.2 m/d (0.6 ft/d). Pumping test results for the wells screened in Ringold E had hydraulic

conductivity ranging from 1.8 to 34 m/d (6 to 111 ft/d). Slug test results for wells screened in Ringold E had hydraulic conductivity ranging from 0.7 to 44 m/d (2 to 145 ft/d). High hydraulic conductivity values in the Hanford formation shows that pumping test results are 2-3 times higher than the slug test results (SGW-44022). However, no wells in 100-K were available for which both pumping and slug test were performed. In general, actual field hydraulic conductivity should be couple of times higher than the slug test results and should be similar to the pumping test results.

Table 2-1. Horizontal Hydraulic Conductivity Estimates for 100-K Sediments

Well Number	Geologic Unit	Hydraulic Conductivity		Test Type/Analysis Method	Reference
		ft/day	m/day		
199-K-10	Ringold E	52	16	Pumping/Cooper-Jacob	PNL-10886
199-K-18	Ringold E	9	2.8	Pumping/Cooper-Jacob	CCN 024566
199-K-19	Ringold E	6	1.8	Pumping/Cooper-Jacob	CCN 024566
199-K-20	Ringold E	111	34	Pumping/Cooper-Jacob	CCN 024566
199-K-21	Ringold E	16	5	Pumping/Cooper-Jacob	CCN 024566
199-K-22	Ringold E	3	0.88	Pumping/Cooper-Jacob	CCN 024566
199-K-32A	Ringold E	80	24	Slug/Bouwer-Rice	DOE/RL-93-79
199-K-33	Ringold E	19	5.8	Slug/Bouwer-Rice	DOE/RL-93-79
199-K-34	Ringold E	68	21	Slug/Bouwer-Rice	DOE/RL-93-79
199-K-35	Ringold E	124	38	Slug/Bouwer-Rice	DOE/RL-93-79
199-K-36	Ringold E	87	27	Slug/Bouwer-Rice	DOE/RL-93-79
199-K-37	Ringold E	145	44	Slug/Bouwer-Rice	DOE/RL-93-79
199-K-106A	Ringold E	9	2.7	Slug/Bouwer-Rice	WHC-SD-EN-DP-090
199-K-107A	Ringold E	5	1.6	Slug/Bouwer-Rice	WHC-SD-EN-DP-090
199-K-108A	Ringold E	3	0.98	Slug/Bouwer-Rice	WHC-SD-EN-DP-090
199-K-110A	Ringold E	4	1.1	Slug/Bouwer-Rice	WHC-SD-EN-DP-090
	Ringold E	32	9.8	Slug/Bouwer-Rice	WHC-SD-EN-TI-221
199-K-111A	Ringold E	27	8.4	Slug/Bouwer-Rice	WHC-SD-EN-TI-221
199-K-183	Ringold E	43	13	Slug/KGS	ECF-100KR4-12-0010
199-K-184	Ringold E	22	6.8	Slug/KGS	ECF-100KR4-12-0010
199-K-185	Ringold E	8	2.3	Slug/KGS	ECF-100KR4-12-0010
199-K-187	Ringold E	52	28	Slug/KGS	ECF-100KR4-12-0010
199-K-188	Ringold E	52	16	Slug/KGS	ECF-100KR4-12-0010
199-K-189	Ringold E	3	0.9	Slug/KGS	ECF-100KR4-12-0010

Table 2-1. Horizontal Hydraulic Conductivity Estimates for 100-K Sediments

Well Number	Geologic Unit	Hydraulic Conductivity		Test Type/Analysis Method	Reference
		ft/day	m/day		
199-K-190	Ringold E	39	12	Slug/KGS	ECF-100KR4-12-0010
199-K-191	Ringold E	3	1	Slug/KGS	ECF-100KR4-12-0010
199-K-192	RUM	0.66	0.2	Slug/KGS	ECF-100KR4-12-0010
199-K-193	Ringold E	4	1.1	Slug/KGS	ECF-100KR4-12-0010
199-K-194	Ringold E	2	0.7	Slug/KGS	ECF-100KR4-12-0010
199-K-195	Ringold E	49	15	Slug/KGS	ECF-100KR4-12-0010
199-K-196	Ringold E	49	8.8	Slug/KGS	ECF-100KR4-12-0010
199-K-199	Ringold E	17	5.1	Slug/KGS	ECF-100KR4-12-0010
199-N-119	Ringold E	14	4.3	Slug/Bouwer-Rice	PNNL-16894
	Ringold E	22	6.7	Slug/Type curve Butler	PNNL-16894
199-N-120	Ringold E	17	5.3	Slug/Bouwer-Rice	PNNL-16894
	Ringold E	21	6.4	Slug/Type curve Butler	PNNL-16894
199-N-121	Ringold E	12	3.7	Slug/Bouwer-Rice	PNNL-16894
	Ringold E	12	3.8	Slug/Bouwer-Rice	PNNL-16894
199-N-182	Ringold E	13.4	4.1	Slug/KGS	ECF-100NR2-12-0031
199-N-183	Ringold E	21.3	6.5	Slug/KGS	ECF-100NR2-12-0031
199-N-184	Ringold E	12.4	3.8	Slug/KGS	ECF-100NR2-12-0031
199-N-185	Ringold E	8.5	2.6	Slug/KGS	ECF-100NR2-12-0031
199-N-186	Ringold E	14.3	4.4	Slug/KGS	ECF-100NR2-12-0031
199-N-187	Ringold E	18.3	5.6	Slug/KGS	ECF-100NR2-12-0031
199-N-188	Ringold E	22.2	6.8	Slug/KGS	ECF-100NR2-12-0031
199-N-189	Ringold E	30.7	9.4	Slug/KGS	ECF-100NR2-12-0031

Table 2-1. Horizontal Hydraulic Conductivity Estimates for 100-K Sediments

Well Number	Geologic Unit	Hydraulic Conductivity		Test Type/Analysis Method	Reference
		ft/day	m/day		
PNL-10886, <i>Development of a Three-Dimensional Ground-Water Model of the Hanford Site Unconfined Aquifer System: FY 1995 Status Report.</i>					
CCN 024566, "Field Summary Report 100-H Area Well Production Testing"					
DOE/RL-93-79, <i>Limited Field Investigation Report for the 100-KR-4 Operable Unit.</i>					
WHC-SD-EN-DP-090, <i>Borehole Data Package for the 100-K Area Ground Water Wells, CY 1994.</i>					
WHC-SD-EN-TI-221, <i>Geology of the 100-FR-3 Operable Unit, Hanford Site South-Central Washington.</i>					
ECF-100KR4-12-0010, <i>Analysis of Slug Test Data at the 100-KR-4 OU.</i>					
PNNL-16894, <i>Investigation of the Strontium-90 Contaminant Plume Along the Shoreline of the Columbia River at the 10-N Area of the Hanford Site.</i>					
ECF-100NR2-12-0031, <i>Analysis of Data Collected from Slug Tests Conducted in Remedial Investigation Boreholes within the 100-NR-2 Groundwater Operable Unit.</i>					

Bierschenk (*Aquifer Characteristics and Ground-Water Movement at Hanford*, 1959) used the Ferris analytic approach to estimate hydraulic conductivity for Hanford “glaciofluvial” deposits in the 100 Area and got results between 200 and 700 m/d. These wells ranged from about 1 to 5 km inland from the river; thus, these values represent bulk effective Hanford properties.

Slug and single-well pumping tests do not provide reliable estimates of storativity even though the analytic test solutions incorporate the parameter (*Ground-Water Hydraulics*, Lohman, 1972).

PNNL-18732 (*Field Test Report: Preliminary Aquifer Test Characterization Results for Well 299-W15-225: Supporting Phase I of the 200-ZP-1 Groundwater Operable Unit Remedial Design*) reports aquifer characterization in the 200-ZP-1 OU located in the 200 West area. The Ringold E was the tested formation. Storativity of 9.7×10^{-4} was reported for a saturated thickness of 55.4 m giving a specific storage of 1.7×10^{-5} 1/m. Specific yield was estimated at 0.097; similar type curve matches could be generated with specific yield ranging from 0.08 to 0.13.

Bierschenk (1959) cites an S value of 0.06 from a multiple-well test at 699-62-43; the magnitude indicates this should be interpreted as specific yield (S_y).

2.2 Features, Events, and Processes (FEPs)

2.2.1 FEP: Anthropogenic Recharge

Untreated (that is, raw) Columbia River water is used in 100-K to control fugitive dust from remedial action processes. Typical remedial action processes and site features that contribute to fugitive dust include digging, open excavations, soil stock piles, and vehicle use on dirt roads. During remedial action, it has been important to control fugitive dust primarily for contamination control, worker inhalation concerns, and offsite perceptions. Control is maintained by applying water and by halting remediation activities when fugitive dust cannot be controlled because of wind conditions. According to the 100 Area RDR/RAWP (DOE/RL-96-17, *Remedial Design Report/Remedial Action Work Plan for the 100 Area*), “...use of water for dust control is minimized.” This means that the quantity of water used is sufficient to control airborne emissions but excessive quantities of dust control water are not applied to minimize

potential adverse impacts on groundwater. In the future, remedial actions will have less impact within 100-K because most of the waste sites have been remediated and revegetated.

2.2.2 FEP: Natural Recharge

Recharge is the result of net infiltration through the vadose zone reaching the aquifer and is driven by the partition of precipitation (meteoric water, including snow) into potential evaporation, transpiration, run-off, run-on, and net recharge. In an arid or semi-arid climate such as at the Hanford Site, the net downward recharge flux that results from the partition of these fluxes is episodic and usually infrequent. However, this effect is typically damped towards a nearly constant rate with increasing depth as soil moisture variability with depth measured at Hanford Site lysimeters shows (PNNL-17841, *Compendium of Data for the Hanford Site (Fiscal Years 2004 to 2008) Applicable to Estimation of Recharge Rates*). This is the basis for representing recharge in the vadose zone model using a constant rate applicable to a given soil type and vegetation cover (DOE/RL-2011-50, *Regulatory Basis and Implementation of a Graded Approach to Evaluation of Groundwater Protection*).

Direct measurement of recharge at the water table is typically impractical due to inaccessibility, especially for many areas of the Hanford Site where the water table is commonly located at depths below ground surface (bgs) of 80 m or more. Other aquifer-influencing operations, such as artificial discharges (from anthropogenic discharges such as those associated with past waste management operations at the Hanford Site) or perturbations to the aquifer system from remedial action pump and treat systems, where present, complicate efforts at making a direct measurement of natural recharge for a deep water table. Instead, measurements and analyses in the unsaturated zone at shallow depths are used to characterize deep drainage. Deep drainage here is defined here as the water flux leaving the depth below which the processes of evapotranspiration can return water from the unsaturated soil to the atmosphere (PNNL-17841). This deep drainage, with sufficient time, will be manifest as the natural recharge flux. The time required for this to happen will depend on the thickness and hydraulic properties of the vadose zone and the deep drainage rate itself. Changes in the deep drainage rate, such as would result from changes in surface vegetative conditions that increase or decrease the evapotranspiration rate, can take many years to be reflected in the recharge rate for a thick vadose zone in arid conditions such as at the Hanford Site and can be an important consideration in characterizing recharge as well (PNNL-17841).

Important physical properties and processes that influence recharge include climate, soil hydraulic properties and stratigraphy, vegetative cover, land use, and topography (PNNL-17841). Climate determines the driving forces for recharge, namely the quantity of precipitation available for the land surface water balance, and the energy fluxes that are determinant in the partitioning of precipitation into evaporation, transpiration, and recharge. Soil hydraulic properties and stratigraphy determine the rate at which water is transmitted through the vadose zone, and hence the effective time for processes of evaporation and transpiration to influence the net downward flux. Vegetative cover determines the strength of the transpiration portion of the land surface water balance. Land use will change the influencing factors including the vegetative cover and surface soils, and hence the hydraulic properties and soil stratigraphy of a site, and hence transpiration rates. Topography is the primary determinant for the portion of precipitation that is subject to overland flow, either “run-on” or “run-off,” for a given site. Knowledge of all the influences is important to the estimation of recharge at a given location.

Natural recharge from precipitation at the Hanford Site is highly variable both spatially and temporally, ranging from near-zero to more than 100 mm/yr depending on climate, vegetation, and soil texture (“Variations in Recharge at the Hanford Site” [Gee et al., 1992] and PNL-10285, *Estimated Recharge Rates at the Hanford Site*). Vegetative areas and fine-textured soil, like silt loams, tend to have lower recharge rates, while areas with little vegetation and coarse-textured soil, such as dune sands, tend to have higher recharge rates. PNL-10285 developed estimates of natural recharge for 1992 conditions using a

systematic procedure. First, distributions of soil and vegetation types were mapped. Then, a recharge rate was assigned to each combination of soil/vegetation type based on data from lysimeters, tracer studies, neutron probe measurements, and computer modeling. The data used for these estimates derive from several sources, such as distribution of recharge estimated using the 1992 climate, a 1966 soil map (*Soil Survey Hanford Project in Benton County, Washington* [Hajek, 1966]), and 1979 vegetation/land use patterns. Estimated recharge rates for 1992 ranged from 2.6 to 127 mm/yr, and the total volume of natural recharge from precipitation over the Hanford Site was estimated to be $2.35 \times 10^4 \text{ m}^3/\text{d}$.

For numerical simulation, two general approaches are available regarding addressing recharge. In the first, the surface energy and fluid balance can be explicitly simulated as part of the larger vadose model numerical implementation. In this approach, meteorological data (precipitation, wind speed, humidity, solar radiation, air temperature), surface soil parameters, and vegetation parameters (root density and depth with time, leaf area index with time, growth cycle dates, etc.) would be used to directly simulate the surface water balance and thereby estimate net deep recharge. Under this approach, the processes simulated for the upper boundary would dominate time step control of the simulation, particularly as this approach would require high-temporal-resolution meteorological data (e.g., hourly) to support a reasonably accurate simulation of the processes in question. A second approach is to segregate the simulation of the surface balance processes to arrive at a net recharge rate used for deeper vadose zone simulations. In this approach the full process-based simulation described for the surface soil is still performed, but only for the near surface. This has been done, and the effective net recharge rates are available in references such as PNNL-14702 Rev .1, *Vadose Zone Hydrogeology Data Package for Hanford Assessments*, for application to deeper vadose zone simulations. The second approach is clearly more efficient and is preferred. It is noted that the recharge rates from the second approach are strongly a function of vegetation cover and surface soil type, and that, due to land surface condition changes in time, these rates will change over time. A typical progression might be from a pre-operational natural vegetation cover (low recharge due to vegetation efficiently returning a high proportion of meteoric water to the atmosphere through transpiration) to an operational cover (such as gravel maintained vegetation free with high recharge) to a transitional period following remediation with declining recharge rates, and finally a return to a mature native plant community with low recharge once again. Thus, the historic and projected land cover condition is the determining factor for selecting recharge rates to apply with time.

There has been considerable study devoted to estimation of recharge rates at the Hanford Site to support flow and transport modeling needs. PNL-10285 produced a defensible map of estimated recharge rates across the Hanford Site for current climate and 1991 vegetation/and use patterns. Various recharge data packages have been prepared to support performance assessments (e.g., PNNL-13033, *Recharge Data Package for the Immobilized Low-Activity Waste 2001 Performance Assessment*, PNNL-14744, *Recharge Data Package for the 2005 Integrated Disposal Facility Performance Assessment*; PNNL-16688, *Recharge Data Package for Hanford Single-Shell Tank Waste Management Areas*) and site-wide assessments (e.g., PNNL-14702 Rev. 1). These studies, in turn, have been supported by a significant field research program (e.g., PNL-6403, *Recharge at the Hanford Site: Status Report*; PNL-6810, *The Field Lysimeter Test Facility (FLTF) at the Hanford Site: Installation and Initial Tests*; PNL-7209, *Field Lysimeter Test Facility: Second Year (FY 1989) Test Results*; Gee et al. [2005], "Measurement and Prediction of Deep Drainage from Bare Sediments at a Semiarid Site"; Gee et al. [2007], "Hanford Site Vadose Zone Studies: An Overview"; PNNL-17841).

The 100 Area specific recharge rates reported in PNNL-14702 Rev. 1 vary with surface soil type, providing an estimate of the range of possible recharge rates for various land uses. The three surface soil types were the Ephrata sandy loam or stony loam, Burbank sandy loam and Rupert sand. Additionally, PNNL-14702 Rev. 1 also provides recharge rates for disturbed soil conditions: the disturbed soil rates

were selected for use in calculation of soil screening levels (SSLs) and preliminary remediation goals (PRGs) for the 100 Area source OUs using vadose zone models.

For the groundwater model of the 100-K area that is the subject of this report, an important improvement in this model is the treatment of the natural recharge for this model as spatially- and temporally variable, using recharge rates that vary by surface soil type and vegetation cover type, and that are fully consistent with the rates used for vadose zone models used to derive SSL and PRG values. Rates of net recharge from precipitation were acquired from DOE/RL-2011-50, which summarized net natural recharge rates compiled in PNNL-14702 Rev. 1. These are the same sources of recharge rates used for vadose zone modeling. An example of temporal variability, already applied in vadose zone models, is the natural vegetation recharge scenario illustrated in Figure 2-8 using values tabulated in Table 2-2. Note the higher recharge rates during the operation period, when a waste site was cleared and maintained in gravel-covered, vegetation-free state. In contrast, revegetation following remedial activities vastly reduces the recharge rates expected in the future as the surface condition changes within the expectations of this scenario. The purpose of such a recharge scenario is to define the upper boundary condition for a vadose zone model of a waste site in terms of a recharge rate that changes in time as a function of the surface soil and vegetation present during the history and expected future condition of that site.

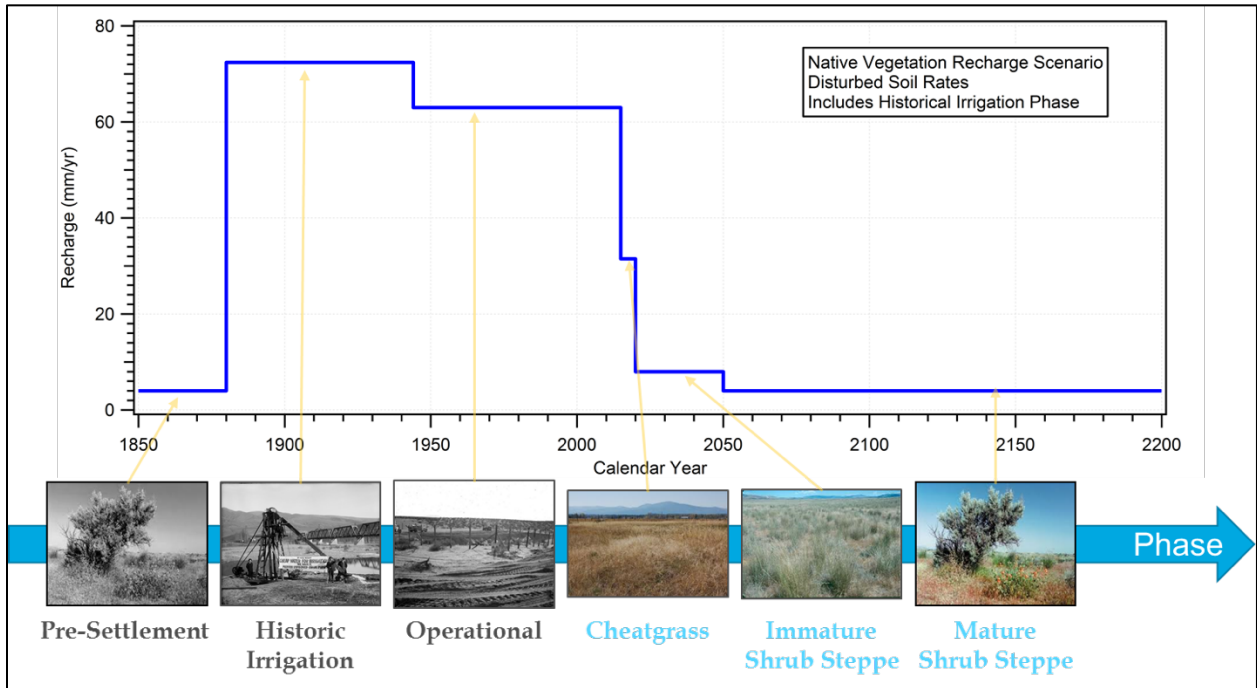


Figure 2-8. Natural Vegetation Recharge Scenario Applied for Preliminary Remediation Goal Calculation in 100-Area Waste Sites Subject to Historic Irrigation

Table 2-2. Native Vegetation Recharge Scenario Phases and Recharge Rates (mm/yr)

Surface Soil Type	Historic Simulation (pre-2010) (calculation of initial hydraulic conditions)			Predictive Simulation (post-2010) (calculation of peak groundwater concentration)			
	Pre-Settlement (< 1880)	Historic Irrigation ^(a) (1880-1944)	Hanford Operations (1944-2010)	Bare Soil (2010-2015)	Cheatgrass (2015-2020)	Developing Shrub Steppe (2020-2050)	Mature Shrub Steppe (2050 >)
Hanford sand, disturbed	4.0 ^(b)	72.4 ^(c)	63.0 ^(d)	63.0 ^(d)	31.5 ^(e)	8.0 ^(f)	4.0 ^(g)

- a. Irrigated agriculture was prevalent in some 100-Area sites prior to Hanford Site construction; irrigation therefore was conservatively assumed applicable throughout any operational units with historic irrigation, applied from calendar years 1880 through 1944.
- b. Source: PNNL-14702 Rev. 1, Table 4-15, all areas with soils disturbed by excavations; shrub steppe.
- c. Recharge rates for historic irrigation phase is that from the long-term irrigation rate (Irrigation II) under the irrigation recharge scenario.
- d. Source: PNNL-14702 Rev. 1, Table 4-15, all areas with soils disturbed by excavations; no vegetation.
- e. Source: PNNL-14702 Rev. 1, Table 4-15, all areas with soils disturbed by excavations; cheatgrass.
- f. Source: PNNL-14702 Rev. 1, Table 4-15, all areas with soils disturbed by excavations; young shrub steppe.
- g. Source: PNNL-14702 Rev. 1, Table 4-15, all areas with soils disturbed by excavations; shrub steppe.

Applying the recharge scenario concept to a groundwater model, it is acknowledged that spatial variability needs to be included in the representation of this process. Figure 2-9 shows aerial imagery that illustrates the variability in surface conditions present in calendar year 2011; some portions of the model domain are highly disturbed and vegetation free, associated with higher recharge rates, while other portions show undisturbed natural vegetation cover that will have commensurately lower recharge rates.



Source: NAIP 4 Band Imagery (7/15/2011); image courtesy of University of Washington.

Figure 2-9. Aerial Imagery of 100-K Model Domain Showing Spatial Variability of Surface Conditions that are Reflected in Natural Recharge Rates that Depend on Surface Soil Type and Vegetation Density

The extent of the groundwater model incorporates a variety of surface soil types and vegetation types that evolve over different portions of the model domain in different ways. This makes the management of this boundary condition, varying in both time and space, a process that can best be addressed using a geographic information system (GIS) approach. The GIS representation of natural recharge with spatial and temporal variability is conceptualized as shown in Figure 2-10. In this concept, waste sites follow the

same temporally variable recharge scenario developed for vadose zone models used to calculate PRGs and reflect disturbed soil conditions. Other land areas outside of the waste sites follow different evolutions; some may remain in pre-Hanford mature shrub steppe with native surface soil types throughout the historic and projected future periods. Other areas may currently be covered in the invasive cheatgrass species and will remain this way.

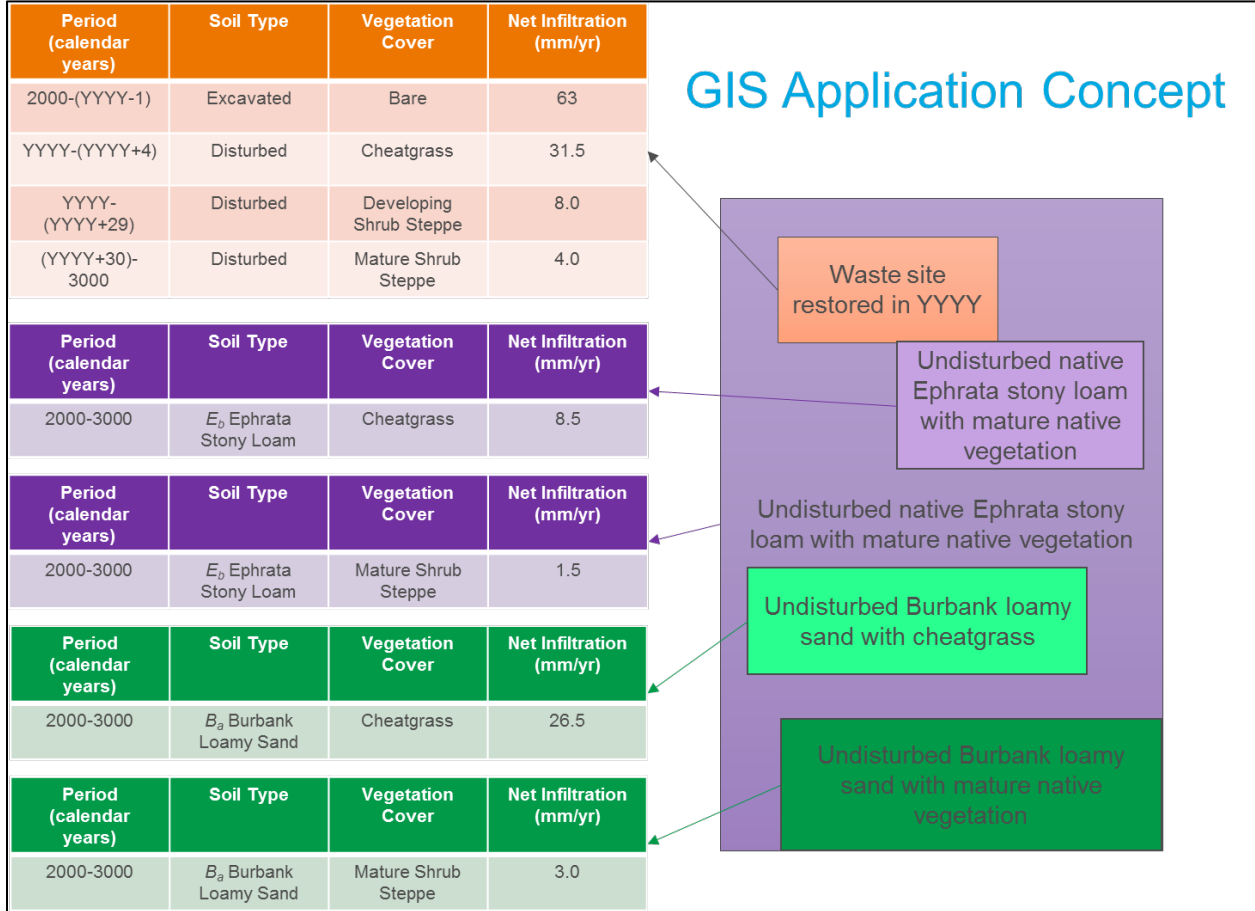


Figure 2-10. Conceptualization of Spatially and Temporally Variable Natural Recharge Rate Boundary Condition

Using aerial imagery, National Land Cover Database (NLCD 2011), Biological Resources Management Plan Vegetation Class (DOE/RL-96-32 Rev. 2, *Hanford Site Biological Resources Management Plan*), and other spatial data sources, a GIS approach is implemented to provide spatially variable recharge rate maps that are a function of surface soil type and vegetation cover present throughout the 100-K groundwater model domain at selected time periods. Use of multiple time-period maps to represent the natural recharge process in this groundwater model provides temporal variability, reflecting changing conditions during the simulation time.

The described approach to specify spatially and temporally variable representation of the natural recharge process as a boundary condition of the groundwater model provides the following advantages:

- Full consistency of natural recharge rates for waste sites as simulated in vadose zone models for PRG development to the recharge rates applied to the spatial extent of those waste sites within the larger groundwater model

- Increased model fidelity by prescribing higher recharge rates in waste site areas of the groundwater (maintained vegetation free with disturbed soil) and lower recharge rates in other areas, ensures that the higher driving force of increased recharge focused over contaminant plume source areas is represented in the model (in contrast to approaches that apply a spatially-averaged natural recharge rate across the model domain)
- Increased model fidelity by prescribing recharge rates that vary in time, ensuring that the impact of reducing recharge through revegetation activities is factored into groundwater model (in contrast to applying a temporally-constant recharge rate that assumes present conditions persist in the future)

2.2.3 FEP: Columbia River Interaction

Groundwater and surface water interactions are critical to understanding the rate and magnitude of contaminants potentially entering the Columbia River. The flow of the Columbia River at 100-K is to the northeast and is controlled mainly by Priest Rapids Dam. The flow rate at Priest Rapids from 1992 through 2011 averaged approximately 3,240 m³/sec (114,500 ft³/sec). Flow volumes are highest from April through early July because of run-off from regional and high elevation snowmelt. Flows are lowest from September through October. The width of the Columbia River through the Hanford Reach at 100-K can vary from approximately 300 to 1,000 m (1,000 to 3,300 ft), depending on the flow rate.

The elevation of the river also changes with the flow rate, resulting in wetting and drying of the shoreline area (PNNL-6415 Rev. 18, *Hanford Site National Environmental Policy Act (NEPA) Characterization*).

High river stage can be greater than 123 m (404 ft) AMSL and generally occurs in May or June. Low river stage, approximately 118.5 m (389 ft), typically occurs in September or October. Diurnal fluctuations in 100-K river stage range up to 1.5 m (5 ft). Seasonal fluctuations average 4.0 m (13 ft) over a year, and have ranged up to 5.6 m (18 ft). Figure 2-11 shows that the annual river changes are a repeatable cycle with a similar pattern from year to year.

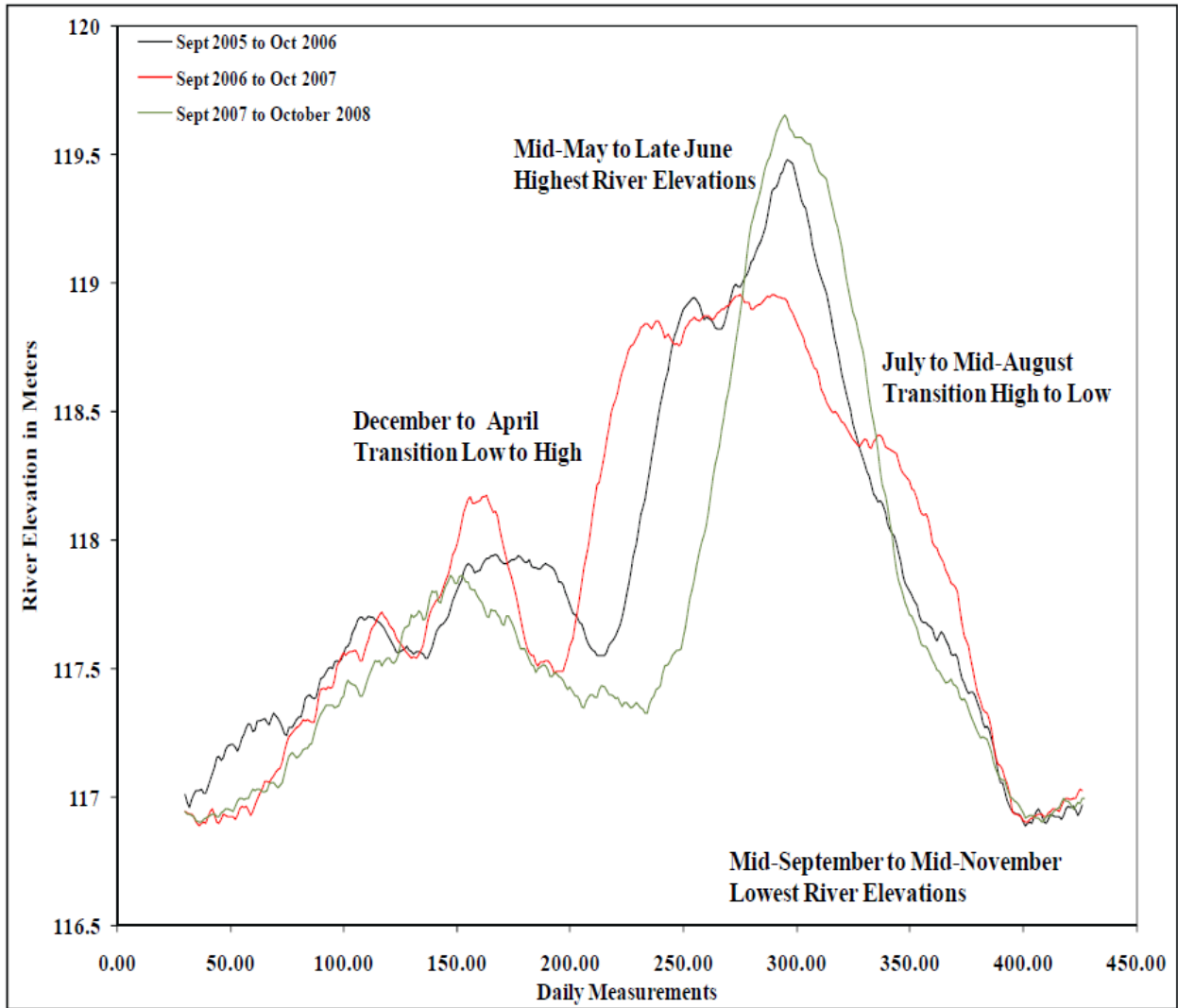


Figure 2-11. Annual Trends in River Stage at One Location Illustrating Repeatable Annual Cycles (from DOE/RL-2010-97, DRAFT A)

Contaminant flow paths from 100-K to the Columbia River are related to the locations of geologic units both on shore and beneath the Columbia River. **The evaluation of the near-river well geology indicates that the top of the aquitard (RUM) is beneath the bottom of the Columbia River - the RUM does not intersect the bottom of the Columbia River at 100-K.** Therefore, the river partially penetrates the unconfined aquifer system.

Groundwater discharges to the Columbia River via seeps and upwelling to the riverbed. This groundwater flow provides a pathway for contaminant transport to the Columbia River. Rapid, periodic, or cyclic elevation fluctuations of the river stage occur in controlled response to flood conditions, hydroelectric production, and salmon spawning programs at a series of dams and reservoirs upriver of the site. These rapid elevation changes in the river cause periodic influences on flow conditions within the aquifer. Daily fluctuations up to 1.5 m (5 ft) are common. Even greater changes (up to 5.6 m [18 ft]) are observed seasonally, with a period of high river stage in the spring or early summer and low river stage in the fall. Periods of high or low river flow affect the unconfined aquifer flow the most.

The nature and extent of groundwater contaminants entering the Columbia River is of great interest, especially about how it may affect water quality and aquatic plants and animals. Groundwater seeps (small water streams flowing across shoreline areas during low river stage periods) have been identified and studied in the 100 Areas (*Sampling and Analysis of 100 Area Springs* [DOE/RL-92-12]) and 300 Area. Pore water or groundwater upwelling (groundwater entering into the space between rocks and sediment of the riverbed) have also been studied in the 100 and 300 Areas. These upwelling areas have been identified using specific conductivity and/or water temperature data (riverbed locations with higher conductivities and/or warmer temperatures than the Columbia River water column are indicative of groundwater entering the bottom of the river), then subsequently characterized to determine contaminant concentrations in surface water, sediment, and pore water at those locations. Specific conductance of groundwater in 100-K ranges from 300 to 550 $\mu\text{S}/\text{cm}$, while that of river water averages 150 $\mu\text{S}/\text{cm}$. Figure 2-12 shows electrical conductivity and temperature of pore water samples collected from the riverbed near 100-K (WCH-380, *Field Summary Report for Remedial Investigation of Hanford Site Releases to the Columbia, Hanford Site, Washington: Collection of Surface Water, Pore Water, and Sediment Samples for Characterization of Groundwater Upwelling*).

The nearshore groundwater conditions are directly affected by river stage. A wide range of mixing ratios has been observed between upwelling water at the bottom of the river and groundwater at nearshore locations (*Technical Evaluation of the Interaction of Groundwater with the Columbia River at the Department of Energy Hanford Site, 100-D Area* [SGW-39305]). This mixing ratio represents a continuum from pure groundwater to pure river water, depending on where in the groundwater pathway the measurement is taken. Water from the zone of interaction is a mixture of groundwater and river water.

Geologic control on the connection between river and aquifer can occur from the presence of altered river bed properties. For instance, PNNL-17708 (*Three-Dimensional Groundwater Models of the 300 Area at the Hanford Site, Washington State*) identified a preferential aquifer-river connection from Hanford/Ringold contacts in the 300 Area.

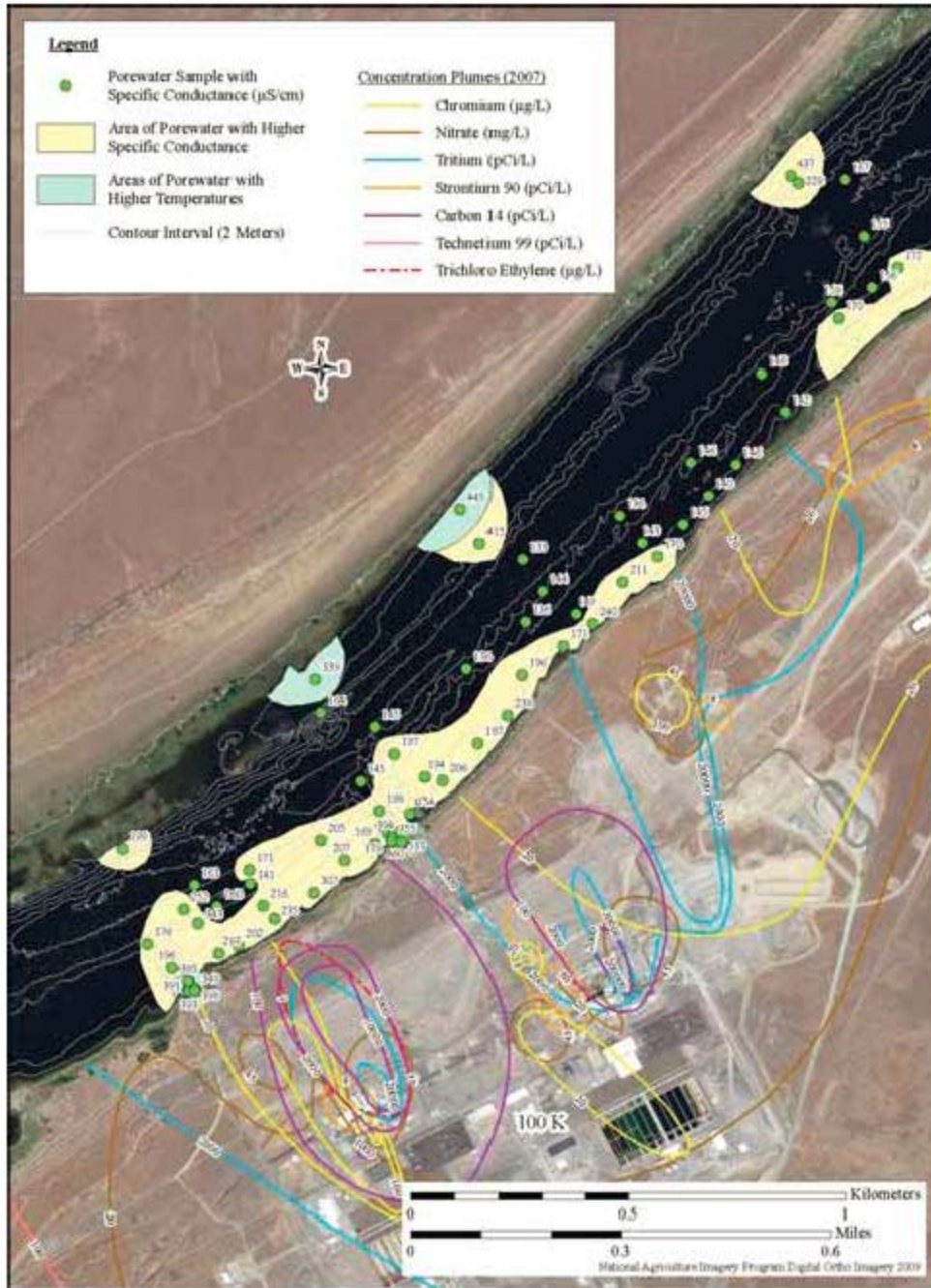


Figure 2-12. Pore Water Samples from the Columbia River Bed

Source: *Field Summary Report for Remedial Investigation of Hanford Site Releases to the Columbia River, Hanford Site, Washington: Collection of Surface Water, Pore Water, and Sediment Samples for Characterization of Groundwater Upwelling (WCH-380).*

2.2.4 FEP: Groundwater Flow

Groundwater in 100-KR-4 flows generally to the northwest towards the Columbia River as illustrated in Figure 2-13. Groundwater discharges to the river through riverbank seeps (springs); most discharge occurs as upwelling through the riverbed. Operating the pump and treat system has changed groundwater

flow direction and velocity; groundwater mounding near injection wells and drawdown near extraction wells creates radial diverging and converging flow patterns, respectively, that would not be present in natural conditions. Groundwater further inland generally flows to the north and northeast towards the 100-N as suggested by data from 1989 (Figure 2-14).

In addition to water movement in and out of the riverbank (i.e., one-dimensional flow perpendicular to the shoreline), there is a component of flow in the downstream direction (Newcomb and Brown, 1961). Because the river flows downstream in response to an elevation gradient, groundwater and bank storage also tend to travel downstream, although at a considerably slower rate than the river flow. Finally, vertical components of flow are induced by the river that does not fully penetrate the aquifer.

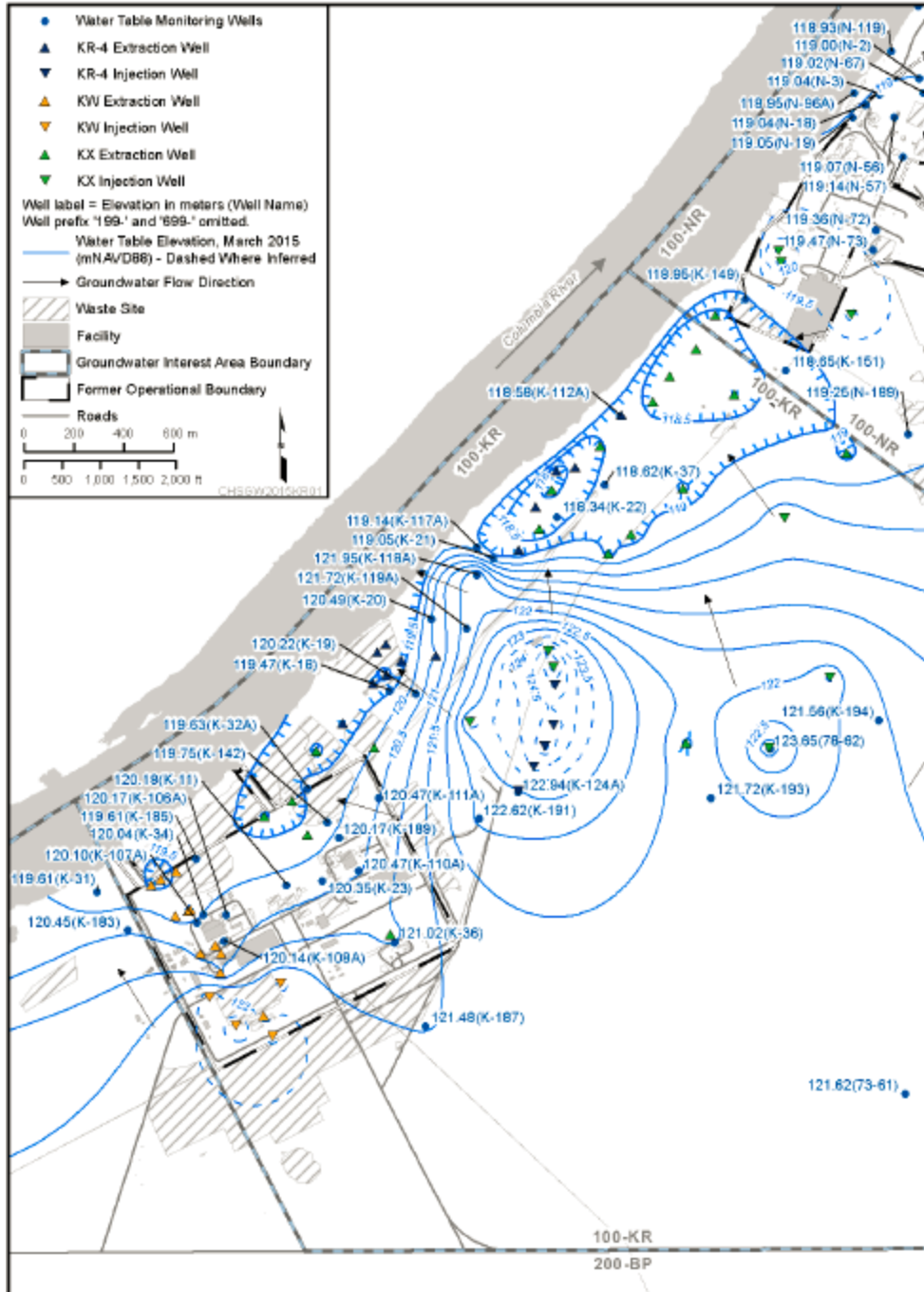


Figure 2-13. 100-K Water Table March 2015 (from DOE/RL-2016-09, Rev. 0)

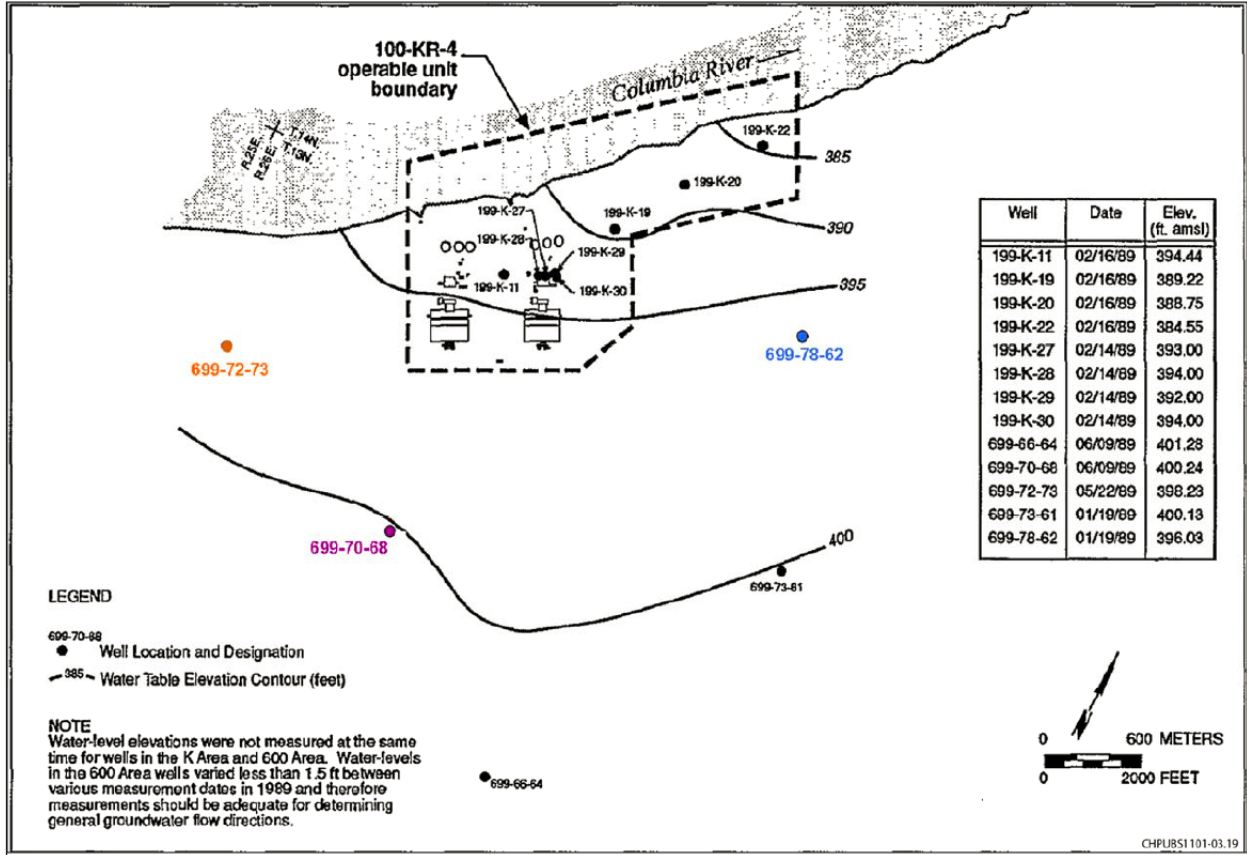


Figure 2-14. 1989 Water Table Elevations in the 100-KR-4 OU (from DOE/RL-90-21)

The effect of the seasonal changes in river stage on groundwater levels is illustrated in Figure 2-15. The well closest to the river, 199-K-114A, has little or no temporal delay to river changes, and the magnitude is nearly identical to the river. The well farthest from the river, 199-K-108A, shows the smoothest hydrograph because all the short-term river changes are attenuated in the aquifer. There is a delay in the response, and there is less response magnitude at this distance from the river.

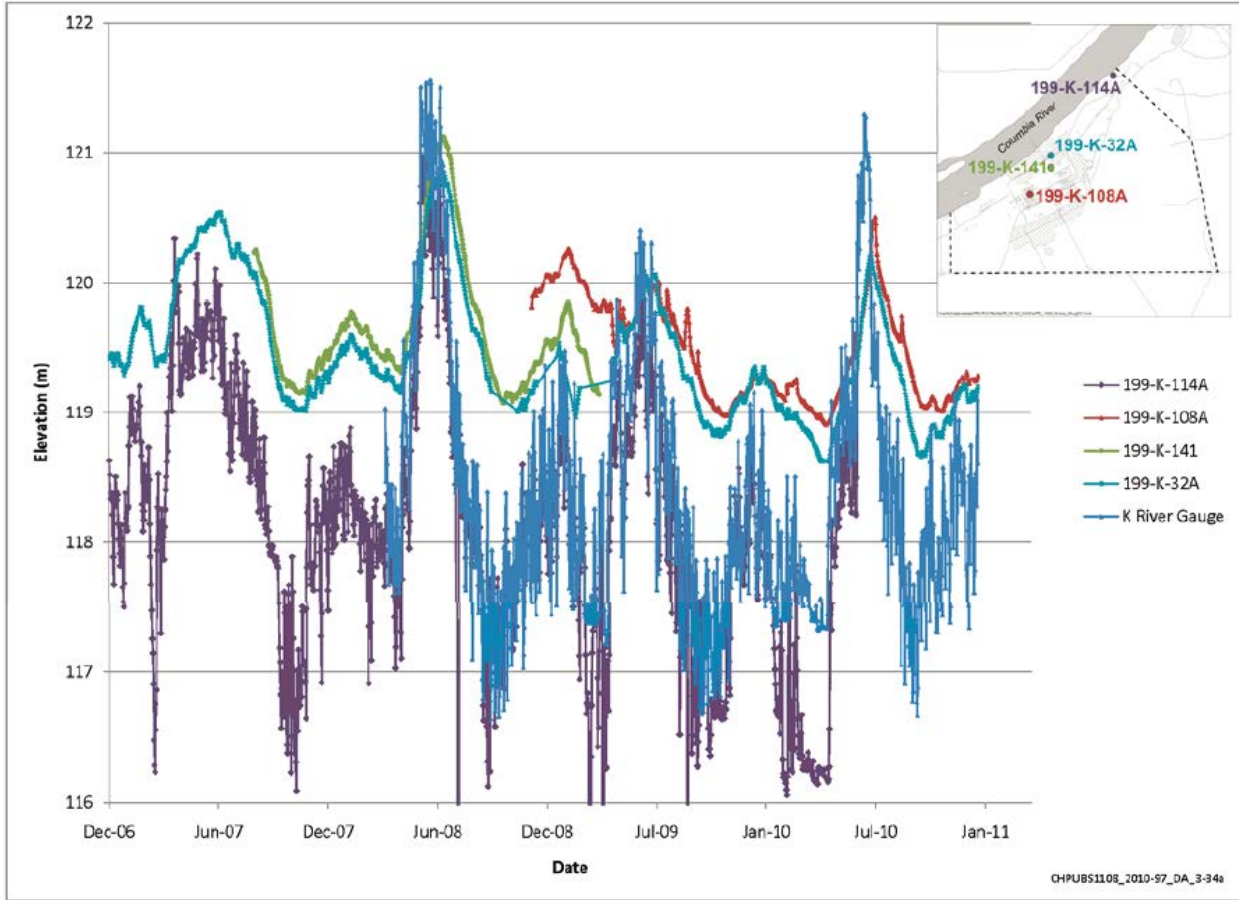


Figure 2-15. Columbia River Stage and Selected Well Water Level Elevations

The water table on the north side of the Columbia River in Grant County is much higher than in 100-K (150 to 300 m [490 to 980 ft] AMSL; *Hanford Site Groundwater Monitoring for Fiscal Year 2006* [PNNL-16346]; Figure 2-16). **Groundwater from Grant County north of the river and 100-K south of the river discharges to the Columbia River.**

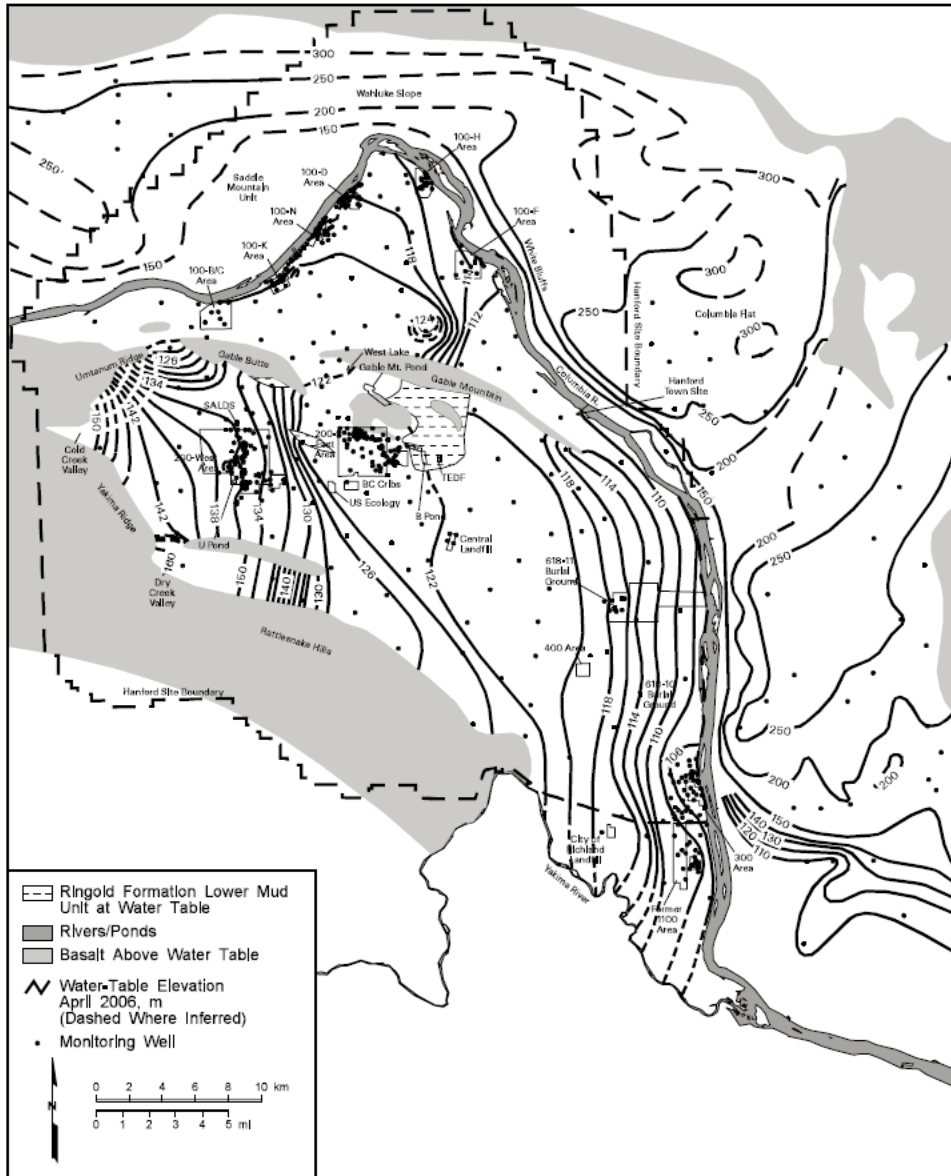


Figure 2-16. Hanford Site and Outlying Areas Water Table Map, April/May 2006 (from PNNL-16346)

2.2.5 FEP: Pump and Treat System

Three pump and treat (P&T) systems have been operational at various periods over the history of the 100-KR-4 OU. The operational time-frames and the number of extraction and injection wells for each of the P&T systems are shown in Table 2-3.

Table 2-3. 100-KR-4 OU Pump and Treat System Specifications

Treatment System	Number of Extraction Wells	Number of Injection Wells	System Start Date	System End Date
KR4	17	6	9/1/1997	(ongoing)
KW	10	6	1/29/2007	(paused on 5/17/2016 for rebound study and restarted on 4/12/2017)
KX	18	10	2/3/2009	(ongoing)

Flow conditions in the 100-KR-4 OU are largely controlled by the P&T system. Over time, water level elevations at each extraction well have generally been held constant (constant pressure constraints) while pumping rates have varied. As the interim system has been developed additional wells have been added or removed. In general, the extraction wells are located downgradient of the plumes near the river. Along the former location of the 116-K-2 disposal trench, only extraction was occurring in December 2014. The efficacy of the system is illustrated by the reduction in estimated plume areas as shown in Figure 2-17.

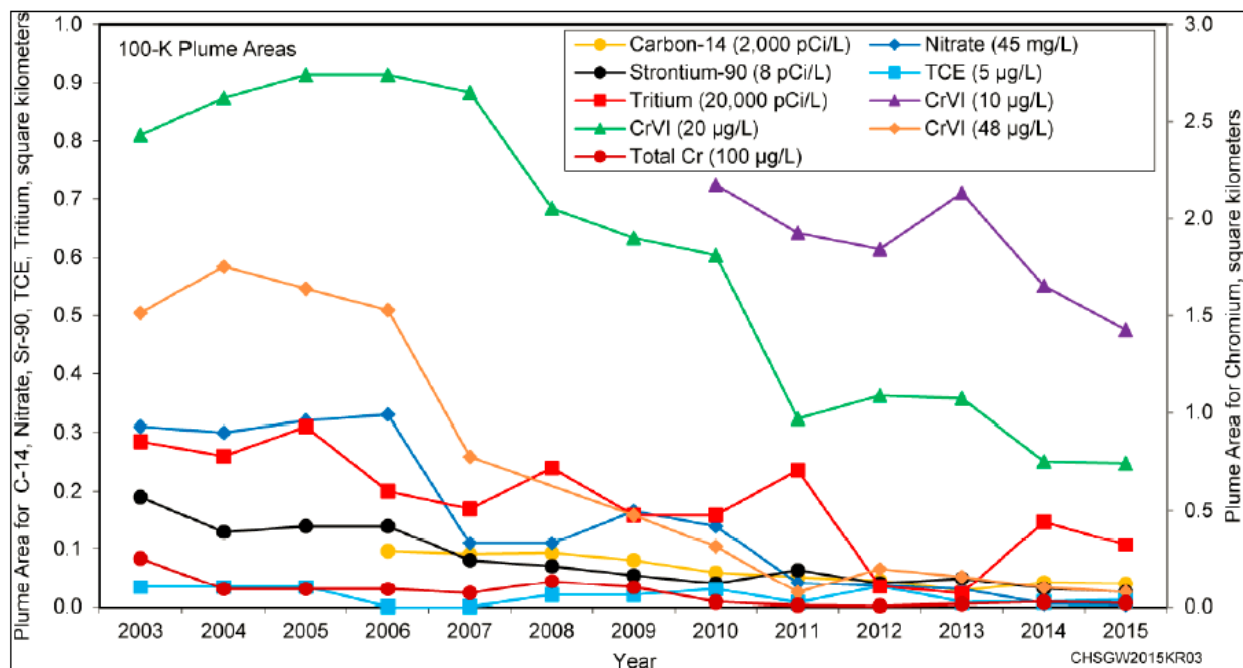


Figure 2-17. Changes in Selected 100-KR-4 OU Plume Areas since 2003 (from DOE/RL-2016-09)

2.2.6 FEP: Potential Hexavalent Chromium Sources

Relatively stable concentrations at some wells, especially in the shallow unconfined aquifer, are suggestive of continuing sources. In addition, P&T system shutdown at KW area to study Cr(VI) concentration rebound clearly indicated the presence of continuing source at or near the reactors, headhouses, and gas condensate cribs. For example, concentrations at wells 199-K-173 and 199-K-205 show an increasing trend (Figure 2-18) after shutting down the P&T system at KW area. There are a few more locations (e.g., wells 199-K132, 199-K-137, 199-K-166, and 199-K-184) in KW area where Cr(VI)

is observed to persist. Similarly, Cr(VI) concentrations at well 199-K-220 persist for last two years although nearby well 199-K-188 shows declining trend.

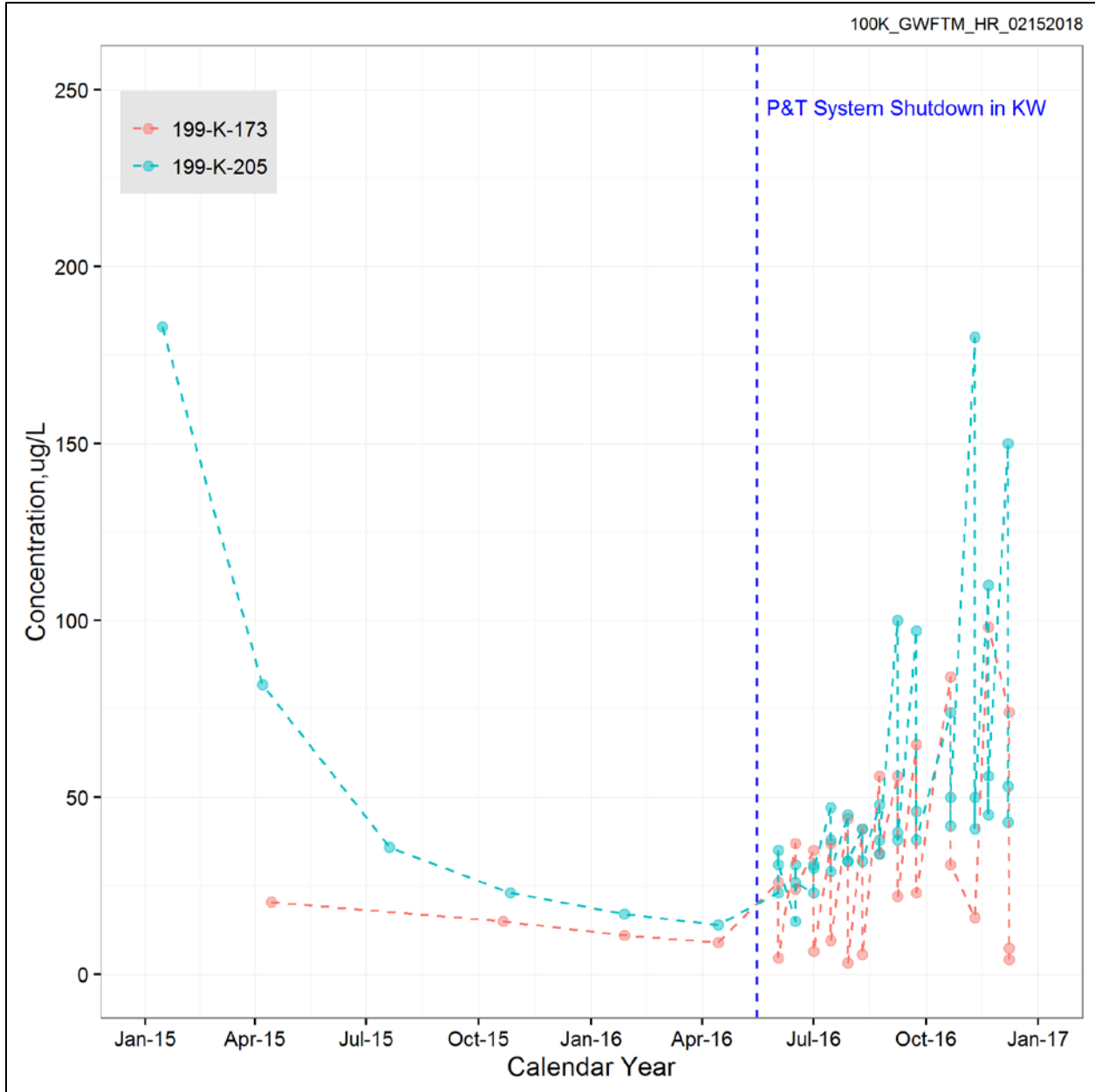


Figure 2-18. Observed Hexavalent Chromium Concentrations at Wells 199-K-173 and 199-K-205

2.2.7 FEP: Potential Strontium-90 Sources

Strontium-90 concentrations in some wells are steady or declining slower than the rate expected solely due to radioactive decay. This suggests potential residual sources. Recently, two boreholes (199-K-221 and 199-K-222) were installed at UPR-100-K-1 and 116-KE-3 crib for evaluating strontium-90 leaching characteristics as well as monitoring the strontium-90 concentrations in the shallow aquifer. In 2017, two very high concentrations, 13,900 pCi/L in August and 15,600 pCi/L in October, were reported at well 199-K-222. Additional wells near 116-KW-2 crib (e.g., well 199-K-107A, 199-K-34), fuel storage basin

in KE area (e.g., well 199-K-141), and 199-K-2 trench (e.g., well 199-K-200) have shown persistent strontium-90 concentrations.

2.2.8 FEP: Potential Tritium, Nitrate, and Carbon-14 Sources

Tritium, nitrate and carbon-14 concentrations at some wells near gas condensate cribs in KW and KE area show steady or increasing trends. In addition, 118-K-1 burial ground is assumed to be a potential continuing source for tritium as some very high tritium concentrations were reported at wells 199-K-207 (935,000 pCi/L in August 2015) and 199-K-111A (379,000 pCi/L in August 2016).

2.3 Nature and Extent of Contamination

Groundwater at 100-K was contaminated by waste releases associated with past operations of the KE and KW reactors and associated support facilities. Contaminants of interest in the unconfined aquifer include hexavalent chromium and total chromium, tritium, nitrate, strontium-90, carbon-14, and trichloroethene. Figure 2-17 illustrates changes in the contaminant plume area since 2003 for strontium-90, nitrate, hexavalent chromium, and tritium, demonstrating that the P&T systems in the 100-KR-4 OU are consistently reducing the size of the contaminant plumes.

Hexavalent chromium is mobile in groundwater at 100-KR-4. Plumes are associated with three general areas: (1) at or near the 183.1KW Headhouse chemical storage tank farm, (2) at or near the 183.1KE Headhouse chemical storage tank farm, and (3) at the 116-K-1 crib and 116-K-2 trench.

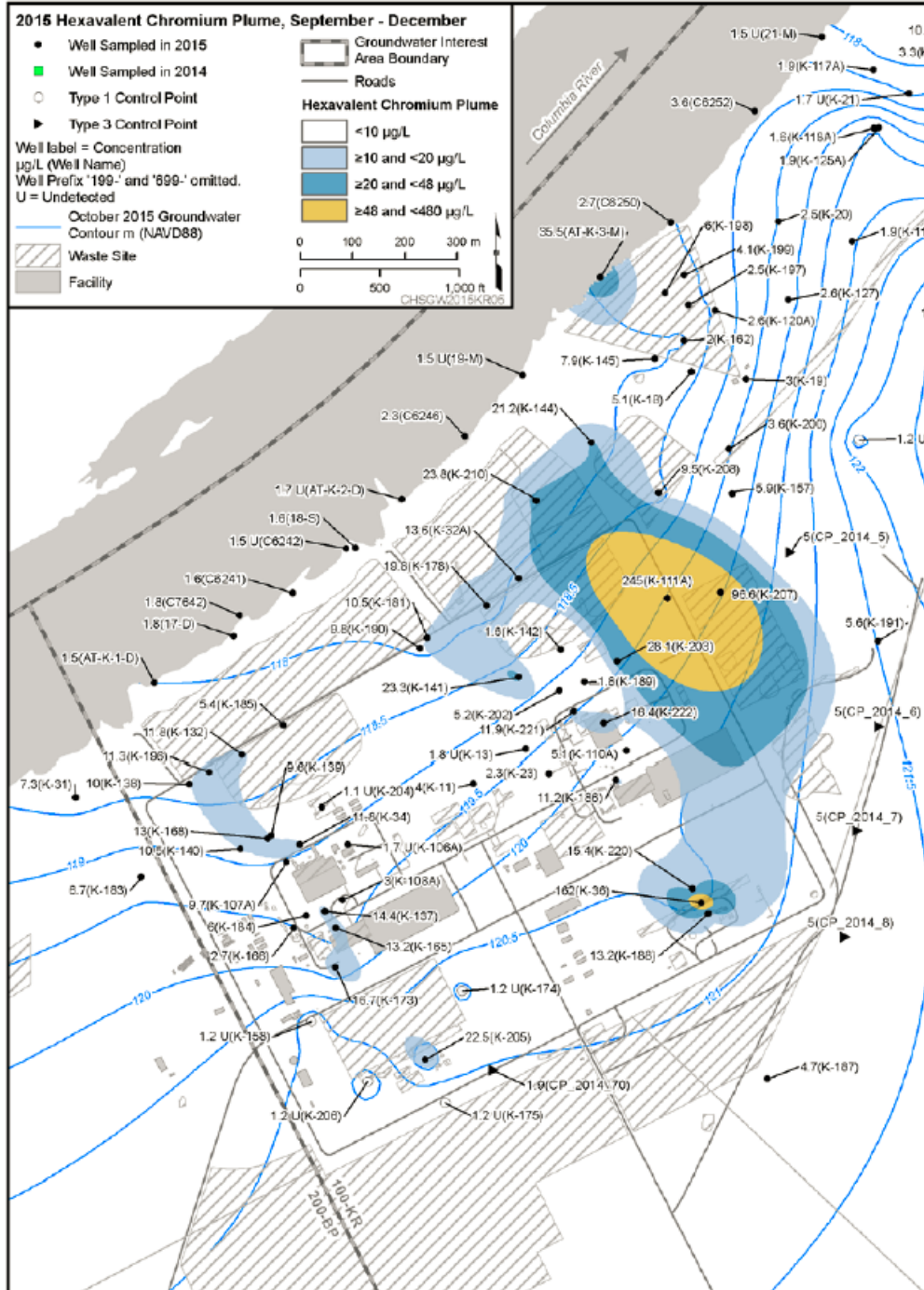


Figure 2-19. 100-KR Cr(VI) Plume in the Unconfined Aquifer (2015 Low River Stage), KE and KW Reactor Vicinity (from DOE/RL-2016-09)

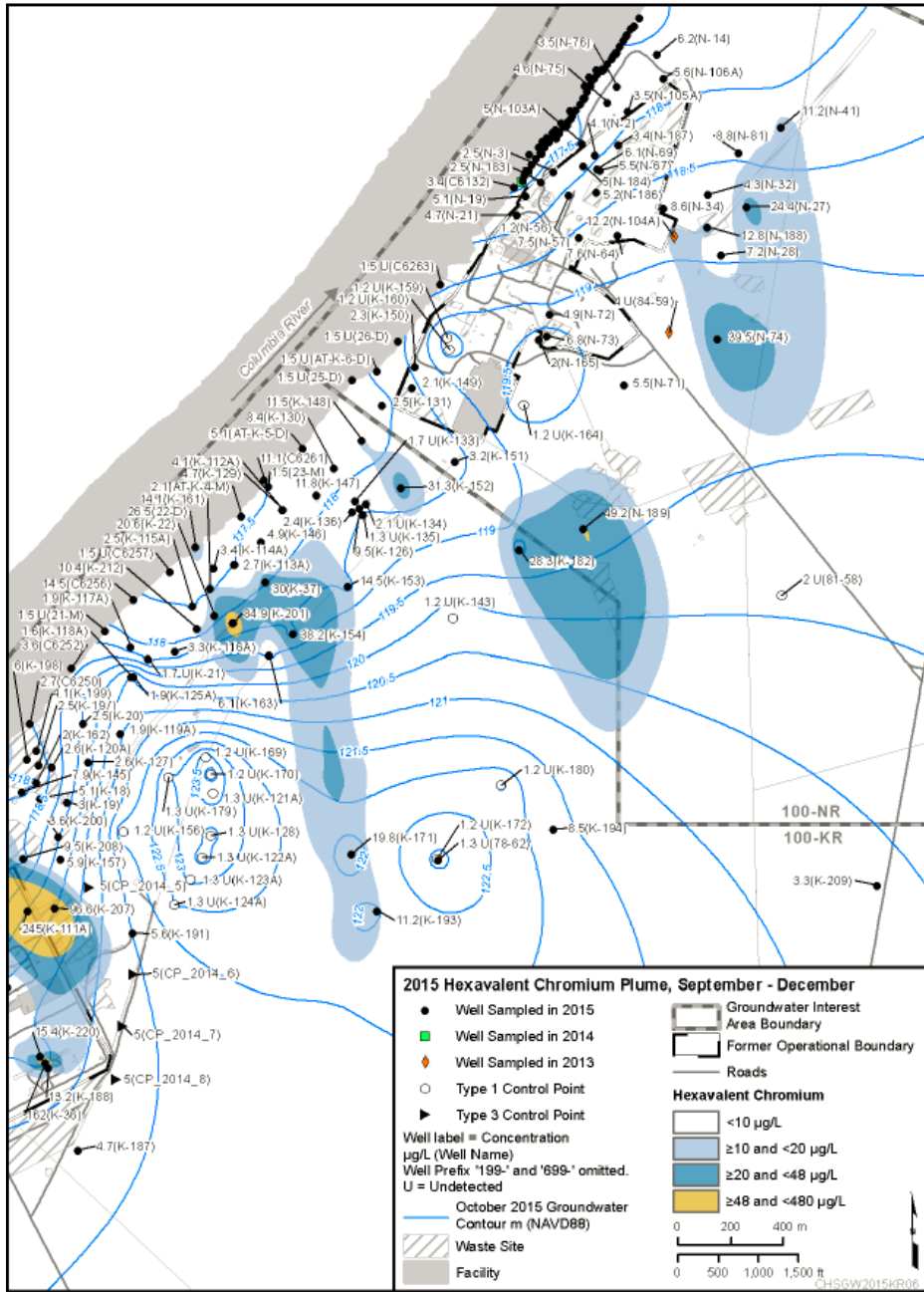
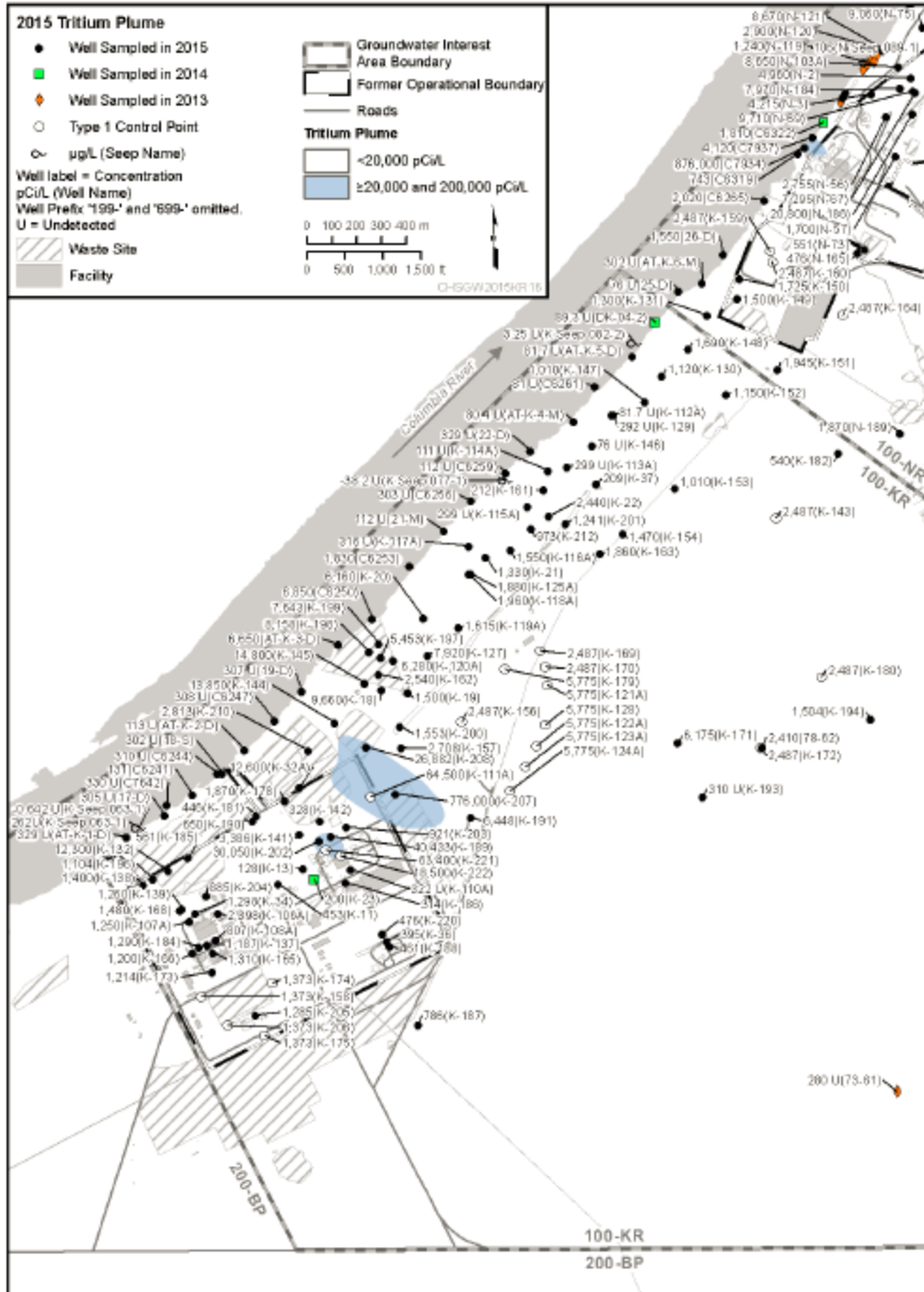


Figure 2-20. 100-KR Cr(VI) Plume in the Unconfined Aquifer (2015 Low River Stage), 116-K-2 Trench and 100-N Vicinity (from DOE/RL-2016-09)

Tritium is mobile in 100-KR groundwater, and is present as a diffuse plume (Figure 2-21).



Nitrate is attributed primarily to oxidation of high concentration ammonia in reactor gas dryer condensate that was discharged to the 116-KW-1 and 116-KE-1 gas condensate cribs and is above the cleanup level of 45 mg/L in a few locations. Additional nitrate may have come from sanitary waste drain fields. However, nitrate plume has depleted significantly in recent years (Figure 2-22).

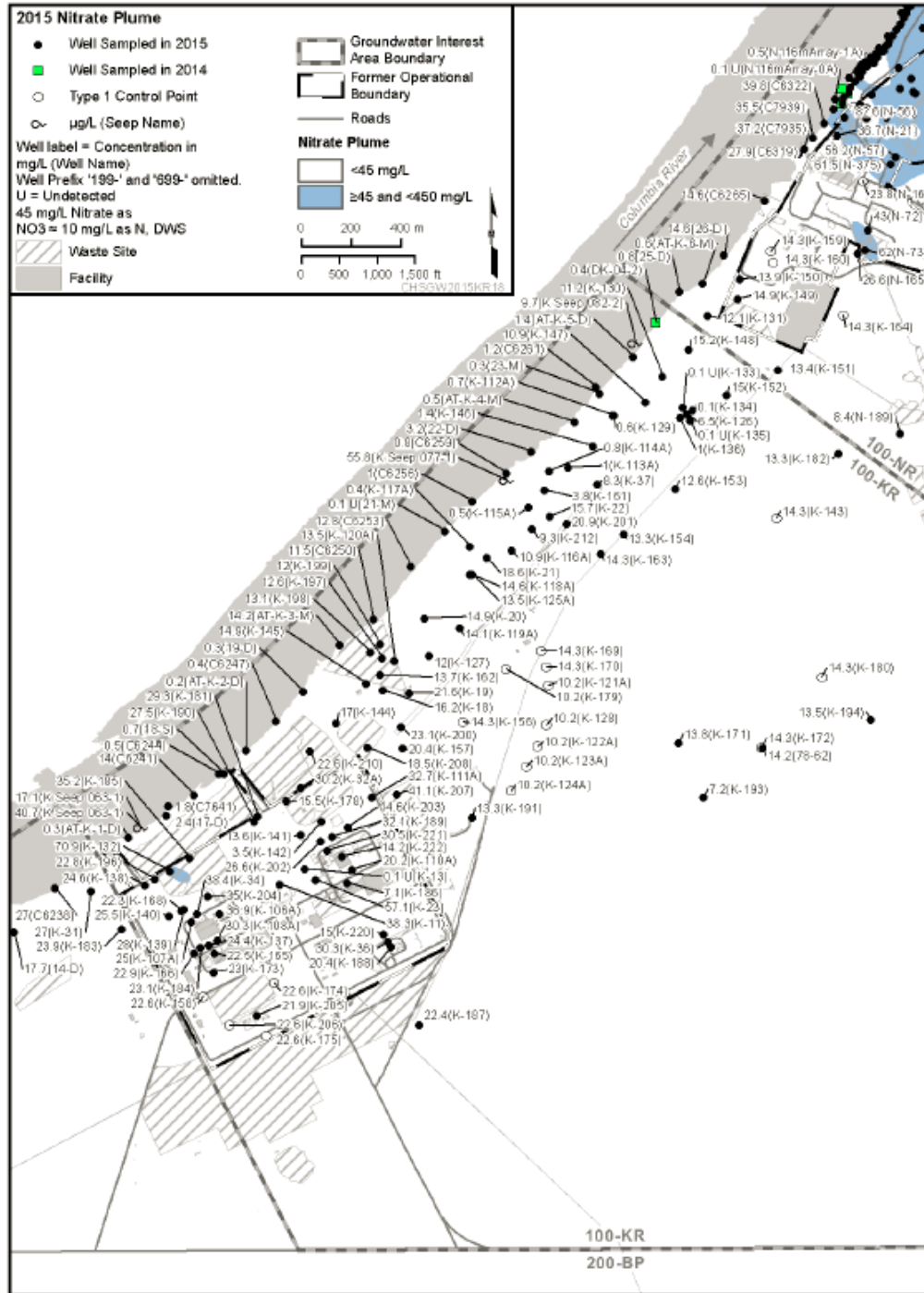


Figure 2-22. 100-KR Nitrate Plume in the Unconfined Aquifer (from DOE/RL-2016-09)

Strontium-90, a fission product, was released during fuel failure events and resulted in contamination of reactor cooling water. This water could be released to the 116-K-2 trench and the fuel storage basins. Figure 2-23 shows mapped strontium-90 plume reported in DOE/RL-2016-09.

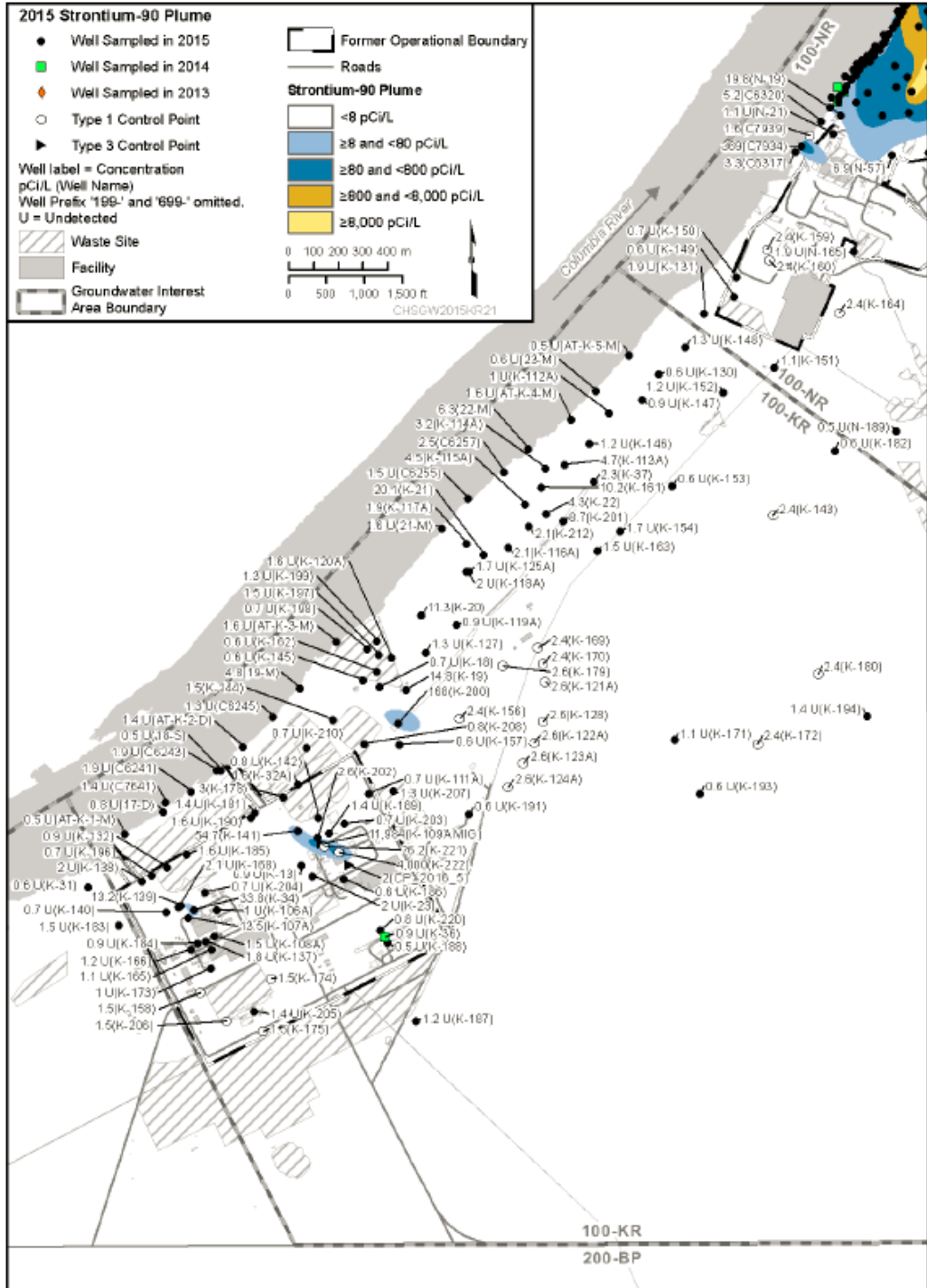


Figure 2-23. 100-KR Strontium-90 Plume in the Unconfined Aquifer (from DOE/RL-2016-09)

Most of the carbon-14 (Figure 2-24) in 100-KR groundwater originated from historical discharges of reactor gas dryer regeneration condensate to the 116-KE-1 and 116-KW-1 cribs. The presence of TCE in the groundwater is likely related to the use of solvents during equipment maintenance activities. TCE continues to be detected in some 100-KR wells, primarily in the K west region (Figure 2-25).

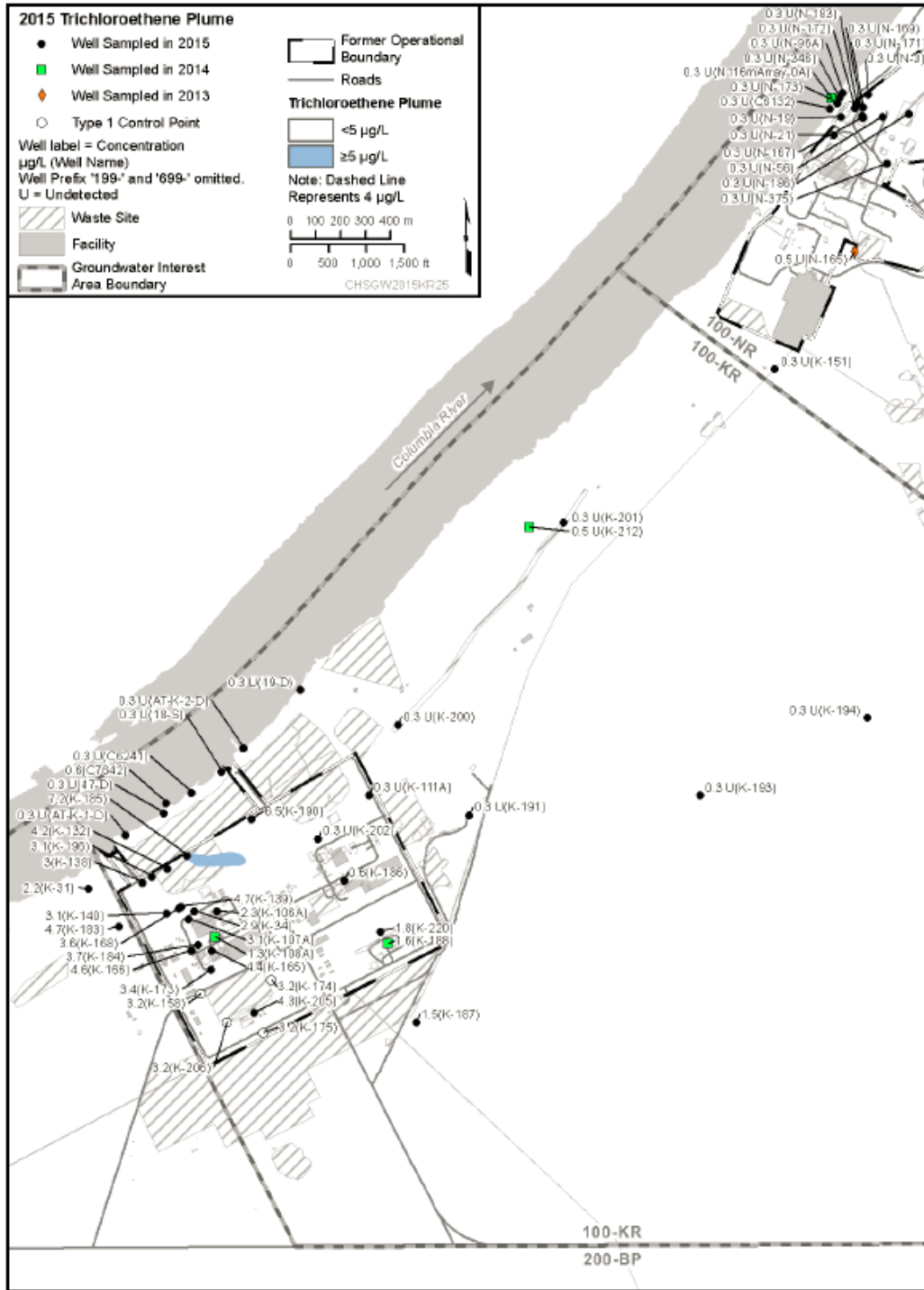


Figure 2-25. 100-KR Trichloroethene Plume in the Unconfined Aquifer (from DOE/RL-2016-09)

2.4 Conceptual Model Summary

Key elements (FEPs and their components) include the following:

1. Contaminant migration in units below the RUM is very unlikely because the low hydraulic conductivity of the RUM makes it an effective aquitard where it underlies the Ringold unit E throughout 100-K.
2. The Ringold E is the major component of the unconfined aquifer under the 100-KR-4 OU.
3. The Hanford formation has systematically higher hydraulic conductivity than the Ringold, but is largely unsaturated in the area of the plumes.
4. The flow of the Columbia River at 100-K is to the northeast and is controlled mainly by Priest Rapids Dam.
5. Groundwater discharges to the Columbia River via seeps and upwelling to the riverbed.
6. The evaluation of the near-river well geology indicates that the top of the aquitard (RUM) is projected to come near to the deepest part of the river channel towards the northern shore. This limits the unconfined geometry for discharge under the river. However, this interpretation is uncertain, and data from the river bed clearly shows groundwater discharge indicating that an appreciable amount of unconfined aquifer exists.
7. Groundwater from Grant County north of the river and 100-K south of the river discharges to the Columbia River implying that a groundwater divide exists under the Columbia River.
8. As revegetation continues recharge rates will continue to decline, reducing the driving force for moving potential residual contaminants through the vadose zone.
9. Chromium contamination is highest near the top of the unconfined aquifer and decline with depth.
10. Strontium-90 contamination is limited to the upper portion of the unconfined aquifer.
11. Tritium concentrations are highest near the top or middle of the unconfined aquifer and lower at the bottom.

3 Model Implementation

3.1 Software

MODFLOW 2000 (USGS Open File Report 00-92, *MODFLOW-2000, the U.S. Geological Survey Modular Ground-water Model - User Guide to Modularization Concepts and the Ground-Water Flow*) and MT3DMS (SERDP-99-1, *MT3DMS: A Modular Three-Dimensional Multispecies Transport Model for Simulation of Advection, Dispersion, and Chemical Reactions of Contaminants in Groundwater Systems; Documentation and User's Guide*) were selected for implementation of the 100-K Model because they fulfill the following specifications:

- Among the more versatile and widely used software packages for models of this type.
- Are freely available and distributed with the source code.
- It is fully documented and has been verified in applications similar to those at the Hanford Site.
- There is wide expertise in use of these software packages.
- Together, these software packages are capable of directly simulating the principal FEPs that are relevant to the 100-K simulation requirements.
- For those FEPs that they do not directly simulate, the needs can be met through links to other codes, such as linking to STOMP for vadose calculations as described in the FEP section on recharge.

Use of MODFLOW is in keeping with DOE direction for simulation of groundwater at the Hanford Site (“Hanford Groundwater Modeling Integration” [Klein, 2006]). DOE has not specified a groundwater transport simulator for use with MODFLOW; however, MT3DMS is the most commonly applied transport simulator used with MODFLOW. All software for implementation of this model was used in accordance with a CHPRC procedure implementing the requirements of DOE O 414.1D, *Quality Assurance*.

The software used to implement this model and perform calculations and was approved under the requirements of, and use was compliant with CHPRC’s procedure implementing the requirements of DOE O 414.1D, *Quality Assurance*. This software is managed under the following software quality assurance documents consistent with that implementing procedure:

- CHPRC-00257, *MODFLOW and Related Codes Functional Requirements Document*
- CHPRC-00258, *MODFLOW and Related Codes Software Management Plan*
- CHPRC-00259, *MODFLOW and Related Codes Software Test Plan*
- CHPRC-00260, *MODFLOW and Related Codes Acceptance Test Report*
- CHPRC-00261, *MODFLOW and Related Codes Requirements Traceability Matrix*

CHPRC-00259 distinguishes between safety software and support software based on whether the software managed calculates reportable results or provides run support, visualization, or other similar functions.

The following describes the MODFLOW controlled calculation software:

- Software Title: MODFLOW-2000 (MODFLOW-2000, *The U.S. Geological Survey Modular Ground-water Model - User Guide to Modularization Concepts and the Ground-Water Flow* [USGS Open File Report 00-92])—solves transient groundwater flow equations using the finite difference discretization technique.
- Software Version: MODFLOW-2000-SSPA Version 1.19.01 modified by S.S. Papadopolous and Associates for minimum saturated thickness and to use the ORTHOMIN Solver— approved as CHPRC Build 8 using acceptance-tested executables mf2k-chprc08dpl.exe and mf2k-chprc08spl.exe for single and double precision real variables, respectively.
- Hanford Information System Inventory (HISI) Identification Number: 2517 (Safety Software S3, graded Level C).

The following describes the MT3DMS controlled calculation software:

- Software Title: MT3DMS (SERDP-99-1, *MT3DMS: A Modular Three-Dimensional Multispecies Transport Model for Simulation of Advection, Dispersion, and Chemical Reactions of Contaminants in Groundwater Systems; Documentation and User's Guide*).
- Software Version: Standard MT3DMS Version 5.30 approved as CHPRC Build 8 using acceptance-tested executables mt3d-chprc08dpl.exe and mt3d-chprc08spl.exe for single and double precision real variables, respectively.
- HISI Identification Number: 2518 (Safety Software S3, graded Level C).

Support software is used that has been identified in CHPRC-00258, or is scheduled by the software owner to be included as support software in the next revision to that document. Software with a trademark designation is commercial software. Software listed without a trademark has been developed internally.

- **Groundwater Vistas™²**: (*Guide to Using Groundwater Vistas Version 6* [Rumbaugh and Rumbaugh, 2011]). It provides graphical tools used for model quality assurance.
- **ArcGIS™³**: (*The ESRI Guide to GIS Analysis, Volume 1: Geographic Patterns and Relationships* [Mitchell, 1999]). Provided visualization tool for assessing validity of interpolated hydrostratigraphic unit (HSU) surfaces and HSU extents.
- **PEST**: (*PEST Model-Independent Parameter Estimation User Manual* [Doherty, 2007]). Used for automated calibration and run coordination.
- **Leapfrog Hydro®⁴**: (Version 3.0.0). Used for evaluating the 100 Area Geologic Framework Model (GFM) onto the MODFLOW computational grid.

Safety Software (MODFLOW and MT3DMS) is checked out and installation tested before quality-affecting use in accordance with procedures specified in CHPRC-00258. Executable files are obtained

² Groundwater Vistas is a registered trademark of ESI.

³ ArcGIS is a registered trademark of ESRI.

⁴ Leapfrog-Hydro and Leapfrog-Geo are registered trademarks of ARANZ Geo Limited of Christchurch, New Zealand.

from the CHPRC software owner who maintains the configuration-managed copies in MKS Integrity™⁵, installation tests identified in CHPRC-00259, are performed and successful installation confirmed, and software installation and checkout forms are required and must be approved for installations used to perform model runs.

Use of the software previously identified must be consistent with intended use for CHPRC as identified in CHPRC-00257, and be a valid use of this software for the problem addressed in this application. The software must be used within its limitations as identified in CHPRC-00257.

3.2 Discretization

3.2.1 Temporal Discretization

Generally, Columbia River stage is relatively steady from October to March and fluctuates from April to September. Automated Water Level Network (AWLN) wells used for calibration show a time delay from river stage changes from between about 10 to 40 days. Manual water level data collected during sampling is also available at a much lower frequency. Additionally, simulation of the no further action scenario for 125 years requires a different time discretization for efficiency. These factors dictated multiple temporal discretizations.

The 100-K groundwater flow model was implemented three different ways for distinct purposes as follows:

1. **Calibration to river induced changes to establish aquifer hydraulic properties emphasizing the most recent and extensive data.** This period was from January 2013 through December 2016 with stress periods of 5 or 30 days. Care was taken to increase temporal discretization during periods of rapid river stage change to accurately capture the transient effects that provide information on hydraulic properties. Thus, a 5-day stress period length was used for April to September (i.e., rising limb to the peak river stage and falling limb from the peak river stage) of each year to capture this response, and a 30-day stress period length was used for October to March of each year. Figure 3-1 shows the comparison between daily river stage and average river stage based on stress period length at K-River gauge for January 2013 to December 2016.
2. **Calibration of the interpreted contaminant plumes migration.** The calibration period was selected based on the most representative interpreted plume in between 2012 and 2015 so that the transport model can be started with a good initial condition. Moreover, the calibration period was kept as long as possible so that more data can be used for calibration. Transport calibration for hexavalent chromium and nitrate simulates between 2014 and 2016. On the other hand, transport calibration for the remaining contaminants of potential concern (COPCs) (carbon-14, strontium-90, tritium, and TCE) simulates only calendar year 2016. This is because plume footprint/definition for these COPCs keeps changing significantly with the newly available concentration data. As a result, most recent interpreted plume (i.e., plumes from 2015 Annual Groundwater Monitoring Report for these COPCs) was used as the initial condition for the transport model calibration. In all cases, stress period lengths of 5 or 30 days (i.e., similar to flow calibration model) were used.

⁵ PTC, The Product Development Company, MKS Integrity, Integrity and all other PTC product names and logos are trademarks or registered trademarks of Parametric Technology Corporation or its subsidiaries in the United States and in other countries

- Long-term forecast of solute concentrations.** Based on a detailed flow budget analysis of aquifer discharge to the river longer stress periods could be used for solute transport analysis. A 30-day/31-day stress period length was used for 48 years beginning January 2018. For the last 77 years March 2016 was selected as an average condition and applied for 77 one-year stress periods. Figure 3-2 shows the comparison between daily river stage and average river stage based on stress period length at K-River gauge for the 3-year predictive model.

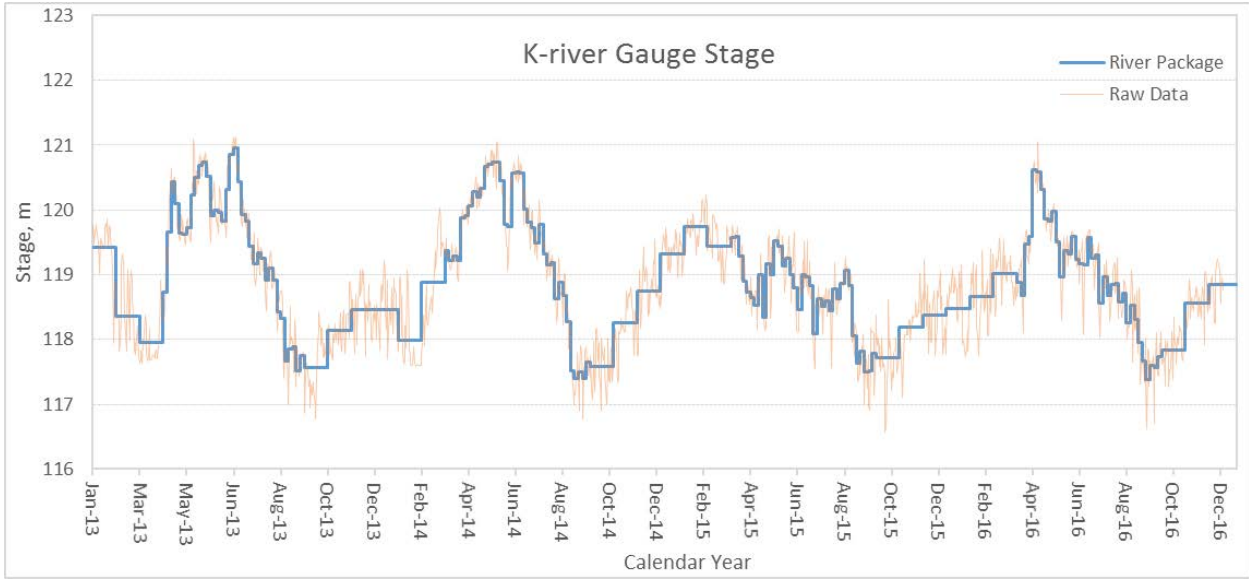


Figure 3-1. Comparison between Daily River Stage and Average River Stage Based on Stress Period Length at K-River Gauge for January 2013 to December 2016

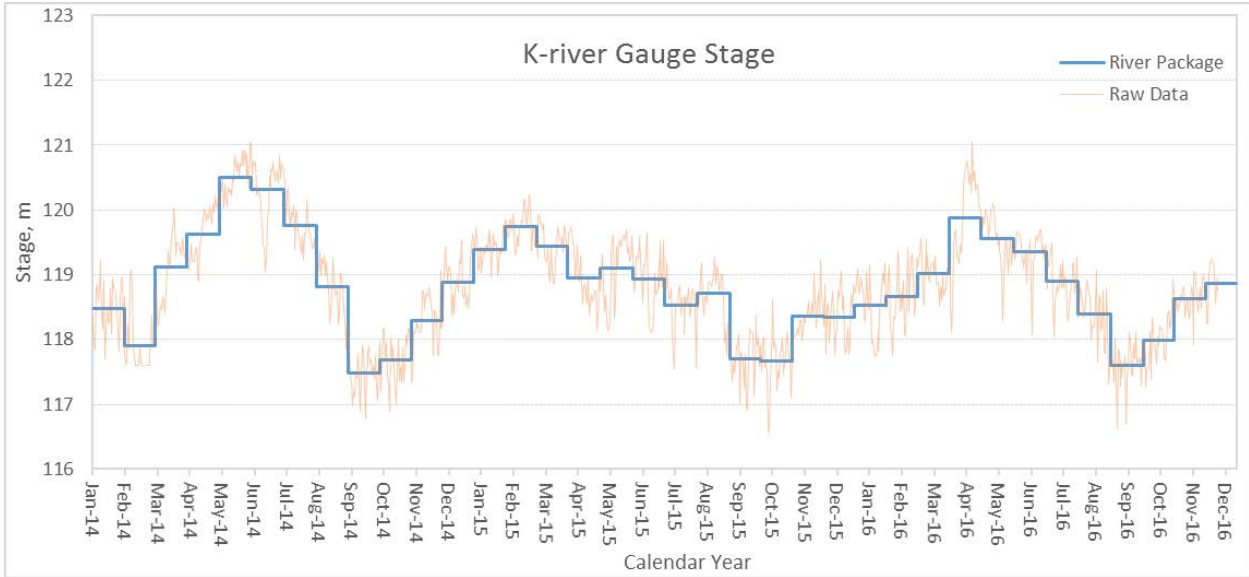


Figure 3-2. Comparison between Daily River Stage and Average River Stage Based on Stress Period Length at K-River Gauge for the Predictive Model

3.2.2 Spatial Discretization

Spatial discretization is the same for all models. The finest grid spacing of 10 m was used where chromium and strontium plumes are currently interpreted to exist. The largest row and column spacing was 50 m. A total of 712,880 cells are in the model, of which 500,848 are active. The model origin is at 567,450 m easting and 142,640 m northing in Washington South NAD83 HARN.

The 100-K Groundwater Flow and Transport Model (GWFTM) extends to the Columbia River on the north side of the model, and uses a general head boundary on the south, east and west sides of the model. A small portion in the southeast corner of the model was assigned no-flow boundary where basalt outcrops above water table. Land surface is the top of the model and the bottom of Ringold Formation Unit E comprises the lower model boundary. The 100-K GWFTM is restricted to approximately center of the width of the Columbia River by a polyline lateral extent and is assigned no-flow for the cells north of the center line of the river. Features of the 100-K GWFTM are shown in Figure 3-3.



Figure 3-3. 100-K Groundwater Flow and Transport Model Plan View Grid

Columbia River bathymetry (PNNL-19878) comprises the upper boundary surface of the broader 100-Area GFM along the Hanford Reach within the model domain. This also applies to the 100-K model since it lies completely within the domain of the 100-Area GFM. To create the original 100-Area GFM upper boundary surface, high-resolution land surface LiDAR (Aero-Metric LiDAR, 2008, “RCCC-Hanford Battelle/PNNL/DOE, Digital Orthophotography & LiDAR Surveys Photogrammetric Report”) was mosaicked with the river bathymetry using GIS (ECF-HANFORD-13-0020, Rev. 3 *Process for Constructing a Three-dimensional Geological Framework Model of the Hanford Site, 100 Area*).

The model boundary was selected to contain two key natural boundaries (e.g., river, no-flow), well locations with extensive data, and COPC plume extents within the 100-KR-4 OU. The 100-Area GFM uses top of basalt as its lower boundary surfaces and are comprised (from land surface down) of the Hanford formation (HF), Ringold E (Rwie) and RUM hydro-stratigraphic units (HSUs). Because the RUM is assumed to be a no-flow boundary, only Hf and Rwie are utilized in the 100-K GWFTM.

The MODFLOW grid for the 100-K GWFTM was built using Groundwater Vistas software and an R script for pre- and post-processing of the HSU contact surfaces. It was required to discretize the model grid as finely as possible so that all the flow and transport properties can be well-represented by the model cells. However, model cells need to be limited to avoid longer runtimes and other numerical issues. The 100-K GWFTM was created with 469 rows, 380 columns, and 4 layers so that the model satisfies these criteria. The Rwie is split into four layers; the Hanford formation only occurs in the southern part of the domain. The following procedures were performed to generate model and HSU assignment at model cells:

- MODFLOW grid with 469 rows, 380 columns, and 4 layers was created using Groundwater Vistas.
- Model cells to the north of approximately center of Columbia River were made inactive. Model cells within the Columbia River footprint are defined as river cells.
- The surfer grid contact surfaces from Leapfrog Hydro (i.e., Land surface with river bathymetry, 2014 water table with river bathymetry, and Rwie-RUM contact) were imported to Groundwater Vistas and exported as MODFLOW readable array.
- A surface was generated by subtracting 4.0 m from the 2014 annual groundwater table with river bathymetry and was imported to Groundwater Vistas as the bottom elevation of layer 1. This allows at least 4.0 m saturated thickness in layer 1 which is important in preventing wet-dry issues during MODFLOW model simulation. The remaining saturated thickness in the unconfined aquifer is split into 3 equally spaced layers.
- Model cells, where basalt pinches out above water table, were made inactive.
- HSU assignment at each model cell is done by evaluating the 100 Area GFM onto the model grid center.

A base map showing the three geologic cross section locations within 100-K GWFTM is shown in Figure 3-4. Figure 3-5 through Figure 3-7 show cross-sectional view of the 100-Area GFM within the 100-K GWFTM along with Columbia River, MODFLOW model layering, and 2014 Water Table.

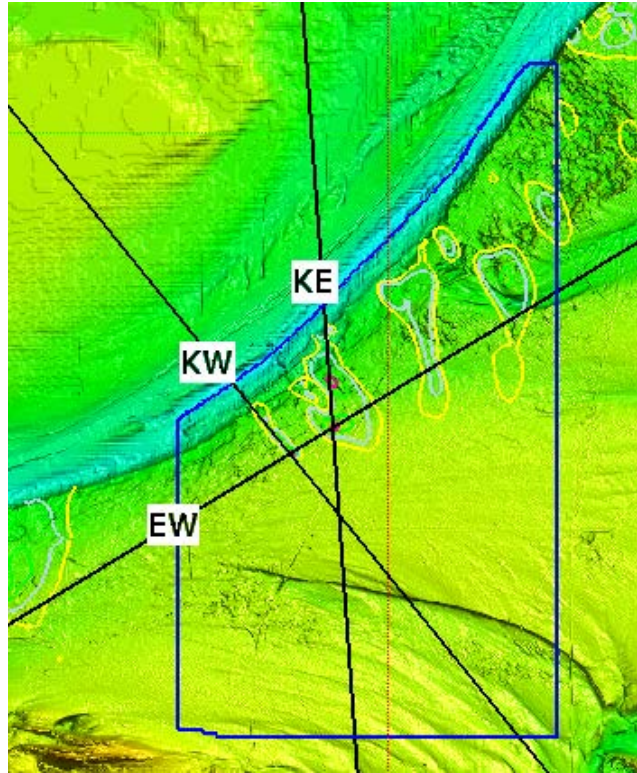


Figure 3-4. Hydrogeological Cross Section Base Map for 100-Area GFM within 100-K GWFTM Model Domain

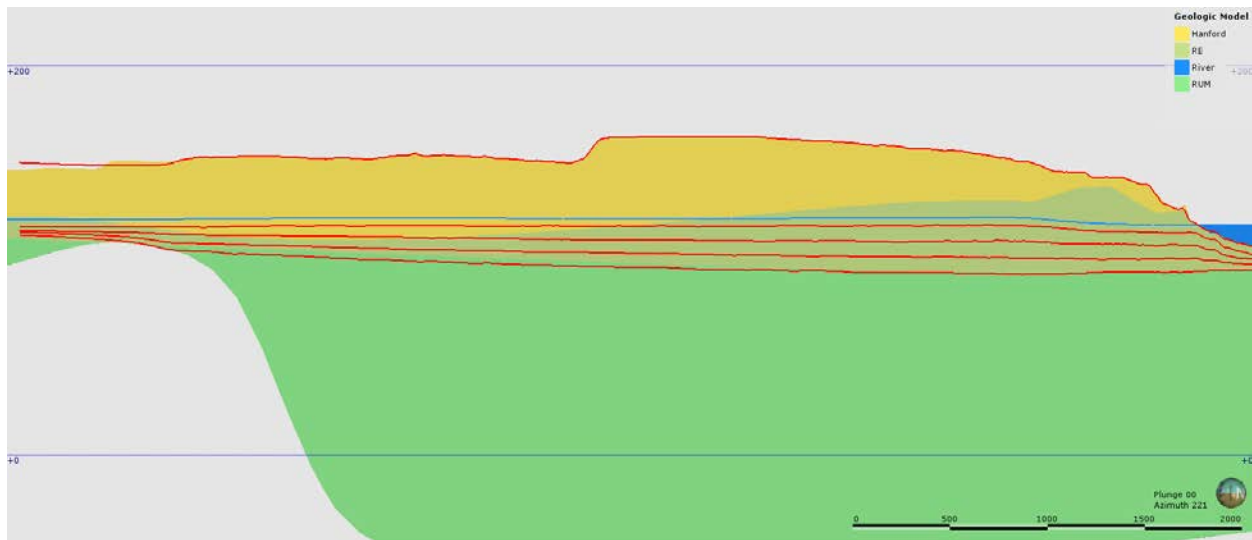


Figure 3-5. 100-Area GFM with Columbia River, MODFLOW Model Layers and 2014 Water Table through Cr(VI) Plume in KW Area

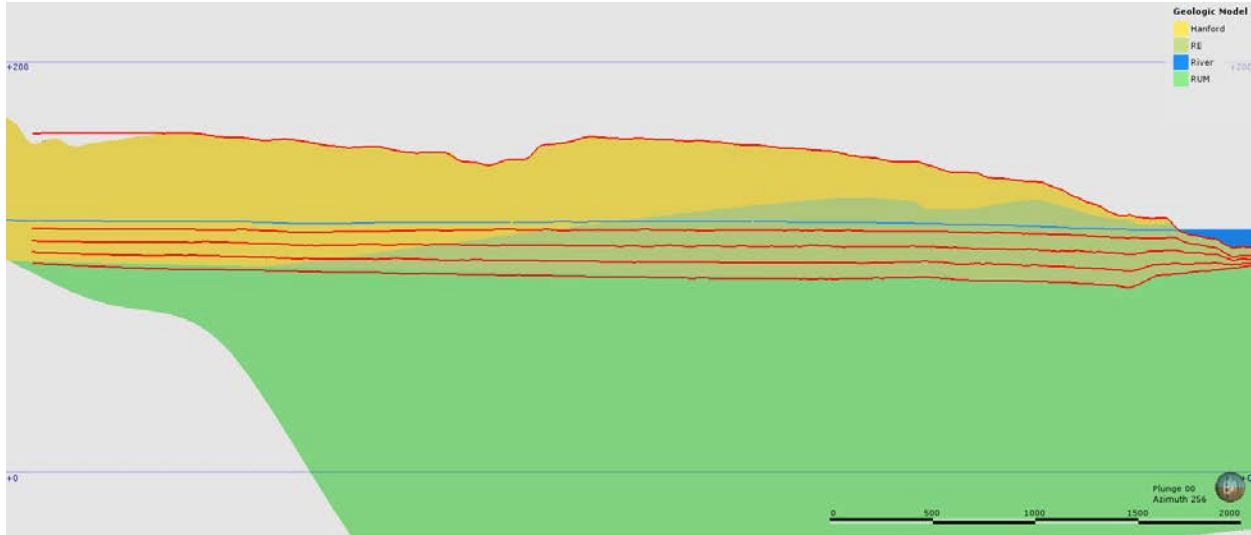


Figure 3-6. 100-Area GFM with Columbia River, MODFLOW Model Layers and 2014 Water Table through Cr(VI) Plume in KE Area

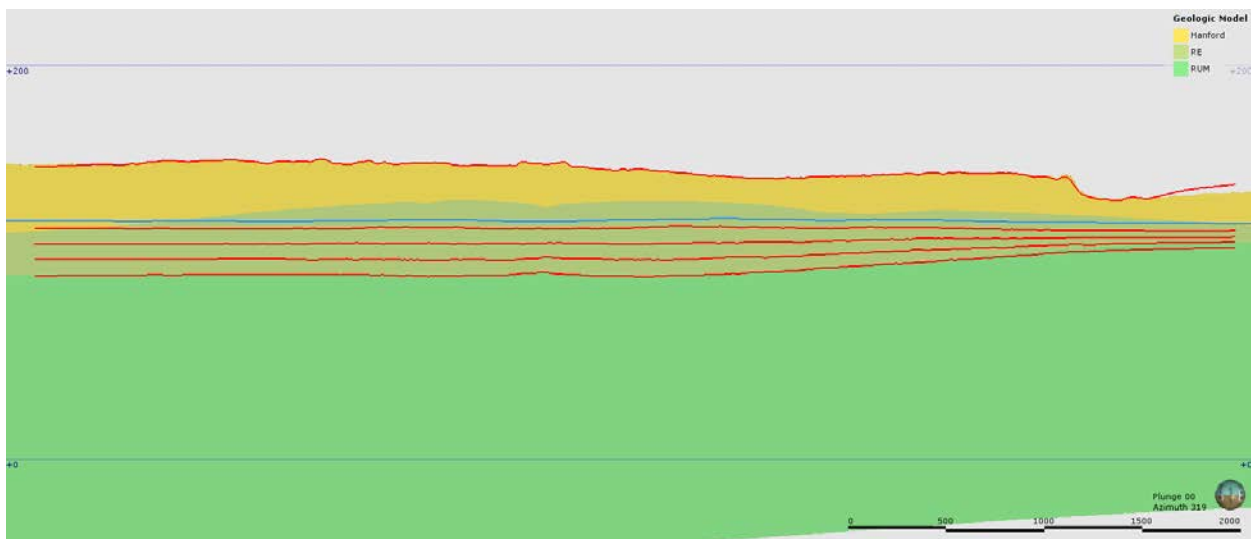


Figure 3-7. EW Cross Section at 100-Area GFM with MODFLOW Model Layers and 2014 Water Table

3.3 Parameterization

3.3.1 Recharge Boundary Condition

The Recharge Estimation Tool (RET) was developed using the concept described above to compute recharge rates both temporally and spatially. The RET was developed for ArcGIS®⁶ using python scripts and to enable users to determine the spatial-temporal variation in recharge for their model domain and over their time of interest. The site-specific information produced by the RET is used in the MODFLOW recharge package. The RET scripts use a dictionary which identifies all the years where a change in recharge rate occurs over the Hanford Site. This dictionary contains a list of all the waste sites at the

⁶ ArcGIS is a registered trademark of ESRI, Redlands, California.

Hanford Site, their associated remediation action and date from the disposition baseline report (CP-60254, *Hanford Site Composite Analysis Technical Approach Description: Hanford Site Disposition Baseline*) and incorporates vegetation succession over time (ECF-HANFORD-15-0019, *Hanford Site-Wide Natural Recharge Boundary Condition for Groundwater Models*). The first RET script uses 13 spatial data sources and three tabular data sources to develop recharge estimates for the Hanford Site. This script produces a geodatabase of recharge rates over the Hanford Site for all years identified as having a change in recharge rate as listed in the dictionary. The second RET uses the user-provided model boundary (i.e., 100-K GWFTM) to identify the waste sites within the model domain and references the dictionary to identify for which years over the time of interest there are changes in recharge rate. This step is repeated for all the waste sites and the list is compiled to create a comprehensive list of years for the user-provided model domain and time of interest. The RET then samples the relevant years in the geodatabase from the first RET script, clips them to the model domain, and compiles them into a new geodatabase or individual shapefiles as preferred by the user. Figure 3-8 shows the recharge rates that were applied to the calibration model for calendar year 2013 thru 2016. An R script was used for evaluating the shapefiles onto the model grid and output to a MODFLOW readable array format. The RET tool did not include some of the future estimates of the sequential recharge rates for the waste sites. This adjustment was made using an R script.

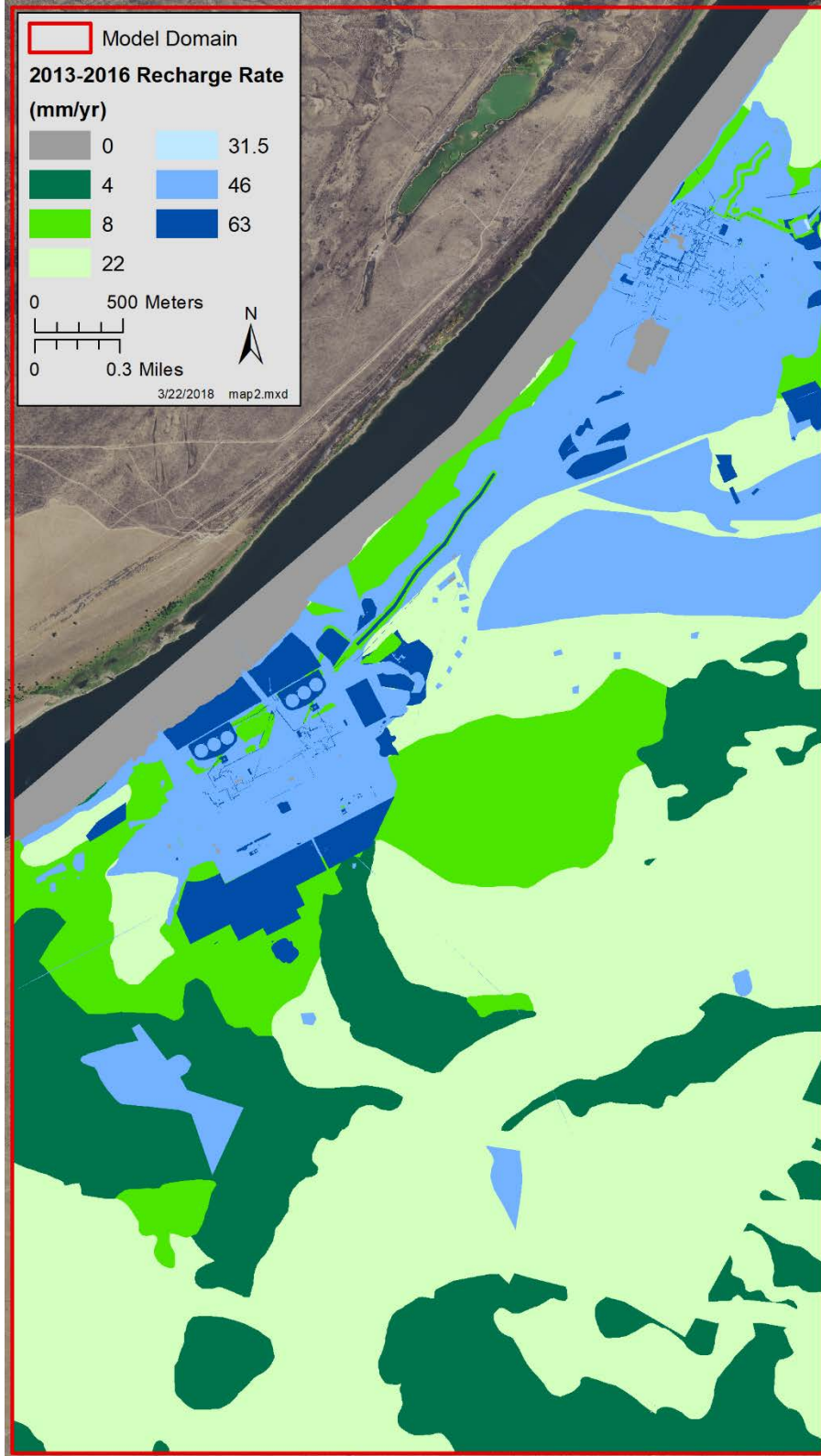


Figure 3-8. 2013-2016 Recharge

3.3.2 West, South, and East Landward Boundary Conditions

General head boundary (GHB) conditions are used at western and eastern boundaries of the 100-K GWFTM to represent the influence of the unconfined aquifer not included in the model domain. The fluctuations in the Columbia River stage are conceptualized to impact the head at these lateral boundaries with the impact of the river being largest near the river and lessening with increasing distance from the river. Active P&T systems within the 100-KR-4 OU disturbs this relationship between the Columbia River and the aquifer near the P&T system. No significant number of wells with long record of high frequency data outside the influence of P&T system were found to evaluate this relationship. However, aquifer responses to Columbia River fluctuation is already evaluated and the parameters are calibrated at nearby 100-BC area as part of the 100-BC RI/FS. The observed water levels at several wells within the 100-BC area were compared to the B-gage stage data and a synthetic formula was developed to incorporate both the B-gage stage and the prior groundwater level at those locations using a damping parameter. The synthetic formula also allowed for a systematic increase in the groundwater levels at those locations to account for the regional groundwater gradient towards the river and a time lag to account for the time required for river fluctuations to propagate through the aquifer. The formula was fit to the observed water levels as a function of distance of the wells from the river. In this way, the effect of the Columbia River fluctuations as well as the aquifer between points along the boundaries was accounted for in generating the heads and conductance along the western and eastern boundaries. The GHB head over distance along the boundary for 100-BC GWFTM is illustrated for the first eight calibration stress periods in Figure 3-9. The boundary shows the effects of low river stage beginning in January (sp1) and then rising and becoming more variable in April. Note that, at about 1,500 m from the river, the fluctuations are strongly damped, broadly consistent with the well water levels near the southern boundary of the 100-BC GWFTM. Similar relationship can be used and calibrated for the 100-K GWFTM.

The southern boundary is 3,500 to 8,000 m away from the Columbia River where response to river fluctuation would be very minimum. As expected, wells near the southern boundary show relatively steady water level. General-head boundary conditions with a fixed GHB head is applied to the southern boundary.

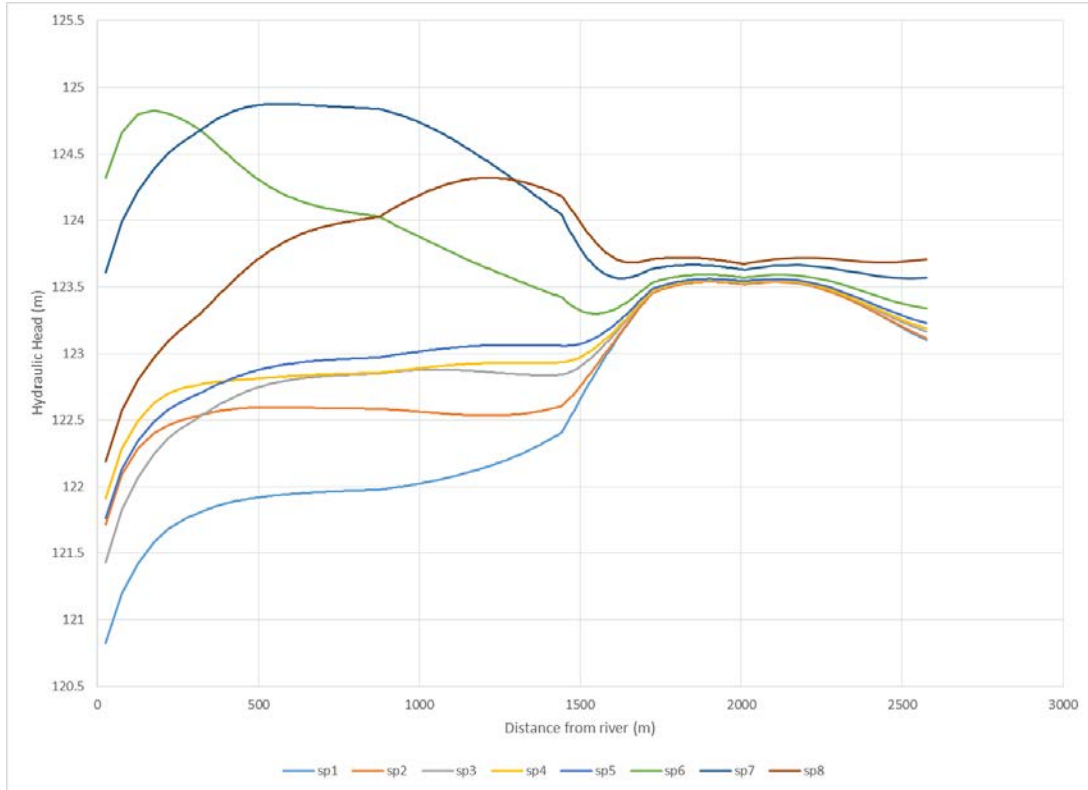


Figure 3-9. GHB Head vs. Distance Considering Stage, Gradient, Prior Levels, and Distance Correction for the First Eight Stress Periods of the 100-BC GWFTM

3.3.3 River Boundary Conditions

PNNL-14753 Rev. 1 (*Groundwater Data Package for Hanford Assessments*) documents the steady-state water surface of the Columbia River from the MASS1 surface water model. This data is assumed to adequately represent the variation in the slope of the river over all times of interest. Practically, this assumption may be violated during sharp increases in stage as the flood wave propagates downstream. The MASS1 simulated stages were interpolated onto the PNNL groundwater model river nodes; in turn this data was interpolated and sampled at the 100-K GWFTM grid centers underlying the river. The relative stage at each location was then used with the K-gauge data to compute the river stage. The K-gauge transducer data was averaged over each stress period.

As stage changes over time the area of the riverbed that is submerged also changes – this phenomenon is noted as seeps along the river. To account for this a river boundary is only assigned to a cell when the average stage in the stress period is above the cells bathymetry- only cells within the river are included in the computation. For grid cells where the stage is below the bathymetry a drain boundary condition is substituted and the elevation set to the land (bathymetric) surface to emulate riverbank seeps that occur when the river drops.

Riverbed hydraulic conductivity (with an assumed riverbed thickness of 1 m) for the Ringold E was made adjustable during calibration, but not spatially variable. The quality assurance checking performed for this algorithm is not shown here, but is preserved in the Environmental Model Management Archive (EMMA) under this model name and version.

3.3.4 Initial Head Condition

The initial hydraulic head everywhere in the model was assigned from January 2013 water table conditions as published in the 2013 annual groundwater monitoring report (DOE/RL-2014-32, Rev. 0, *Hanford Site Groundwater Monitoring Report for 2013*). This was done by importing the shape files into Groundwater Vistas to perform the interpolation. Because this is a transient solution that uses an iterative solver, the primary effect of specifying the initial head is to speed up the solution.

3.3.5 Initial Concentrations

The DOE publishes concentration plumes every year for each COPC for each OU as part of their extensive annual groundwater monitoring program at Hanford Site. These are essentially a two-dimensional (2D) concentration plume based on the interpretation of known site-specific knowledge and the observed concentration over a year irrespective of depth of the collected sample. The plume delineation could change significantly from one year to another if new information is available from recently drilled monitoring wells. For contaminant transport calibration, it is important to start the model from a good initial concentration. In addition, the calibration period needs to be as long as possible to build confidence on the calibration results. As a result, concentration plumes reported in the annual groundwater monitoring report between 2012 and 2015 were examined for selecting initial concentration for each COPC. The 2D concentration plumes reported in the annual groundwater monitoring report are applied to all the layers in the 100-K GWFTM.

3.3.5.1 Hexavalent Chromium Initial Concentration

Hexavalent chromium contamination is extensive throughout the 100-KR-4 OU and is considered the most important COPC. The P&T system in 100-KR-4 OU was installed to remediate Cr(VI) contamination and protect the Columbia River from Cr(VI) discharges to the river. There are two Cr(VI) plumes, one at or near each reactor, in groundwater. According to the annual groundwater monitoring reports, the 100-K hexavalent chromium plumes in 2013 are significantly different from 2012, especially near high concentration (and source) areas near the KW and KE headhouses. The details of these differences are explained in DOE/RL-2014-32. Conceptually, the inferred plumes from 2013 thru 2015 are consistent. The 2013 plume from annual groundwater monitoring report was selected for the transport model calibration.

There are also several Cr(VI) plumes which originated from the 116-K-2 trench, but migrated towards the 100-N OU. The migration towards 100-N OU could be due to the historical discharges during the operational period. Among those migrated plumes, one completely lies within 100-K OU boundary, one partially lies between 100-K and 100-N OU boundary, and one completely lies within 100-N OU boundary. It would be inefficient to include 100-N OU within 100-K GWFTM domain just to simulate one Cr(VI) plume that has migrated away from the Cr(VI) source area when a groundwater fate and transport model already exists which was built to support RI/FS in 100-N OU. This isolated plume was not included in the 100-K GWFTM and modeled during predictive simulations by using the 100-N GWFTM documented in CP-59563, Rev. 0 (*100-N Scale-Appropriate Fate and Transport Groundwater Model*).

3.3.5.2 Strontium-90 Initial Concentration

Strontium-90 contamination in 100-KR-4 OU was limited to around Fuel Storage Basin (FSB) in KE area and 116-K-2 trench. Based on the information about historical discharges, the plume delineation for strontium-90 at the FSB was significantly bigger in the past and subsequently reduced in the later years as information from the newly drilled monitoring wells were available. Strontium-90 has very strong affinity to soil and adsorbs with soil as contaminated groundwater flow through the pore spaces. Therefore, it is

expected that strontium-90 will move very slowly with groundwater flow and the plume footprint should remain very similar within couple of years. However, that was not the case for strontium-90 plume in between 2012 and 2015. Strontium-90 plume from 2015 annual groundwater monitoring report is assumed to be most representative of latest observed data. Therefore, the plume from 2015 annual groundwater monitoring report (DOE/RL-2016-09) was selected as the initial concentrations for the transport calibration model simulation.

3.3.5.3 Nitrate Initial Concentration

According to the annual groundwater monitoring reports between 2012 and 2015, the nitrate plume footprint has shrunk significantly in the later years. However, the most recent annual groundwater monitoring report in 2016 (DOE/RL-2016-67, Rev. 0, *Hanford Site Groundwater Monitoring Report for 2016*) shows a significantly larger plume footprint in response to observed high concentrations (above cleanup level) at some wells in KW area. It should be noted that some of these well locations are not at or near the suspected potential continuing sources. A slug of contaminant mass coming from the upstream could have migrated to these downstream wells and contributed to the observed high concentrations. There is a lot uncertainty with these migrating slug of masses where no continuing sources are expected. Moreover, modifying the initial concentrations at these locations would improve the calibration results but would not contribute much to the predictive simulations as those masses would be depleted in couple of years. Therefore, the plume from 2013 annual groundwater monitoring report (most mass conservative) was selected as the initial concentrations for the transport calibration model simulation.

3.3.5.4 Carbon-14, Tritium, and Trichloroethene Initial Concentrations

Like the above COPCs, plume footprints of carbon-14, tritium, trichloroethene reported in the annual groundwater monitoring reports between 2012 and 2015 were evaluated for selecting the most representative initial concentration, and the most recent ones (i.e., 2015) was selected for the transport calibration model simulation.

3.3.6 Aquifer Hydraulic Property Parameterization

Simulation of transient groundwater flow under unconfined conditions requires the following input data:

- Horizontal hydraulic conductivity in each model layer of the Hanford and/or Ringold
- The ratio of vertical to horizontal hydraulic conductivity (K_v/K_h) used to compute vertical hydraulic conductivity
- Specific storage (S_s), and
- Specific yield (S_y).

These properties were specified using the MODFLOW LPF (Layer Property Flow) package. The first model layer is unconfined (type 1) where transmissivity is a function of saturated thickness, and the remaining layers are convertible (type 3) where transmissivity is computed from layer thickness when simulated head is above the layer or as saturated thickness when head is below the top of the layer.

Uniform values of the ratio of vertical to horizontal hydraulic conductivity (K_v/K_h) for the Hanford and Ringold were specified, and used to multiply horizontal hydraulic conductivity to yield vertical hydraulic conductivity for model input, S_s and S_y were input as constant values for all layers and formations. Upper and lower bounds on K_v/K_h were set at 0.01 and 0.5, respectively. Specific storage upper and lower bounds were set at 1×10^{-4} and 5×10^{-6} 1/m, respectively. Specific yield upper and lower bounds were set at 0.4 and 0.1, respectively.

Two HSUs are present in the model:

1. Hanford formation, only in the southern part of the model domain in layers 1 thru 4.
2. Ringold E formation, in layers 1 thru layer 4.

Horizontal hydraulic conductivity was parameterized by points interpolated over the model grid via ordinary kriging. This approach is termed the “pilot point” method of parameterization (Doherty, 2003). Pilot points at each layer are placed based on the following criteria:

1. Uniform distribution of the pilot points over the entire model domain so that at least 2-3 points are available for interpolation within the correlation scale (range)
2. High density of pilot points in vicinity of calibration targets (e.g., AWLN wells, manual measurement wells)

In the context of this application the correlation scale (range) of the semivariogram represents an influence distance for interpolation, not the actual correlation scale of hydraulic conductivity; insufficient data exist to determine the correlation scale of hydraulic conductivity. The PEST groundwater utility PPK2FAC was used to generate kriging factors from the pilot points in each layer for all the model cells. A spherical variogram with a correlation range of 1,000 m was used to interpolate hydraulic conductivity. A total of 36 pilot points were used where 35 of those lie within the Ringold E and one lies within the Hanford formation. The PEST groundwater utility FAC2REAL was used to calculate hydraulic conductivity at each model cell based on the pilot point values and kriging factors generated by PPK2FAC program. PEST was run with regularization constraints computed from the PPKREG utility so that FAC2REAL program always generates hydraulic conductivity values based on smoothness constraints. Figure 3-10 thru Figure 3-13 show the location of the pilot points with respect to HSUs, calibration wells, and 2013 Cr(VI) plume outline in layers 1 through 4, respectively.

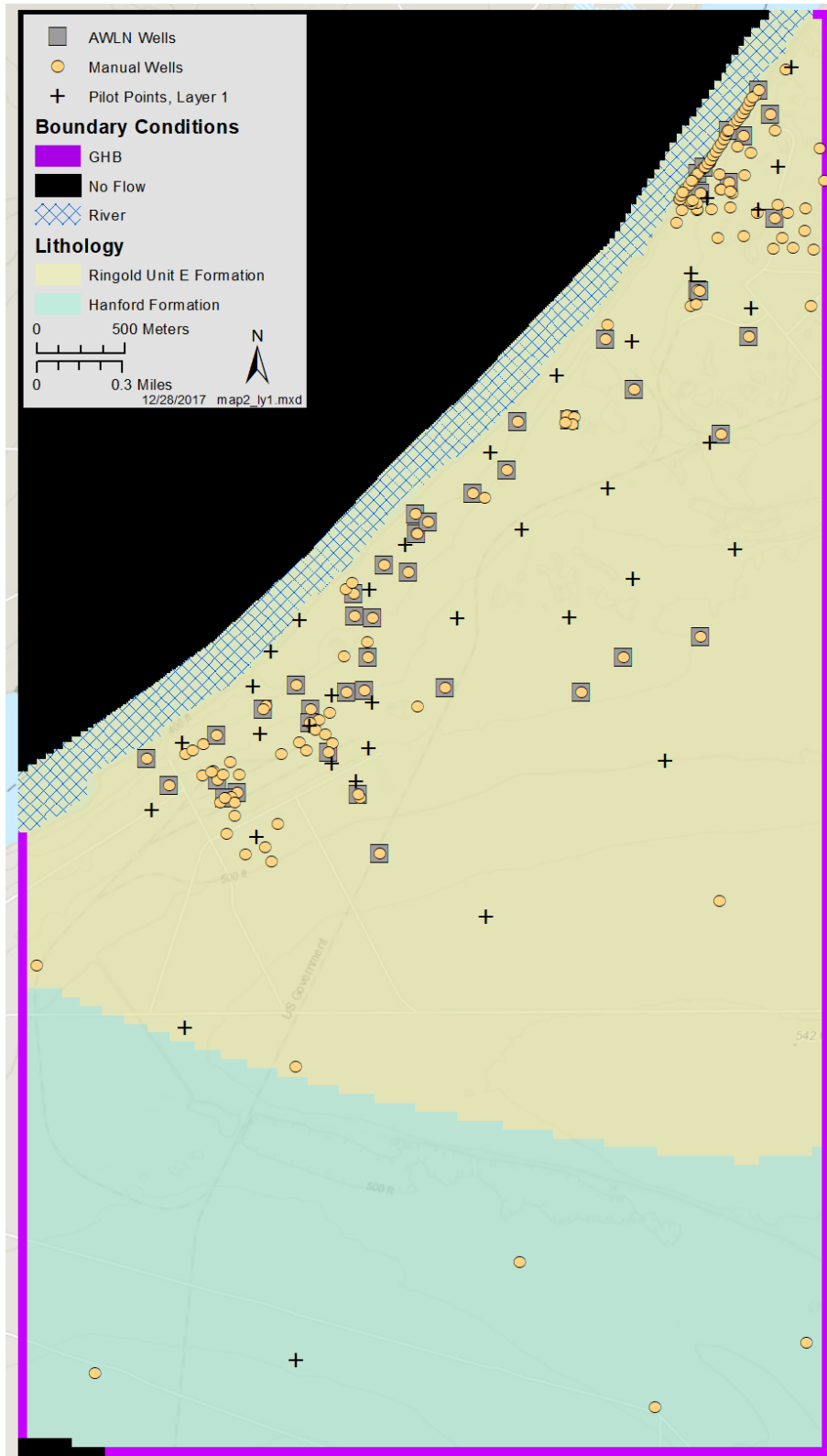


Figure 3-10. Pilot Point Locations with Hydrostratigraphic Unit Distribution in Layer 1

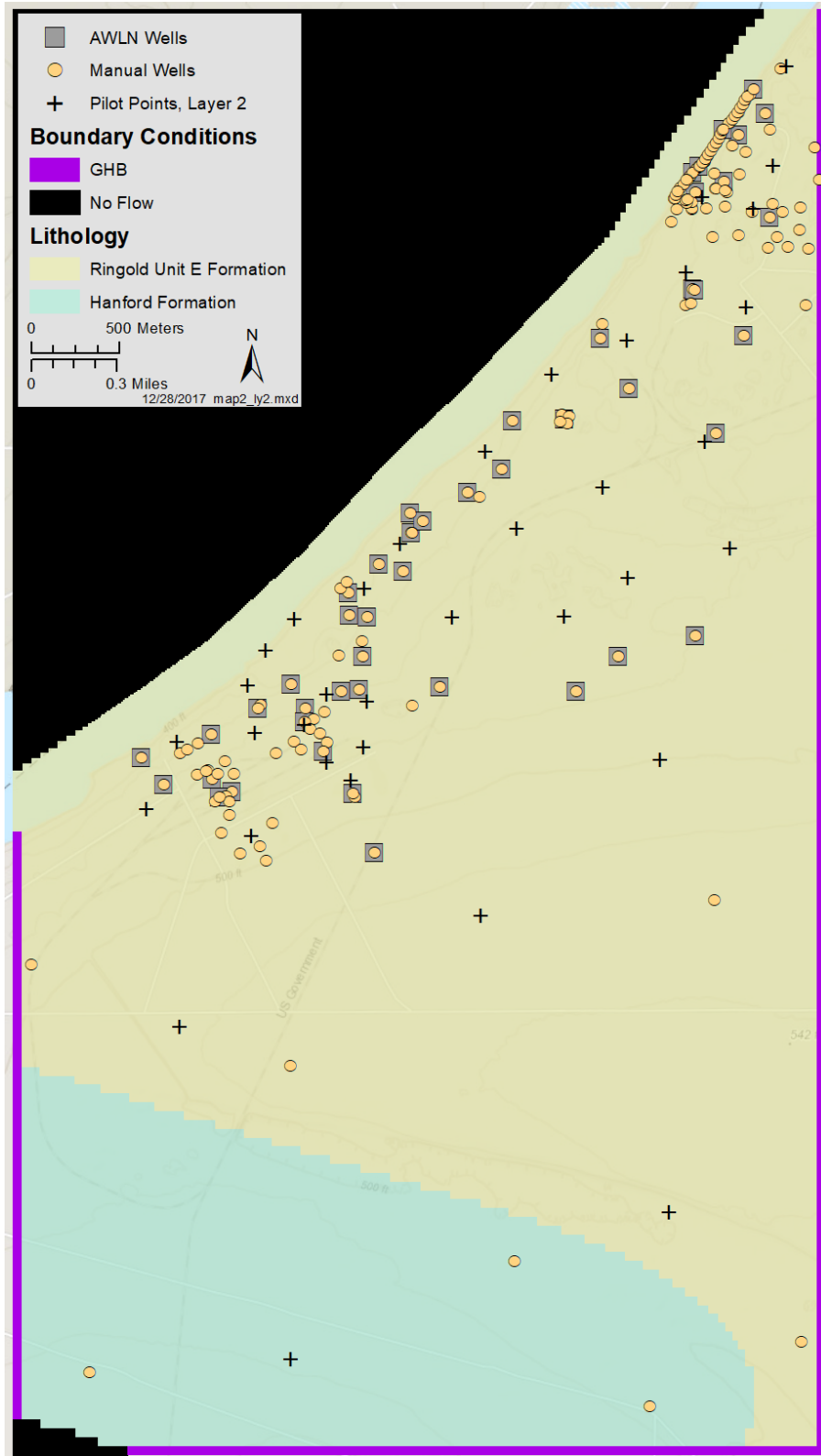


Figure 3-11. Pilot Point Locations with Hydrostratigraphic Unit Distribution in Layer 2

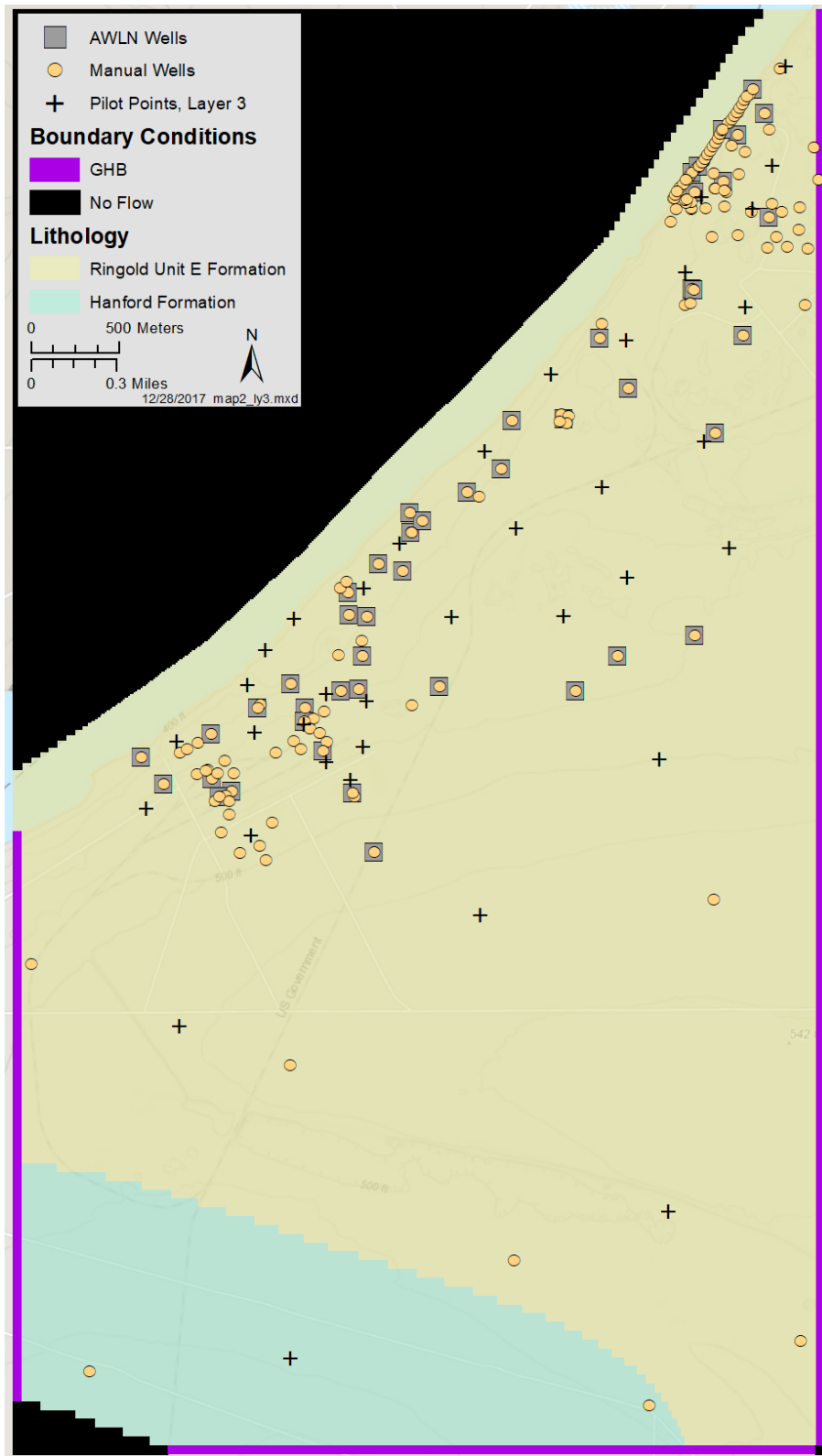


Figure 3-12. Pilot Point Locations with Hydrostratigraphic Unit Distribution in Layer 3

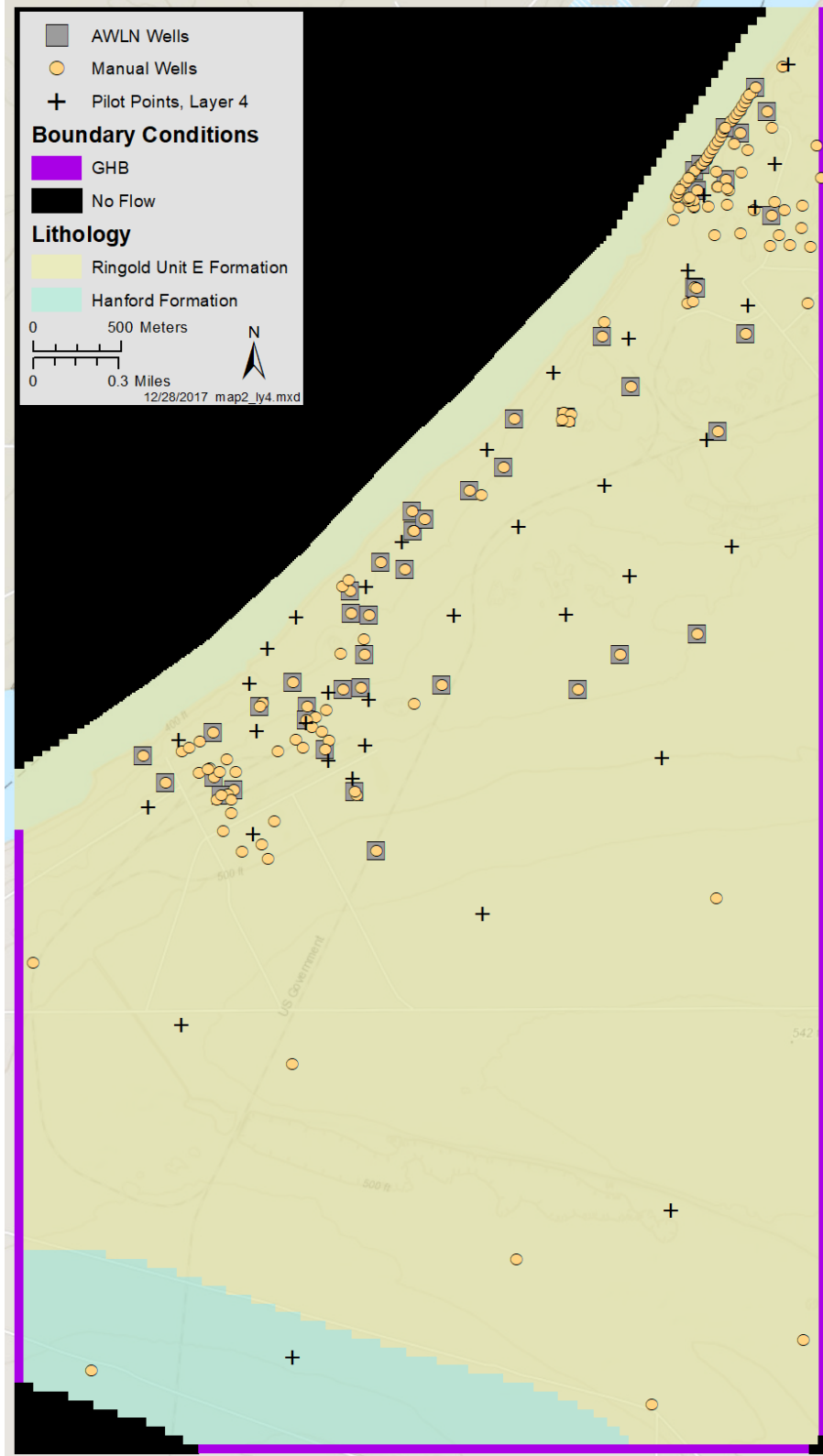


Figure 3-13. Pilot Point Locations with Hydrostratigraphic Unit Distribution in Layer 4

3.3.7 Effective Porosity

PNNL-21845, *Investigation of Hexavalent Chromium Flux to Groundwater at the 100-C-7:1 Excavation Site*, estimates the effective porosity of the Hanford formation from tracer tests at 0.18 with a range from 0.24 to 0.14. The uncertainty was due to the simplified methodology. A uniform value of 0.18 was used throughout the model domain for both Ringold E and Hanford formation.

3.3.8 Dispersivity

Dispersivity is a characteristic property of the geologic system, often found to be scale-dependent (e.g., a function of mean travel distance of solutes). Representative dispersivity values are typically determined from examination of values at similar transport scales from tracer tests and modeling of contaminant plumes. Dispersivity data from the scientific literature was evaluated and appropriate dispersivity values for use in the 100-K transport model selected. This analysis supersedes that in SGW-44022.

Schulze-Makuch (2005) gathered data from additional sources and added this data to the data presented by Gelhar et al. (1992). Schulze-Makuch (2005) presents 184 additional dispersivity values from 39 authors in a similar fashion to that of Gelhar et al. (1992). An evaluation of some of the data summarized by Schulze-Makuch (2005) revealed a number of discrepancies such as: (1) incorrect reporting of dispersivity (e.g., average dispersivity value referenced from Rivett et al. [1994] should be 49 cm, not 49 m; and transverse horizontal dispersivities from Lavenue and Domenico [1986] were reported as longitudinal dispersivities), (2) from two to five dispersivity values were tabulated for identical flow paths from some reference sources, which could lead to over representation and bias if multiple values are included in the dataset for the same tested flow path (e.g., Ptak and Teutsch [1994]; D'Alessandro et al. [1997]; Himmelsbach et al. [1998]), (3) inappropriate selection of transport scale (e.g., use of the total model grid length rather than the mean travel distance for regional plumes presented in Avon and Bredehoeft [1989] and Chapelle [1986]), and (4) omitting dispersivities reported in sources (e.g., Chiang et al. [1989]; Engesgaard et al. [1996]; Mas-Pla et al. [1992]; D'Alessandro et al. [1997]). Because direct inclusion of all of the data reported in Schulze-Makuch (2005) could lead to undesirable uncertainty in the combined dataset constructed to support development of a dispersivity-scale relation, it was decided to use only data from those original sources that could be readily obtained and verified with emphasis on field studies with scales of interest (i.e., greater than 1 m). Where multiple dispersivity values were reported for the same flow path (e.g., from multiple tests and/or multiple analysis methods) in the original data sources, a geometric mean value was calculated for inclusion in the dataset. Schulze-Makuch (2005) adopted the reliability classification system above defined by Gelhar et al. (1992).

Literature data other than that cited in Gelhar et al. (1992) and Schulze-Makuch (2005) for tracer tests conducted at the Nevada National Security Site (IT Corp, 1998; Reimus et al., 1999; SNJV, 2006, 2007) and analysis of a long plume in Canada (van der Kamp et al., 1994) are also included in the dataset. Reliability codes were assigned to these data based on the criteria in Gelhar et al. (1992). For these data, a geometric mean value was calculated for inclusion in the dataset where multiple dispersivity values were reported for the same flow path.

Plots of the longitudinal dispersivity versus scale in log-log space are shown in Figure 3-14 and Figure 3-15 by rock type and reliability level, respectively. The data show a systematic increase in longitudinal dispersivity with increasing transport scale, which is consistent with findings by previous authors (e.g., Gelhar et al., 1992). The equations for these fits are given in Table 3-1. At 100-K, the unconfined aquifer is located within the alluvial sediments of the Ringold Formation. Therefore, linear and log fits were obtained for the data from only alluvial sediments (Figure 3-16). The equations for these fits, which are very similar to those for the fits to all the data, are also given in Table 3-1. Recommended values as a function of transport distance are given in Table 3-2. Transverse horizontal and vertical dispersivities

were selected based on a ratio of longitudinal to transverse horizontal dispersivity of about 10 and a ratio of longitudinal to transverse vertical dispersivity of about 100, respectively. Because groundwater contamination from sources at greatly different transport distances from the river intermingle, it was not possible to implement scale-dependent dispersivity. Lower-end values of 10, 1, and 0.1 m were used for horizontal longitudinal, horizontal transverse, and vertical transverse dispersivity to minimize plume spreading but still account for the dispersion process.

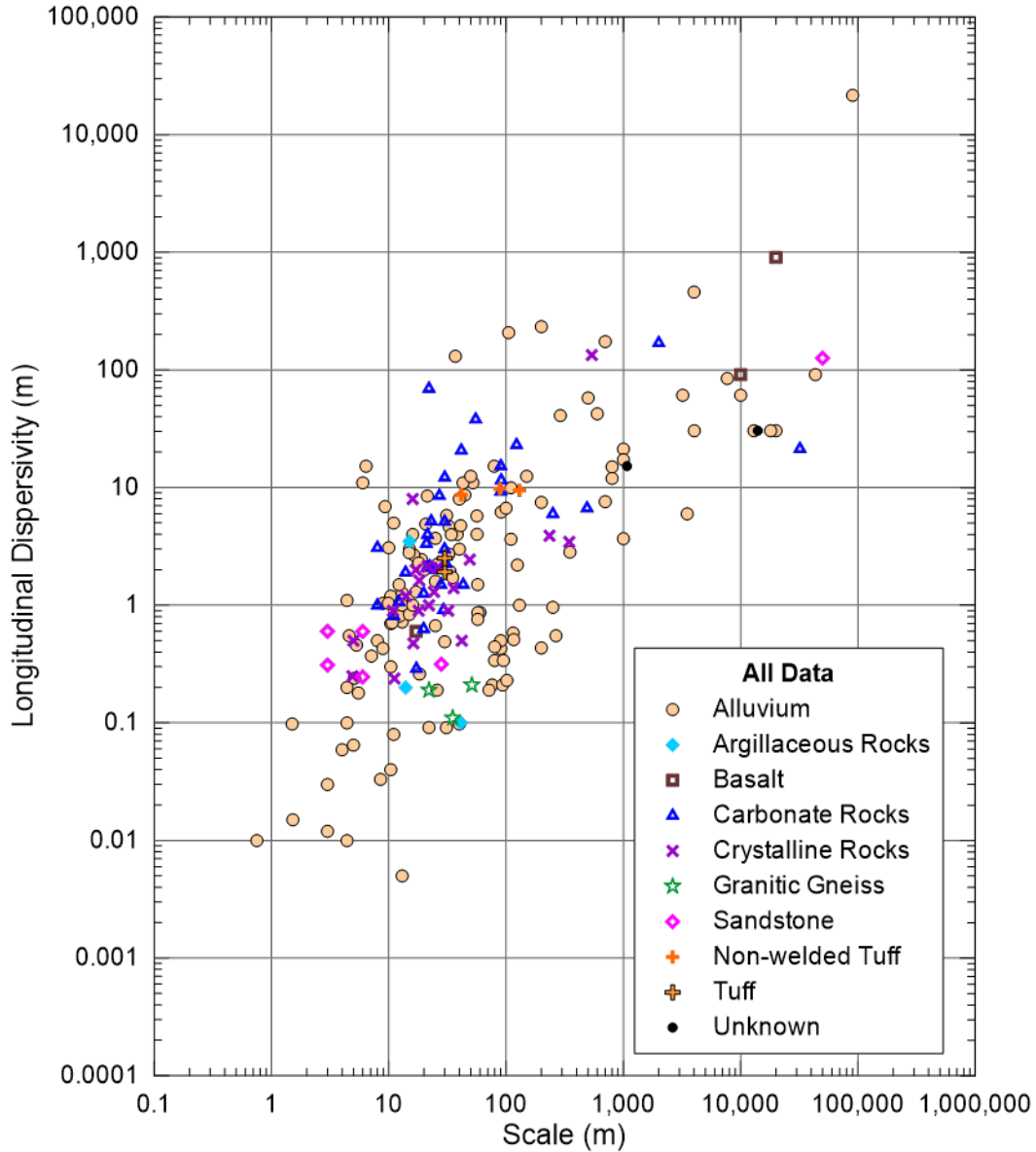


Figure 3-14. Longitudinal Dispersivity by Rock Type

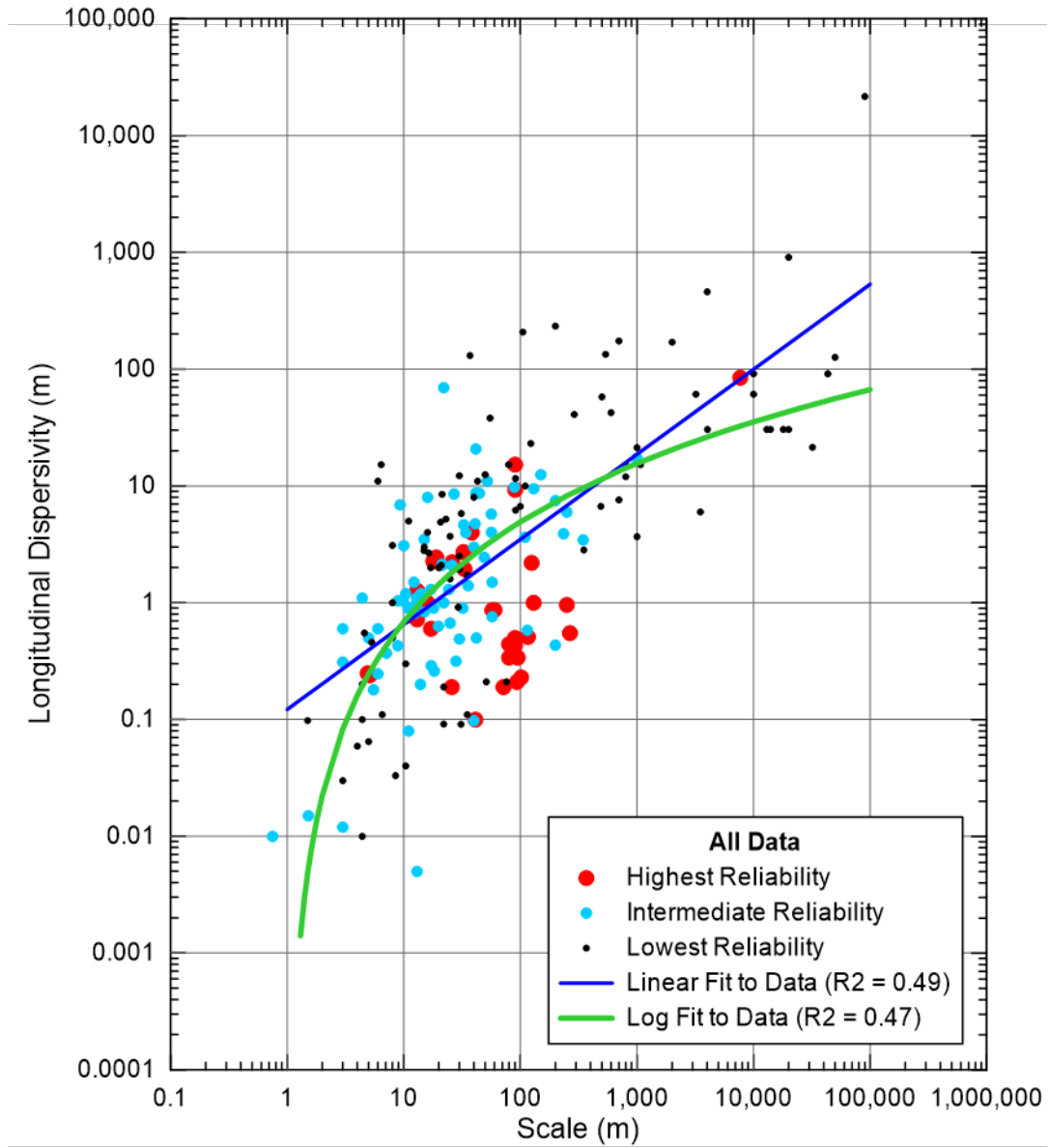


Figure 3-15. Longitudinal Dispersivity by Reliability Level for all Rock Types with Linear and Log Fits

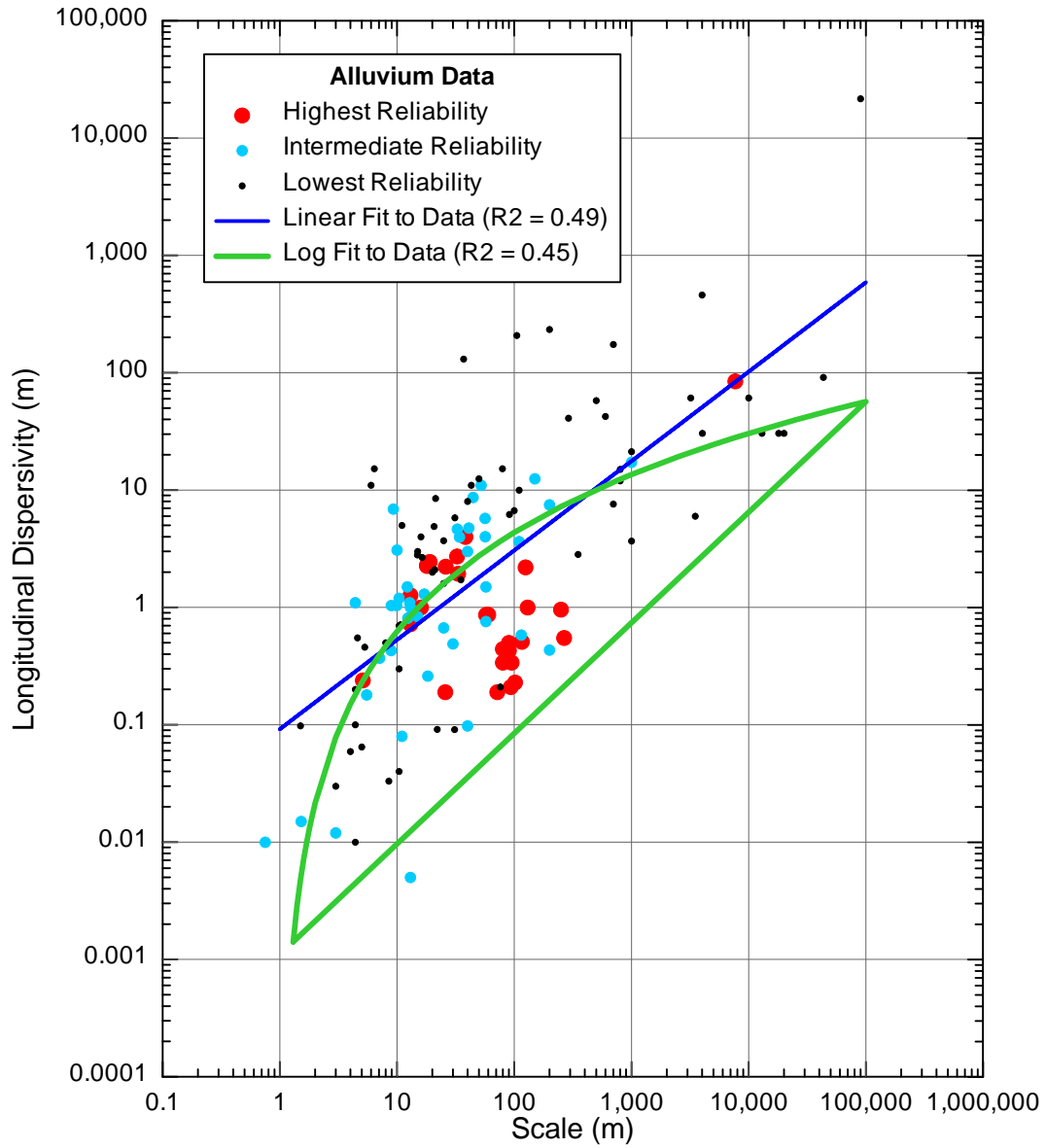


Figure 3-16. Longitudinal Dispersivity by Reliability Level for Alluvial Sediments Only with Linear and Log Fits

Table 3-1. Dispersivity-scale Relationships

Relationship Type	Relationship ⁽¹⁾	Coefficient of Determination (R ²)
All Data		
linear	$\log(\alpha) = 0.7282 * \log(x) - 0.9141$	0.49
log	$\log(\alpha) = 1.2367 * \log(x) - 0.1658$	0.47
Alluvium Data		
linear	$\log(\alpha) = 0.7615 * \log(x) - 1.0369$	0.49
log	$\log(\alpha) = 1.2176 * \log(x) - 0.2050$	0.45
(1) α = longitudinal dispersivity; x = transport distance		

Table 3-2. Recommended Dispersivity Values for 100-K

Transport Distance	Calculated Longitudinal Dispersivity (m) ⁽¹⁾				Recommended Longitudinal Dispersivity (m) ⁽²⁾	Recommended Horizontal Transverse Dispersivity (m) ⁽³⁾	Recommended Vertical Transverse Dispersivity (m) ⁽⁴⁾
	All Data - Linear	All Data - Log	Alluvium Data - Linear	Alluvium Data - Log			
500	11	12	10	12	10	1	0.1
1000	19	16	18	14	18	1.8	0.18
5000	60	28	60	24	60	6	0.6
7000	77	32	82	27	82	8.2	0.82

(1) Calculated using the equations in Table 3-1.

(2) Based on the linear fit to the alluvial sediment data only.

(3) An order of magnitude lower than the longitudinal dispersivity.

(4) Two orders of magnitude lower than the longitudinal dispersivity.

Dispersivity is not an intrinsic property of the medium. In order to have a basis for predicting dispersivity from statistical distributions, its dependence on the scale of the measurement and on the type of test and method of analysis must be known. Such data are not available for the Hanford Site. The trends in dispersivity with travel distance are compiled from data obtained from locations around the world. As a result, the appropriate longitudinal dispersivity to apply at large scales for Hanford Site models has uncertainty associated with the range and distribution of data.

3.3.9 Adsorption

PNL-10899, *Strontium-90 Adsorption-Desorption Properties and Sediment Characterization at the 100 N-Area*, characterized the adsorption and desorption of strontium-90 for the 100-NR2-OU. Results showed a range of K_d values from 7 to 59 mL/g, and K_d decreases as the particle size of the sediment increases. In addition, K_d of 15 mL/g was estimated for bulk sediments more representative of actual field conditions. A more site-specific (i.e., 100-K) study was performed recently using samples collected at UPR-100-K-1 and 116-KE-3 for evaluating leaching characteristics of strontium-90 (ECF-100KR2-16-0127). A K_d value of 12 mL/g was recommended for use in evaluating the transport of strontium-90 for the 100-KR-4 OU. The K_d value assigned for strontium-90 in the 100-K GWFTM was 12 mL/g obtained from ECF-100KR2-16-0127, *Evaluation of Strontium-90 Leaching Characteristics from Borehole Sediment Samples Collected at UPR-100-K-1 and 116-KE-3 Crib within the 100-K Area of the Hanford Site*.

PNNL-17674, *Geochemical Characterization of Chromate Contaminant in the 100 Area Vadose Zone at the Hanford Site*, investigated the mobility of chromium in 100 Area sediments, and found that K_d was close to zero (retardation factor near 1). Therefore, Cr(VI) is considered not to sorb in this analysis. The remaining COPCs (i.e., carbon-14, nitrate, tritium, and TCE) were found to be highly mobile (PNNL-18564, *Selection and Traceability of Parameters to Support Hanford-Specific RESRAD Analyses: Fiscal Year 2008 Status Report*).

3.3.10 Contaminant Treatment System (CTS)

The P&T system in 100-KR-4 OU mainly focuses on treating Cr(VI) and recirculates other COPCs into the aquifer without any treatment through the injection wells. The process of extracting high concentration plume mass from the aquifer, mixing and treatment at the P&T facilities, and re-injecting the fully/partially treated water into the aquifer need to be included in the fate and transport simulation to track the recirculating contaminant mass. A CTS module was developed and added to the standard MT3DMS software to incorporate the processes related to the P&T system.

3.4 Flow Model Calibration

3.4.1 General Approach

MODFLOW solves the following mathematical-conceptual model:

$$\frac{\partial}{\partial x} \left(K_{xx} \frac{\partial h}{\partial x} \right) + \frac{\partial}{\partial y} \left(K_{yy} \frac{\partial h}{\partial y} \right) + \frac{\partial}{\partial z} \left(K_{zz} \frac{\partial h}{\partial z} \right) + W = S_s \frac{\partial h}{\partial t}$$

Where x , y , and z are Cartesian coordinate axes, K is the hydraulic conductivity coincident with each axis, W is water source or sink rate, S_s is specific storage, t is time, and h is hydraulic head (the state variable).

MT3DMS solves the following mathematical-conceptual model:

$$\frac{\partial(\theta C^k)}{\partial t} = \frac{\partial}{\partial x_i} \left(\theta D_{ij} \frac{\partial C^k}{\partial x_j} \right) - \frac{\partial}{\partial x_i} (\theta v_i C^k) + q_s C_s^k + \sum R_n$$

Where θ is effective porosity, t is time, x is Cartesian coordinate, C is concentration, k is transport component, D is dispersion tensor, v is groundwater velocity, q_s is water source/sink volume, C_s is source/sink concentration, and R_n is the chemical reaction term (i.e., aqueous-solid surface reaction or sorption and first-order rate reaction).

The transport equation is related to the flow equation by velocity determined from the hydraulic head computed by the flow model and Darcy's Law:

$$v_i = \frac{q_i}{\theta} = -\frac{K_i}{\theta} \frac{\partial h}{\partial x_i}$$

Transport model predictive power can be improved by:

1. Refining estimates of hydraulic conductivity by calibration to hydraulic head responses to river stage fluctuations.
2. Acquiring site-specific knowledge of effective porosity.
3. Incorporating hydraulic gradient estimates ($\partial h/\partial x_i$) and improving their model representation.
4. Incorporating independent estimates of velocity to act as an additional constraint on K , θ , and hydraulic gradient.

The ultimate use of the model is as a tool to evaluate potential groundwater remediation times and strategies. To improve the representation of the groundwater system for transport model development, the following approaches to address the items above were included.

- Ferris (1963) presents a conceptual model and analytic solution that allows estimation of hydraulic diffusivity (T/S), which could be used to independently estimate T , assuming S to supply a flow model constraint. Idealized assumptions include uniform aquifer thickness, completely penetrating river, great inland aquifer extent from its subcrop in the river, observation wells are far enough from the river to be unaffected by vertical flow, and that the range in fluctuations is a small fraction of the saturated thickness. As seen in Section 2 many of these assumptions are violated at 100-K. However, the conceptual approach is still useful when implemented within the framework of a numerical model that overcomes Ferris' simplifying assumptions. To this end AWLN data from 47 wells was used for flow model calibration because it provides a multiyear record of detailed aquifer water level changes responding to the Columbia River.
- PNNL-21845 estimated site-specific effective porosity of the Hanford formation at 0.18.

Figure 3-17 shows the location of the AWLN wells and manual measurement wells with respect to 2013 mapped Cr(VI) plume.

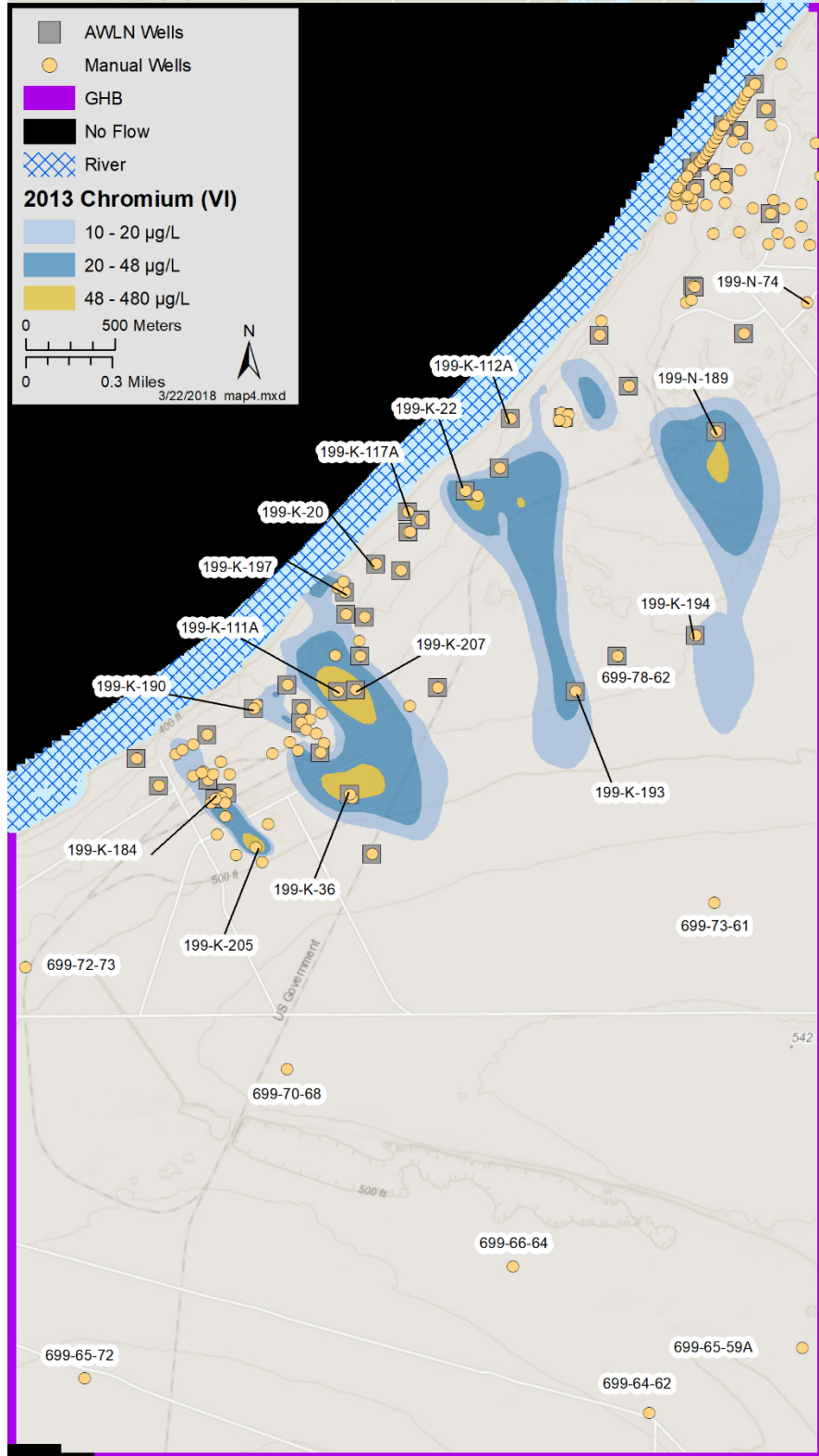


Figure 3-17. Calibration Features

The use of the AWLN data provides a constraint on the bulk aquifer properties that affect plume migration. It also can help identify different hydraulic diffusivity (T/S) paths that can be a surrogate for transport paths (Knudby and Carrera, 2006).

3.4.2 Parameter Estimation Framework

The PEST (Doherty, 2007) parameter estimation software was used to facilitate model calibration in concert with manual adjustments. The 2013 through 2016 calibration dataset incorporated the following elements:

1. Stress period averaged water levels from 47 AWLN wells (5701 total data points). These AWLN wells are spatially distributed across both KW and KE area and a significant portion of 100-N OU near the Columbia River. However, no AWLN wells occur in the southern portion of the 100-K GWFTM
2. Manual water level measurements from 171 wells (2308 data points). Wells with manual measurement data covers more area than the AWLN wells. It includes four wells near the southern boundary and one well each near western and eastern boundary. Manual measurement well list also includes the measurements recorded from some of the pump and treat operation system during the pumping shut down events.
3. Change from initial observed water level for 47 AWLN wells (5701 total data points).

All the available observed water level data were examined and cross-referenced with nearby well data and measurement methods (i.e., AWLN vs manual measurement) prior to including in the calibration dataset. The outliers or noisy data were given zero weight during calibration so that those measurements do not contribute to the objective function. Below is a brief description of the water level measurement that were considered noisy:

- Well 199-K-108A: The AWLN data from 7/9/2015 thru 12/31/2016 are useable for calibration. Earlier data are either missing or don't match the manual measurements.
- Well 199-K-118A: The AWLN data from 1/3/2013 thru 2/4/2014 are quite noisy although the underlying trend looks fine. The data from 2/4/2014 thru 12/31/2016 are good and they compare well with the manual measurements. However, the head in this well is higher than expected for this well's location. The heads at two nearby wells (199-K-117A and 199-K-21) are about 2 m less than the head at 199-K-118A. This well was examined several times with regard to water table mapping and was considered valid. There has been no change to the casing elevation or any other change to the well itself that would account for the higher water level. The water level elevation increased about 2 to 3 m from late 2008 into 2010. This could be due to response from the injection of water to the south at injection wells 199-K-169, 199-K-170, and 199-K-179.
- Well 199-K-125A: This well is located very close to well 199-K-118A. The manual water level measurements are around 2 m higher than the other nearby wells similar to 199-K-118A. As mentioned above, these data were considered valid to be included in the calibration dataset.
- Well 199-K-142: The early AWLN data for this well are either missing or not valid. The data from 6/16/2014 thru 2/18/2015 and 3/19/2015 thru 12/31/2015 are good and can be used for calibration. The data become noisy near the end but still look reasonable. Data are missing from 2/18/2015 to 3/19/2015.
- Well 199-K-151: The early AWLN data from 1/3/2013 thru 3/14/2014 have numerous data quality issues and periods of missing data. The data from 3/14/2014 thru 12/31/2016 are good.

The AWLN measurements are biased high compared to the manual measurements, but only by about 0.1 m so the data should still be useful for calibration (the 4/18/2014 manual measurement is an outlier).

- Well 199-K-32A: Much of the AWLN data for this well are not useable. The data from 1/1/2013 thru 2/18/2015 exhibit poor agreement with the manual measurements and there are many data gaps. However, the data from 2/18/2015 thru 12/31/2016 agree well with the manual measurements, so the data for this period can be used for calibration.
- Well 699-78-62: The AWLN data prior to 2/17/2015 are mostly missing, and what is not missing doesn't agree with the manual measurements. However, the data from 2/17/2015 thru 12/31/2016 are good and agree well with the manual measurements (the 7/16/2015 manual measurement is an outlier). Some data appear noisy because this well is located only about 5 m from injection well 199-K-172, so it responds very quickly to changes in the injection rate.

If a well is completed in confined units beneath the uppermost mud layer, the water level data for that well was not included in the calibration dataset. In addition, water level data was not included for the wells that are drilled to 100 ft or more and open to the basalt aquifers. Such wells include 199-K-192, 199-K-32B, 199-N-80, 699-81-62, and 699-84-59.

The deviation between observed and simulated values (objective function) is mathematically minimized using singular value decomposition with regularization as described by Doherty (2007). Weights were assigned to account for magnitude and contribution to the objective function.

The overall calibration process was as follows:

- Run the PEST software
- Review estimated model parameters and model fit to data for reasonableness and agreement
- Identify potential conceptual or parameter issues to be resolved and an approach
- Implement parameter, model setup, or other change
- Repeat

PEST provides several outputs of the process, including a file listing the residual between simulated and observed data. This was used to review goodness of fit. No absolute value of goodness of fit was set as a stopping criterion; an overall weight of evidence was considered including goodness of fit and plausibility of estimated parameters.

A qualitative transport evaluation was also conducted as part of this cycle with the criteria of matching interpreted chromium plume migration between 2014 and 2016 as documented by maps produced every fall as part of annual groundwater or other reports. Flow models were adjusted to preserve the interpreted chromium plume trajectory and velocity even at the expense of better fitting hydraulic data. The ultimate model use is for transport and this is judged to be an acceptable compromise.

3.4.3 Flow Model Calibration Results

A plot of observed versus simulated hydraulic head from the AWLN network is shown in Figure 3-18. The same data for manual water levels is shown in Figure 3-19. Appendix B shows the hydrographs of observed and simulated head for each calibration well. In general, the simulated head matched well with observed head. Both the wells near the river and the inland area show good match except some wells near the river. The model was able to capture the overall trend at well 199-K-118A but was off by around 1.75

to 2.0 m consistently throughout the simulation period. As described in section 3.4.2, the observed higher head in this well compared to the nearby wells are well known and no further calibration was done to improve calibration at this location in absence of additional site-specific information. Similarly, well 199-K-125A which is very close to well 199-K-118A simulates consistently lower heads. Well 199-K-117A and 199-K-21 are located near well 199-K-118A and the model captures the overall observed trend but could not match some lower heads during low river stage.

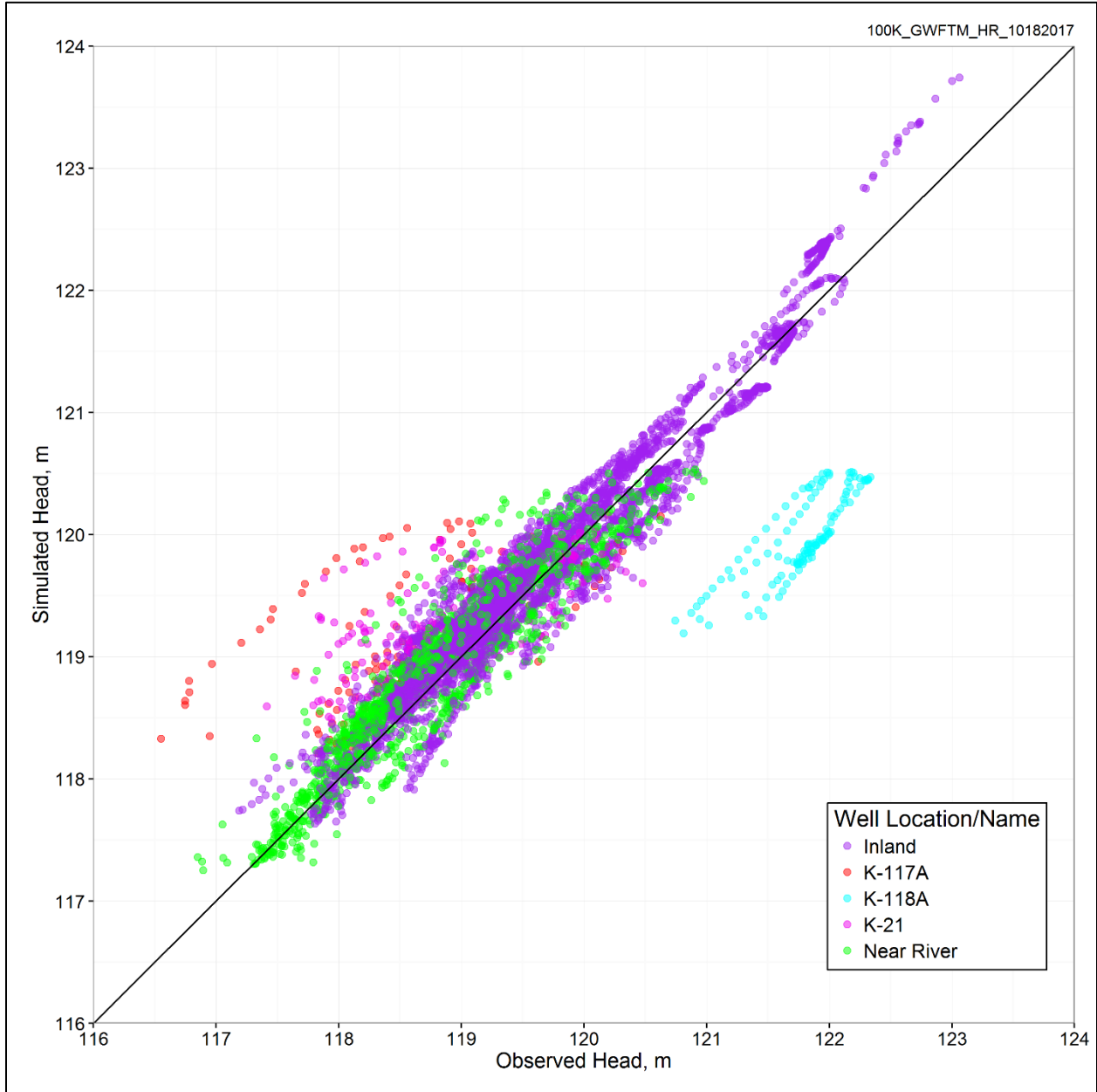


Figure 3-18. Observed Versus Simulated AWLN Heads

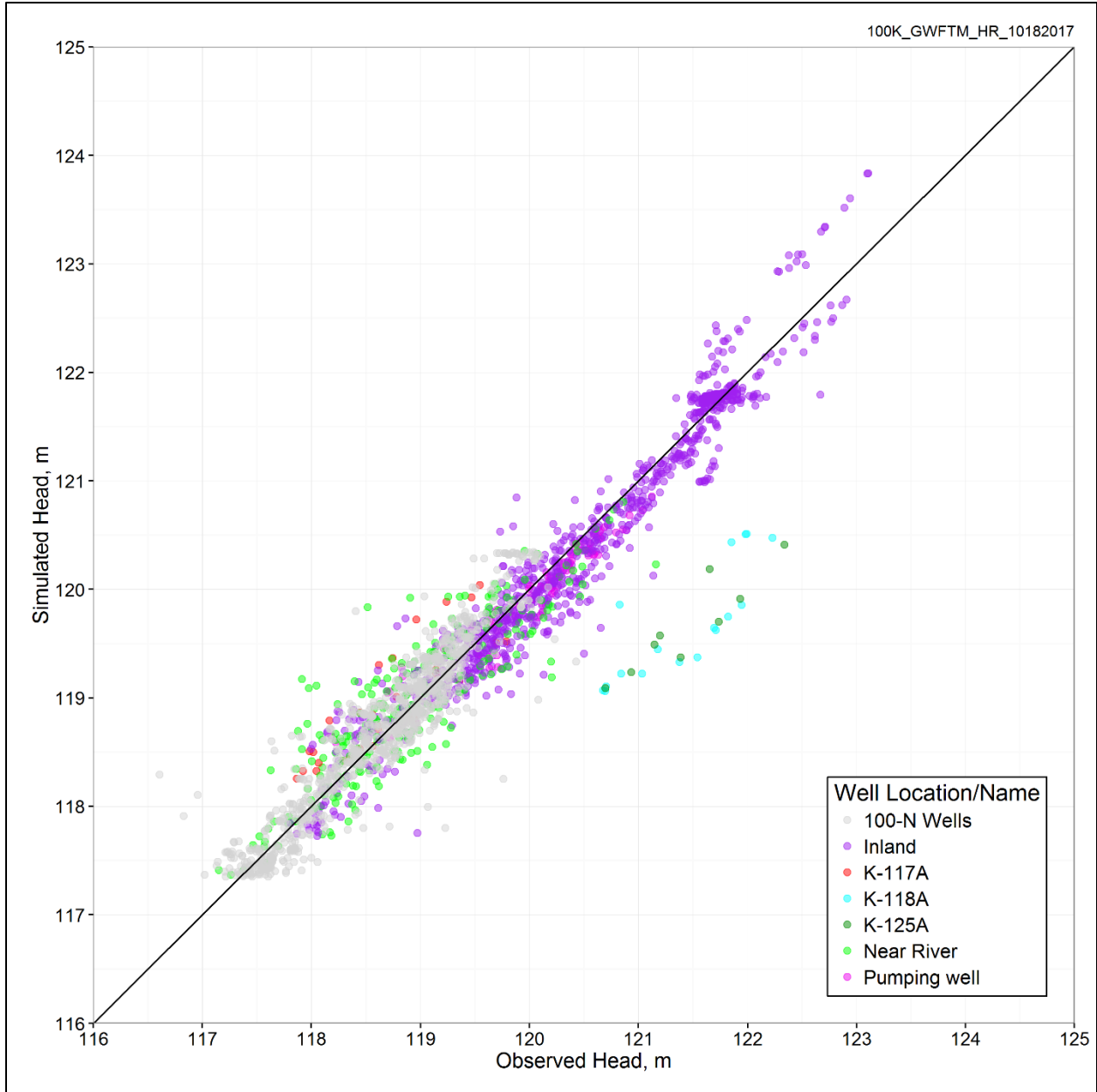


Figure 3-19. Observed Versus Simulated Manually Measured Heads

3.4.4 Qualitative Flow Model Evaluation

In addition to quantitative metrics a qualitative check on the flow was performed by comparing the interpreted flow field from groundwater annual reports to the simulated flow field. Figure 3-20 and Figure 3-21 show the interpreted water table from the 2015 and 2016 annual groundwater monitoring reports and the simulated results for the same times. Agreement is qualitatively good with very low hydraulic gradient (no contours) in the south and higher hydraulic gradient to the north with flow converging on the river.

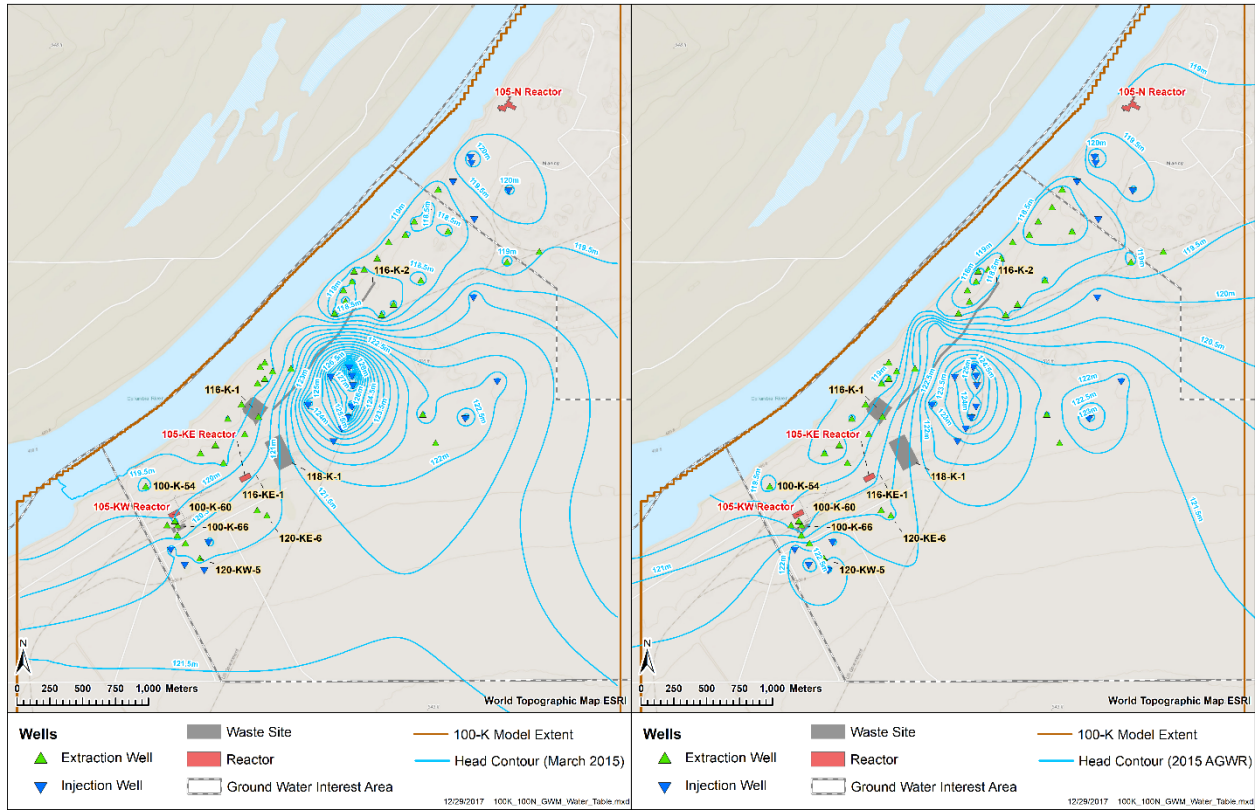


Figure 3-20. March 2015 Annual Groundwater Monitoring Report (Right) and Model Simulated (Left) Maps

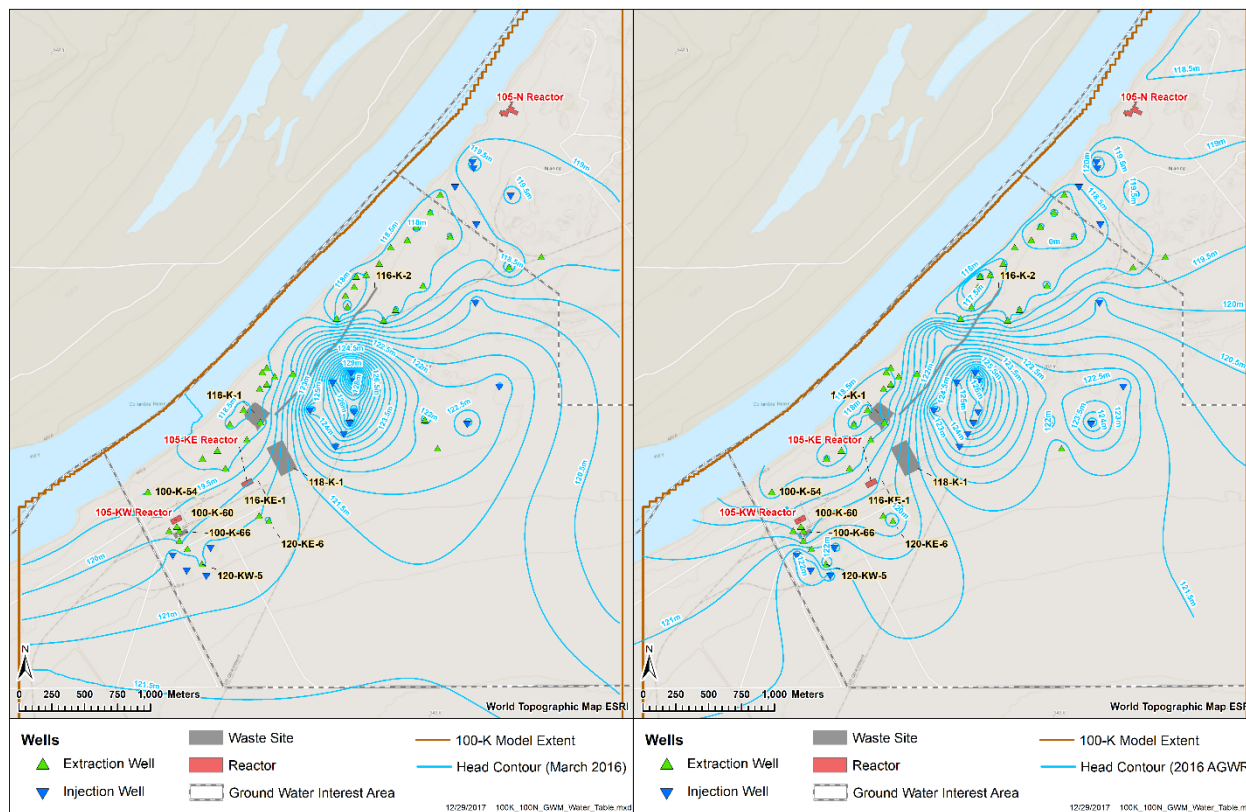


Figure 3-21. March 2016 Annual Groundwater Monitoring Report (Right) and Model Simulated (Left) Maps

3.4.5 Calibrated Flow Model Properties

Properties estimated as single values over some or all of the model domain are shown in Table 3-3.

Table 3-3. Single-Value Parameter Estimates

Parameter	Value
Specific yield	8.16×10^{-2}
Specific storage (1/m)	1.01×10^{-5}
Hanford vertical to horizontal hydraulic conductivity ratio	0.011
Ringold E vertical to horizontal hydraulic conductivity ratio	0.055
Ringold E riverbed hydraulic conductivity (m/d)	123.9

Figure 3-22 through Figure 3-25 show model layer calibrated hydraulic conductivity along with the 2013 Cr(VI) plume 10, 20, and 48 $\mu\text{g/L}$ contours and AWLN monitoring wells (shown regardless of layer). The saturated zone in the southern portion of the 100-K GWFTM (i.e., 200-BP-5 OU) contains both Hanford and Ringold E formations whereas water table in the northern portion (i.e., 100-K and 100-N) of the

model lies solely within Ringold E. The calibrated hydraulic conductivity within 100-K OU varies from 1.5 to 43 m/d. These values are within acceptable range for the hydraulic conductivity in the Ringold E and are consistent with pumping/slug test results. The calibrated hydraulic conductivity within 100-N OU varies from 3.0 to 86 m/d. The upper bound is higher than the expected hydraulic conductivity for Ringold E. The higher values of Ringold E are prominent in the north-east corner of the model. The calibrated hydraulic conductivity for Hanford formation in the southern portion of the model is 1,494 m/d. The highly conductive inferred paleo-channel in the Hanford Site is expected to pass through the southern portion of the model domain although the extent of the channel is not precisely known. Therefore, hydraulic conductivities of thousands m/d are expected in some portion of the Hanford formation. Only one hydraulic conductivity value for Hanford formation was calibrated due to the lack of water level measurement coverage in the southern portion of the model. The well hydrographs in these areas show good qualitative responses, and if the geologic interpretation is correct, all the groundwater flow in the Hanford must pass into and through the Ringold E. This area is where the Hanford formation saturated thickness is declining from a maximum of 30 m to under 5 m. Thus, the Ringold E must have higher transmissivity to accommodate groundwater flow from the Hanford formation and still replicate groundwater potentials. Slight misidentification of the Hanford/Ringold E contact, especially if the Hanford deposits are cataclysmic flood gravels, would have a large impact on transmissivity given the approximate two orders of magnitude difference in hydraulic conductivity.

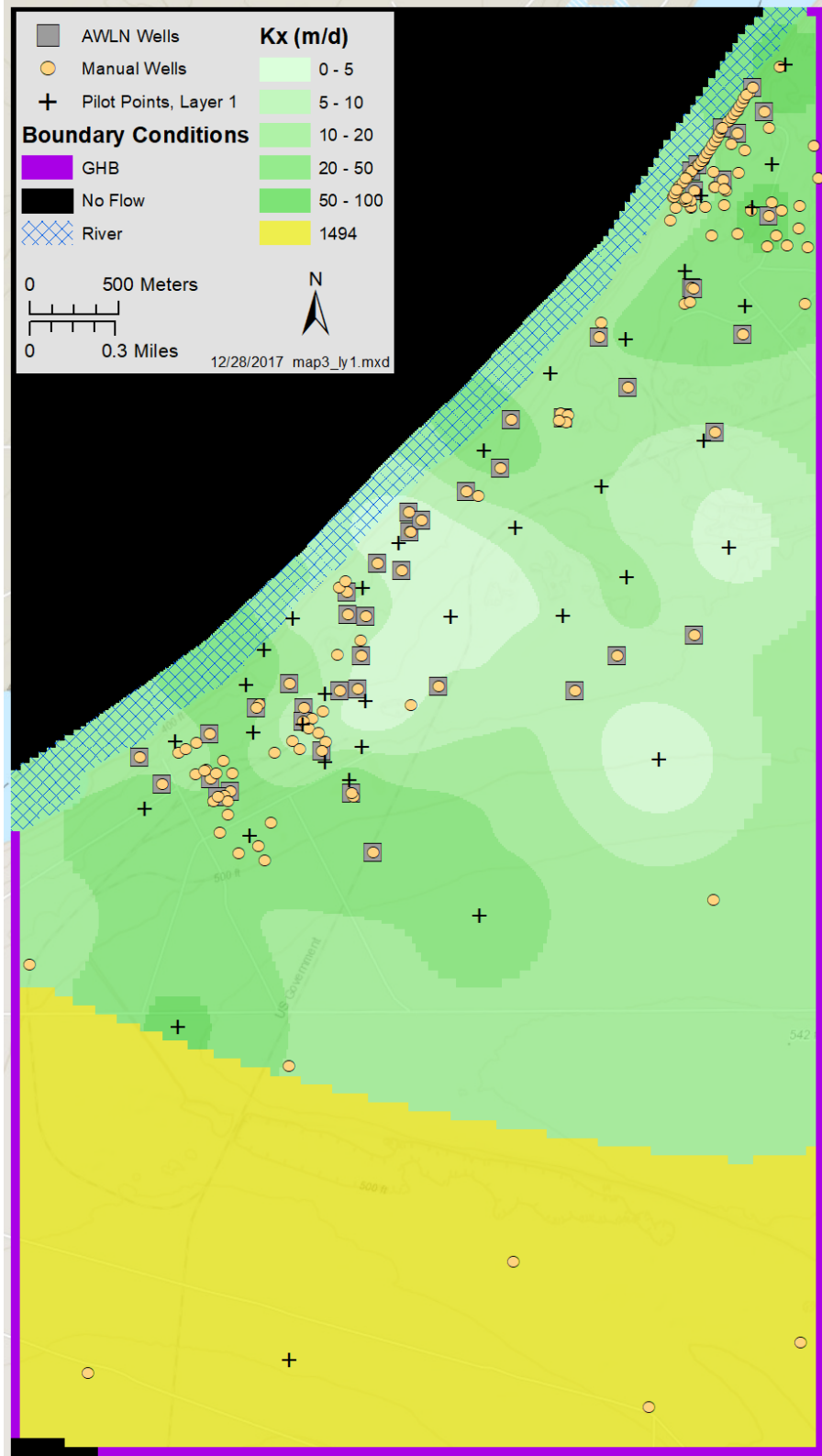


Figure 3-22. Layer 1 Hydraulic Conductivity

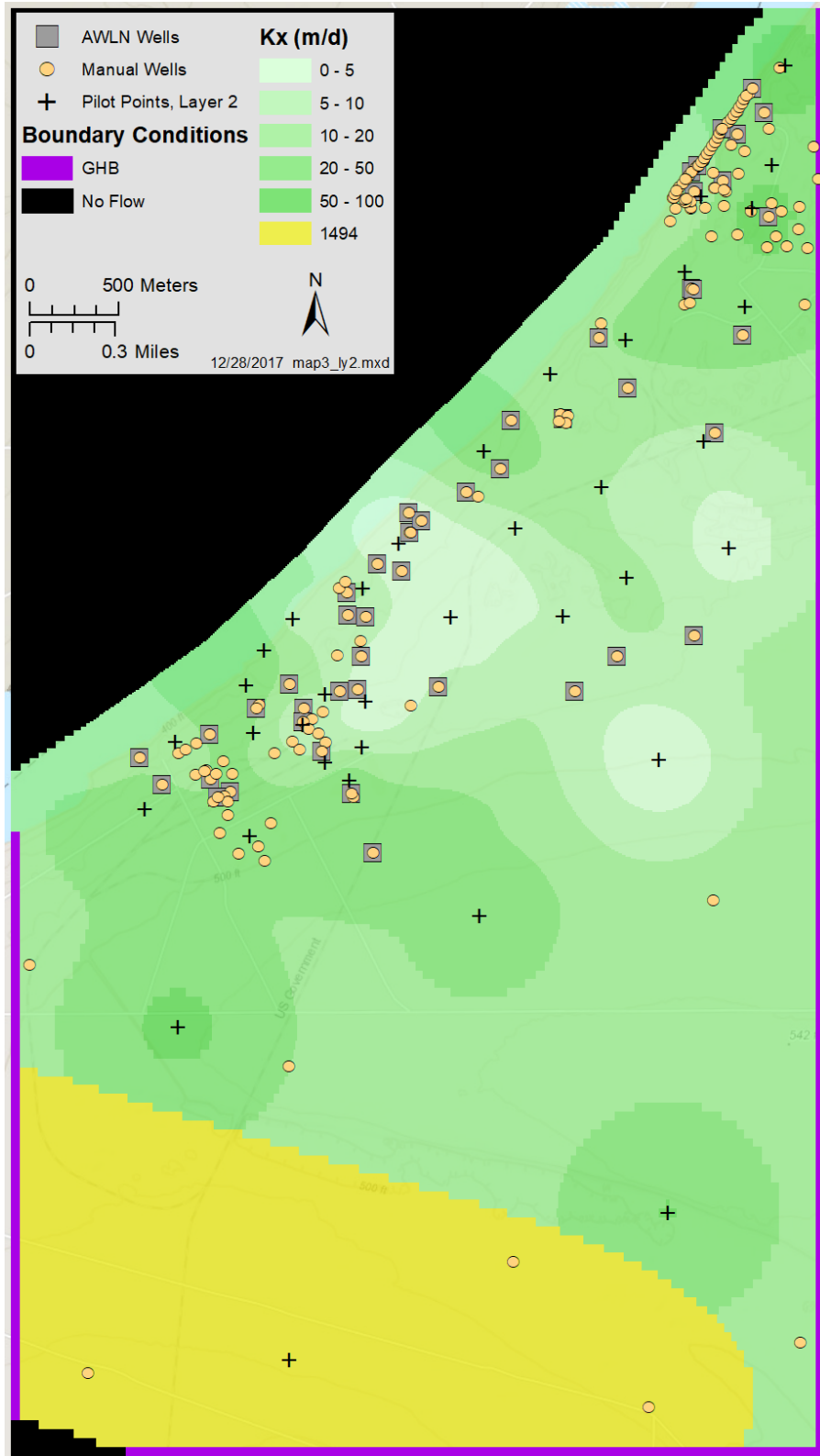


Figure 3-23. Layer 2 Hydraulic Conductivity

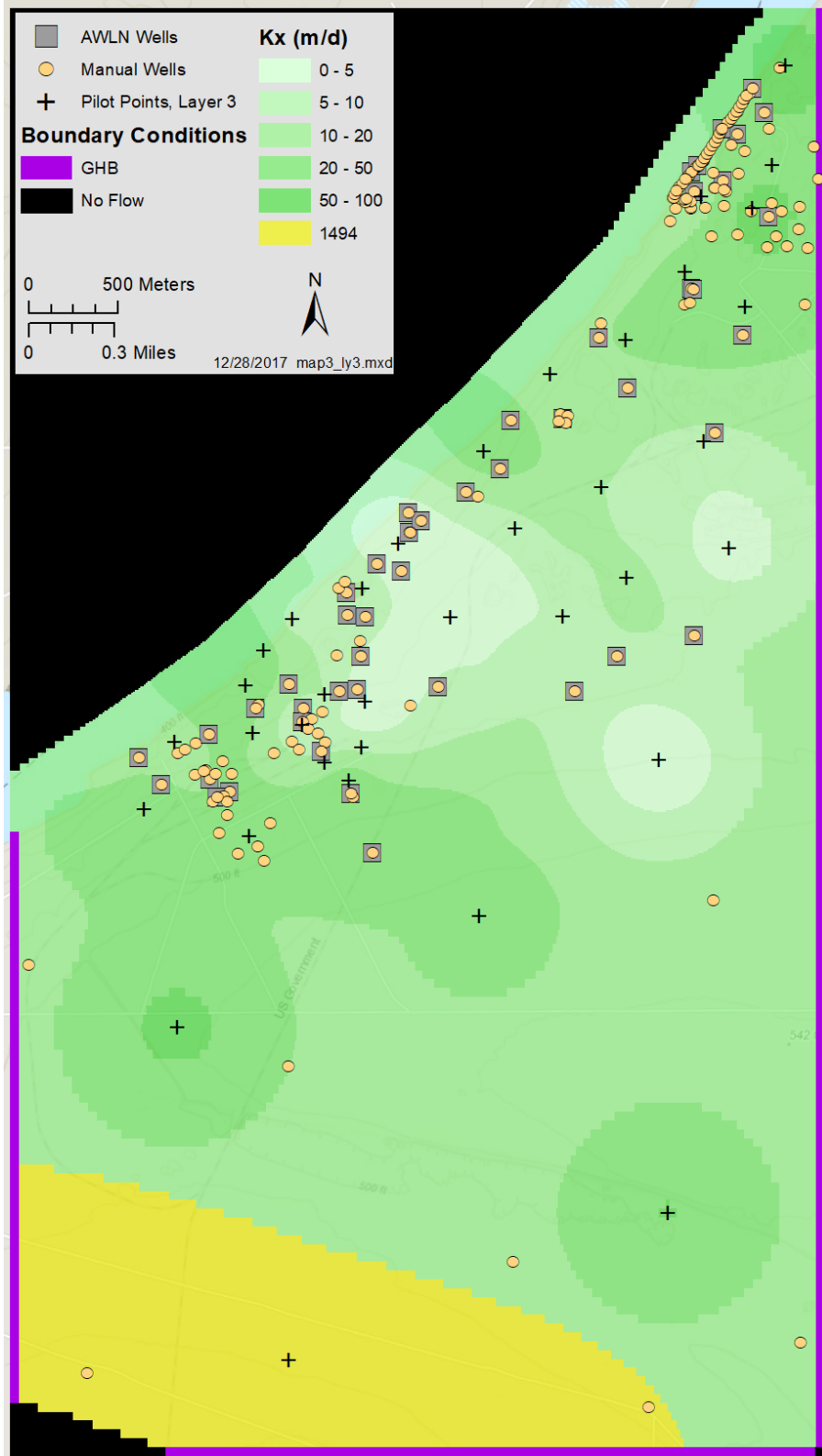


Figure 3-24. Layer 3 Hydraulic Conductivity

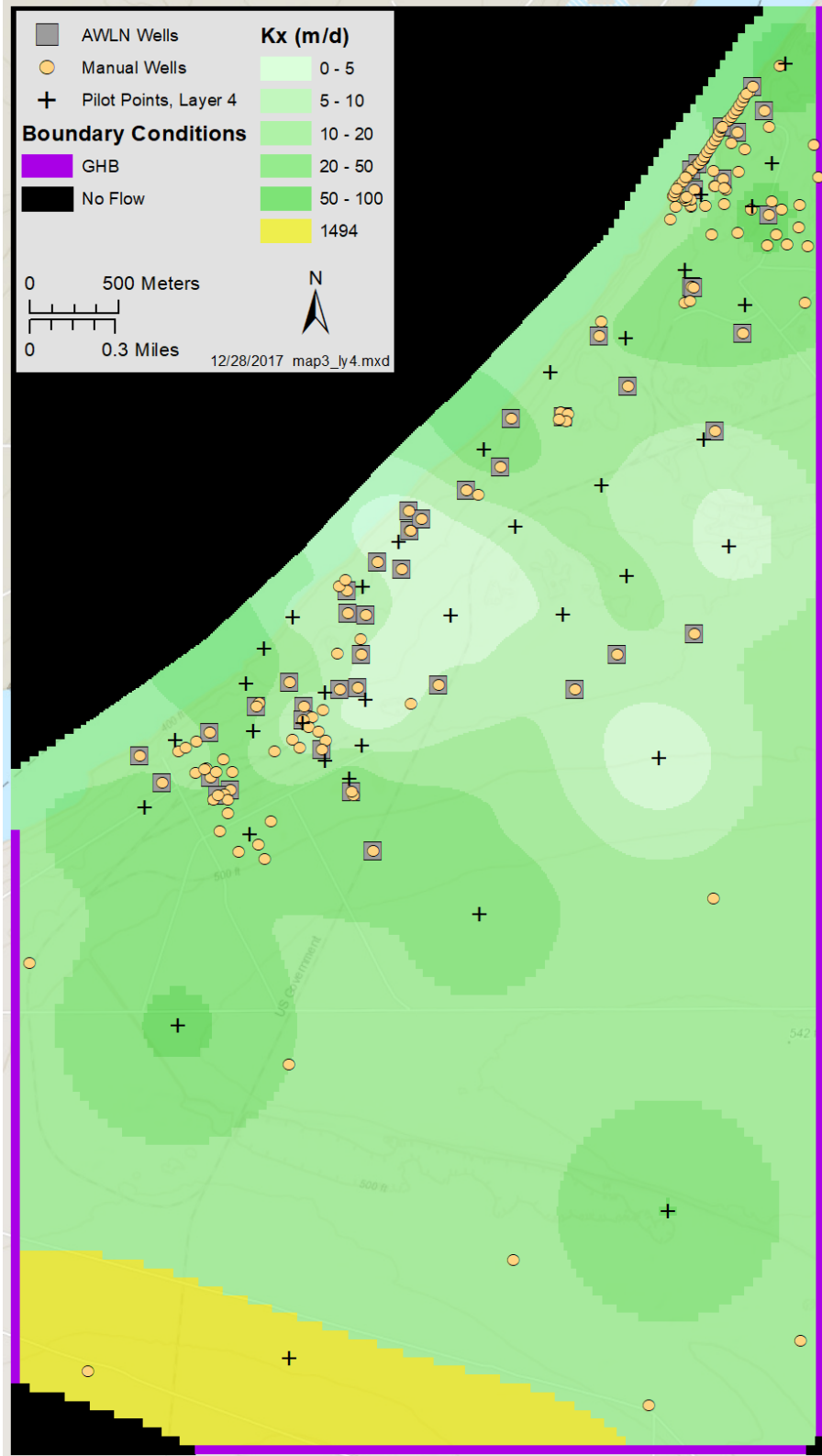


Figure 3-25. Layer 4 Hydraulic Conductivity

3.5 Transport Model Calibration

Transport calibration was mostly focused on the potential continuing source locations and initial concentration that was inferred from the annual groundwater monitoring report. As described in section 3.3.5, 2D concentration plumes reported in the annual groundwater monitoring report between 2012 and 2015 were examined to select most representative initial concentrations for the transport models. No further calibration was performed to initial concentrations for all the COPCs except hexavalent chromium. Possible continuing source locations for each COPC were identified based on prior knowledge, and observed groundwater concentrations over the years. The upper vadose zone of significant number of waste sites at the 100-K area was excavated as part of the DOE's remedial action goals. However, no soil remediation of the deep vadose zone was performed. Moreover, no characterization of the deep vadose zone is available for the waste sites within 100-K area. Scarcity of information on the areal extent, vertical distribution, and strength of the soil contamination had made it difficult for a comprehensive vadose zone modeling for estimating contribution from the continuing sources to the groundwater at the potential source locations. Therefore, a simple one-dimensional soil column was simulated for estimating a characteristic release rate curve for each COPC at each potential source location. These characteristic release rate curves are based on a unit source concentration in the soil column. An upscaling/downscaling of these release rate curves was performed using PEST to calibrate on the observed groundwater concentration at or near the source locations. A similar approach was followed for estimating vadose zone contribution to the groundwater for strontium-90 at 100-BC-5 OU (ECF-100BC5-16-0051, Rev. 0, *Calibration of Continuing Source for Strontium-90 in the 100-BC-5 Operable Unit*).

3.5.1 Vadose Zone Modeling

The vadose zone calculation is performed with models implemented in the STOMP fate and transport simulation software (PNNL-11216, *STOMP Subsurface Transport Over Multiple Phases: Application Guide*; PNNL-12030, *STOMP Subsurface Transport Over Multiple Phases: Theory Guide*; PNNL-15782, *STOMP Subsurface Transport Over Multiple Phases: Version 4.0: User's Guide*). STOMP one-dimensional (1D) model framework used in this analysis is identical to that used in ECF-100KR1-17-0087, *Determination of Soil Screening Levels and Preliminary Remediation Goals for Waste Sites in the 100-K Source Operable Units*. However, a few changes were made to the STOMP 1D model framework so that the parameters were consistent with the 100-K GWFTM.

3.5.1.1 Identification of Vadose Zone Source Area

The 105-KE and 105-KW Reactors were the largest production reactors at the Hanford Site. Leaks from these reactors and their support facilities are responsible for the groundwater contamination in 100-KR-4 OU. Contaminated soil at a handful of waste sites, known as suspected leakers, were cleaned up as part of Remedial Action Goal at the 100-K area. Most of these cleanup operations were limited to the shallow vadose zone. However, persistent groundwater plume near some waste sites indicated the presence of continuing sources from the deep vadose zone to the groundwater. The details on the operational history, waste releases, and potential continuing sources are described in the previous 100-K RI/FS ((DOE/RL-2010-97, *Remedial Investigation/Feasibility Study for the 100-KR-1, 100-KR-2, and 100-KR-4 Operable Units*, Draft A) and *Hanford Site Groundwater Monitoring Report for 2015* (DOE/RL-2016-09). Based on the prior knowledge about the waste sites suspected to have contributed to groundwater contamination and groundwater concentration data at the nearby wells, nine waste site locations were identified and selected for the STOMP 1D simulation. Table 3-4 lists all the waste sites with their associated COPCs.

Table 3-4. List of Waste Sites for Potential Continuing Sources to the Groundwater

Primary Waste Site	Nearby Related Waste Sites	Operational History	COPCs	Nearby wells	Cleanup Status
183.1KW Headhouse	120-KW-5, 100-K-18, 100-K-19, 100-K-21, 100-K-79, 100-K-97	Unplanned releases of the sodium dichromate dihydrate solution during transfer and material handling events along with some intentional releases to the ground during cleaning of tanks and conveyance lines	Cr(VI)	199-K-205	Contaminated soil was excavated up to 10.96 m from ground surface (DOE/RL-88-30)
183.1KE Headhouse	120-KE-6, 100-K-58, 100-K-79, 100-K-101, 100-K-123	Some sodium dichromate dihydrate solution remained in tank farm pipelines and was released during demolition of the headhouse	Cr(VI)	199-K-36, 199-K-188, 199-K-220	Site was not excavated
165-KW and 190-KW	100-K-59, 100-K-60, 100-K-66	Possible migration of sodium dichromate dihydrate solution from 183.1KW headhouse	Cr(VI)	199-K-173	Site was not excavated
116-KW-1 crib	100-K-47, 100-K-54, 100-K-61	Discharges of condensate generated by the reactor gas dryer system	C-14, nitrate, tritium	199-K-106A, 199-K-204	Contaminated soil was excavated up to 9.1 m from ground surface (DOE/RL-88-30)
116-KE-1 crib		Discharges of condensate generated by the reactor gas dryer system	C-14, nitrate, tritium	199-K-222	Contaminated soil was excavated up to 9.1 m from ground surface (DOE/RL-88-30)
105-KW FSB	116-KW-2 crib/reverse well, 100-K-43	Contamination of water in the FSB by fuel ruptures entered the FSB during reactor defueling operations	Strontium-90	199-K-107A, 199-K-34	Site was not excavated
105-KE FSB	100-K-42, UPR-100-K-1, 116-KW-2 crib	Same as 105-KW FSB but substantially more contaminated	Strontium-90, tritium	199-K-221, 199-K-222	Contaminated soil was excavated up to 8.5 m near well 199-K-221 and 4.5 m near well 199-K-222

Table 3-4. List of Waste Sites for Potential Continuing Sources to the Groundwater

Primary Waste Site	Nearby Related Waste Sites	Operational History	COPCs	Nearby wells	Cleanup Status
116-K-2 trench	116-K-1		Strontium-90	199-K-200	Contaminated soil was excavated up to 7.6 m from ground surface (116-K-2 CVP)
118-K-1 burial ground		Contaminated solid waste disposed at the burial ground	Tritium	199-K-111A, 199-K-207	Contaminated soil was excavated up to 12.2 m from ground surface (DOE/RL-88-30)
DOE/RL-88-30, Hanford Site Waste Management Units Report. CVP-2006-00001, Cleanup Verification Package for the 116-K-2 Effluent Trench.					

Most of the selected waste site locations are not well characterized to define the lateral extent of these continuing sources. In addition, the plumes beneath these locations are not well defined due to insufficient monitoring wells around the sources. Therefore, the lateral extent of the continuing sources was calibrated only to satisfy the observed concentration at the nearby wells. That means if a downgradient well is not impacted by an upstream source it was not included to the continuing source boundary. However, it is possible that there is a continuing source which is not captured by the downgradient monitoring wells. Figure 3-26 and Figure 3-27 show the potential continuing source locations for all the COPCs at KW, and KE area, respectively.

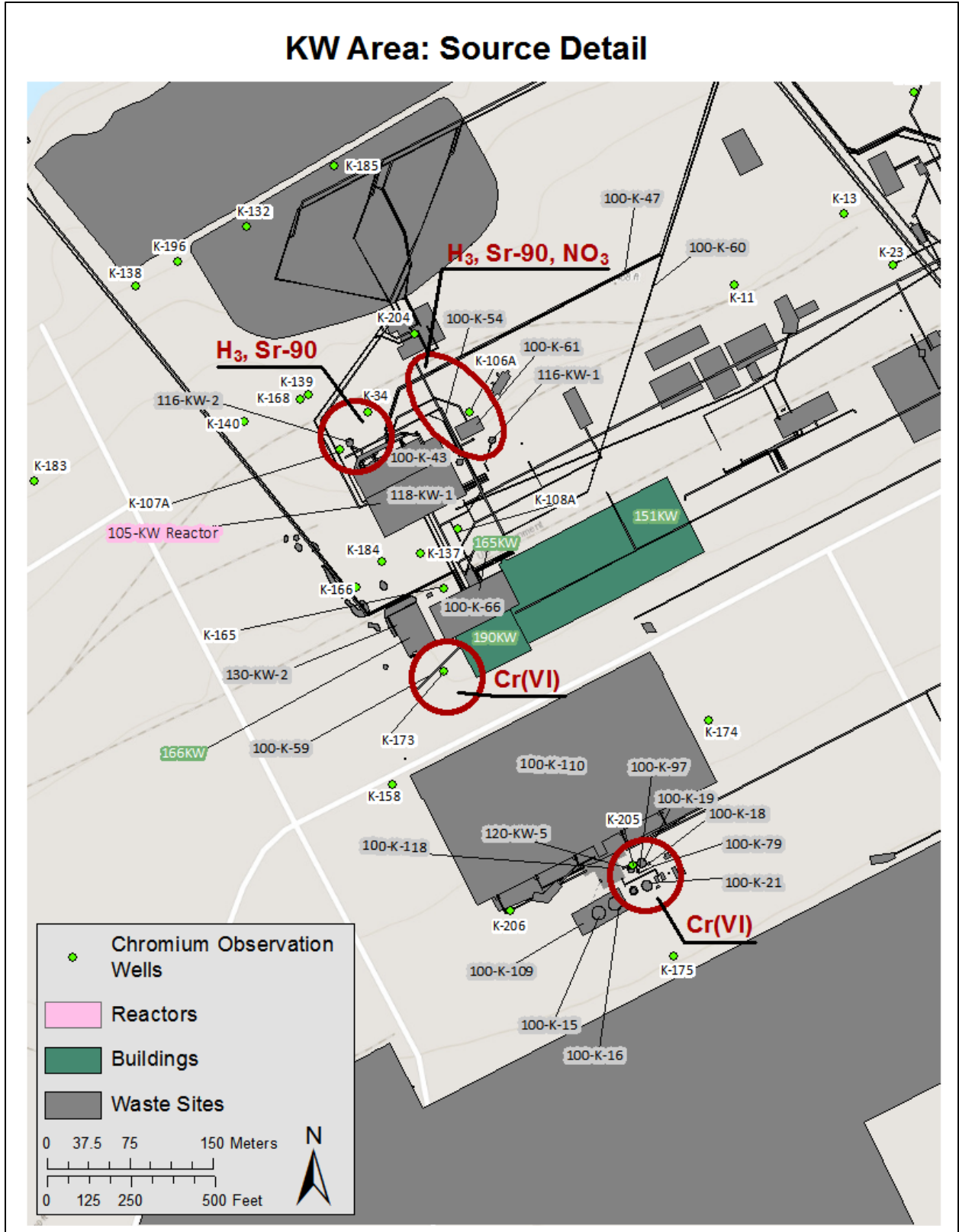


Figure 3-26. Potential Continuing Source Locations at KW Area

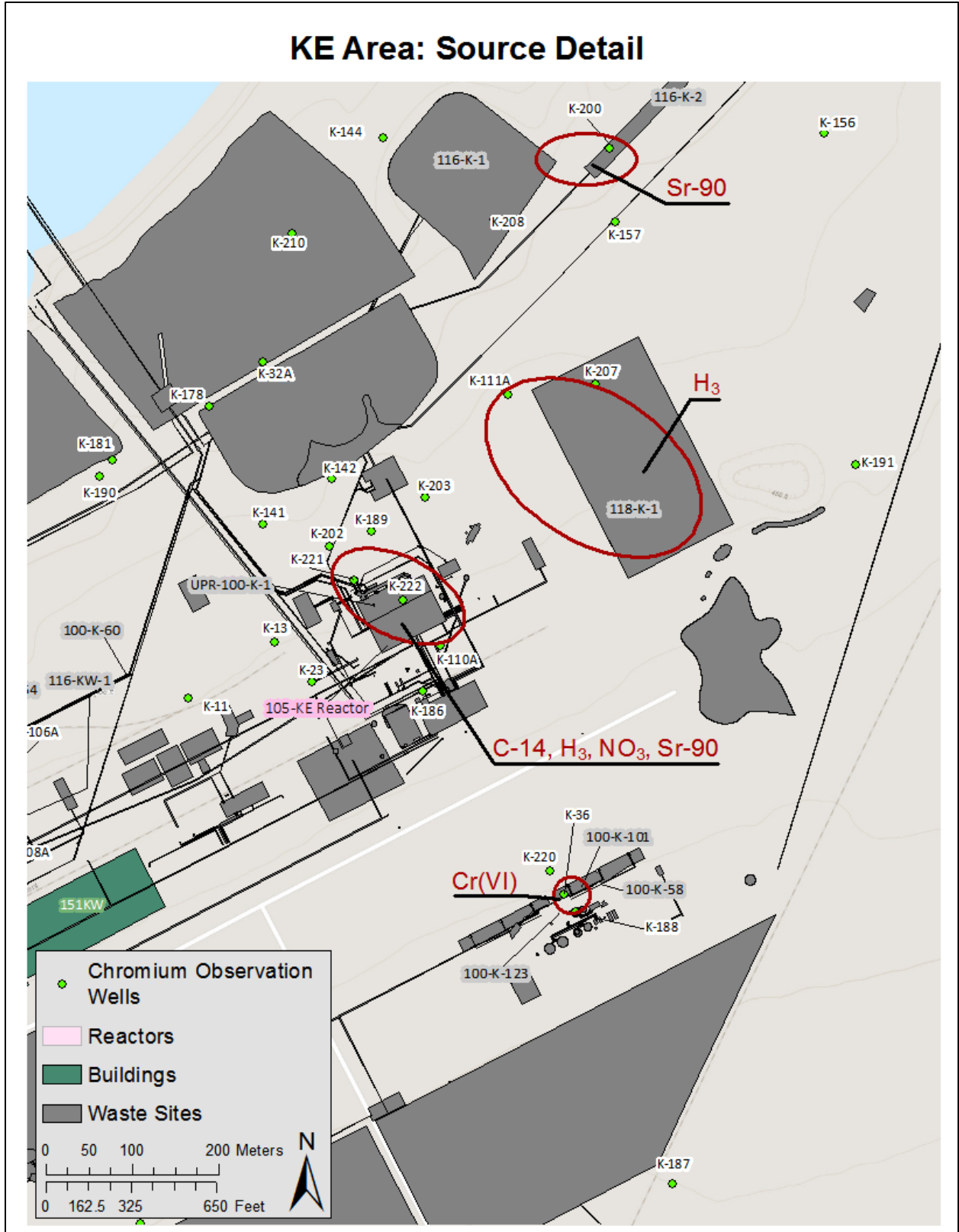


Figure 3-27. Potential Continuing Source Locations at KE Area

3.5.1.2 Identification of Representative Stratigraphic Columns

Two lithologic units are present in the vadose zone in the 100-K source area. These are the gravel-dominated Hanford formation and the Ringold Formation unit E. The Ringold E contains a slightly smaller percentage of coarse-grained sediments and a higher percentage of finer-grained sediments than the Hanford formation (SGW-40781, 100-HR-3 Remedial Process Optimization Modeling Data Package; SGW-46279, *Conceptual Framework and Numerical Implementation of 100 Areas Groundwater Flow and Transport Model*). It's important to identify the thickness of the vadose zone and the location of the Hanford-Ringold E contact within the vadose zone for estimating a characteristic release rate curve for each COPC at each waste site. The 100 Area GFM (ECF-HANFORD-13-0020, Rev.3) was evaluated at the selected waste site locations to get the representative vadose zone thickness and HSU contacts. Then, STOMP 1D model grid were created for these representative columns. Figure 3-28 shows the representative stratigraphic columns at each source area.

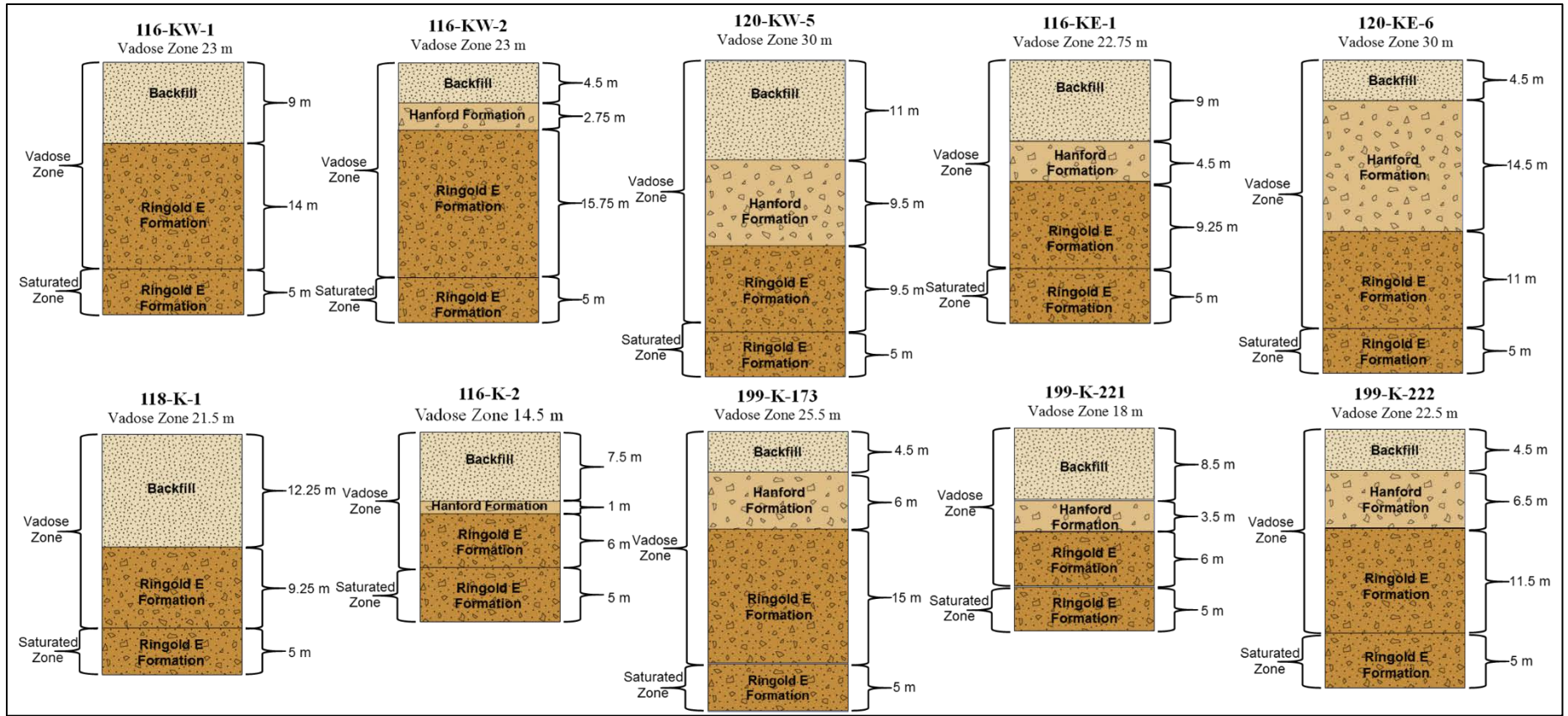


Figure 3-28. Representative Stratigraphic Columns for the Selected Waste Site Locations

The water table elevations from 2014 annual groundwater monitoring report (DOE/RL-2015-07) was used to define the saturated zone in the STOMP 1D column. However, a fluctuating water table boundary condition was used to simulate the periodically rewetted zone (PRZ).

3.5.1.3 *Calculating Characteristic Release Rate Curve*

STOMP is used to solve for water flow and contaminant transport in each of representative stratigraphic columns, under specified recharge scenario, for the appropriate initial uniform concentration of contaminant, for each COPC, for a pair of sequential simulations. The first simulation in this sequential pair is of water flow only for historic recharge conditions, and was needed to obtain the soil moisture conditions throughout the model domain at the start time for the second simulation. The second simulation in the sequential pair is of water flow and contaminant transport for future recharge scenarios, starting from the imposed initial contaminant distribution and the initial soil moisture conditions provided by the first simulation. The second simulation provided solute mass entering the aquifer and exiting the downgradient boundary with the groundwater flow for each representative stratigraphic column under the specified recharge scenario and for each COPC.

All the features and processes of the 1D STOMP model (e.g., hydraulic properties, saturation function parameters, boundary conditions, and initial conditions) were kept as same as ECF-100KR1-17-0087 with few exceptions so that 1D STOMP model is consistent with the 100-K GWFTM. These exceptions are as follows:

1. **Boundary Conditions:** Water level in the 100-K OU fluctuate in response to the Columbia River stage fluctuations. Groundwater gets in contact with the contaminated vadose zone near the water table as the water level rises and increases the solute concentration in the groundwater. The transition between vadose zone and saturated zone due to water table fluctuation is known as PRZ. A fluctuating water table boundary condition was applied to all the STOMP 1D models to represent influence of PRZ to the continuing source. The time varying water table at each waste site location was extracted from the calibrated 100-K groundwater flow model.
2. **Initial Concentrations:** Characterization of the deep vadose zone in the 100-K OU is very minimal to nonexistent. Some of the waste sites were excavated and soil concentration at the bottom of the excavation were reported (Table 3-4). Therefore, defining a representative vertical distribution of initial concentration in a soil column is very difficult. The initial concentration is a major driver for determining the breakthrough and the shape of the characteristic release rate curve. If the soil column below the backfill is assumed to be fully contaminated it would take hundreds of years to flush out the mass from the vadose zone and would be considered as too conservative. Measured concentration at the bottom of some of the excavated sites showed lower concentrations. Therefore, it was assumed that the lower 50% of the vadose zone (i.e., the lower half of the bottom of the backfill to the average water table) is contaminated and concentration is uniform throughout the soil column. The only exception was strontium-90 at the 100-KE FSB. Depth discrete soil concentration data is available for the newly drilled wells 199-K-221 and 199-K-222. This dataset was used for the evaluation of strontium-90 leaching characteristic from the collected contaminated sediment samples (ECF-100KR2-16-0127, Rev.0). The same dataset was used for estimating a characteristic release rate curve at the 100-KE FSB.
3. **Recharge Rates:** 100-K GWFTM uses the RET to develop the recharge boundary conditions as described in Section 3.3.1. For consistency, the recharge rates at each waste site was extracted from the 100-K GWFTM to be used as recharge boundary conditions for the STOMP 1D simulations.

4. Simulation Period: To be consistent with the 100-K GWFTM, STOMP 1D models were simulated in 2 parts: calibration model (2014 to 2016 or only 2016, depending on the COPC), and 125-year predictive model (2018 through 2142).

For the solute mass conservation equation, specified zero-flux boundaries were applied at the top of the model domain, along both edges of the vadose zone except the downgradient portion in the PRZ, along the upgradient edges of the aquifer grid blocks, and the bottom of the aquifer (Section 3.2 in ECF-100KR1-17-0087). The downgradient edges of the aquifer grid blocks were assigned STOMP's outflow solute type boundary condition (see page 6.21 of PNNL-12030, and page 4.4 of PNNL-15782), which transports solute mass out of the domain according to the advective flux term in the solute mass conservation governing equation but does not allow solute to enter back into the domain. The natural recharge flux drives the contaminant in the vadose zone downward towards the water table. Moreover, the contaminant in the PRZ dissolved in groundwater when the fluctuating water table was in contact with the contaminant. These solute masses are captured at the only downgradient outflow boundary and written to a surface flux file, one of STOMP's standard output options. For each time step, STOMP writes the water mass and solute mass flux rates passing through the downgradient surface as well as the cumulative water and solute mass that have passed through the surface. A python script is used for calculating MODFLOW stress period length based average release rate from STOMP surface output file. Figure 3-29 shows the stress period averaged characteristic release rate curves at the Cr(VI) continuing source locations and a few selected waste sites for other COPCs during the calibration period. The characteristic release rate curves for the predictive model at same waste sites and COPCs are shown in Figure 3-30. All the characteristic release rate curves show similar behavior. That is, release rate increases as the water level increases and release rate decreases as the water level decreases. A scaling factor for these characteristic release rate curves were used during transport calibration process.

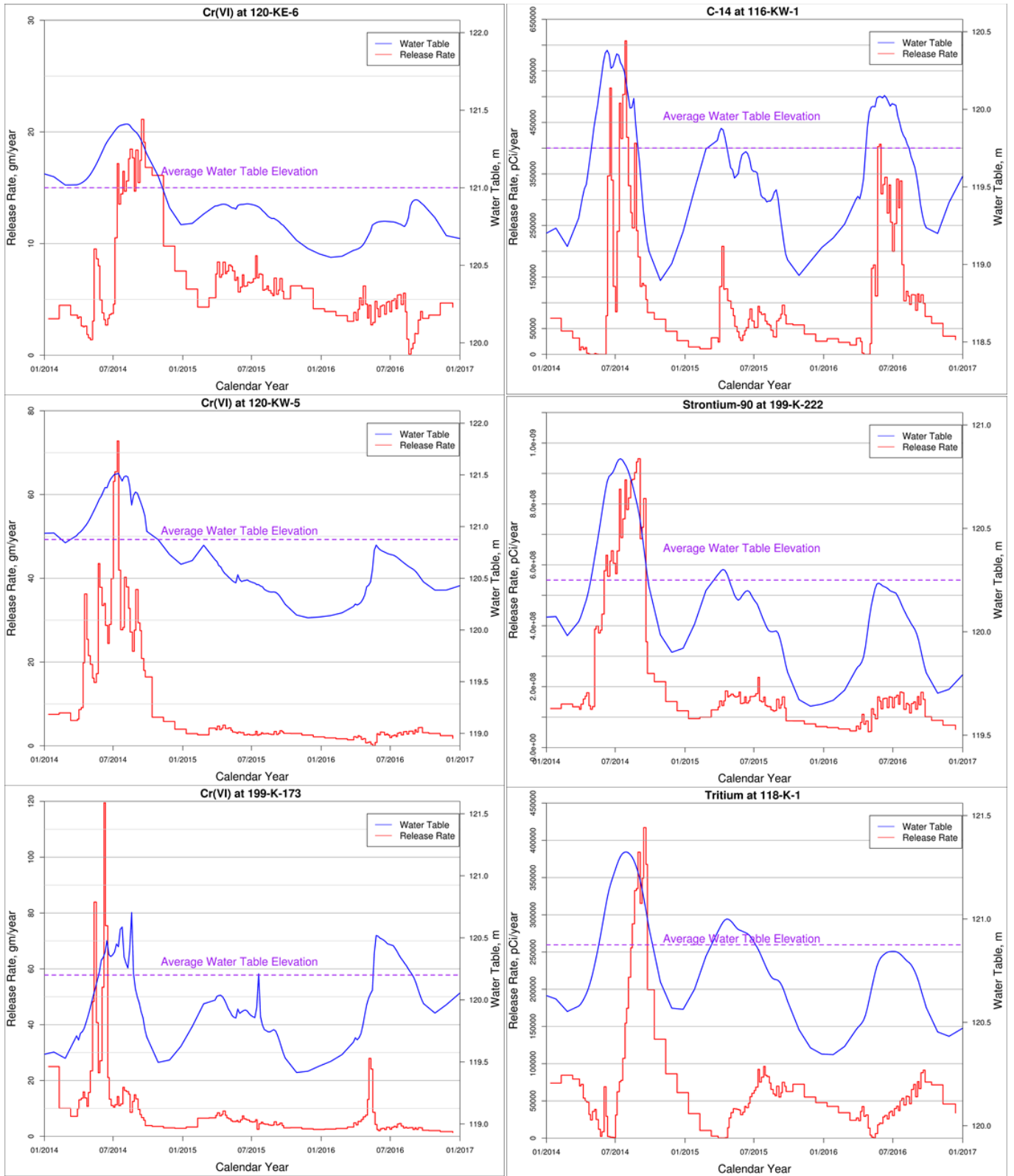


Figure 3-29. Characteristic Release Rate Curves at Continuing Source Locations for Cr(VI), Carbon-14, Strontium-90, and Tritium (Calibration Model)

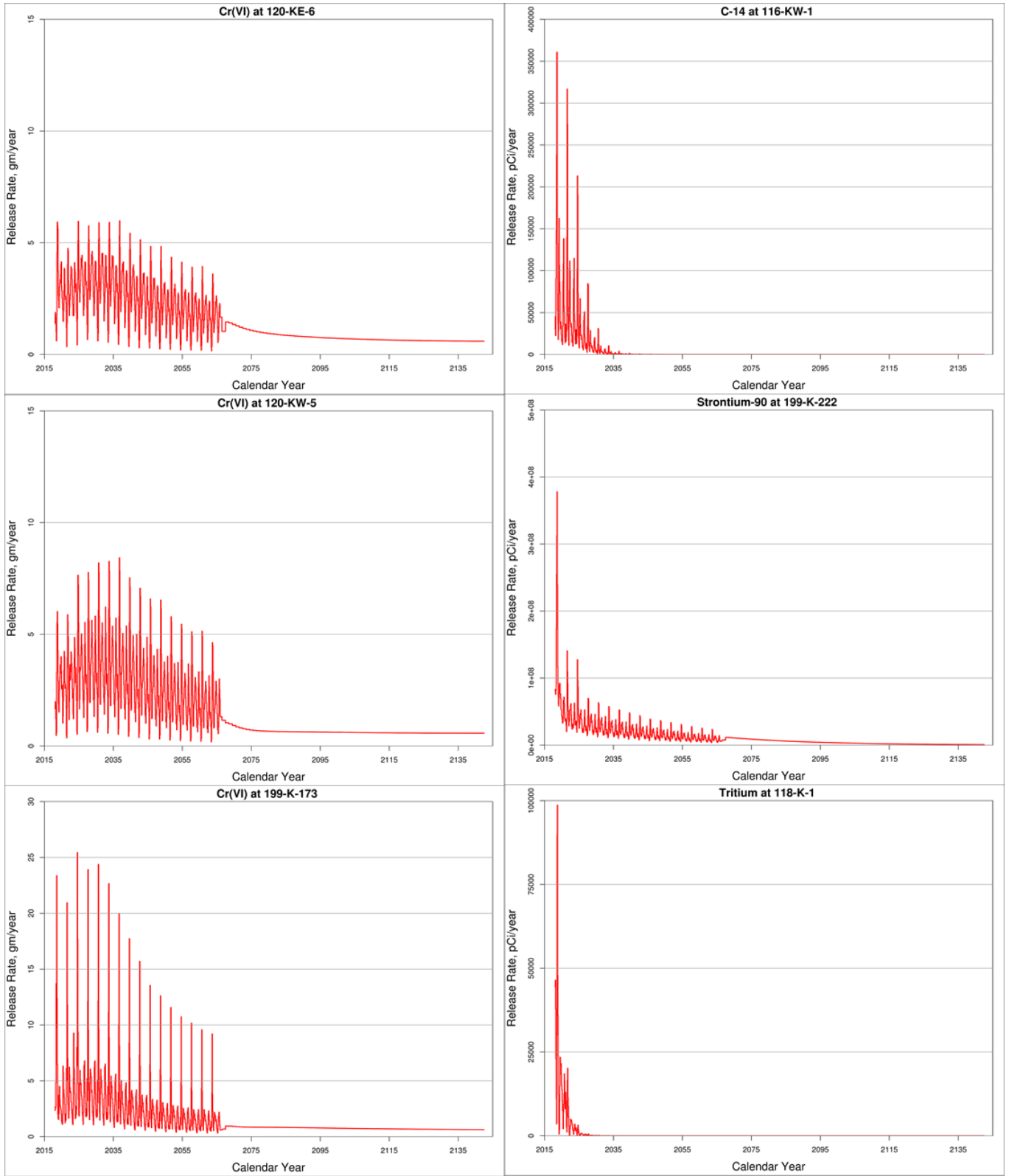


Figure 3-30. Characteristic Release Rate Curves for Cr(VI), Carbon-14, Strontium-90, and Tritium (Predictive Model)

3.5.2 Construction of Source/Sink Mixing Package

The contaminant flux releases from the vadose zone to the aquifer is applied to the transport model through a source/sink mixing (SSM) package. The SSM package allows different ways to apply continuing source in the transport package. Continuing source can be applied as source concentration or mass-loading rate depending on the “ITYPE” flag selected in the SSM package. The mass-loading rate option was selected to avoid any intermediate calculation and directly apply the STOMP output to the transport model. A python script was used for constructing the SSM package using the characteristic release rate curve developed in STOMP, the calibrated number of cells at each waste site, and a calibrated multiplier file to scale release rates.

3.5.3 Processing Observation Data for Calibration

After filtering out data during the quality control process, additional filtering was performed for each of the analytes. This included removing data collected in test holes during characterization, and typically not collected in completed wells. Additionally, for hexavalent chromium, results obtained using field colorimetric methods were removed. Results for total chromium were excluded from the calibration data for hexavalent chromium. For all the analytes, if results were available from multiple samples collected on the same day, the maximum of the measured value was used. Finally, non-detects were replaced with half the reporting limit.

3.5.4 Transport Model Calibration Results

The primary objective of the transport calibration process was to estimate a mass release rate during the calibration period so that simulated concentration at the observation wells near the waste sites would be able to match observed concentrations. In addition, the calibration was done in such a way that the areal footprint of the contaminated zone at each waste site was as small as possible so that the calibrated contaminated zone only contributed to the downgradient observation wells. That is, unless contamination was detected at an observation well no source was introduced even if suggested by process knowledge. These calculations were not meant to directly estimate the spatial distribution and soil concentration in the vadose zone. The consequence of this approach could result in continuing groundwater contamination from vadose zone sources not accounted for in this analysis.

3.5.4.1 Calibration Results for Chromium

All the potential continuing sources for chromium were at or near the high chromium concentrations in the 100-KW and 100-KE area. The P&T system was shut down in May 2016 to study concentration rebound near the suspected source locations. The observation data clearly show a rebound at the wells near the suspected continuing source locations after the P&T system shut down. The simulated concentrations at these locations continue to decline if continuing sources were not included. The introduction of continuing sources at the high concentration zones near 183.1KW Headhouse and 190-KW helped to elevate the concentration at the observation wells 199-K-205 and 199-K-173, which is qualitatively similar to the rebound concentrations. The introduction of continuing source at 183.1KE Headhouse also qualitatively improved calibration at the nearby wells 199-K-36, 199-K-188, and 199-K-220. Observed high concentration near well 199-K-111A and 199-K-207 are probably not due to the contribution from the continuing sources because there were no potential sources for chromium at or near the 118-K-1 burial ground. Lack of monitoring well data around 118-K-1 burial ground probably caused poorly delineated initial concentration in the annual groundwater monitoring report. Installation of a few more wells in this area is planned for better characterization of the chromium plume. However, initial concentration inferred from the annual groundwater monitoring report in this area was calibrated for the purposes of this RI/FS. The observed concentration at well 199-K-111A was as high as 510 µg/L and at well 199-K-207 was around 120 µg/L. The increase in concentrations in these two wells could be due to

the incoming high concentration slug from the upstream. The calibrated chromium concentrations upstream of wells 199-K-111A and 199-K-207 were as high as 2000 µg/L. In addition, initial concentration near 183.1KW Headhouse was changed to 1000 µg/L from inferred value of 450 µg/L reported in the annual groundwater monitoring report. Historically, aquifer below 183.1KW Headhouse had shown high concentrations based on well 199-K-195 which was decommissioned in 2011. An extraction well (199-K-205) was installed near 183.1KW Headhouse in 2014 and measured groundwater concentration after well completion was around 1000 µg/L.

Figure 3-31 shows a qualitative comparison between the simulated and mapped chromium plume at the end of 2016. It should be noted that the Cr(VI) plume which completely lies within 100-N OU boundary was not simulated during the calibration period. The mapped 2016 plume in 100-N was used as the initial concentration for the predictive simulation as described in Section 3.3.5.1.

Figure 3-32 shows comparison between simulated and observed concentrations over the calibration period at wells 199-K-173 and 199-K-205. 199-K-173 is an extraction well within KW P&T system and extracted water at an approximate pumping rate of 60 gpm between 2014 and May 2016. Observed chromium concentration at this location continues to decline during this period. Simulated concentrations agreed with the overall observed trend. However, the model simulates some high concentrations of around 175 µg/L during the summer of 2014, when the water table was higher than the average water table elevation. The rise in water table allows more mass to be in contact with the aquifer. In addition, the travel distance between vadose zone mass and the water table decreases as the water table rises. Therefore, mass releases to the aquifer is always higher for the high-water table condition than low water table condition. A rebound of chromium concentration was observed after the P&T system shut down in the KW area. The simulated concentration agreed well with the observed high rebound concentrations at well 199-K-173. Well 199-K-205 (near 183.1KW Headhouse) is also an extraction well that started operating in September 2014 and operated at an approximate pumping rate of 120 gpm until pump and treat system shut down in May 2016. Some groundwater concentration measurements during well completion were 1000 – 3000 µg/L, which were not included in the calibration dataset (section 3.5.3). However, the simulated concentrations during that period also shows very high concentrations in response to the fluctuating high-water table. The simulated concentrations during P&T system operation agreed very well with the observation data. The model overestimates chromium concentrations during the rebound study period at this location. Figure 3-33 shows comparison between simulated and observed concentrations for selected downstream wells in the 100-KW area.

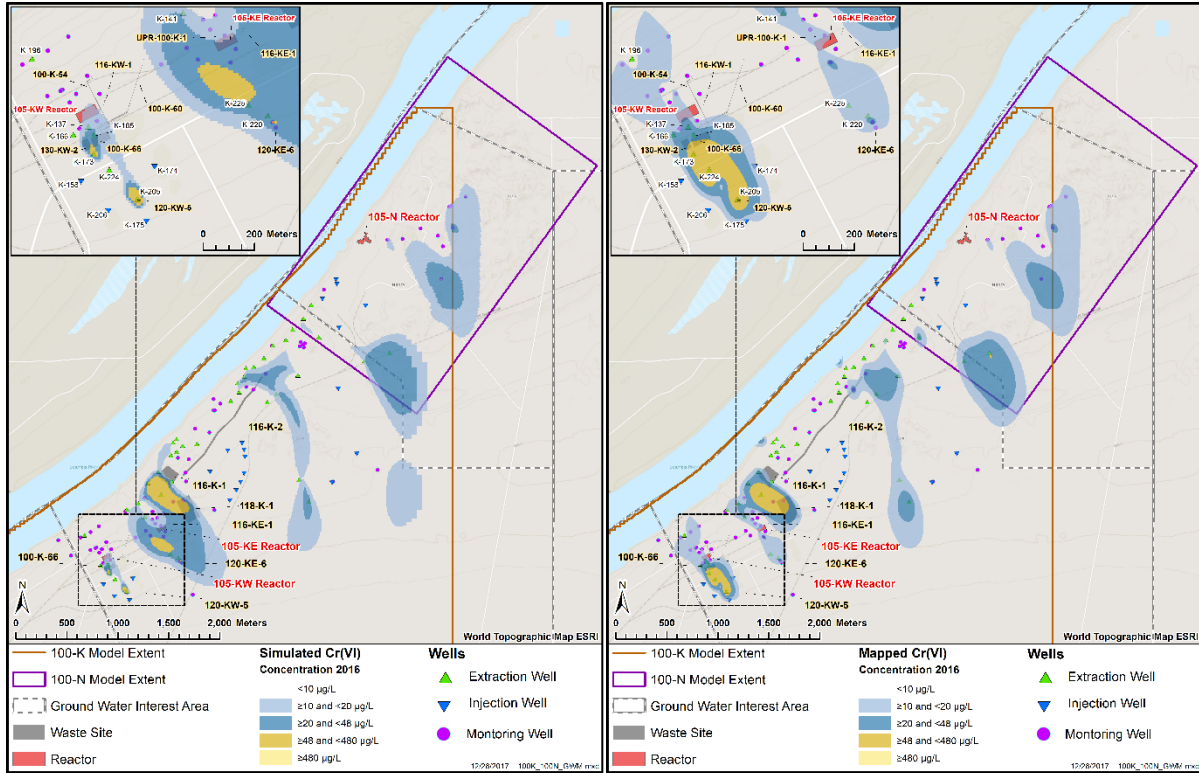


Figure 3-31. Simulated (Left) and Mapped (Right) Chromium Concentrations at the end of 2016 in Layer 1 (Top of Unconfined Aquifer)

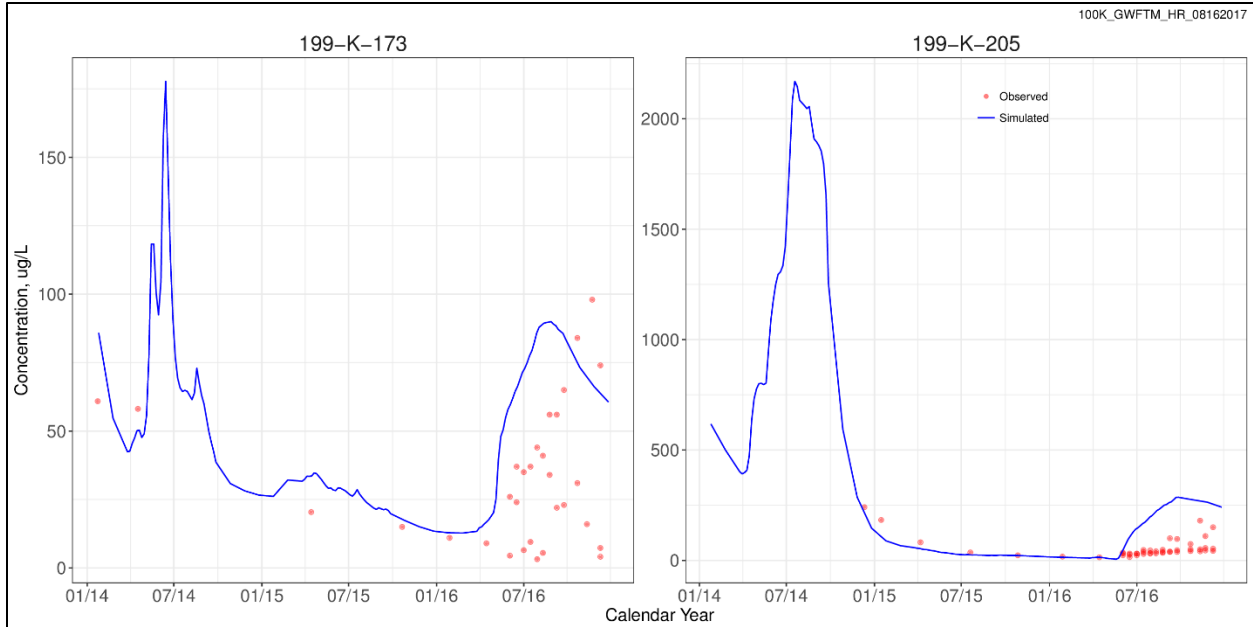


Figure 3-32. Observed vs Simulated Chromium Concentrations at Wells near 183.1KW Headhouse

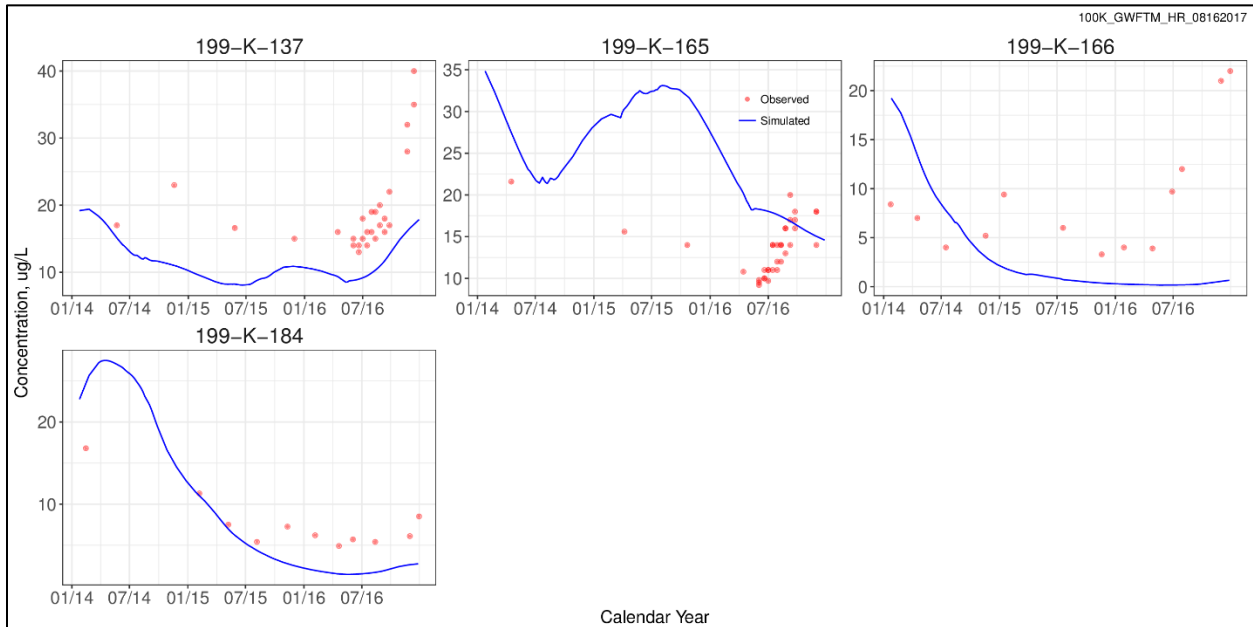


Figure 3-33. Observed vs Simulated Chromium Concentrations at Selected Wells within 100-KW Area

Figure 3-34 shows comparison between simulated and observed concentrations at wells 199-K-188, 199-K-220, and 199-K-36 near 183.1KE Headhouse. Wells 199-K-188 and 199-K-36 are monitoring wells that are 25 m apart from each other. On the other hand, well 199-K-220 is an extraction well within KX P&T operating system and operates at an approximate pumping rate of 60 gpm. This extraction well is 35 m and 60 m downstream of well 199-K-36 and 199-K-188, respectively. Only one measurement at well 199-K-36 show significantly higher concentration than other observed data in all three wells. It's an indication of a small localized continuing source near 183.1KE Headhouse. The calibrated continuing source zone (Figure 3-31) at this location was also found to be very small.

Figure 3-35 shows comparison between simulated and observed concentrations at wells 199-K-111A, 199-K-207, and three other selected downgradient wells near 118-K-1 burial ground. In absence of any continuing source for chromium, the only possibility to explain the observation of high concentration at wells 199-K-111A and 199-K-207 is migration of a high concentration slug from upstream. The initial concentration plume in the annual groundwater monitoring report for the area to the upstream of these two wells is not well defined due to the lack of monitoring wells. The qualitative calibration of initial concentration in this location helped to increase the simulated concentration to the observed level.

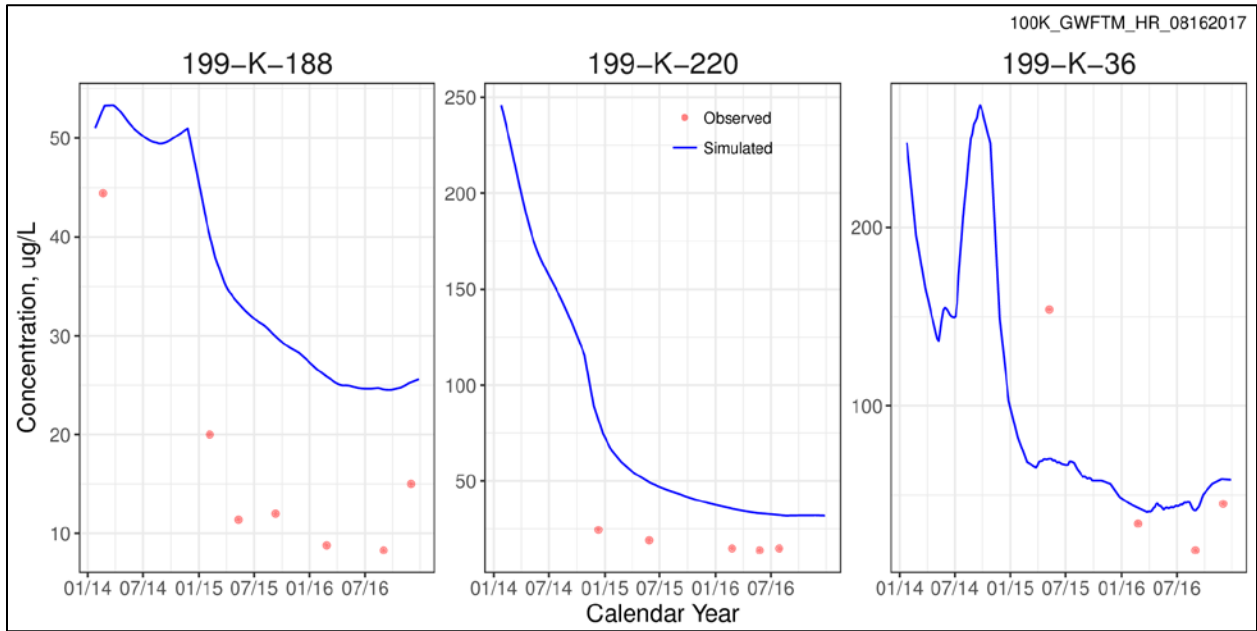


Figure 3-34. Observed vs Simulated Chromium Concentrations at Wells near 183.1KE Headhouse

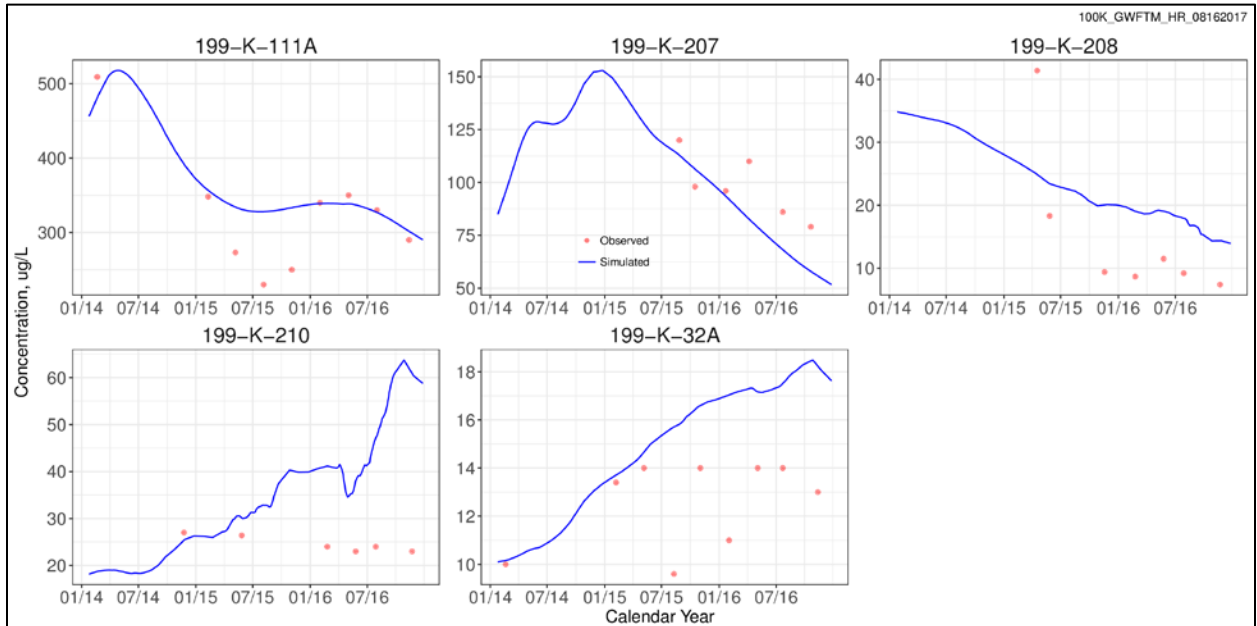


Figure 3-35. Observed vs Simulated Chromium Concentrations at Wells near 118-K-1 Burial Ground

3.5.4.2 Calibration Results for Strontium-90

Strontium-90 has a high distribution coefficient (K_d of 12 mL/g was used for 100-K GWFTM) and is supposed to transport very slowly. However, the plume delineation in the annual groundwater monitoring report had changed from one year to another. Therefore, transport calibration was done using the most recent initial concentration plume (i.e., from 2015 annual groundwater report [DOE/RL-2016-09]). This prevented the addition of strontium-90 in a place where it was not present in the following years based on the most updated plume interpretation. The highest strontium-90 concentrations in 100-KR-4 OU are located near UPR-100-K-1 and FSB in KE area. The estimated maximum concentrations in this area are higher than 3,000 pCi/L whereas all the observed concentrations at two nearby wells (199-K-221 and 199-K-222) in 2016 were couple of orders magnitude lower than the initial concentrations used in the transport model. Some of these measurements are questionable as it was found that the samples for these measurements were collected from bottom of the strontium-90 plume or across the whole screen interval. As a result, reported observed concentrations were very low because all the high concentrations probably lie within the top 2-5 m of the aquifer. The sample collection method was revised in 2016. The most recent (at the time of report preparation) concentrations in August 2017 and October 2017 were 13,900 pCi/L and 15,600 pCi/L, respectively. Although 2017 was not part of the calibration period, these data could not be ignored during the calibration and prediction process.

Based on prior knowledge and observed concentrations, the potential continuing sources for strontium-90 are 116-KW-2 crib in KW area and UPR-100-K-1, FSB, 116-K-1 crib, and 116-K-2 trench in the KE area (Figure 3-26 and Figure 3-27). Figure 3-36 shows a qualitative comparison between the simulated and mapped strontium-90 plume at the end of 2016. Introducing continuing sources at 116-KW-2 crib and at west corner of 116-K-2 trench increased the simulated concentrations similar to the observed concentrations. No continuing source was used at 116-K-1 crib because there was no groundwater data available in support of any continuing source. There are two extraction wells (199-K-144 and 199-K-208) near 116-K-1 crib and all the observed concentrations at these two wells are below drinking water standard (DWS). Depth discrete soil concentration data at wells 199-K-221 and 199-K-222 near UPR-100-K-1/FSB were available to be used in STOMP 1D model for estimating characteristic release rate curves. As described above, the observed concentrations at these two wells in 2016 are a couple of orders magnitude lower than the initial concentrations and in 2017 are couple of times higher than the initial concentrations. Therefore, a multiplier was used to scale the characteristic release rate curve so that simulated concentrations match the observed high concentrations. A better plume delineation and characterization is required to perform any meaningful calibration in this location.

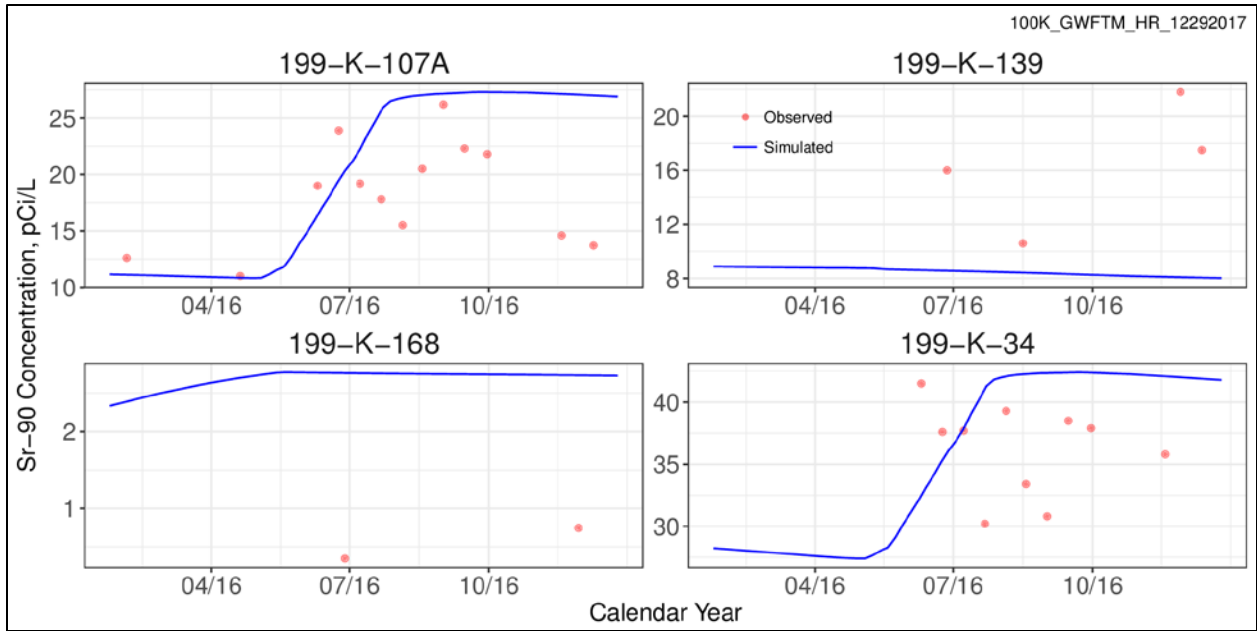


Figure 3-37 through Figure 3-39 show the simulated vs observed concentrations at the selected wells near the continuing source locations.

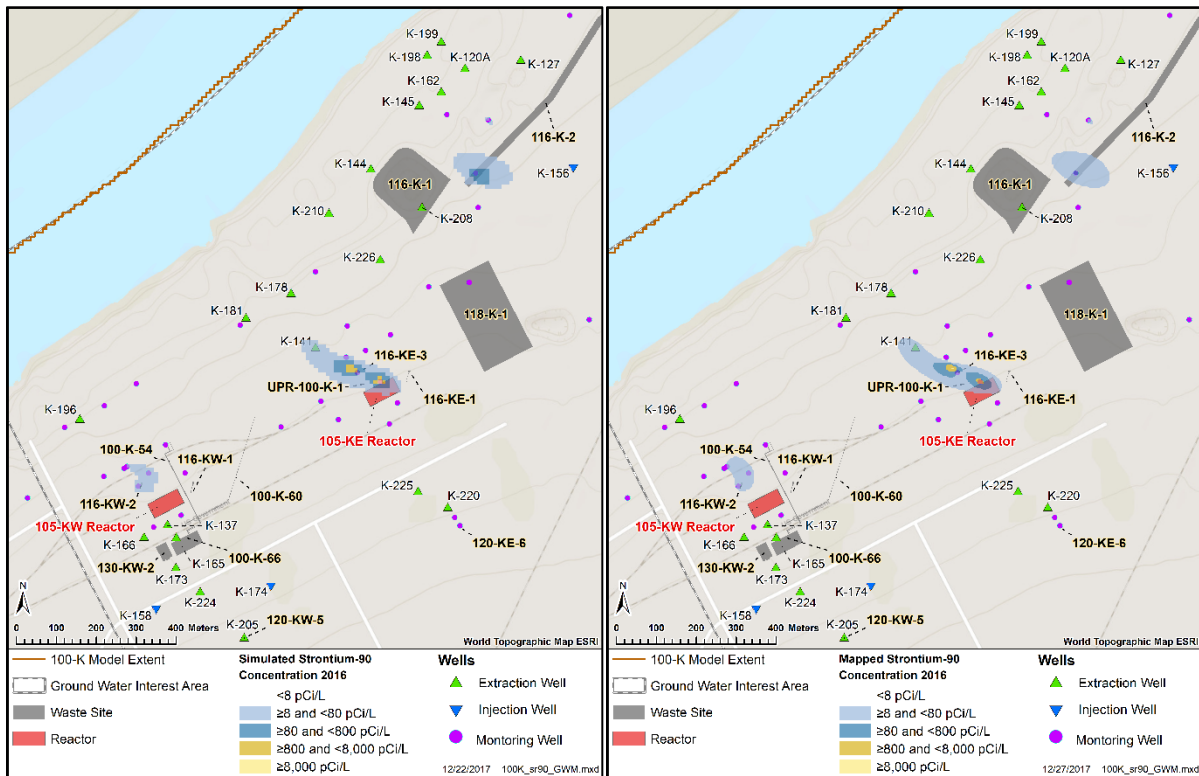


Figure 3-36. Simulated (Left) and Mapped (Right) Strontium-90 Concentrations at the end of 2016 in Layer 1 (Top of Unconfined Aquifer)

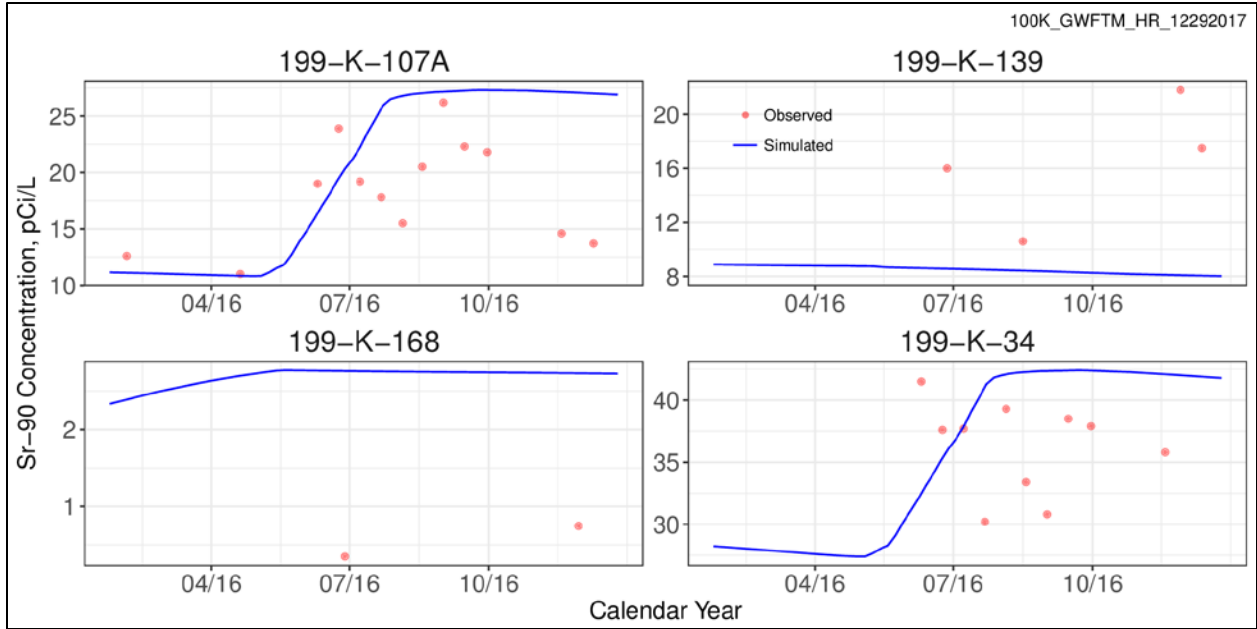


Figure 3-37. Observed vs Simulated Strontium-90 Concentrations at Wells near 116-KW-2 Crib

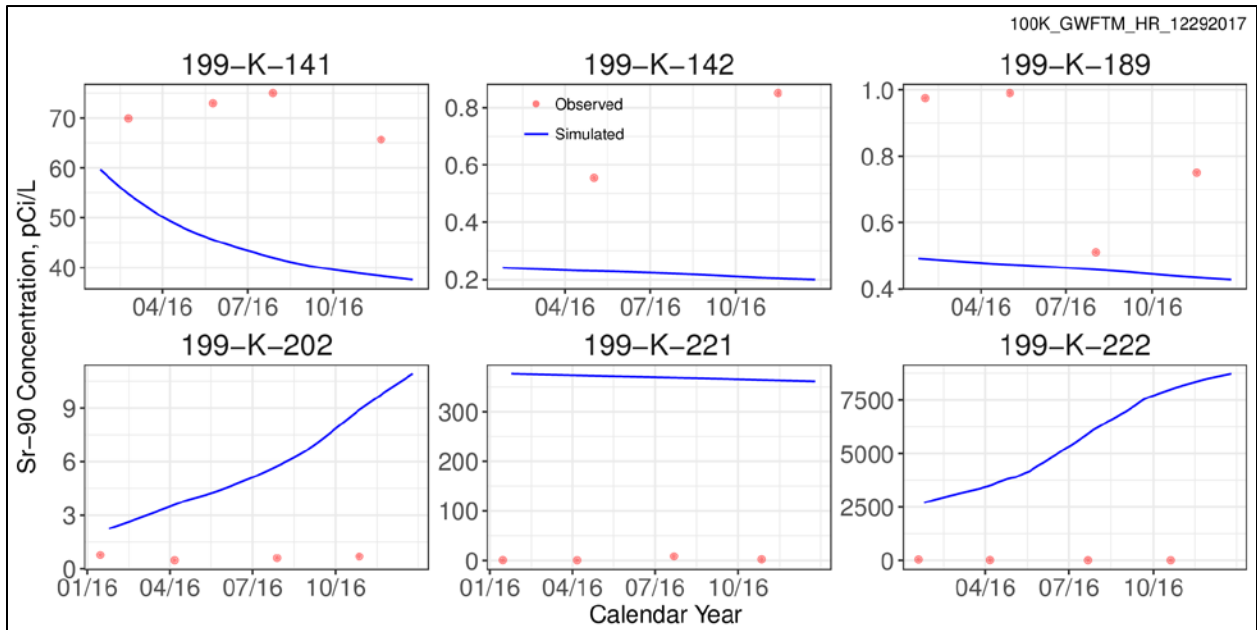


Figure 3-38. Observed vs Simulated Strontium-90 Concentrations at Wells near KE FSB

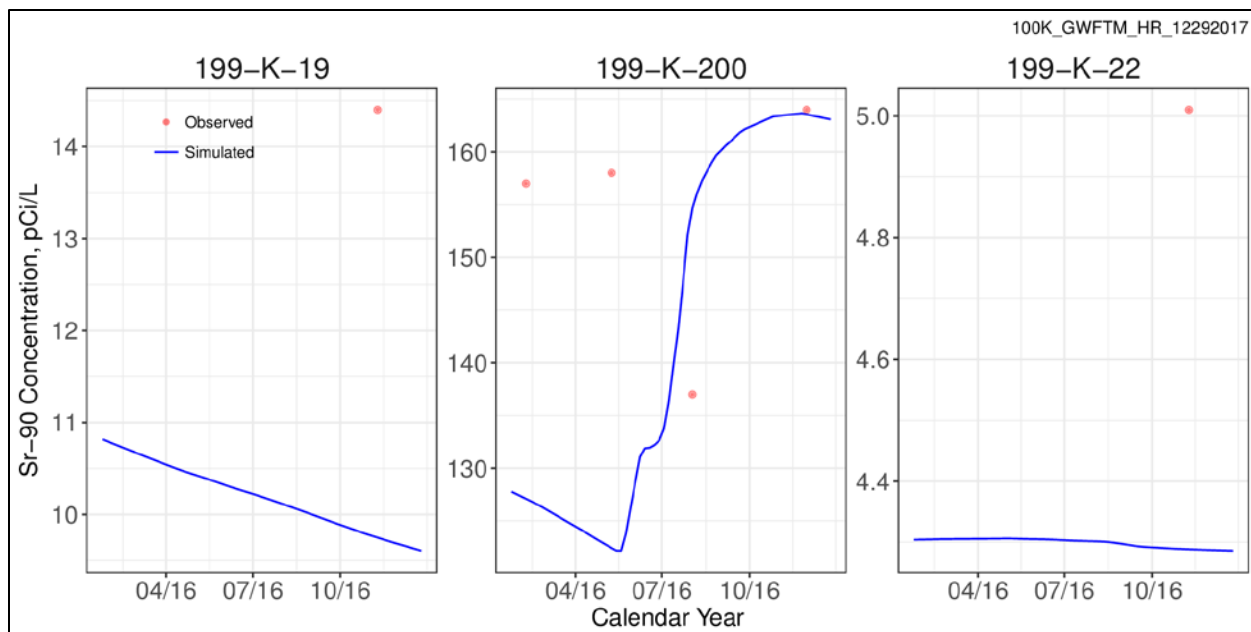


Figure 3-39. Observed vs Simulated Strontium-90 Concentrations at Wells near 116-K-2 Trench

3.5.4.3 Calibration Results for Carbon-14

The presence of carbon-14 in the groundwater is mostly near 116-KW-1 and 116-KE-1 gas condensate cribs. These are also potential continuing source locations considered for the transport model calibration. Carbon-14 plume delineation in the annual groundwater monitoring report between 2013 and 2015 has evolved significantly, especially at KE area, as the concentration measurements at new wells became available during the later years. Figure 3-40 and Figure 3-41 show how the plume delineation has changed between 2013 and 2015 near 116-KW-1 and 116-KE-1, respectively. Starting the model calibration in 2014 would give a long period of observed data to compare but, would not be able to match the locations that were included within the plume footprint in the later years. Carbon-14 plume from 2015 annual groundwater report was selected as the most representative initial concentrations and the transport model was simulated only for calendar year 2016.

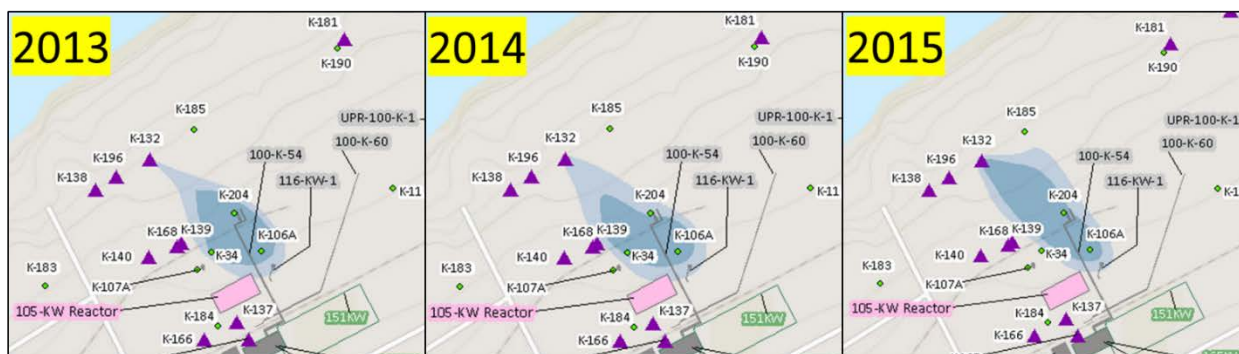


Figure 3-40. Evaluation of Carbon-14 Plume Definition between 2013 and 2015 in KW Area

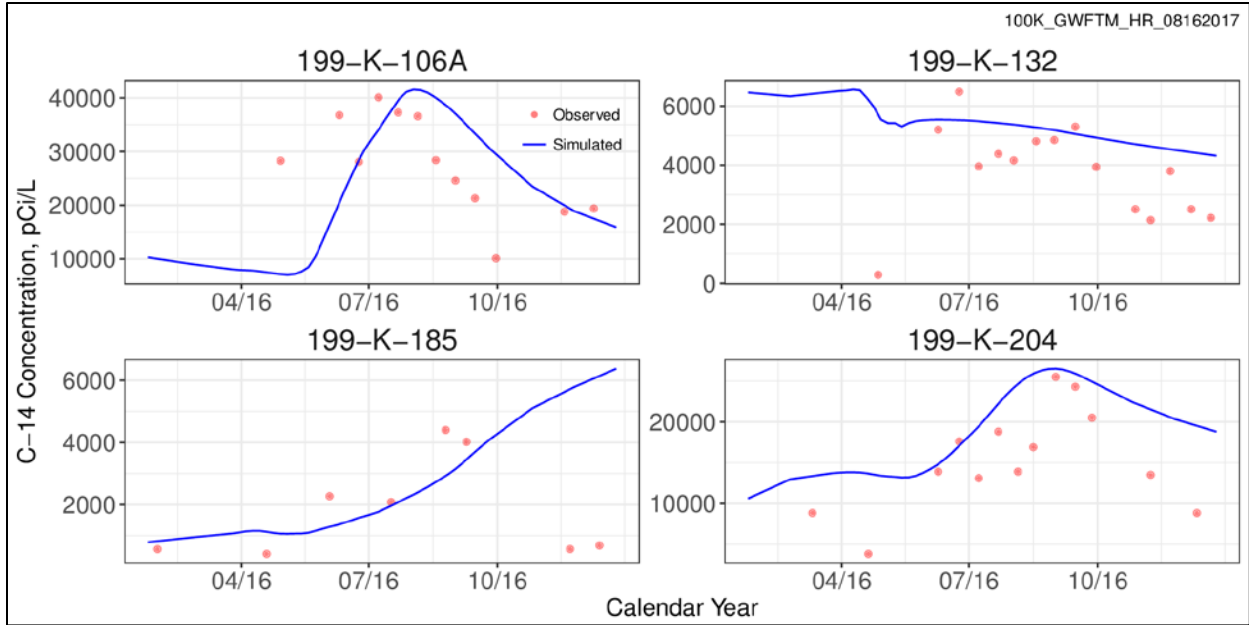


Figure 3-43. Observed vs Simulated Carbon-14 Concentrations at Wells near 116-KW-1 Gas Condensate Crib

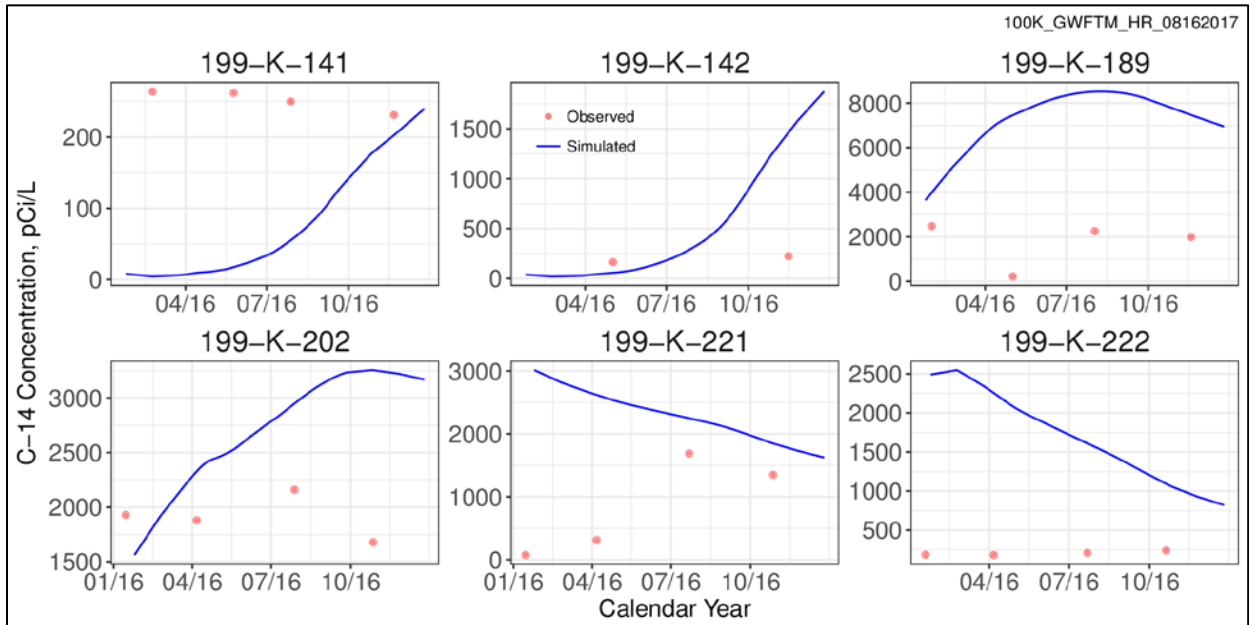


Figure 3-44. Observed vs Simulated Carbon-14 Concentrations at Wells near 116-KE-1 Gas Condensate Crib

3.5.4.4 Calibration Results for Nitrate

The presence of nitrate in the groundwater is mostly near 116-KW-1 gas condensate crib. Although both 116-KW-1 and 116-KE-1 gas condensate cribs are considered to be potential continuing source locations, no calibration of continuing source can be done for 116-KE-1 due to the absence of any plume in the groundwater at least according to the current interpretation. Nitrate plume delineation in the annual groundwater monitoring report between 2013 and 2015 has evolved significantly due to the plume migration and observed data. Figure 3-45 shows how the plume delineation has changed between 2013

and 2015 near 116-KW-1. The plume is highly dependent on the well 199-K-106A and the coverage was expanded by installing another well (199-K-204) to the downstream of 199-K-106A. The most recent observation data show an increase in concentration at wells 199-K-106A and 199-K-204. The data clearly suggest a high concentration slug upstream of these two wells, generated by a continuing source, are migrating towards these wells. The nitrate plume from 2013 annual groundwater report was selected as the most representative initial concentrations and the transport model was simulated for calendar year 2014 through 2016.

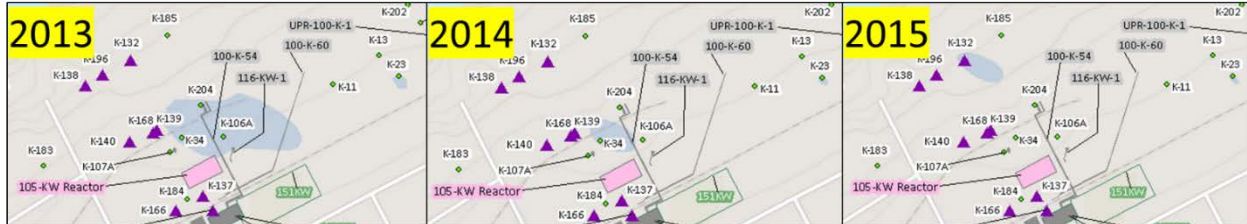


Figure 3-45. Evaluation of Nitrate Plume Definition between 2013 and 2015 in KW Area

Figure 3-46 shows a qualitative comparison between the simulated and mapped nitrate plume at the end of 2016. The mapped plume extent is significantly larger than the simulated plume. It is mainly due to the some recently observed concentrations above DWS which were significantly lower than the DWS in the past and subsequently, were not included in the initial concentration or potential source locations. Figure 3-47 and

Figure 3-48 show the comparison between observed and simulated concentrations at wells near 116-KW-1 and near the river downstream of 116-KW-1, respectively. Introducing continuing sources at 116-KW-1 gas condensate crib increased the simulated concentrations similar to the observed high concentrations at well 199-K-106A and 199-K-204. On the other hand, no continuing source was used near 116-KE-1 as the simulated concentrations were already higher than the observed values.

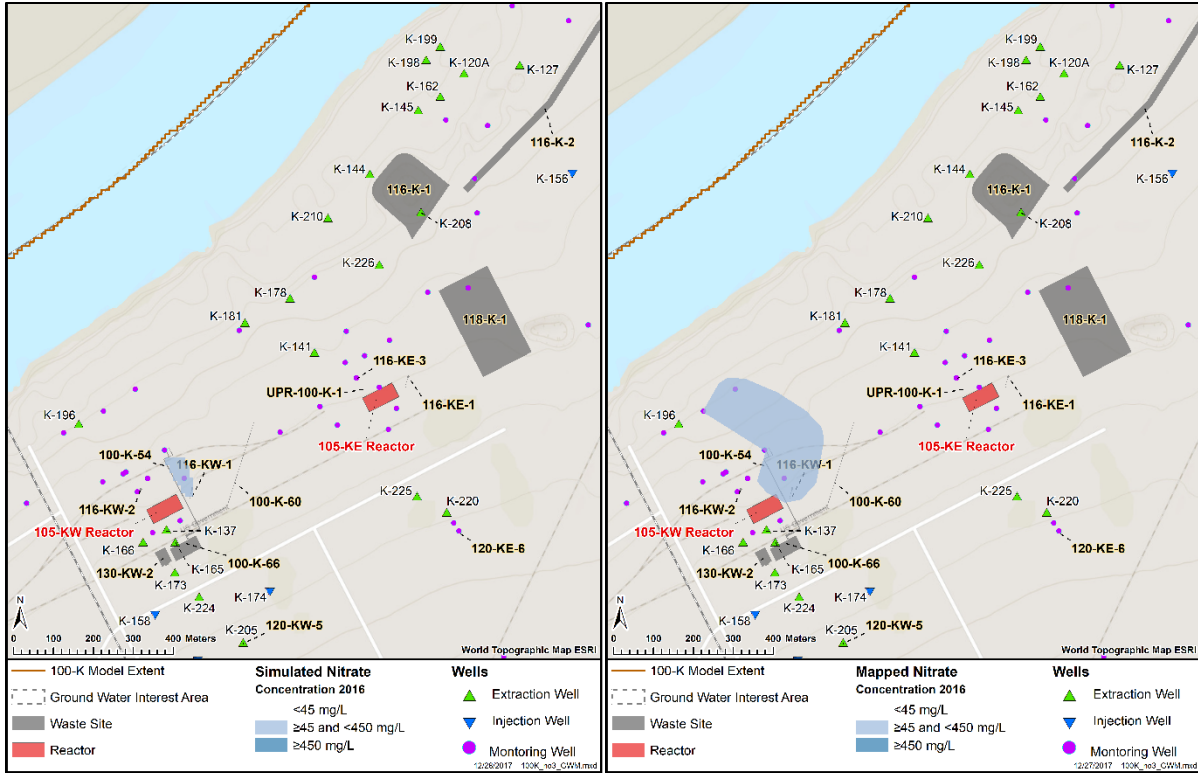


Figure 3-46. Simulated (Left) and Mapped (Right) Nitrate Concentrations at the end of 2016 in Layer 1 (Top of Unconfined Aquifer)

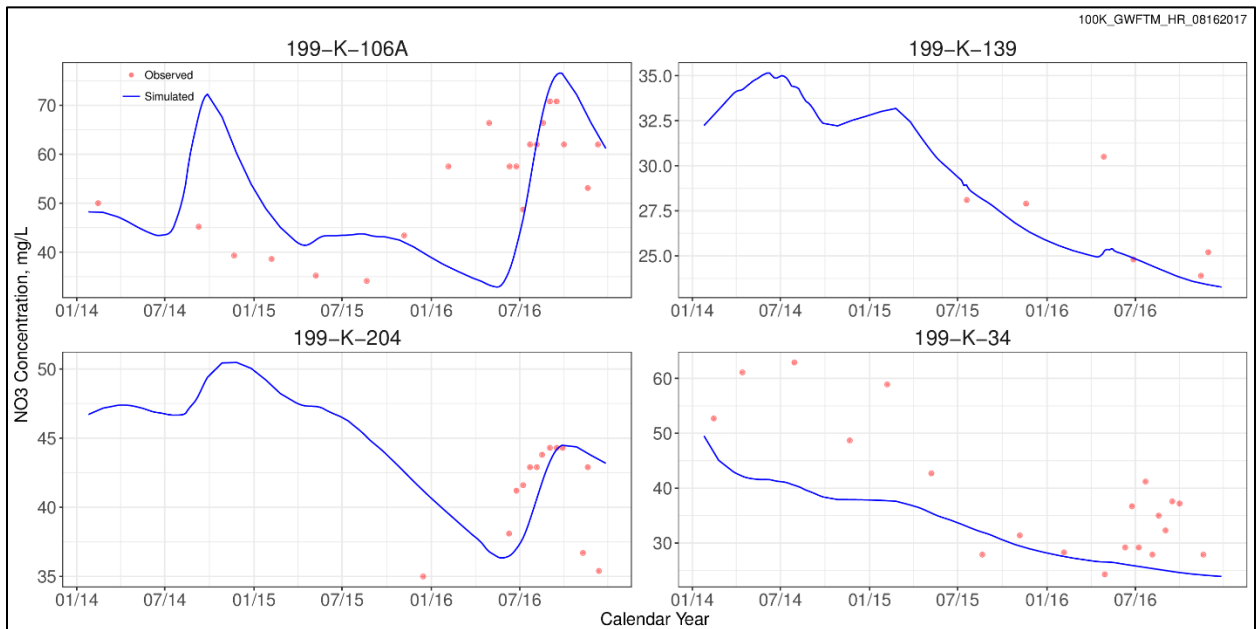


Figure 3-47. Observed vs Simulated Nitrate Concentrations at Wells near 116-KW-1 Gas Condensate Crib

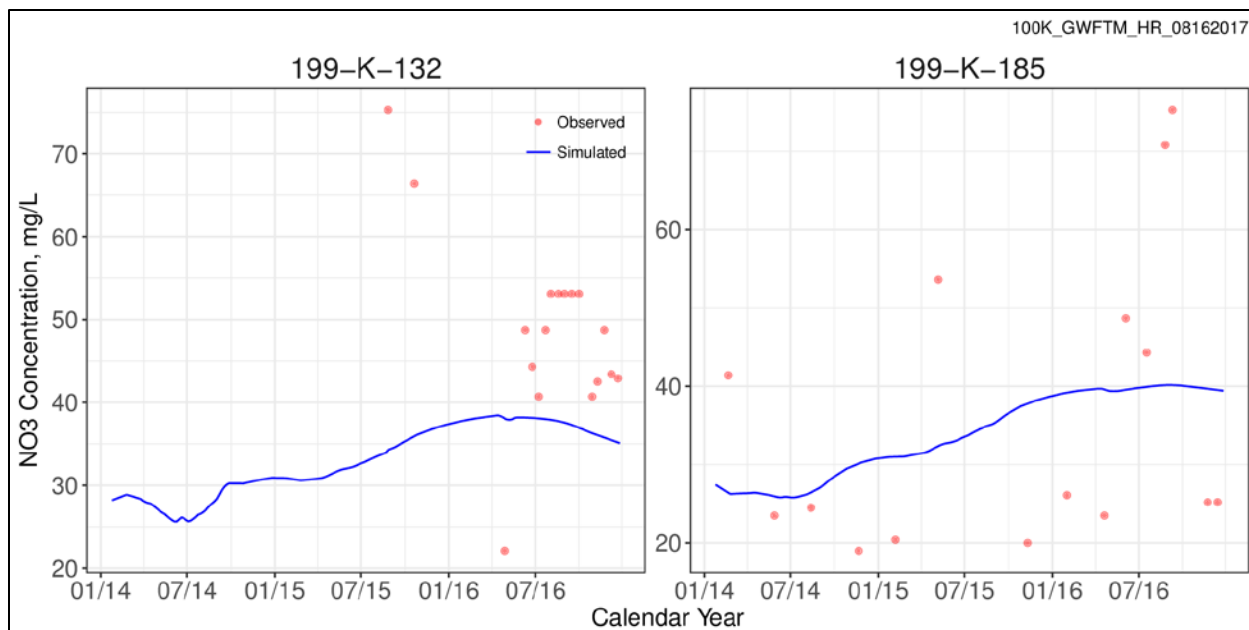


Figure 3-48. Observed vs Simulated Nitrate Concentrations at Selected Wells downstream of 116-KW-1 Gas Condensate Crib

3.5.4.5 Calibration Results for Tritium

Based on the prior knowledge and observed concentrations, the potential continuing sources for tritium are 116-KW-1, and 116-KW-2 crib in KW area and UPR-100-K-1, FSB, 116-K-1 crib, and 118-K-1 burial ground in the KE area (Figure 3-26 and Figure 3-27). Figure 3-49 shows a qualitative comparison between the simulated and mapped tritium plume at the end of 2016. Figure 3-50 shows the comparison between observed and simulated concentrations at wells near the 116-KW-1 gas condensate crib.

Introducing continuing sources near 116-KW-1 gas condensate crib increased the simulated concentrations similar to the observed high concentrations at wells 199-K-106A and 199-K-204. Figure 3-51 shows the comparison between observed and simulated concentrations at wells near the 116-KW-2 crib. The observed concentrations at wells 199-K-107A and 199-K-34 are well below DWS. Therefore, no continuing source was assigned at this waste site. Figure 3-52 shows the comparison between observed and simulated concentrations at wells near the 116-KE-1 gas condensate crib and 118-K-1 burial ground. Introducing continuing sources near 116-KE-1 gas condensate crib and 118-K-1 burial ground increased the simulated concentrations similar to the observed high concentrations at the monitoring wells. Tritium contamination at the 118-K-1 burial ground is well documented (DOE/RL-2016-67) and a significant amount of tritium is expected to remain the deep vadose zone even after excavating 12 m from the land surface.

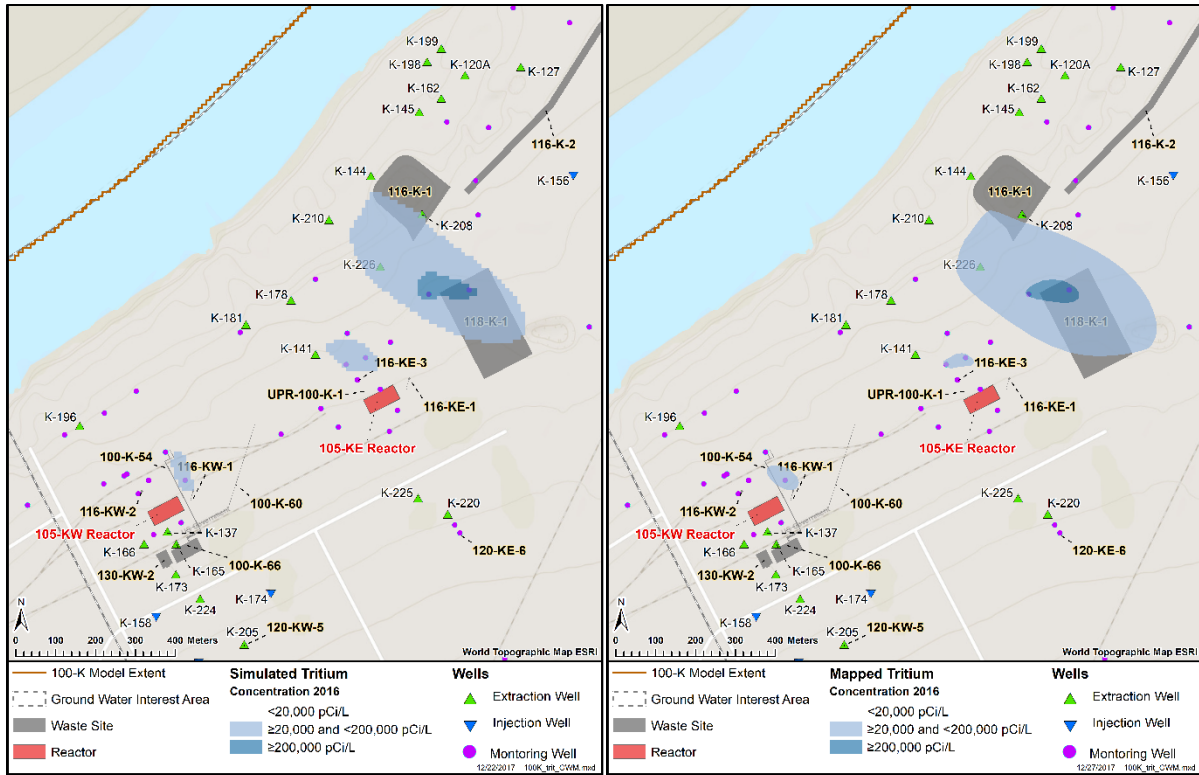


Figure 3-49. Simulated (Left) and Mapped (Right) Tritium Concentrations at the end of 2016 in Layer 1 (Top of Unconfined Aquifer)

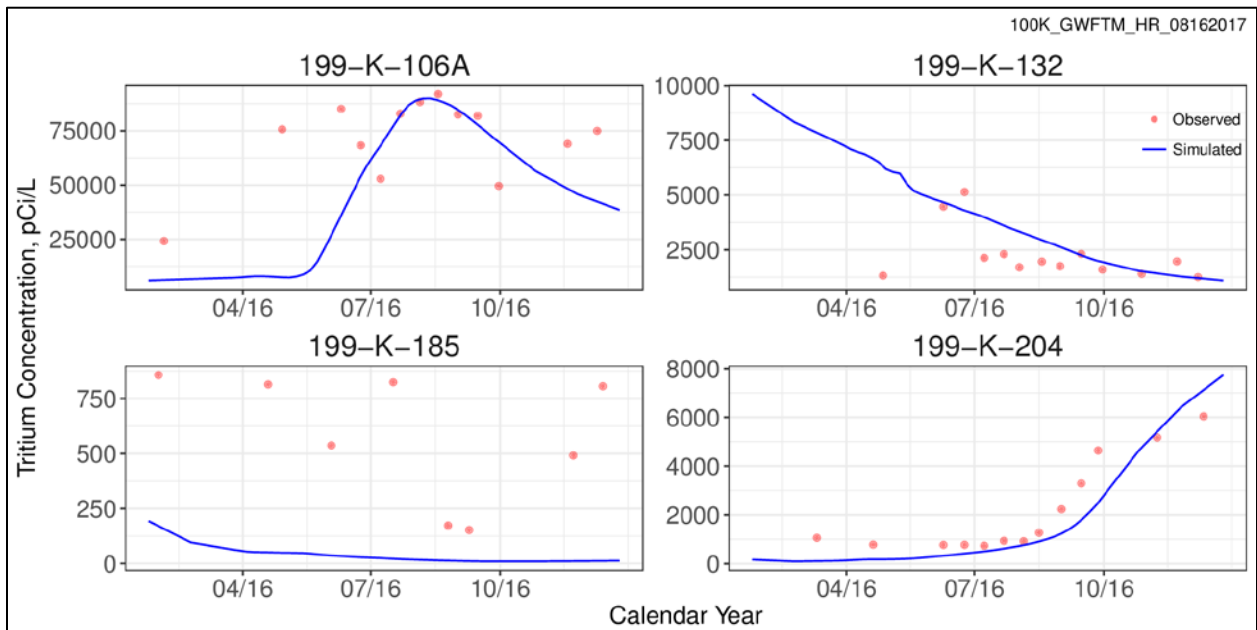


Figure 3-50. Observed vs Simulated Tritium Concentrations at Wells near 116-KW-1 Gas Condensate Crib

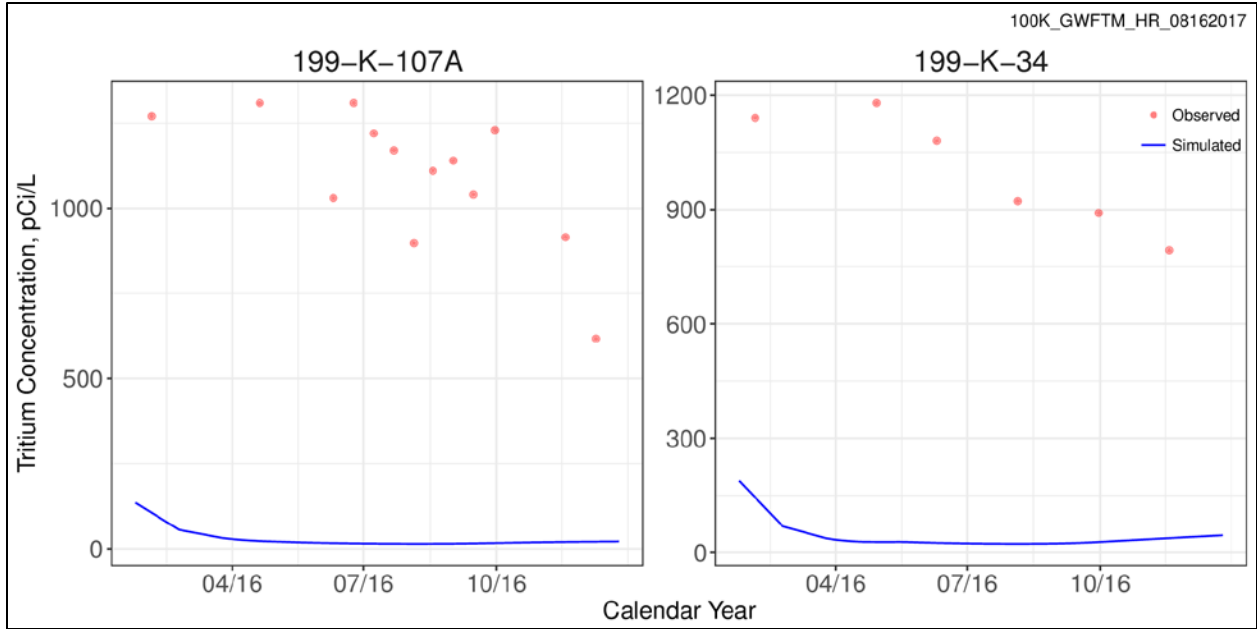


Figure 3-51. Observed vs Simulated Tritium Concentrations at Wells near 116-KW-2 Crib

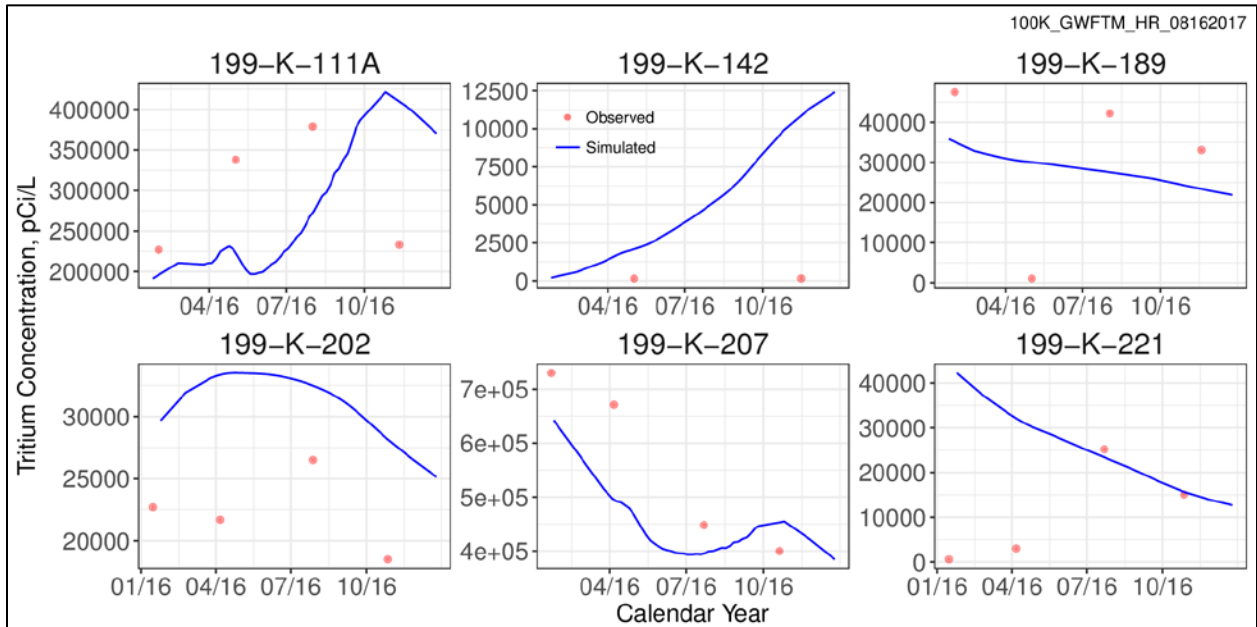


Figure 3-52. Observed vs Simulated Tritium Concentrations at Wells near 116-KE-1 Gas Condensate Crib and 118-K-1 Burial Ground

3.5.4.6 Calibration Results for TCE

TCE above the cleanup level was observed only at a small area near 107-KW retention basin during the last 3-4 years. The observed concentrations remained just barely above the cleanup level in that area. Moreover, no continuing sources for TCE was identified that could be contributing to the persistent TCE concentration near the 107-KW retention basin. Figure 3-53 shows a qualitative comparison between the simulated and mapped TCE plume at the end of 2016. The simulated concentration went below the

cleanup level within one year of simulation as the initial concentration was just above the cleanup level. On the other hand, the mapped plume in 2016 has lot of uncertainty as the apparently larger plume was based on the four slightly above cleanup level concentrations at the corners of the plume. Therefore, no further calibration was done for TCE and the mapped plume reported in 2016 annual groundwater monitoring report was used as the initial concentration for the predictive simulation.

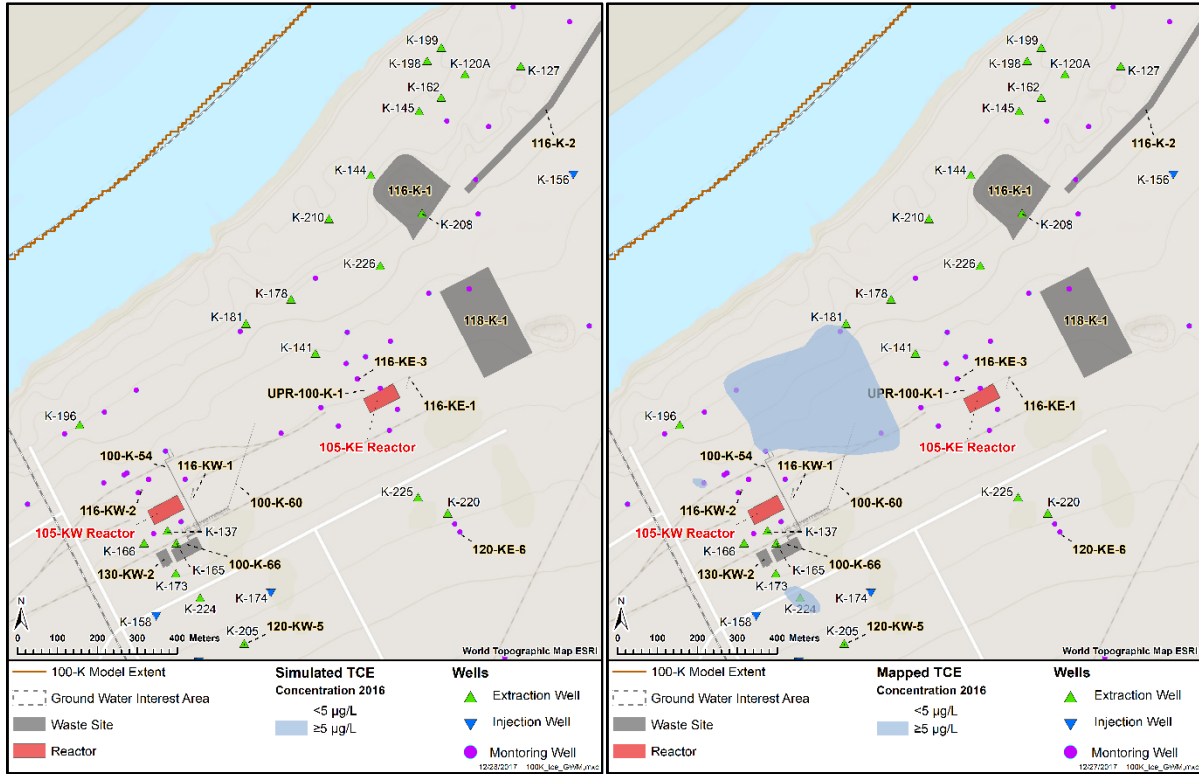


Figure 3-53. Simulated (Left) and Mapped (Right) TCE Concentrations at the End of 2016 in Layer 1 (Top of Unconfined Aquifer)

3.5.5 Predictive Transport Model

The 100-K GWFTM simulation results for the no further action case are presented in the following subsections to establish the basis for action for current groundwater contamination in 100-K. These results also provide the baseline for comparison with fate and transport simulation results for the remediation alternatives developed as part of feasibility study for 100-K RI/FS decisional draft.

Calibration transport simulation ends in year 2016 and predictive transport simulation starts from year 2018 while transport simulation for year 2017 worked as transition period between calibration model and predictive model. The simulated plume footprint at the end of calibration model is qualitatively compared with the plumes depicted in the 2016 annual groundwater monitoring report. If the simulated plume footprint is significantly different from the 2016 annual groundwater monitoring report, the simulated concentration was replaced by the annual groundwater plume as the initial concentration for the 2017 transport simulation. This allows us to start the predictive simulation with the most representative initial concentration based on best available information.

3.5.5.1 Hexavalent Chromium

Simulated concentrations at the end of calibration period shows some differences with the 2016 annual groundwater monitoring report, mostly two plumes near the eastern boundary (Figure 3-31). It is evident that these differences are due to the poor initial concentration setup at those plumes with no sources. For example, the easternmost plume used to have a long tail to the south which is based on measurements at only few monitoring wells. The most recent annual groundwater report does not show the tail. Therefore, simulated concentrations at those two plumes are replaced by the 2016 annual groundwater monitoring report plumes as the initial concentrations for the transport simulation in year 2017.

The no further action case is assumed to begin in January 2020, with the pump and treat system continuing operation as described in SGW-58690, *Remedial Process Optimization Work Plan for 100-HR-3 and 100-KR-4 Groundwater Operable Units Interim Action* until then. Figure 3-54 through Figure 3-58 illustrate the evolution of the Cr(VI) plume from 2017 through 2117. By 2067 (Figure 3-57) the K East and K North plumes have dissipated with the source at the KE headhouse continuing to generate a plume. The plumes that migrated from 100-K into the 100-N area also still remain. Continued depletion of source sources cause the KW plume to diminish, but not disappear, by 2117 (Figure 3-58); the 100-N plume also remains near the N Reactor and river shoreline at low concentrations.

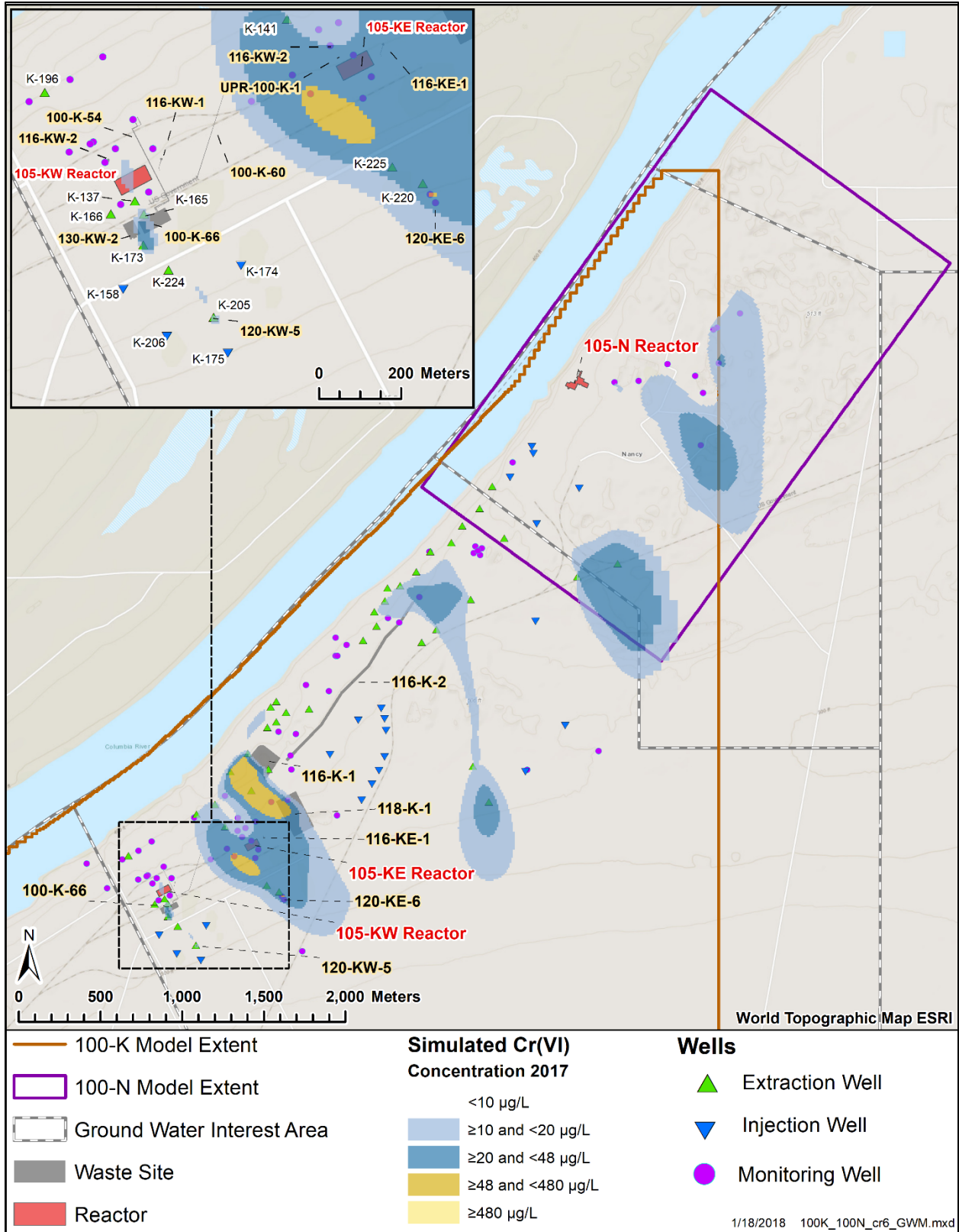


Figure 3-54. Simulated Cr(VI) Plume in 2017 at the Top of the Unconfined Aquifer

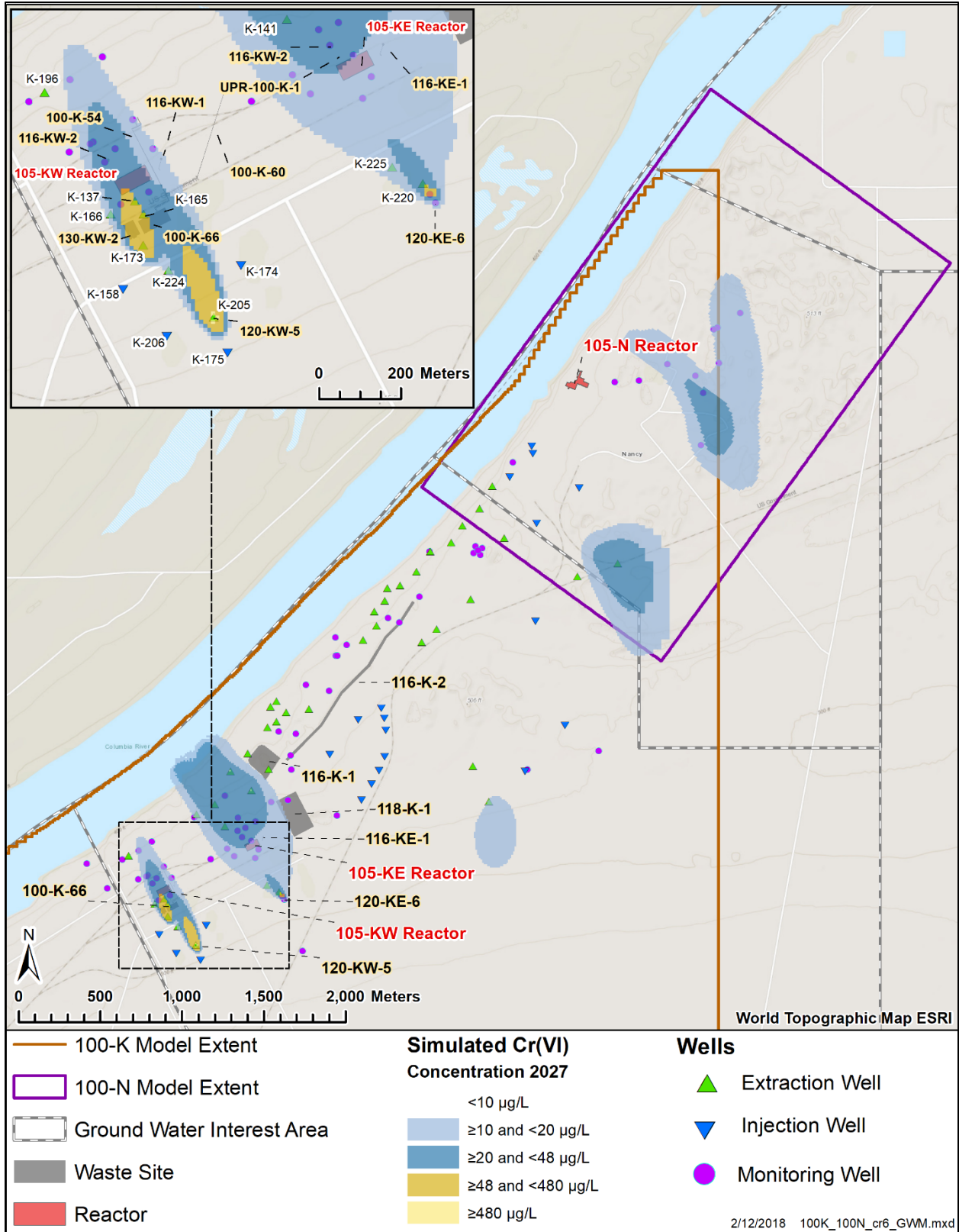


Figure 3-55. Simulated Cr(VI) Plume in 2027 at the Top of the Unconfined Aquifer

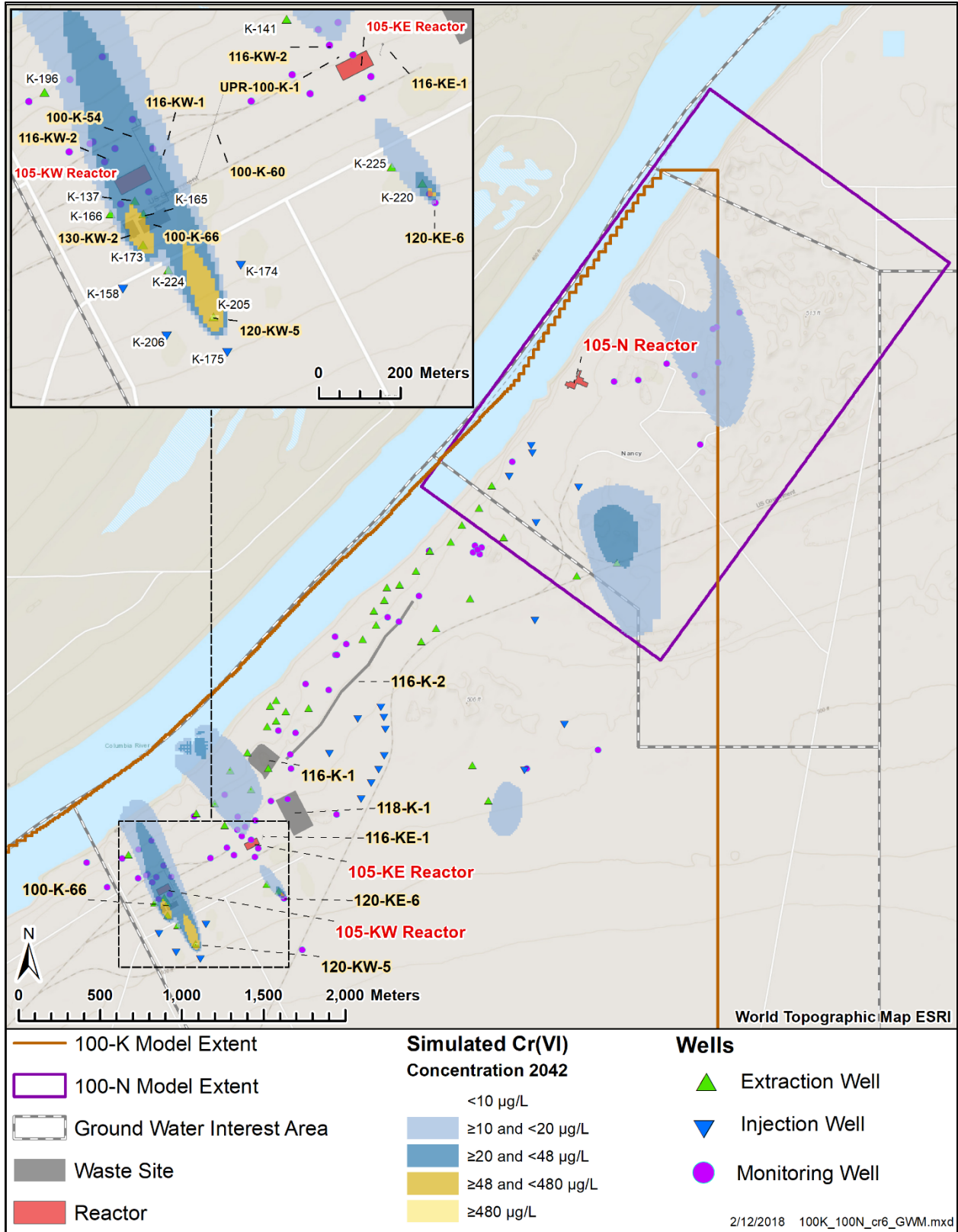


Figure 3-56. Simulated Cr(VI) Plume in 2042 at the Top of the Unconfined Aquifer

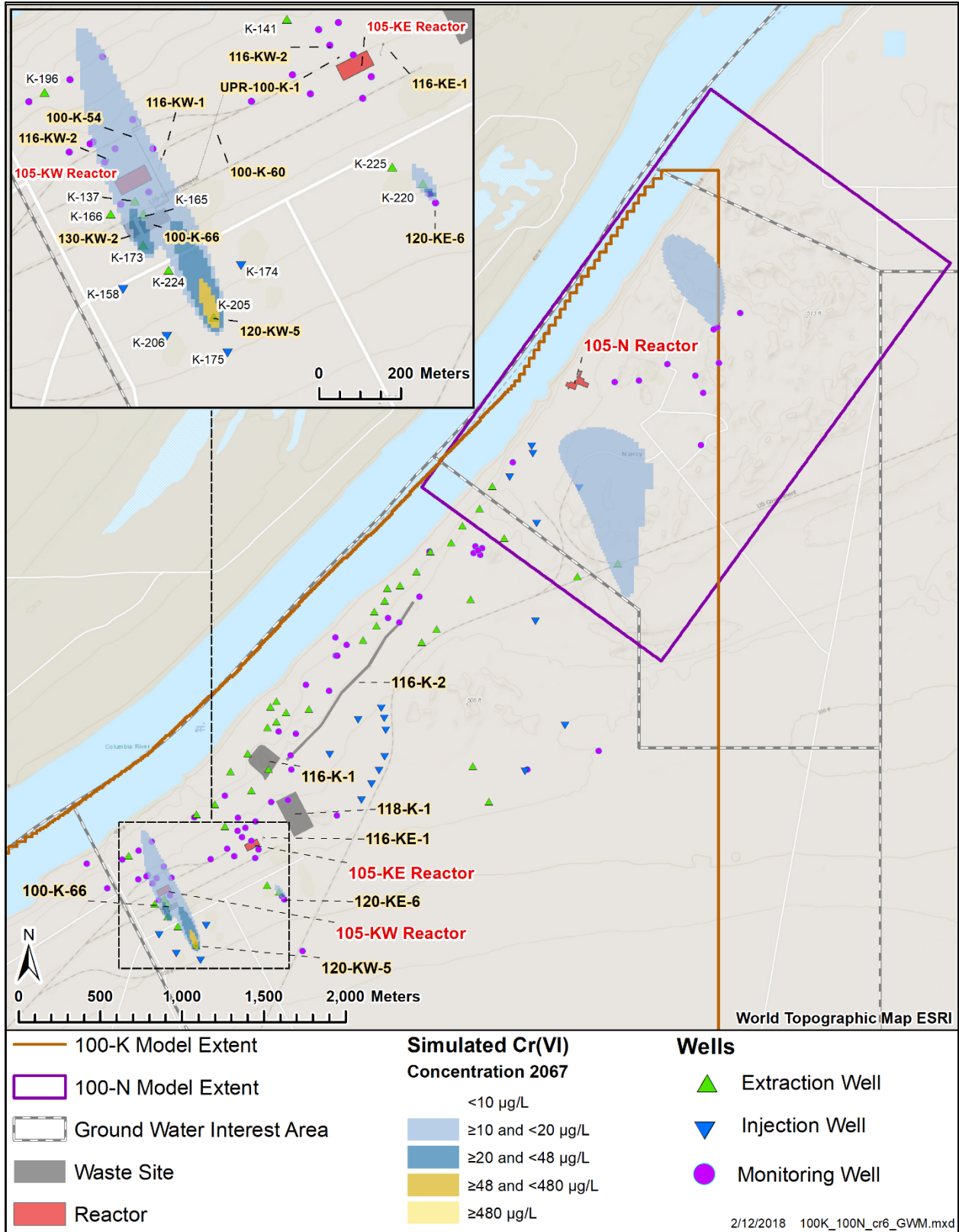


Figure 3-57. Simulated Cr(VI) Plume in 2067 at the Top of the Unconfined Aquifer

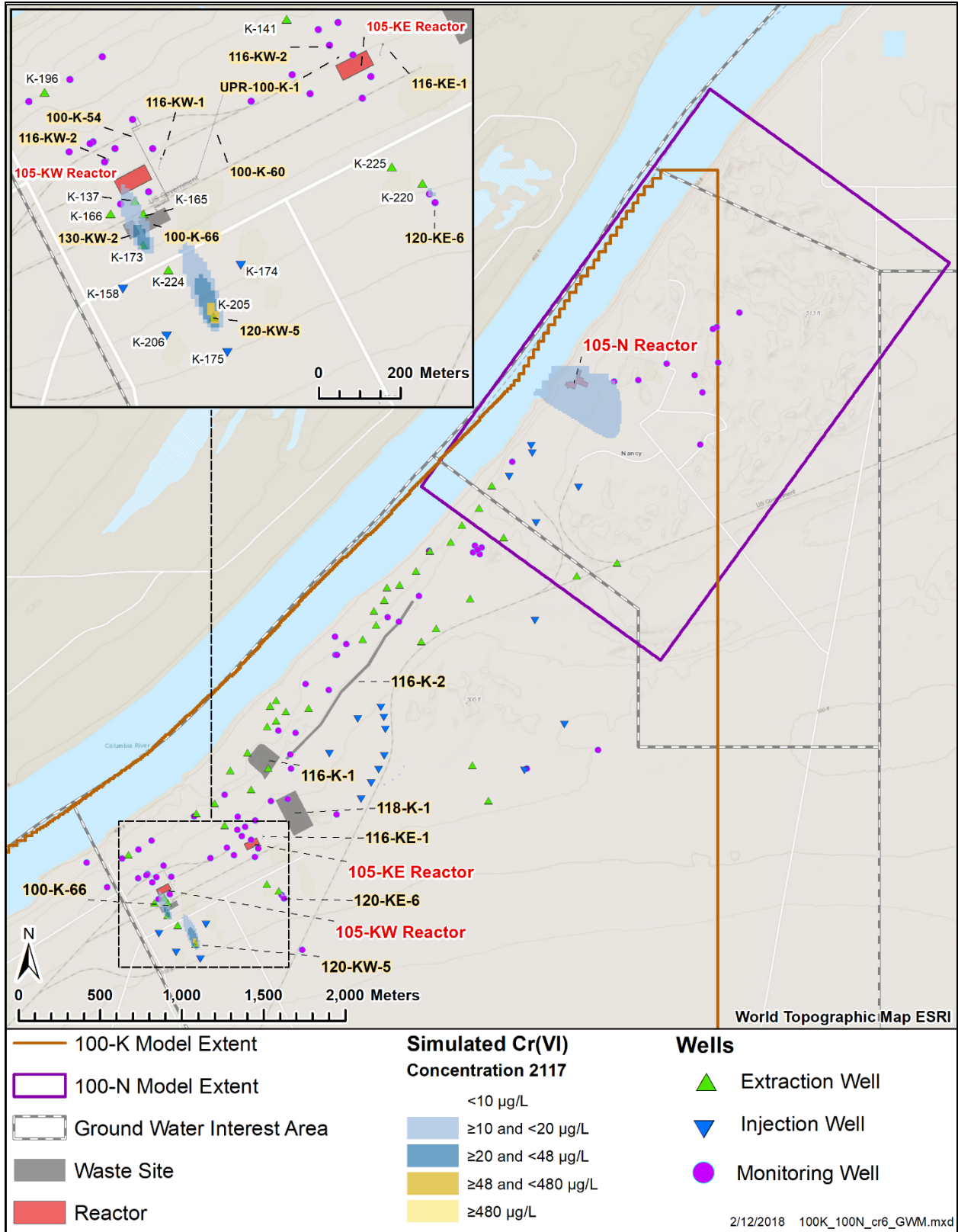


Figure 3-58. Simulated Cr(VI) Plume in 2117 at the Top of the Unconfined Aquifer

3.5.5.2 *Strontium-90*

The no further action case is assumed to begin in January 2020, with the pump and treat system continuing operation as described in SGW-58690, *Remedial Process Optimization Work Plan for 100-HR-3 and 100-KR-4 Groundwater Operable Units Interim Action* until then. Figure 3-59 shows the 2017 Sr-90 plume configuration, and Figure 3-60 shows the simulated extent 100 years later. Note that while radioactive decay has reduced concentrations, the presence of sources near both reactors (especially 100-K-UPR-1) and high initial concentrations result in concentrations greater than 8 pCi/L in 300 years.

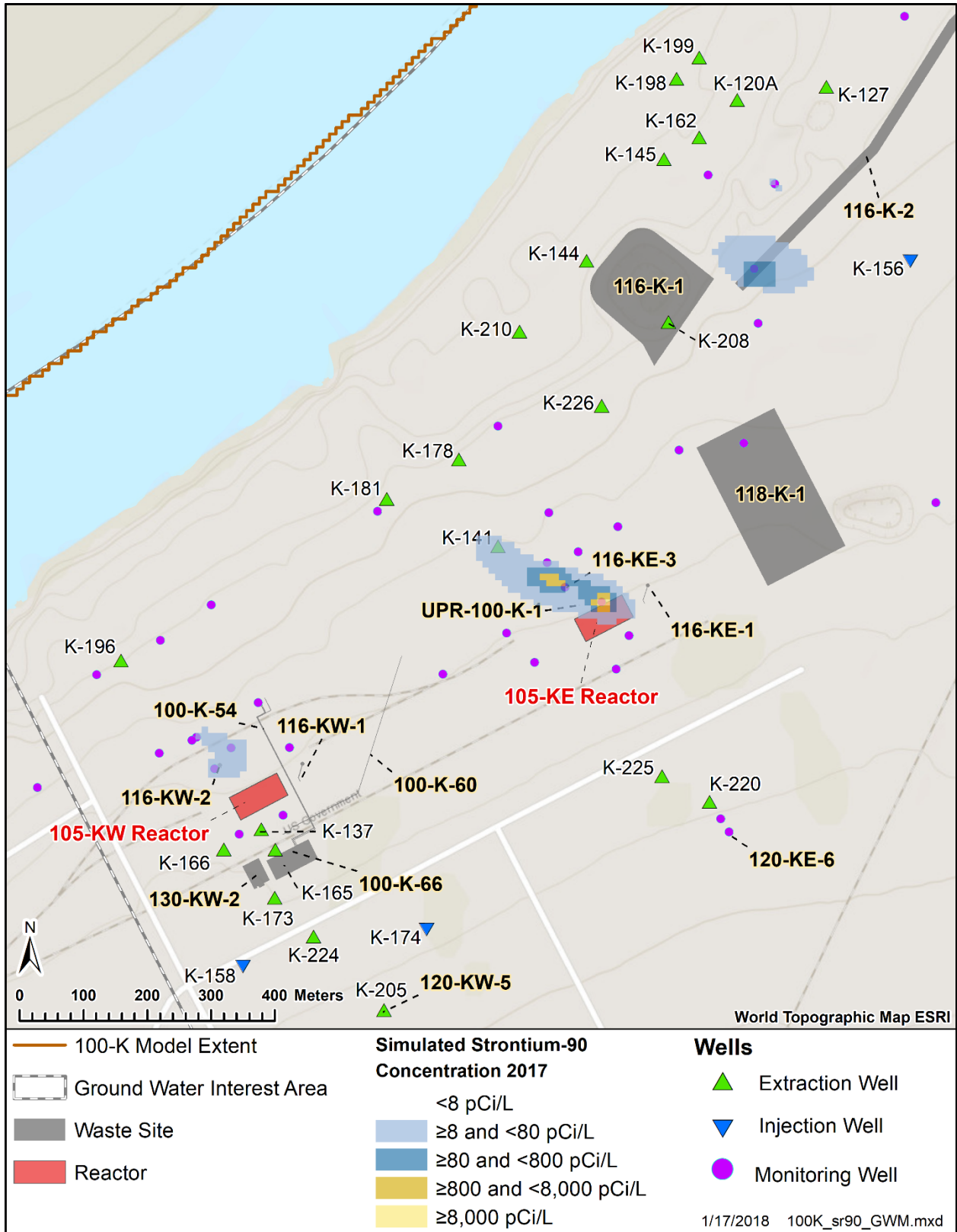


Figure 3-59. Simulated Sr-90 Plume in 2017 at the Top of the Unconfined Aquifer

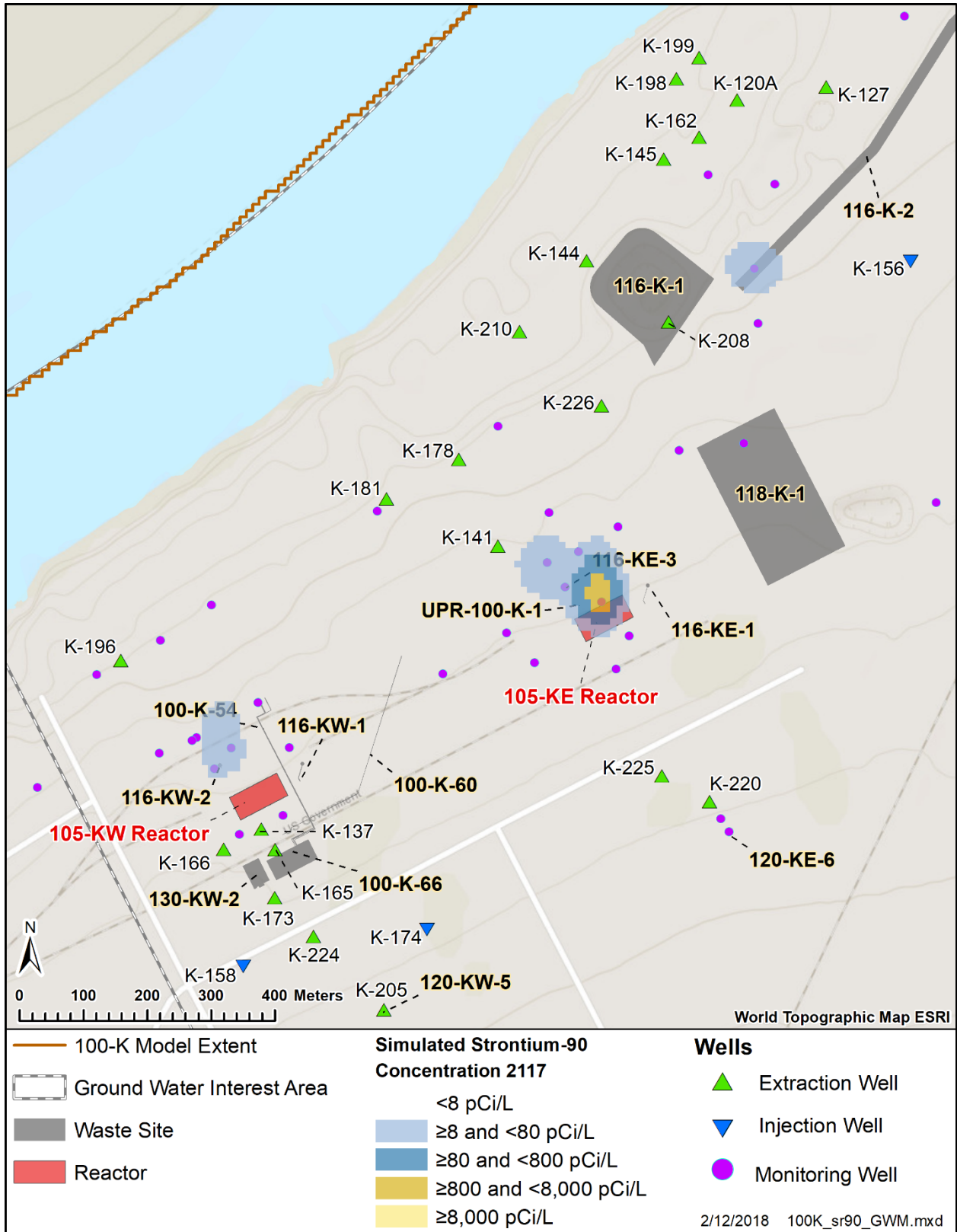


Figure 3-60. Simulated Sr-90 Plume in 2117 at the Top of the Unconfined Aquifer

3.5.5.3 Carbon-14

The no further action case is assumed to begin in January 2020, with the pump and treat system continuing operation as described in SGW-58690, *Remedial Process Optimization Work Plan for 100-HR-3 and 100-KR-4 Groundwater Operable Units Interim Action* until then. Figure 3-61 shows the C-14 plume in 2017, and Figure 3-62 shows the simulated plume in 2027. Due to source depletion – the C-14 half life is too long for radioactive decay to affect the results – the simulated plume extent is shrinking. The plume has dissipated below 2,000 pCi/L by 2033.

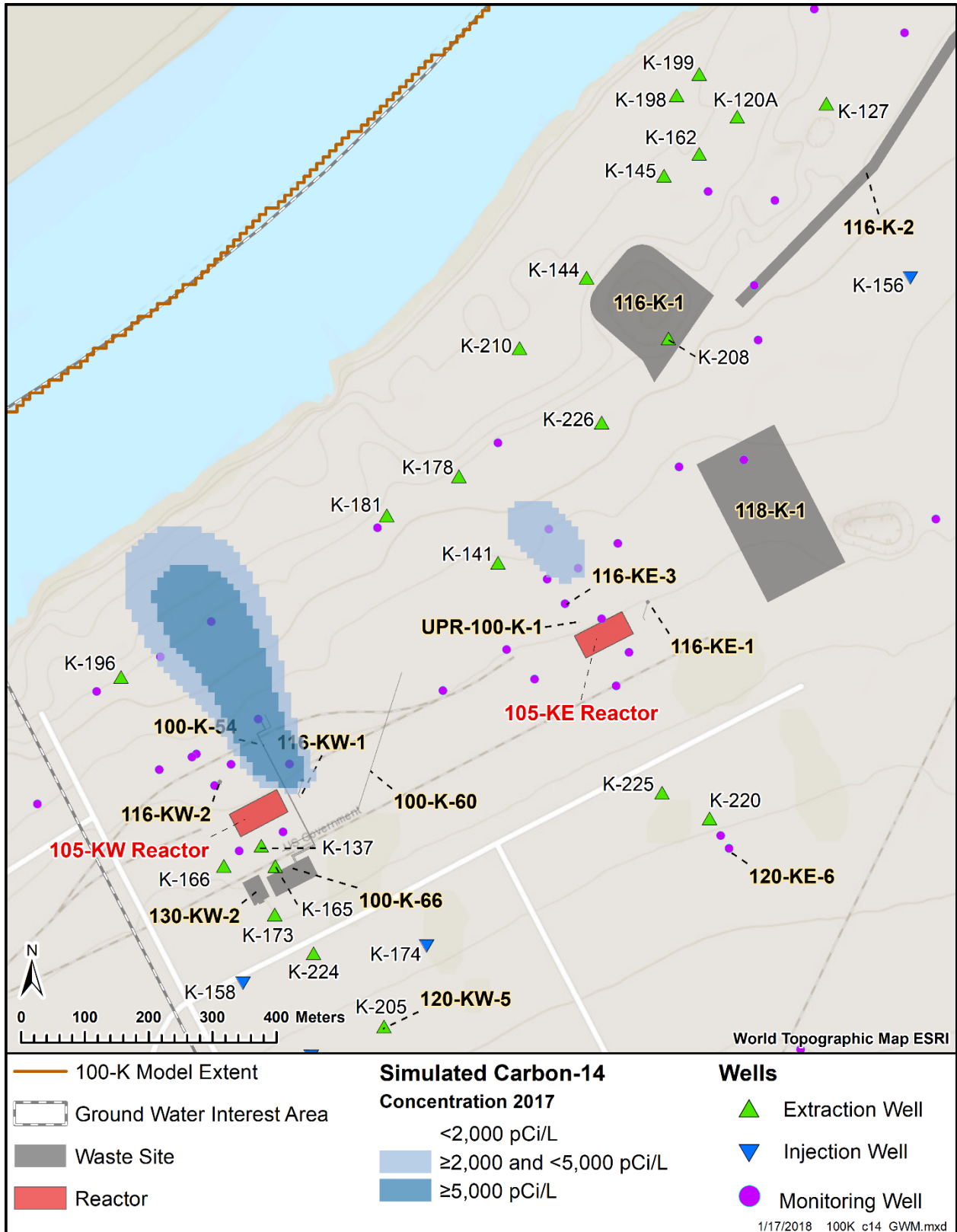


Figure 3-61. Simulated C-14 Plume in 2017 at the Top of the Unconfined Aquifer

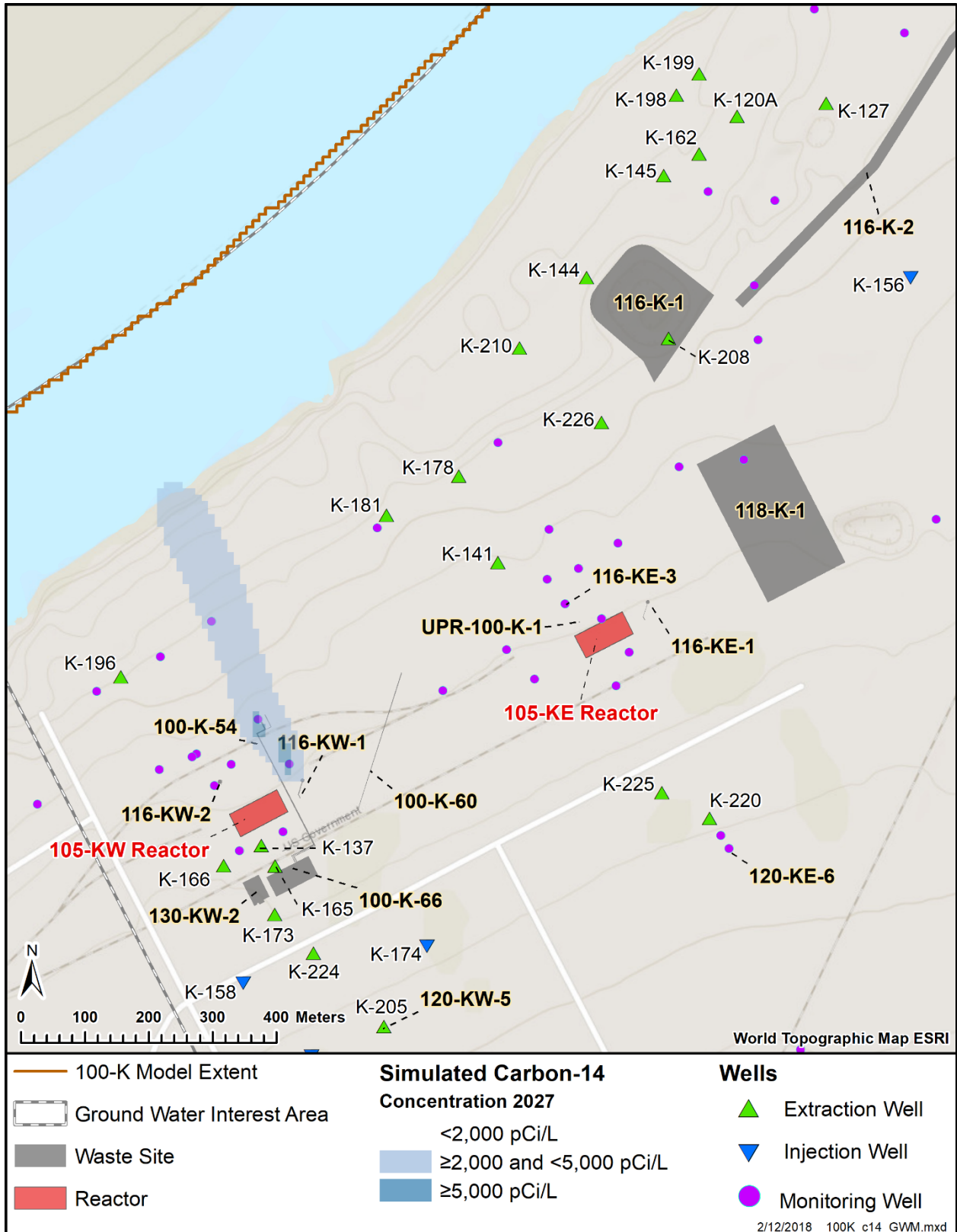


Figure 3-62. Simulated C-14 Plume in 2027 at the Top of the Unconfined Aquifer

3.5.5.4 Nitrate

The calibration model, which used the plume from the 2013 annual groundwater monitoring report as the initial concentration simulated concentrations below cleanup level everywhere except the source location (Figure 3-46). However, the 2016 annual groundwater plume reported a larger plume footprint based on recently observed concentrations. Therefore, simulated concentrations at the end of year 2016 are replaced by the plume from 2016 annual groundwater monitoring report (DOE/RL-2016-67, Rev. 0, *Hanford Site Groundwater Monitoring Report for 2016*) for the predictive simulation.

The no further action case is assumed to begin in January 2020, with the pump and treat system continuing operation as described in SGW-58690, *Remedial Process Optimization Work Plan for 100-HR-3 and 100-KR-4 Groundwater Operable Units Interim Action* until then. Figure 3-63 shows the nitrate plume in 2017, and Figure 3-64 shows the simulated plume in 2024. Due to source depletion at 116-KW-1 the plume extent is greatly reduced, and all simulated concentrations are below 45 mg/L by 2027.

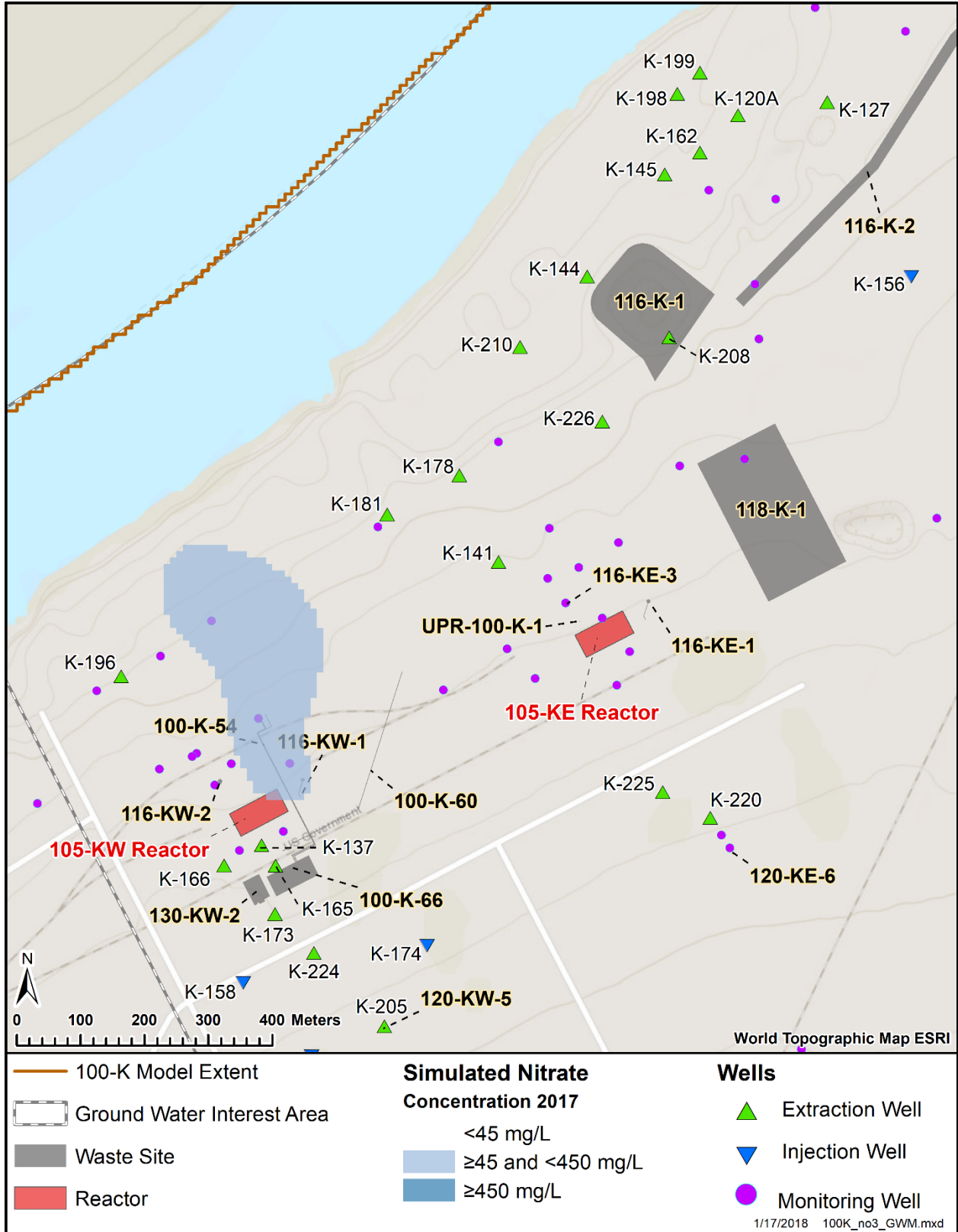


Figure 3-63. Simulated Nitrate Plume in 2017 at the Top of the Unconfined Aquifer

3.5.5.5 Tritium

The no further action case is assumed to begin in January 2020, with the pump and treat system continuing operation as described in SGW-58690, *Remedial Process Optimization Work Plan for 100-HR-3 and 100-KR-4 Groundwater Operable Units Interim Action* until then. Figure 3-65 shows the tritium plume in 2017, and Figure 3-66 shows the simulated plume in 2027. Source depletion and radioactive decay act to reduce impacts to groundwater with no tritium concentrations above 20,000 pCi/L simulated by 2027.

3.5.5.6 Trichloroethene

The calibration model, which used the plume from 2015 annual groundwater monitoring report as the initial concentration, simulates concentrations below cleanup level everywhere in the model domain (Figure 3-53). However, 2016 annual groundwater plume reported a larger plume footprint based on the recently observed concentrations. Therefore, simulated concentrations at the end of year 2016 was replaced by the plume from 2016 annual groundwater monitoring report (DOE/RL-2016-67, Rev. 0, *Hanford Site Groundwater Monitoring Report for 2016*) for the predictive simulation.

The no further action case is assumed to begin in January 2020, with the pump and treat system continuing operation as described in SGW-58690, *Remedial Process Optimization Work Plan for 100-HR-3 and 100-KR-4 Groundwater Operable Units Interim Action* until then. Figure 3-67 shows the TCE plume in 2017, and Figure 3-68 shows the simulated plume extent in 2022; the plume is present only in the aquifer under the river. Concentrations are below 5 µg/L by 2023.

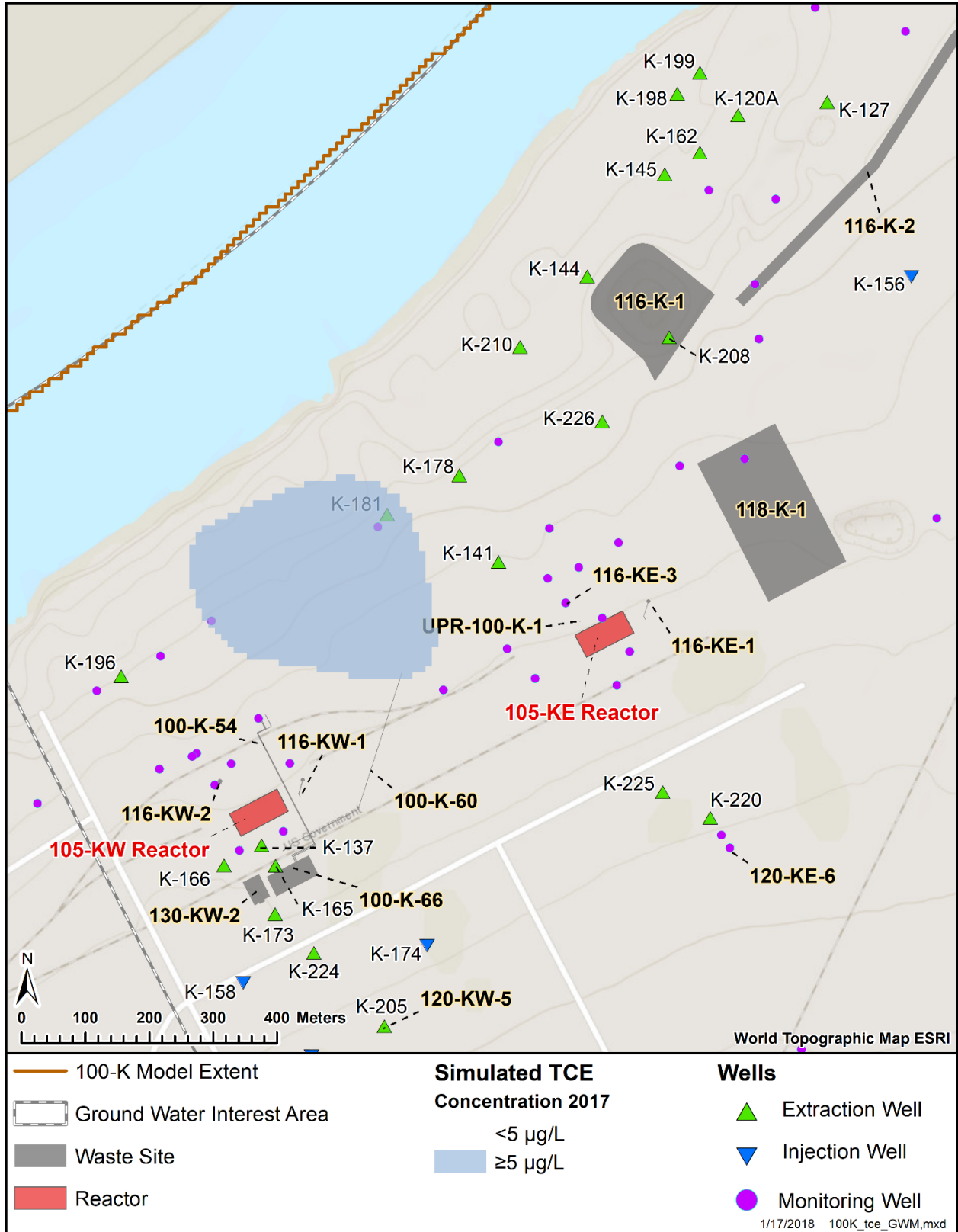


Figure 3-67. Simulated TCE Plume in 2017 at the Top of the Unconfined Aquifer

The no further action case was simulated for 125 years beginning in January 2018 for all the COPCs except for strontium-90. Strontium-90 was simulated for 300 years beginning in January 2018. The maximum aquifer concentration over time for all the COPCs are shown in Figure 3-69 thru Figure 3-74, and the maximum shoreline concentration over time for all the COPCs are shown in Figure 3-75 thru Figure 3-80. Hexavalent chromium and strontium-90 concentrations in the aquifer showed a gradual decline over time but remained above cleanup level near the source areas within simulated 125 and 300 years, respectively. On the other hand, simulated aquifer concentrations for the remaining COPCs declined below cleanup level within next 5 to 17 years.

Simulated concentrations along the Columbia River for all the COPCs were compared against their corresponding aquatic benchmark values. The aquatic benchmark values used for this analysis are documented in Table 7-13 of DOE/RL-2012-15, Rev.0 (*Remedial Investigation/Feasibility Study for 100-NR-1 and 100-NR-2 Operable Units*). Simulated hexavalent chromium concentration along the Columbia River shoreline gradually declines over time but starts to increase again in 50 years due to source concentrations in the aquifer reaching the shoreline. The concentration starts to decline again but never drops below aquatic benchmark of 10 µg/L. Simulated Carbon-14 concentration along the Columbia River shoreline gradually declines over time and drops below aquatic benchmark (609 pCi/L) within 16 years of simulation period. Simulated concentrations along the Columbia River shoreline for the remaining COPCs always stay below aquatic benchmark throughout the simulation period.

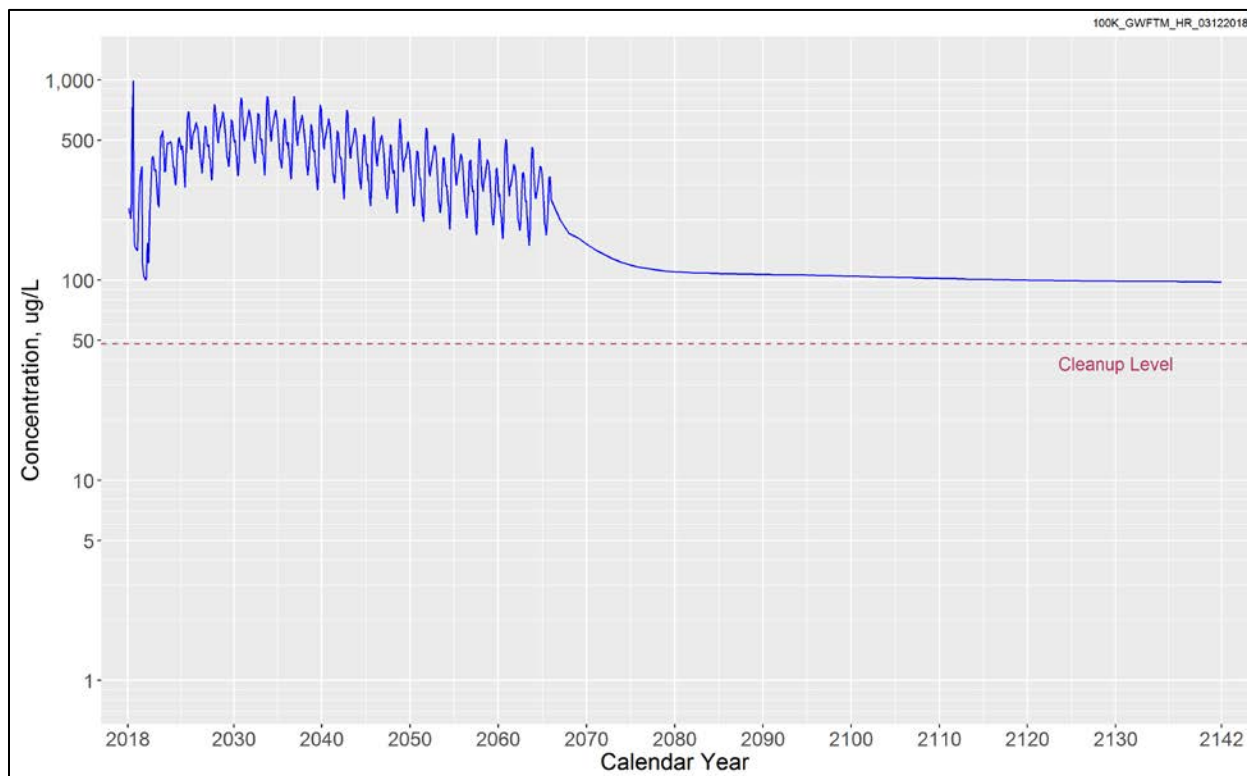


Figure 3-69. Maximum Simulated Cr(VI) Concentration in the Aquifer over 125 Years (No Further Action)

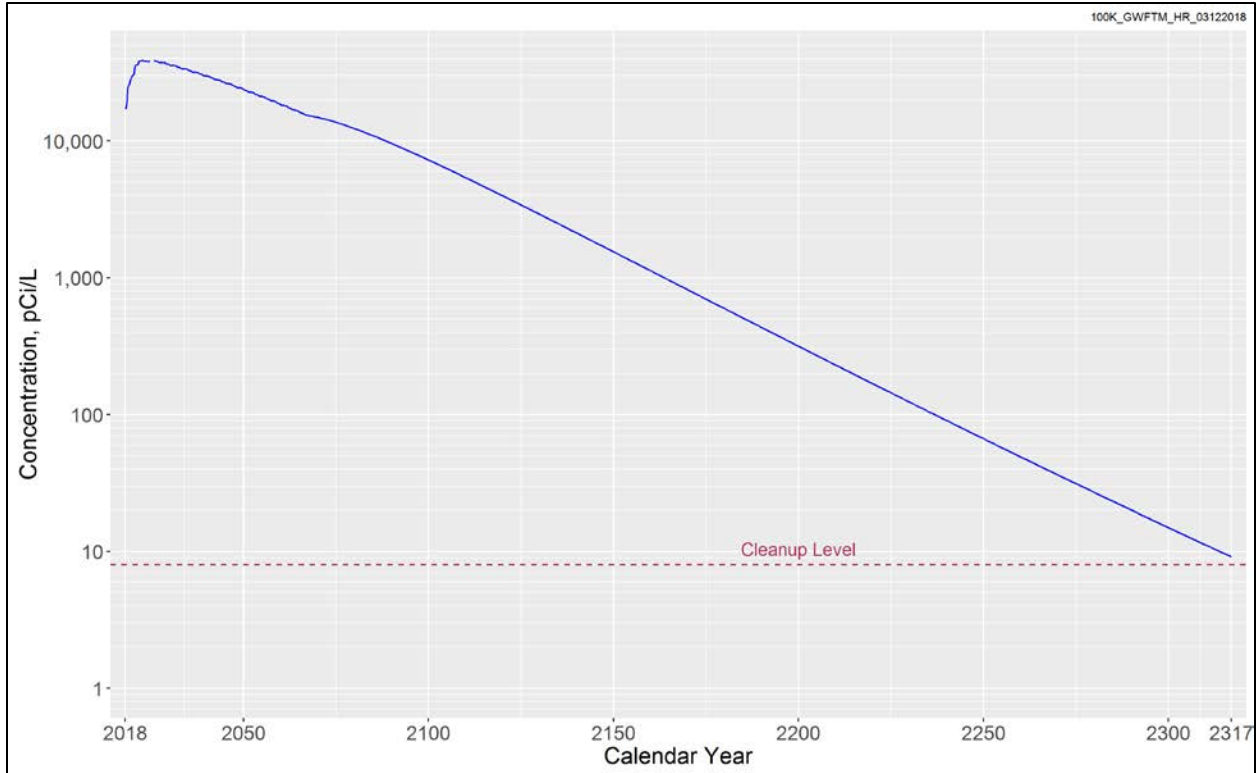


Figure 3-70. Maximum Simulated Sr-90 Concentration in the Aquifer over 300 Years (No Further Action)

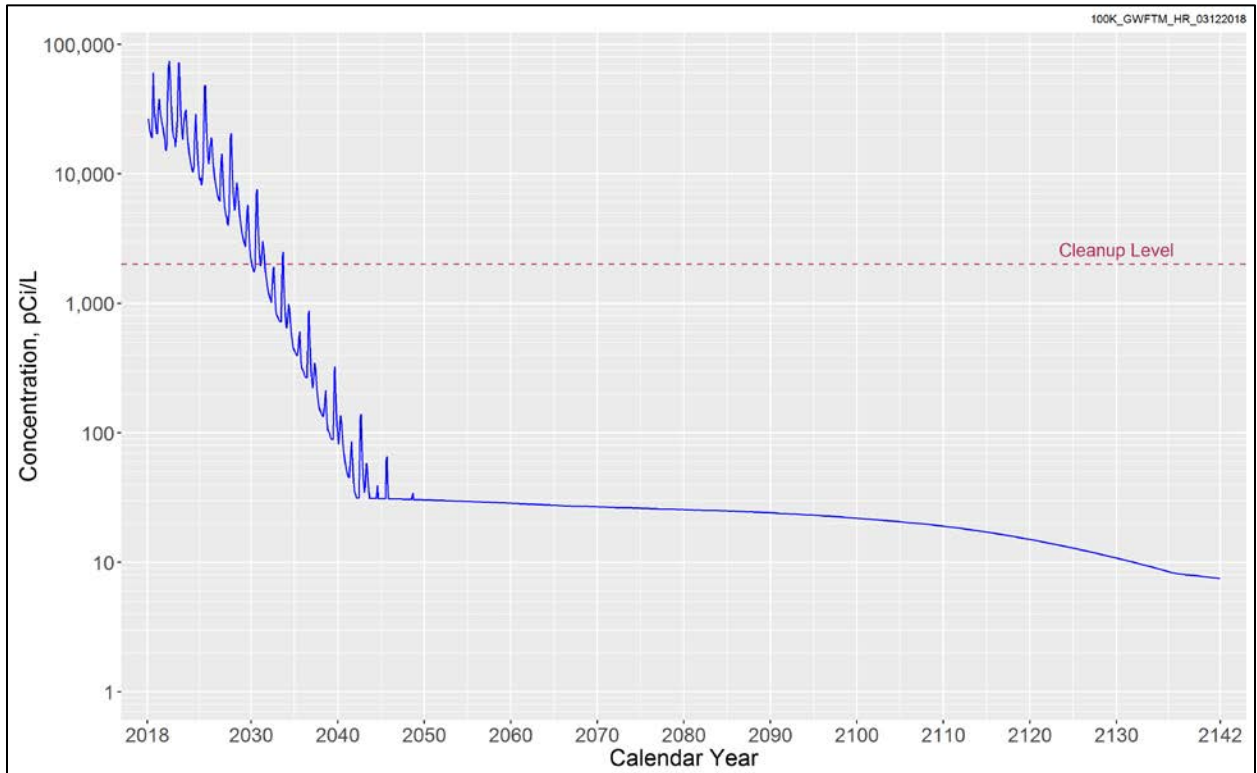


Figure 3-71. Maximum Simulated C-14 Concentration in the Aquifer over 125 Years (No Further Action)

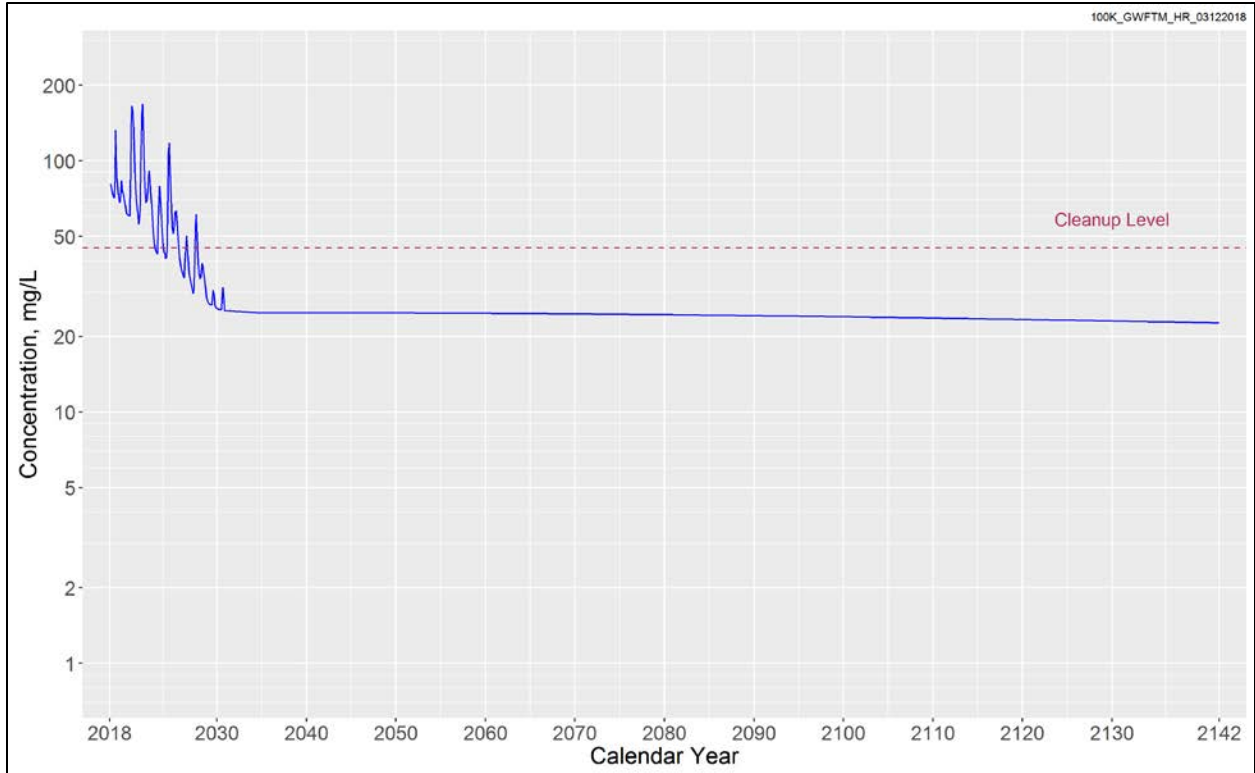


Figure 3-72. Maximum Simulated Nitrate Concentration in the Aquifer over 125 Years (No Further Action)

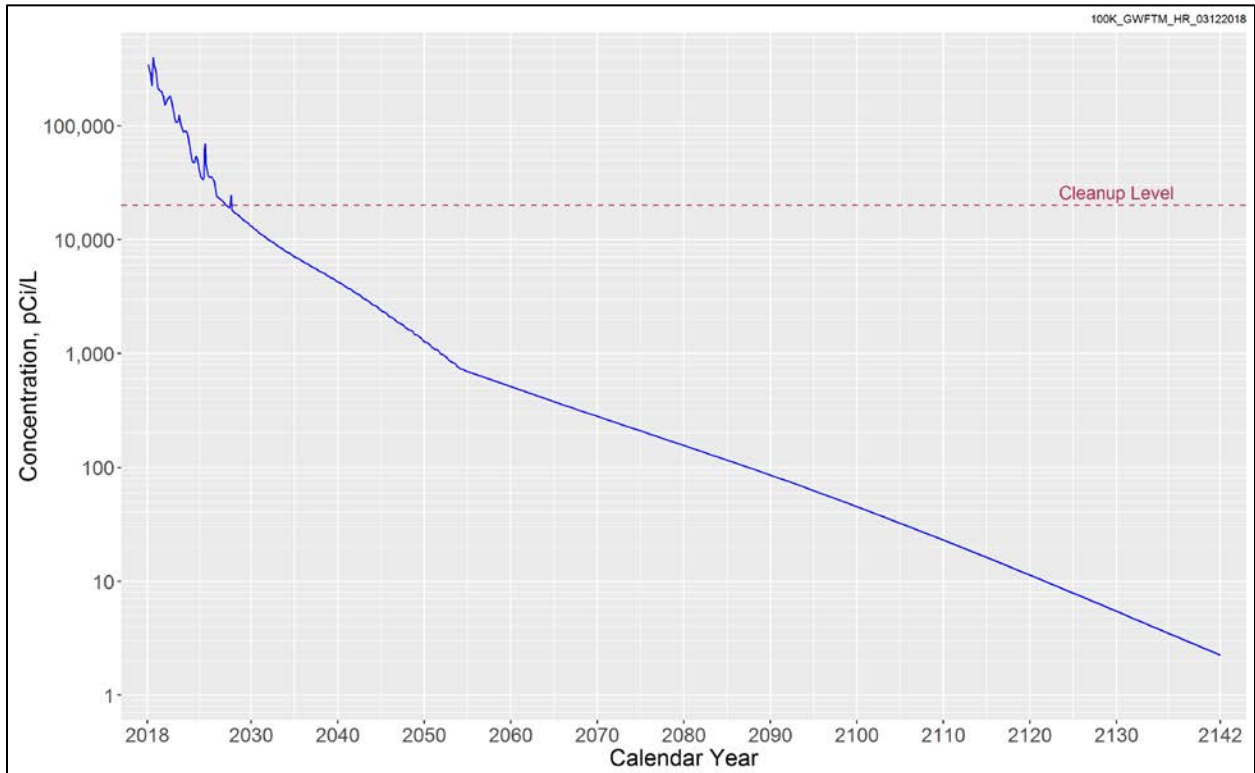


Figure 3-73. Maximum Simulated Tritium Concentration in the Aquifer over 125 Years (No Further Action)

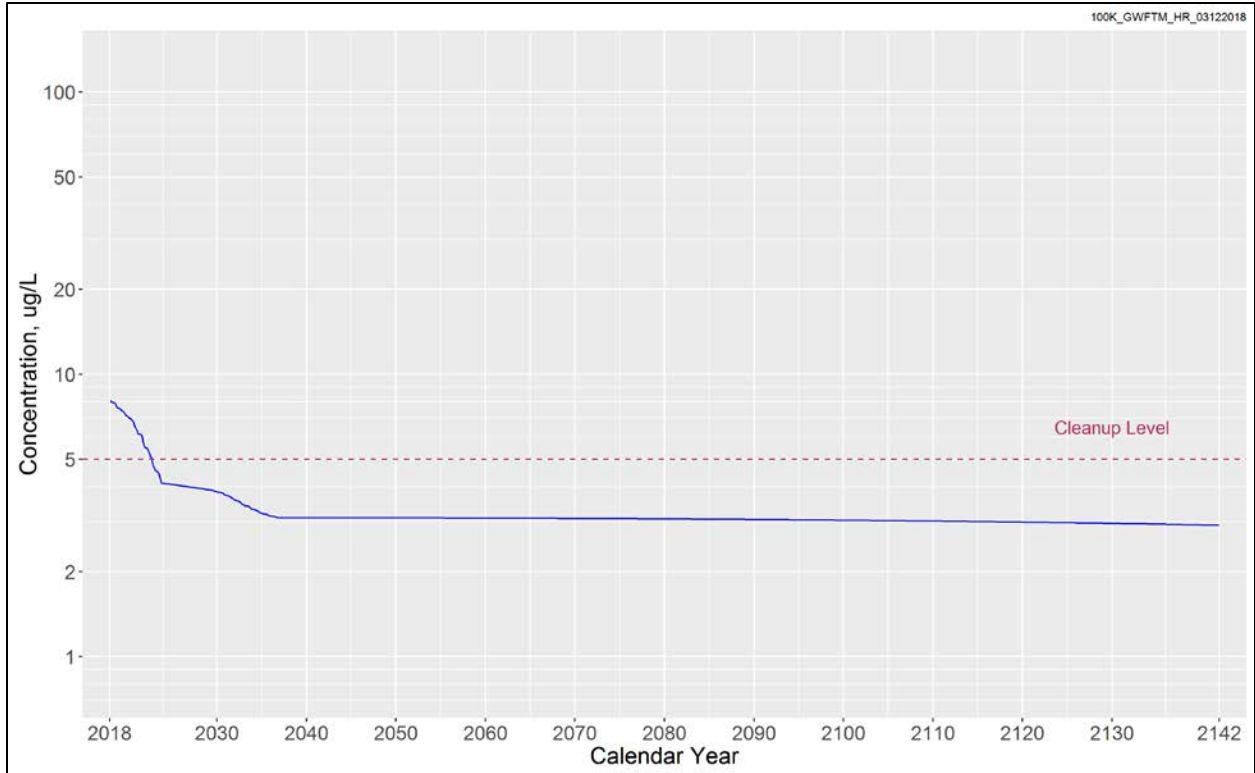


Figure 3-74. Maximum Simulated TCE Concentration in the Aquifer over 125 Years (No Further Action)

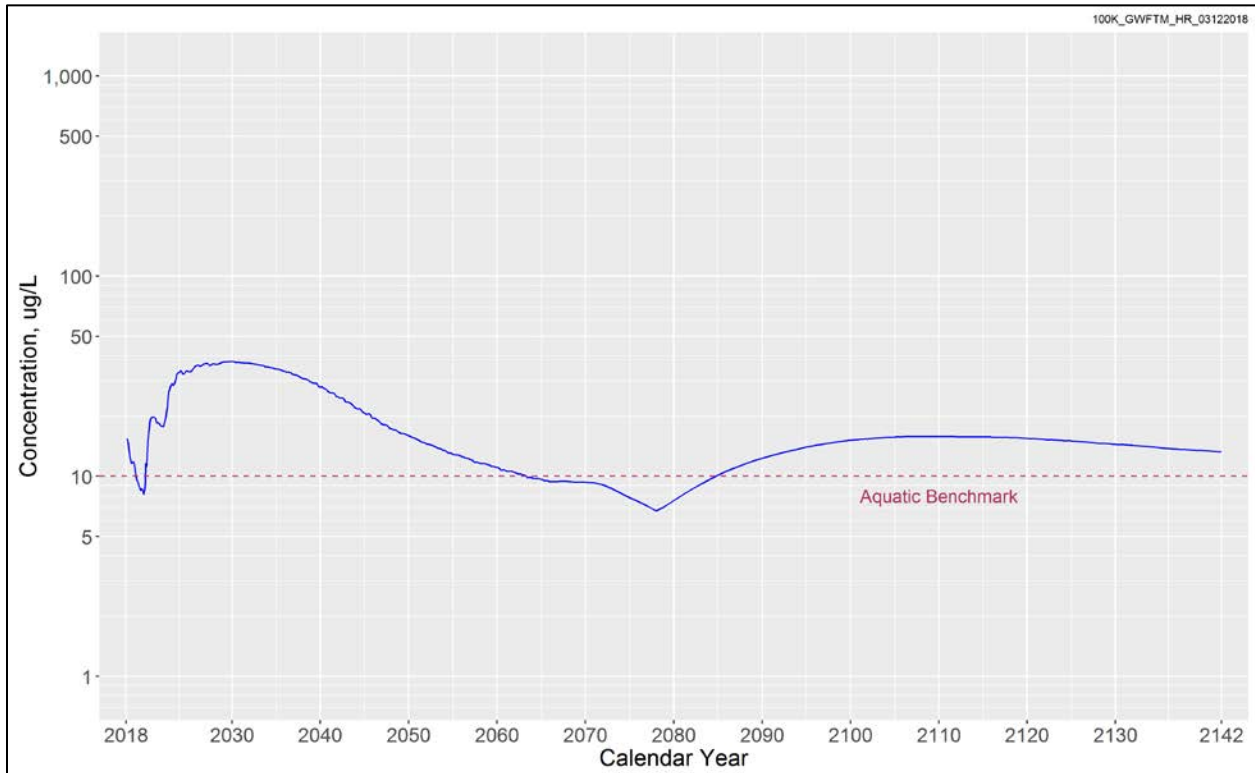


Figure 3-75. Maximum Simulated Cr(VI) Concentration at the Shoreline over 125 Years (No Further Action)

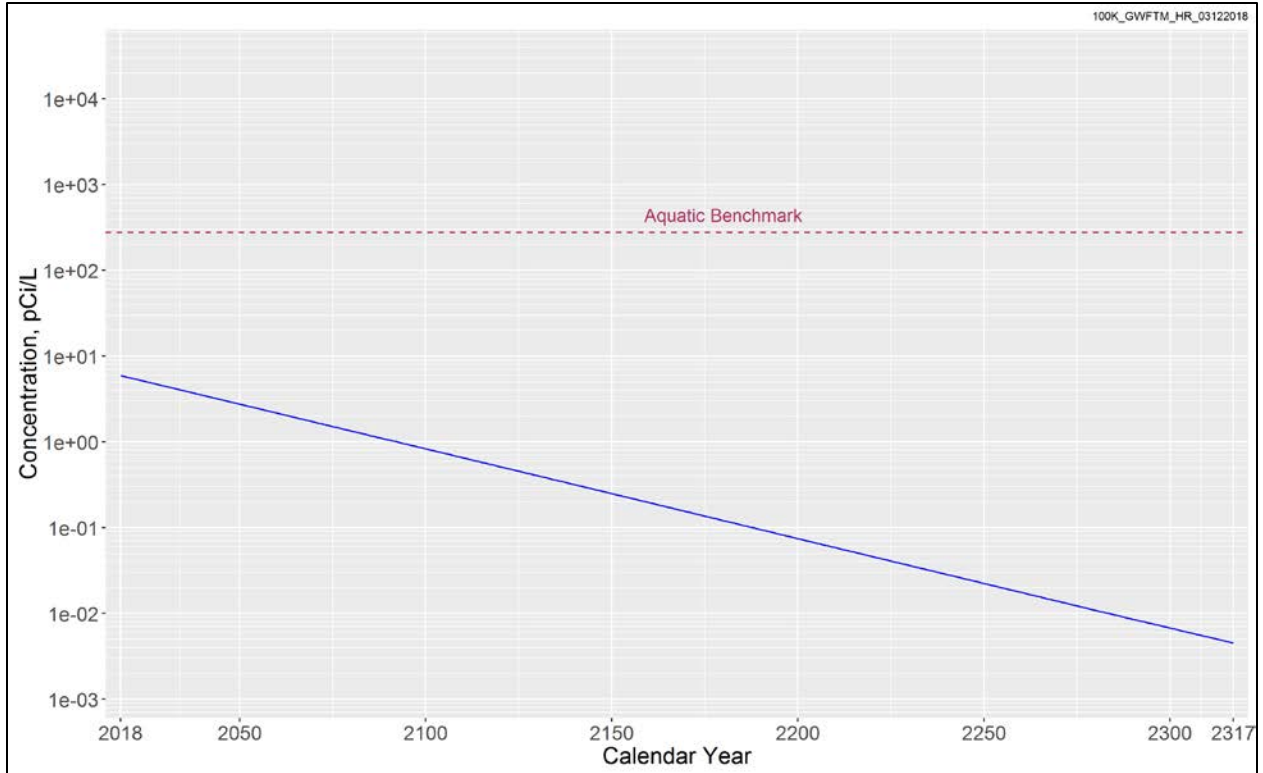


Figure 3-76. Maximum Simulated Sr-90 Concentration at the Shoreline over 300 Years (No Further Action)

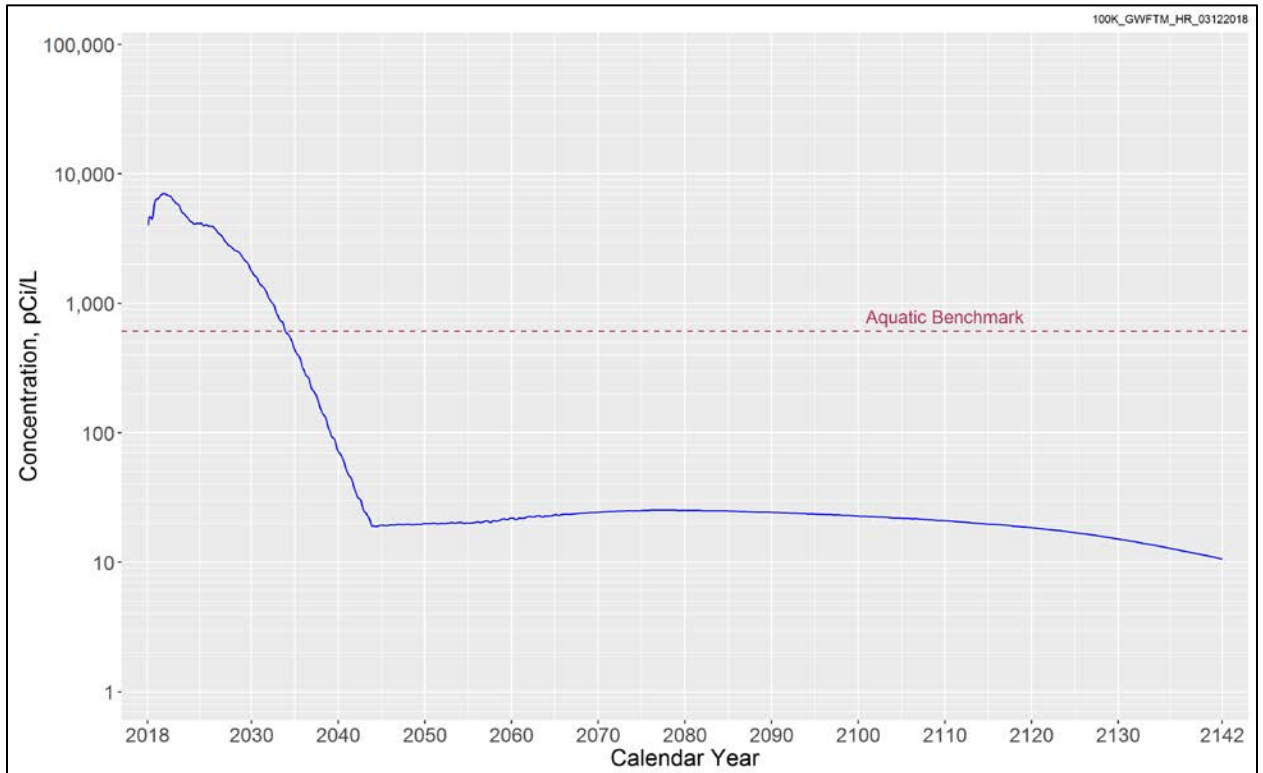


Figure 3-77. Maximum Simulated C-14 Concentration at the Shoreline over 125 Years (No Further Action)

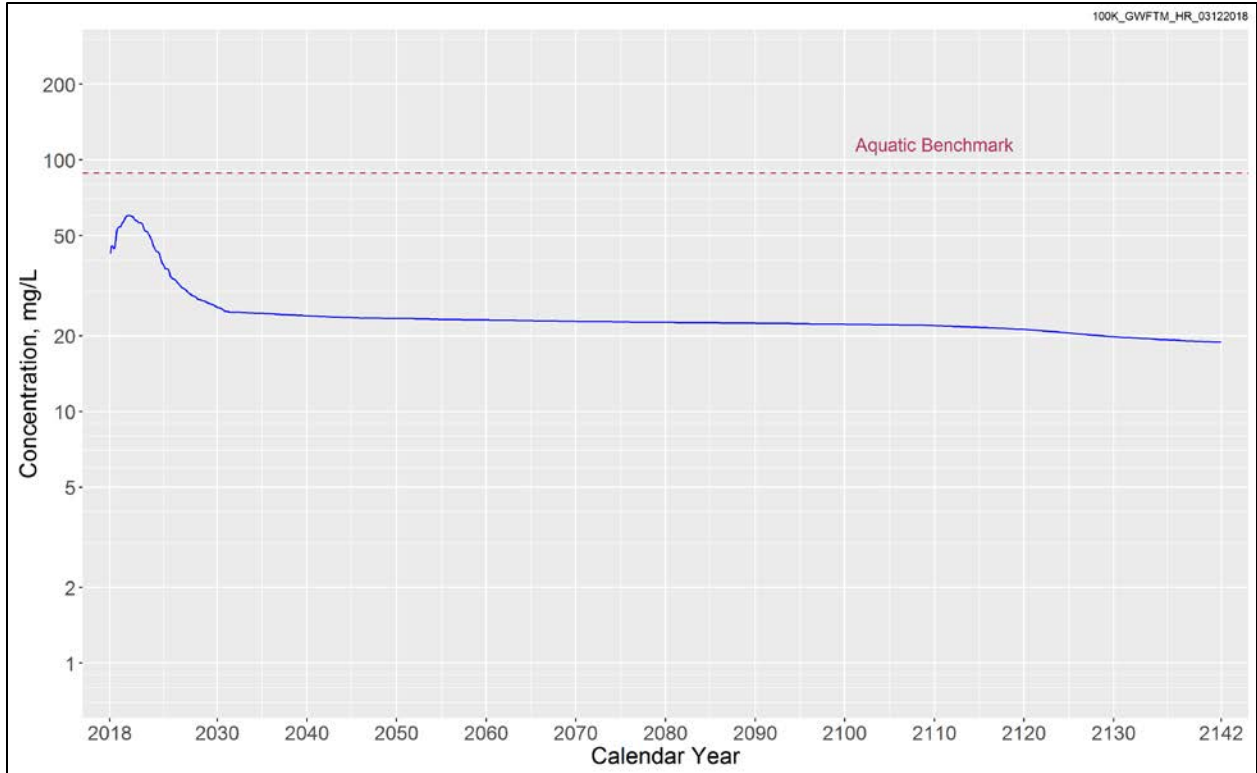


Figure 3-78. Maximum Simulated Nitrate Concentration at the Shoreline over 125 Years (No Further Action)

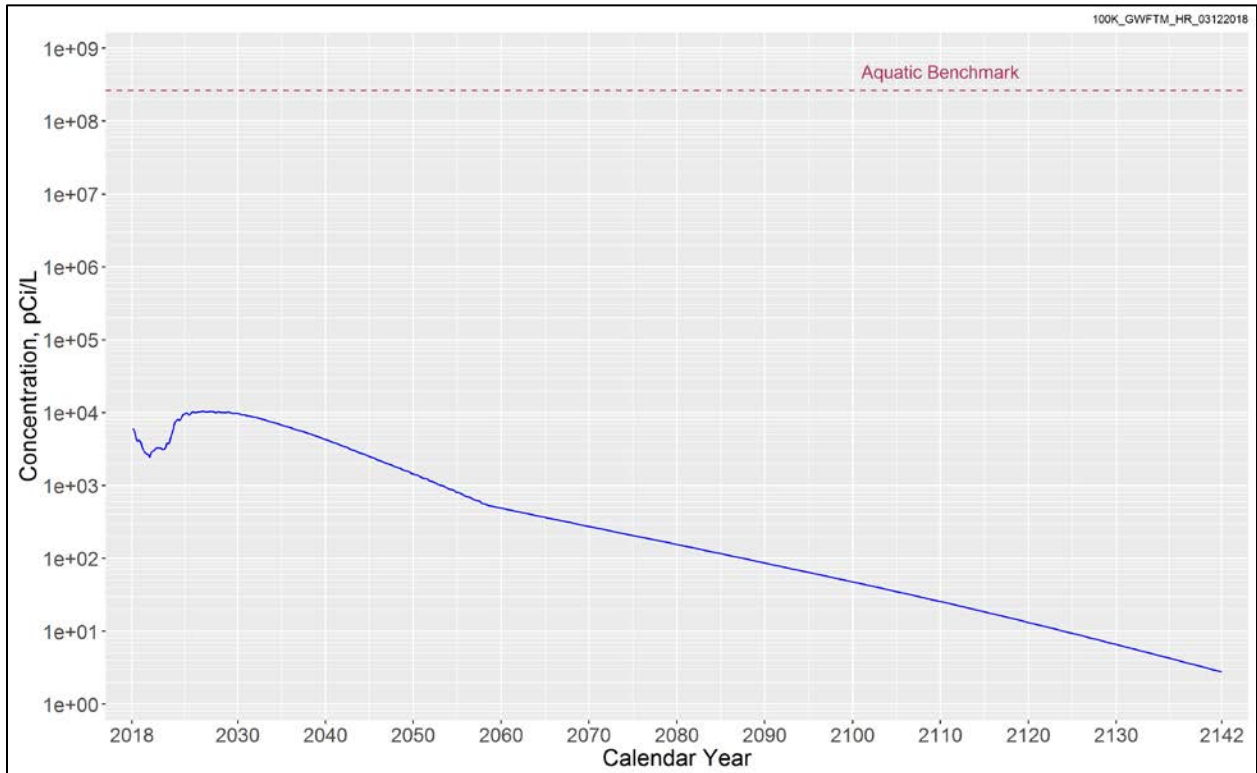


Figure 3-79. Maximum Simulated Tritium Concentration at the Shoreline over 125 Years (No Further Action)

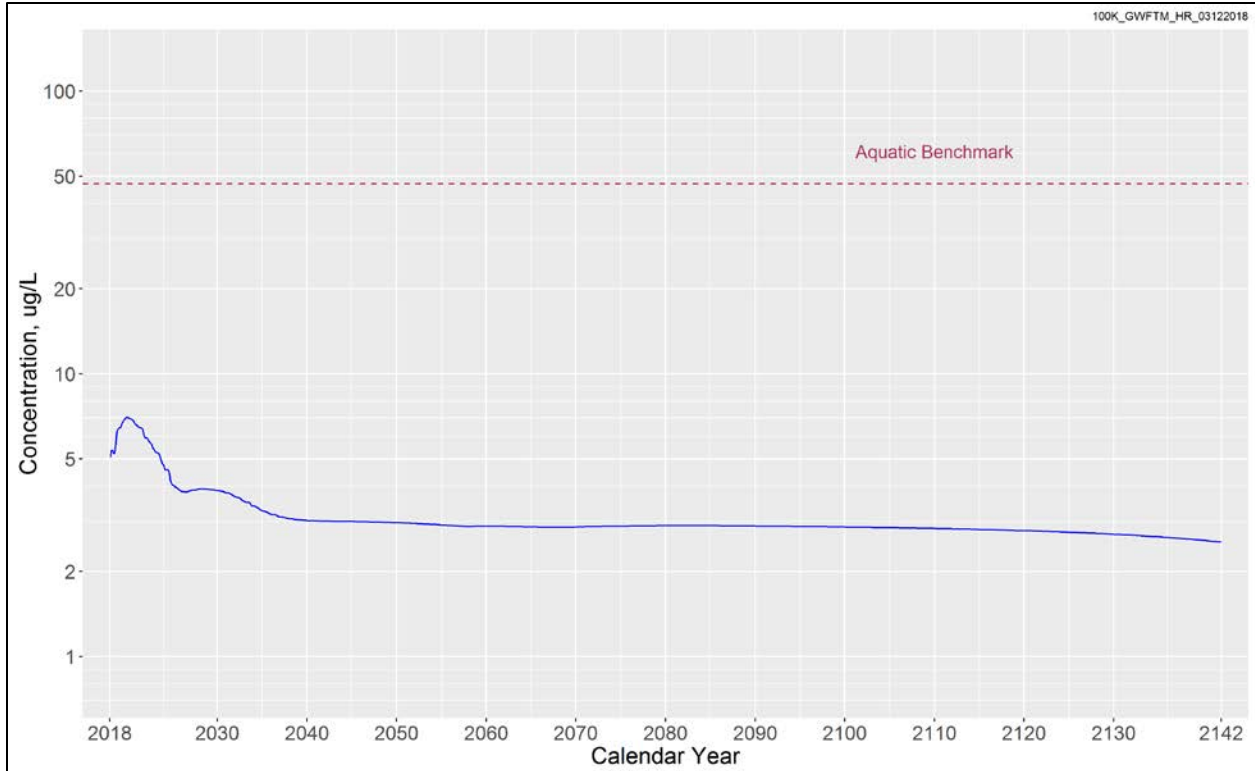


Figure 3-80. Maximum Simulated TCE Concentration at the Shoreline over 125 Years (No Further Action)

4 Model Sensitivity and Uncertainty Analysis

4.1 Sensitivity Analysis

As part of its parameter estimation algorithm PEST computes first derivatives of all adjustable model parameters. Thus, sensitivity analysis was iteratively conducted during model calibration. These derivatives are local parameter sensitivity that can also be analyzed to gain insight into important parameters near the calibrated values.

The IDENTPAR utility (part of PEST suite of software) was also used to assess model parameters. Parameters with a higher value are more informed by the calibration data. Figure 4-1 shows the total identifiability of each PEST adjustable parameter along with the contribution from each solution space eigenvector to each parameter-specific bar. Strongly identifiable model hydraulic parameters (Figure 4-1) include specific yield (sy1), GHB conductance at the eastern (condr) boundary, and some pilot points that generate the hydraulic conductivity field. Pilot points 2, 3, 9, 14, 15, 17, 18, 28, and 36 (Figure 4-2) are located near the high-density calibration dataset and hence, found to be strongly identifiable.

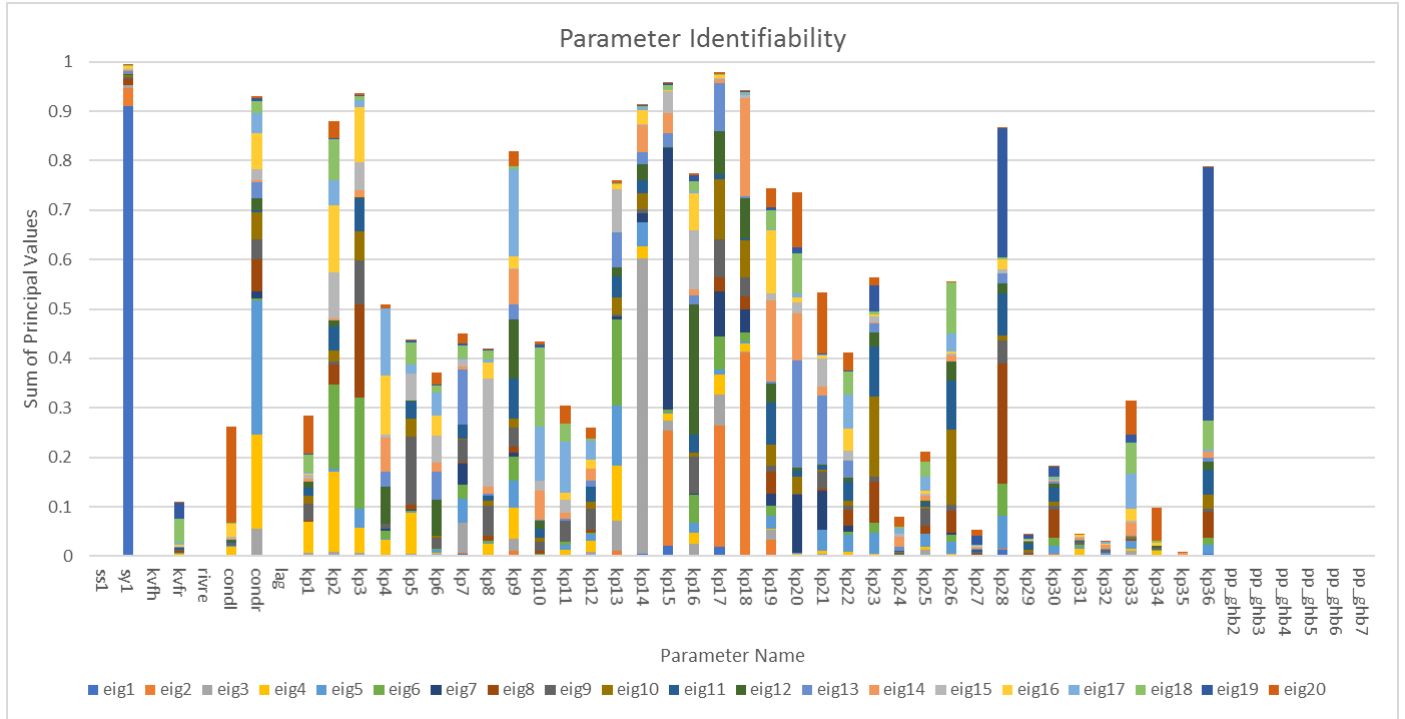


Figure 4-1. Flow Model Parameter Identifiability

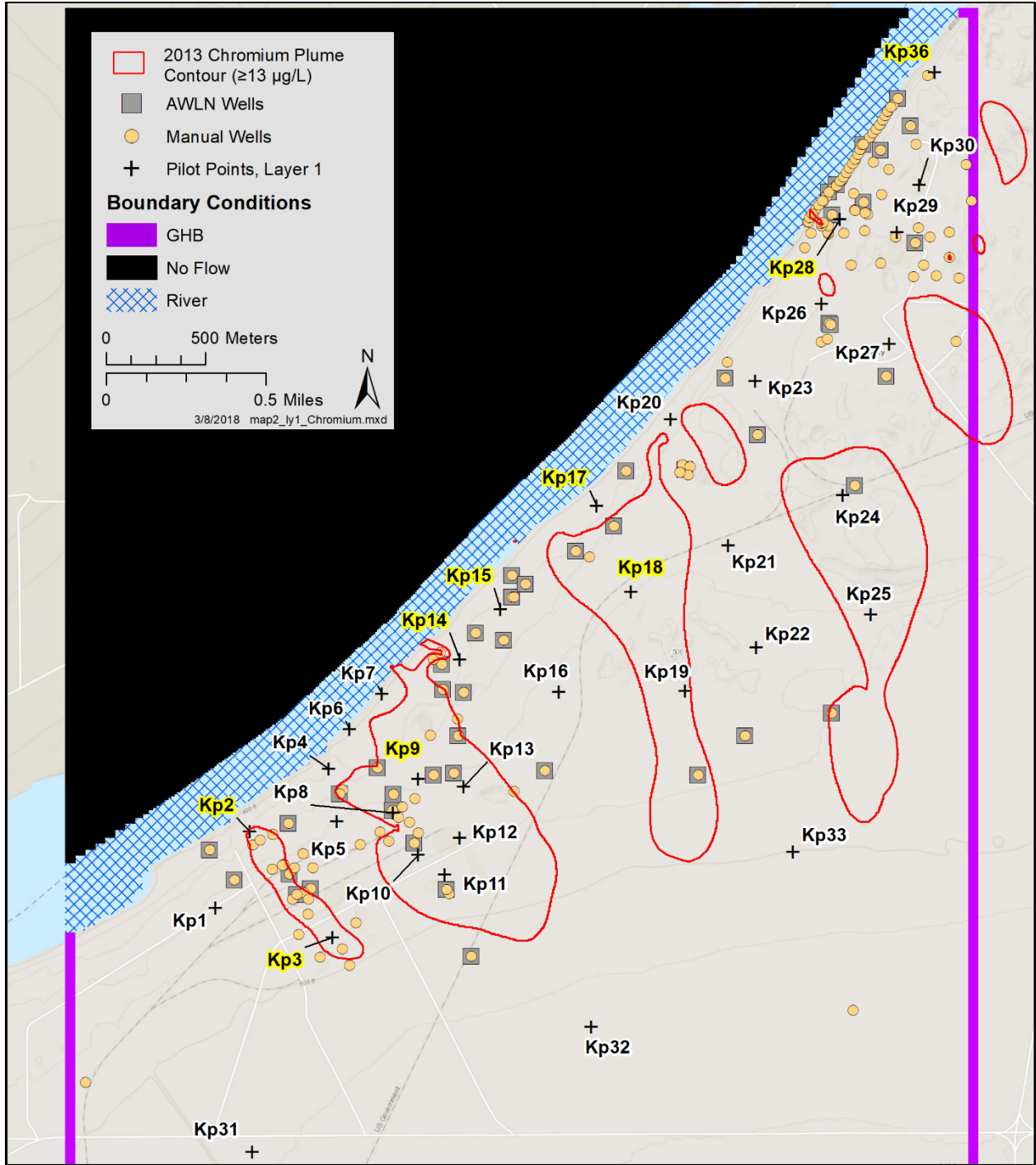


Figure 4-2. Identifiable Pilot Points (Highlighted in Yellow) with Respect to Calibration Dataset and Mapped 2013 Cr(VI) Plume

The range of values for hydraulic conductivity in the Ringold E is shown in Figure 4-3. Note that only one hydraulic conductivity value (1,500 m/d) was used for the entire Hanford formation located in the southern portion of the model. Comparing this figure to Figure 2-6 and Figure 2-7 shows that the lower values are comparable to observed hydraulic conductivity values, as are the ranges. The Ringold E has a smaller range than Hanford. Many of the Hanford values are above 1,000 m/yr, which is consistent with

new geologic data showing the presence of cataclysmic flood gravels over a larger area than previously thought.

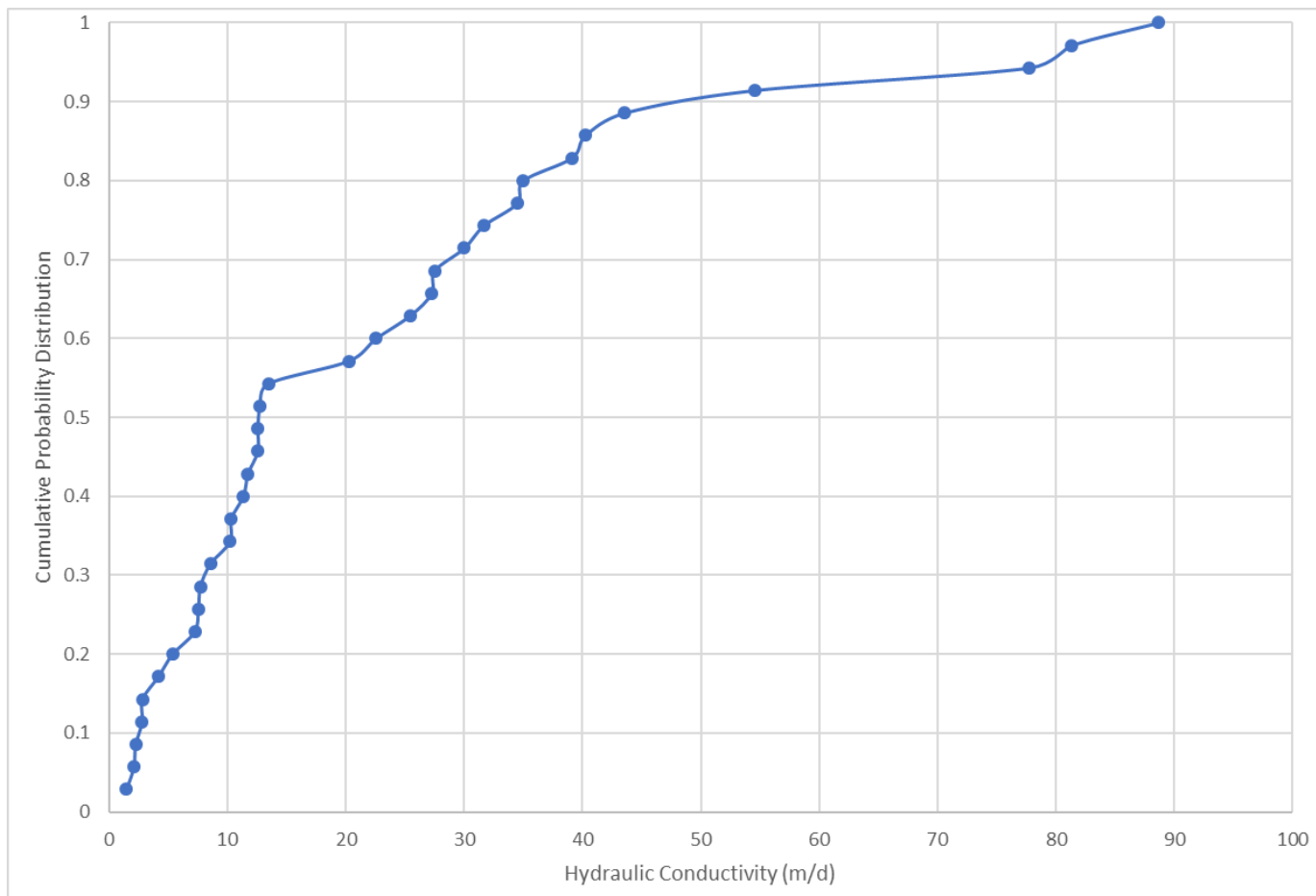


Figure 4-3. CDF of Calibrated Hanford and Ringold E Hydraulic Conductivity Pilot Points

4.2 Uncertainty Analysis

Bredehoeft (2005) suggests that selecting the proper conceptual model (that is, addressing conceptual model uncertainty) is a major problem in groundwater modeling analysis. He suggests that this can be overcome by collecting as much data as feasible using all applicable methods, and by leaving the conceptual model open to change. By using many types of groundwater data, including hydraulic head, concentrations of associated COCs within 100-K, knowledge of source areas, and groundwater discharge patterns to the river model uncertainty has been reduced, but is difficult to quantify. The broad source strengths and locations have been inferred from groundwater monitoring and historical waste site knowledge. However, because the interval of this observation (about the last 15 years or less) is much less than the long-term forecasts required in the RI/FS process uncertainty remains.

Diffusion of solute into stagnant zones (not considering sorption) can result in significant tailing of concentrations. That is, solute is not flushed as fast as anticipated based on the properties of the formation resulting in persistent concentrations above the cleanup level. Suthersan et al. (2009) discuss scale issues with plumes including geologic factors such as paleochannels and changes in depositional environments. Additionally, they observe that plume maps are typically interpreted using a conceptual model of

transport in homogeneous media resulting in relatively smooth concentrations. Field observation has shown that most flow and contaminant flux occurs through the most permeable parts of formations. This can result in advection in some areas and diffusion in others, at greatly differing time scales. This conceptual model is known as the dual-domain, non-equilibrium model (Suthersan et al., 2013). PNNL-21845 identified local-scale heterogeneities beneath 100-C-7:1 (located 100-BC OU) that may lead to large-scale preferential flow paths and potentially the presence of a dual-domain effect. Because of the relatively rapid groundwater flow at 100-K the next several years of groundwater quality data should be useful in detecting this process.

A substantial source of uncertainty in this analysis comes from continuing sources that were inferred to exist in the vadose zone. Calibration of continuing sources was performed by matching the overall observed concentration trends and the observed maximum concentrations at the nearby monitoring wells from the waste sites. However, in absence of robust characterization of the deep vadose zone, the uncertainty on the contaminant mass strength (i.e., concentration, areal extent and vertical distribution) remains high for estimating vadose zone sources. For example, the P&T system in KW area was turned off to perform a Cr(VI) rebound study from May 17, 2016 to April 16, 2017. The calibration of the Cr(VI) continuing sources in KW area was focused on the persistent groundwater concentration at the monitoring wells during the rebound study timeframe. Therefore, it can be said that the calibration of the continuing source is well represented in the PRZ that contributes to the aquifer during the rebound study. However, the contamination in the upper vadose zone and the areal extent of the source remain highly uncertain without any characterization of the deep vadose zone. The estimated release rates from two Cr(VI) waste sites in KW area during the calibration period (i.e., 2014-2016) are shown in Figure 4-4 and Figure 4-5. The release rates are simulated in STOMP using a uniformly distributed contaminated soil column in vertical direction and a source footprint of 400 m² near the 183.1KW Headhouse and 1100 m² near well 199-K-173. Figure 4-6 shows the estimated lateral extent of the source area within KW area which was calibrated based on the observed concentrations of the nearby monitoring wells. However, there is a significant amount of uncertainty on the lateral extent of the source between 183.1KW Headhouse and well 199-K-173.

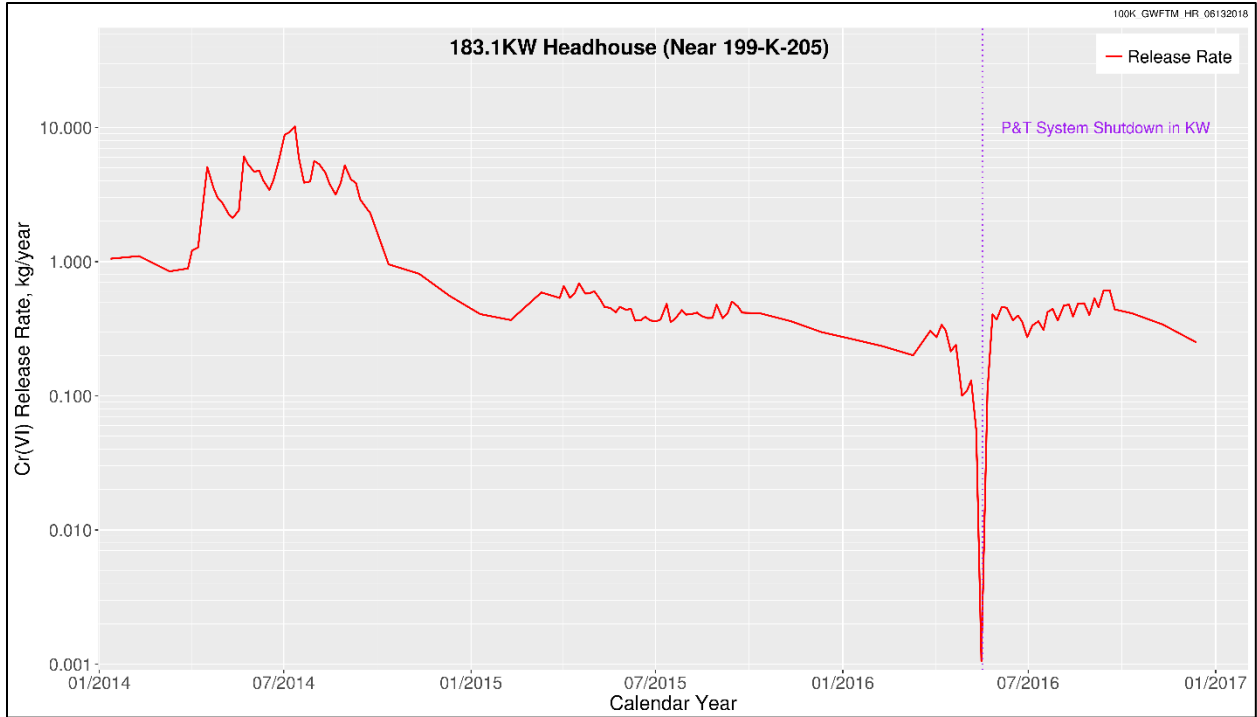


Figure 4-4. Hexavalent Chromium Release Rate from Sources near 183.1KW Headhouse during the Calibration Period

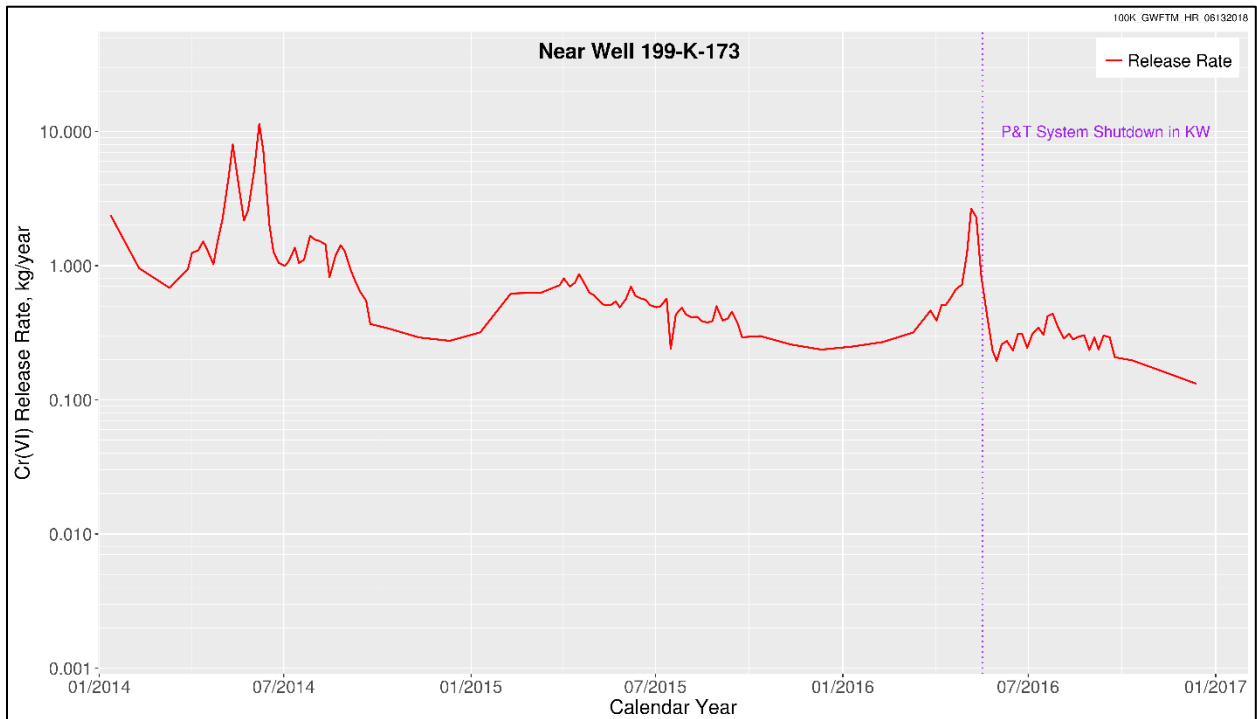


Figure 4-5. Hexavalent Chromium Release Rate from Sources near Well 199-K-173 during the Calibration Period

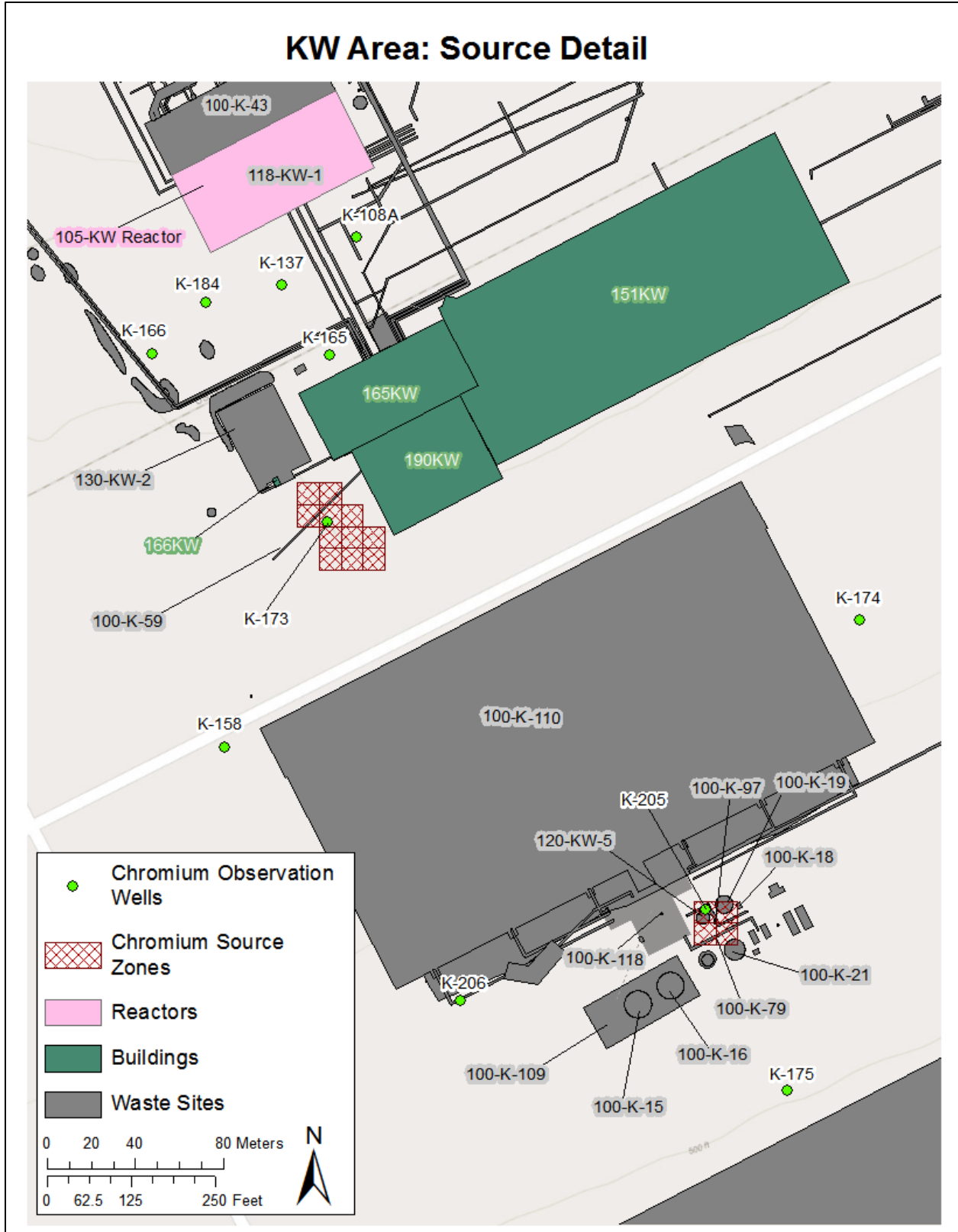


Figure 4-6. The Estimated Lateral Extent of the Hexavalent Chromium Sources in KW Area

5 Model Limitations

The 100-K GWFTM was built for the specific purpose of assessing groundwater remediation options in a small area near the former K reactors. It was calibrated using head and concentration data from 2013 through 2016. Future conditions that dramatically deviate from these may impair its accuracy. Such conditions may occur when the Columbia River Treaty between Canada and the United States is revised in 2024 – as of 2017 both countries have expressed interest in maintaining, but revising the treaty (<http://www.crt2014-2024review.gov/Default.aspx>). The spatial parameterization technique that was used is flexible and allows for non-uniform properties, but it employs a smoothness constraint to limit extrapolation in areas with little information. As new data is collected, conceptual understanding and its associated quantitative representation will change to an unknown degree. Plume maps generated from interpretations of field data were used to initialize the model and help interpret the results. Any errors or data gaps in these maps will be included in the model results, and features that cannot be independently identified cannot be included in the computations.

The National Research Council (2007) stated that while models are useful tools, they have innate limitations including:

- Computational limitations, assumptions, and knowledge gaps.
- Used to describe important, complex, and poorly characterized problems.
- Models in the regulatory process are best seen as tools providing inputs, as opposed to “truth-generating machines”.

Anderson and Lu (2003) compared a pump and treat system capture zone as modeled to actual system performance and found that even with some error the model contributed positively to the system design. Thus, despite these limitations the 100-K GWFTM can contribute to decisions about the site.

6 Model Configuration Management

The model described in this model package report is uniquely designated as the “100-K Groundwater Flow and Transport Model” and in abbreviation form as the “100-K GWFTM”.

Version control for this model will conform to the following version numbering convention:

- 100-K GWFTM Version #.#
 - The first version index will match the sequential calibrations of this model (first calibration = 1, second calibration =2, etc.).
 - The second version index will be used to denote a model modification, in terms of key hydraulic or structural parameters have been changed for specific purposes, without recalibration of the model. The second index is not applied to variations in model stresses (for example, pump and treat rate changes or modification of future recharge rate scenarios applied as a boundary condition).

For example, Model Version 1.0 is used to designate the first calibration and release of the 100-K GWFTM. Similarly, Model Version 2.1 would refer to (as an example) the second calibration of this model, with a subsequent variation in a physical characteristic determined not to require recalibration.

Note that individual simulations (or applications) will have separate configuration controlled following the guidance provided in CHPRC’s quality assurance project plan for modeling. Changes in model stresses (e.g., pump and treat system injection and extraction rates) are not tracked as model changes because these have no impact on model calibration; these are properly the subject of an environmental calculation file; model files for evaluation of changes in model stresses will be archived in the EMMA Application bin, indexed by ECF number.

All inputs and outputs for the development of this model will be committed to EMMA to maintain and preserve this configuration-managed basis of this model. Basis information (that information collected to form the basis for model input parameterization; e.g., historical pump and treat rates) is also stored in the EMMA for traceability purposes.

The software used to implement this model, CHPRC Build 8 of MODFLOW-2000, is configuration managed as discussed in Section 3.1. Configuration-managed software is obtained from the Hanford Site MKS Integrity™ configuration management system as required by CHPRC-00258.

6.1 Version History

Table 6-1 provides the version history of the 100-K GWFTM.

Table 6-1. Version History of the 100-K GWFTM

Version	Date Released	Calibration	Modification	MPR Revision
1.0	21 Mar 2018	Initial	Baseline	0

7 Model Recommendations

The following are recommendations for maintaining and improving the 100-K GWFTM:

1. Use of the AWLN data in model calibration assisted in better definition of aquifer transmissivity. More AWLN data has been collected in additional wells that could not be incorporated due to time constraints. It would be helpful to update the model with this data to improve the transmissivity distribution and resulting groundwater velocity. This would also be useful in years to come for evaluating the remedy performance.
2. An additional constraint useful for building confidence was the qualitative transport assessment using 2012 through 2016 mapped plumes. Given the groundwater velocity at 100-K future comparisons – even quantitative combined flow and transport calibration – would help build confidence in forecasts.
3. The Columbia River Basin Treaty will be renegotiated in 2024. This will result in changes to river operation. The impact of these changes on the groundwater system and associated remedies should be evaluated as they occur in order to ensure regulatory goals are met.

8 References

- ASTM D5979-96, 2014, Standard Guide for Conceptualization and Characterization of Groundwater Systems, ASTM International, West Conshohocken, Pennsylvania.
- Aero-Metric LiDAR, 2008, RCCC-Hanford Battelle/PNNL/DOE, Digital Orthophotography & LiDAR Surveys Photogrammetric Report, prepared by Aero-metric, Seattle, Washington.
- Anderson, P. and S. Lu, 2003, “A Post Audit of a Model-Designed Ground Water Extraction System”, *Groundwater*, Vol. 41, No. 2, pp. 212-218.
- Avon, L., and J.D. Bredehoeft, 1989, “An Analysis of Trichloroethylene Movement in Groundwater at Castle Air Force Base, California”, *Journal of Hydrology*, Vol. 110, p. 23-50.
- Bierschenk, W.H., 1959, *Aquifer Characteristics and Ground-Water Movement at Hanford*, General Electric Company, Richland, Washington. Available at: <https://pdw.hanford.gov/arpir/index.cfm/viewDoc?accession=D196029475>
- Bjornstad et al., 2001, “Long History of Pre- Wisconsin, Ice Age Cataclysmic Floods: Evidence from Southeastern Washington State”, *The Journal of Geology*, Vol. 109, No. 6, pp. 695-713.
- Bredehoeft, J.D., 2005, “The Conceptualization Model Problem – Surprise”, *Hydrogeology Journal*, Vol. 13, No. 1, pp. 37-46.
- Butler and Healey, 1998, “Relationship Between Pumping-Test and Slug-Test Parameters: Scale Effect or Artifact?”, *Ground Water*, Vol. 36, No. 2, pp. 305-313.
- CCN 024566, 1996, “Field Summary Report 100-H Area Well Production Testing” (ERC Interoffice Memorandum from R.S. Edrington to G.L. Kasza), Bechtel Hanford, Inc., Richland, Washington, January 22.
- Chapelle, F.H., 1986, “A Solute-Transport Simulation of Brackish-water Intrusion near Baltimore, Maryland”, *Ground Water*, Vol. 24, No. 3, pp. 304-311.
- Chiang, C.Y., J.P. Salanitro, E.Y. Chai, J.D. Colthart, and C.L. Klein, 1989, “Aerobic Biodegradation of Benzene, Toluene, and Xylene in a Sandy Aquifer – Data Analysis and Computer Modeling”. *Ground Water*, Vol. 27, No. 6, pp. 823-834.
- CHPRC-00257, 2010, *MODFLOW and Related Codes Functional Requirements Document*, Rev. 1, CH2M HILL Plateau Remediation Company, Richland, Washington.
- CHPRC-00258, 2015, *MODFLOW and Related Codes Software Management Plan*, Rev. 4, CH2M HILL Plateau Remediation Company, Richland, Washington.
- CHPRC-00259, 2014, *MODFLOW and Related Codes Software Test Plan*, Rev. 3, CH2M HILL Plateau Remediation Company, Richland, Washington.
- CHPRC-00260, 2015, *MODFLOW and Related Codes Acceptance Test Report: CHPRC Build 8*, Rev. 8, CH2M HILL Plateau Remediation Company, Richland, Washington.
- CHPRC-00261, 2015, *MODFLOW and Related Codes Requirements Traceability Matrix: CHPRC Build 8*, Rev. 8, CH2M HILL Plateau Remediation Company, Richland, Washington.
- CP-59563, 2018, *100-N Scale-Appropriate Fate and Transport Groundwater Model*, Rev. 0, CH2M HILL Plateau Remediation Company, Richland, Washington.

- CP-60254, 2017, *Hanford Site Composite Analysis Technical Approach Description: Hanford Site Disposition Baseline*, Rev. 0, CH2M HILL Plateau Remediation Company, Richland, Washington. Available at: <https://www.osti.gov/servlets/purl/1412547>.
- D' Alessandro, M., F. Mousty, G. Bidoglio, J. Guimera, I. Benet, X. Sanchez-Vila, M.G. Gutierrez, and A.Y. De Llano, 1997, "Field Tracer Experiment in a Low Permeability Fractured Medium: Results from El Berrocal Site", *Journal of Contaminant Hydrology*, Vol. 26, pp. 189-201.
- DOE O 414.1D, Admin Chg 1, 2011, *Quality Assurance*, U.S. Department of Energy, Washington, D.C. Available at: <https://www.directives.doe.gov/directives/0414.1-BOrder-d/view>.
- DOE/RL-88-30, 2016, *Hanford Site Waste Management Units Report*, Rev. 25, U.S. Department of Energy, Richland Operations Office, Richland. Available at: <https://pdw.hanford.gov/arpir/index.cfm/viewDoc?accession=0078250H>; <https://pdw.hanford.gov/arpir/index.cfm/viewDoc?accession=0078019H>; <https://pdw.hanford.gov/arpir/index.cfm/viewDoc?accession=0078018H>; <https://pdw.hanford.gov/arpir/index.cfm/viewDoc?accession=0078017H>.
- DOE/RL-90-21, 1992, *Remedial Investigation/Feasibility Study Work Plan for the 100-KR-1 Operable Unit, Hanford Site, Richland, Washington*, Rev. 0, U.S. Department of Energy, Richland Operations Office, Richland, Washington. Available at: <https://pdw.hanford.gov/arpir/index.cfm/viewDoc?accession=D196117209>.
- DOE/RL-92-12, 1994, *Sampling and Analysis of 100 Area Springs*, Rev. 1. U.S. Department of Energy, Richland Operations Office, Richland, Washington. Available at: <https://pdw.hanford.gov/arpir/index.cfm/viewDoc?accession=D196102723>.
- DOE/RL-93-79, 1994, *Limited Field Investigation Report for the 100-KR-4 Operable Unit*, Rev. 0, U.S. Department of Energy, Richland Operations Office, Richland, Washington. Available at: <https://pdw.hanford.gov/arpir/index.cfm/viewDoc?accession=D196074933>.
- DOE/RL-96-17, 2009, *Remedial Design Report/Remedial Action Work Plan for the 100 Area*, Rev. 6, U.S. Department of Energy, Richland Operations Office, Richland, Washington. Available at: <http://www5.hanford.gov/arpir/?content=findpage&AKey=0095436>.
- DOE/RL-96-32, 2016, *Hanford Site Biological Resources Management Plan*, Rev. 2, U.S. Department of Energy, Richland Operations Office, Richland, Washington. Available at: https://www.emcbc.doe.gov/SEB/HMESC/Documents/Document%20Library/Plans/Hanford%20Site%20Biological%20Resource%20Management%20Plan_%20DOE-RL-96-32,%20Draft%20Rev%202.pdf.
- DOE/RL-2002-39, 2002, *Standardized Stratigraphic Nomenclature for Post Ringold Formation Sediments Within the Central Pasco Basin*, U.S. Department of Energy, Richland Operations Office, Richland, Washington. Available at: <https://pdw.hanford.gov/arpir/index.cfm/viewDoc?accession=0081471H>.
- DOE/RL-2010-97, 2011, *Remedial Investigation/Feasibility Study for the 100-KR-1, 100-KR-2, and 100-KR-4 Operable Units*, Draft A, U.S. Department of Energy, Richland Operations Office, Richland, Washington. Available at: <https://pdw.hanford.gov/arpir/index.cfm/viewDoc?accession=0093616>.

- DOE/RL-2011-50, 2012, *Regulatory Basis and Implementation of a Graded Approach to Evaluation of Groundwater Protection*, Rev. 1, U.S. Department of Energy, Richland Operations Office, Richland, Washington. Available at:
<http://www5.hanford.gov/arpir/?content=findpage&AKey=0093361>.
- DOE/RL-2014-32, 2014, *Hanford Site Groundwater Monitoring Report for 2013*, Rev. 0, U.S. Department of Energy, Richland Operations Office, Richland, Washington. Available at:
<https://pdw.hanford.gov/arpir/index.cfm/viewDoc?accession=0084842>.
- DOE/RL-2012-15, in progress, *Remedial Investigation/Feasibility Study for 100-NR-1 and 100-NR-2 Operable Units*, Rev. 0, U.S. Department of Energy, Richland Operations Office, Richland, Washington.
- DOE/RL-2015-07, 2015, *Hanford Site Groundwater Monitoring Report for 2014*, Rev. 0, U.S. Department of Energy, Richland Operations Office, Richland, Washington. Available at:
<https://pdw.hanford.gov/arpir/index.cfm/viewDoc?accession=0080600H>.
- DOE/RL-2016-09, 2015, *Hanford Site Groundwater Monitoring Report for 2015*, Rev. 0, U.S. Department of Energy, Richland Operations Office, Richland, Washington. Available at:
<https://pdw.hanford.gov/arpir/index.cfm/viewDoc?accession=0075314H>.
- DOE/RL-2016-67, 2016, *Hanford Site Groundwater Monitoring Report for 2016*, Rev. 0, U.S. Department of Energy, Richland Operations Office, Richland, Washington. Available at:
<https://pdw.hanford.gov/arpir/index.cfm/viewDoc?accession=0068229H>.
- Doherty, J., 2003, "Ground Water Model Calibration Using Pilot Points and Regularization", *Groundwater*, Vol. 41, No. 2, pp. 170-177.
- Doherty, J., 2007, *PEST Model-Independent Parameter Estimation User Manual*. Available at:
<https://www.epa.gov/sites/production/files/documents/PESTMAN.PDF>.
- ECF-100BC5-16-0051, 2016, *Calibration of Continuing Source for Strontium-90 in the 100-BC-5 Operable Unit*, Rev. 0, CH2M Hill Plateau Remediation Company, Richland, Washington. Available at: <https://pdw.hanford.gov/arpir/index.cfm/viewDoc?accession=0073929H>.
- ECF-100KR1-17-0087, 2018, *Determination of Soil Screening Levels and Preliminary Remediation Goals for Waste Sites in the 100-K Source Operable Unit*, Rev. 0, CH2M Hill Plateau Remediation Company, Richland, Washington.
- ECF-100KR4-12-0010, 2012, *Analysis of Slug Testing Data at the 100-KR-4 Operable Unit*, Rev. 0, CH2M HILL Plateau Remediation Company, Richland, Washington.
- ECF-100NR2-12-0031, 2012, *Analysis of Data Collected from Slug Tests Conducted in Remedial Investigation Boreholes Within the 100-NR-2 Groundwater Operable Unit*, Rev. 0, CH2M HILL Plateau Remediation Company, Richland, Washington. Available at:
<https://pdw.hanford.gov/arpir/index.cfm/viewDoc?accession=0086683>.
- ECF-HANFORD-13-0020, *Process for Constructing a Three-dimensional Geological Framework Model of the Hanford Site, 100 Area*, Rev. 3, CH2M HILL Plateau Remediation Company, Richland, Washington. Available at:
<https://pdw.hanford.gov/arpir/index.cfm/viewDoc?accession=0079495H>.

- ECF-HANFORD-15-0019, 2016, *Hanford Site-Wide Natural Recharge Boundary Condition for Groundwater Models*, Rev. 0, CH2M HILL Plateau Remediation Company, Richland, Washington.
- Engesgaard, P., K.H. Jensen, J. Molson, E.O. Frind, and H. Olsen, 1996, "Large-scale Dispersion in a Sand Aquifer: Simulation of Subsurface Transport of Environmental Tritium", *Water Resources Research*, Vol. 32, No. 11, pp. 3253-3266.
- EPA QA/G-5M, 2002, *Guidance for Quality Assurance Project Plans for Modeling*, U.S. Environmental Protection Agency, Washington, D.C. Available at: <https://nepis.epa.gov/Exe/ZyPURL.cgi?Dockey=P1000HFX.TXT>.
- Ferris, J.G., 1963, *Cyclic Water-Level Fluctuations as a Basis for Determining Aquifer Transmissibility*, in R. Bentall (compiler), *Methods of Determining Permeability, Transmissibility, and Drawdown*, U.S. Geological Survey Water-Supply Paper 1536-I, Washington, D.C., pp. 305-318.
- Gee, G.W., Fayer, M.J., Rockhold, M.L., and Campbell, M.D., 1992, "Variations in Recharge at the Hanford Site", *Northwest Science*, Vol. 66, No. 4, pp. 237-250.
- Gee, G.W., J.M. Keller and A.L. Ward, 2005, "Measurement and Prediction of Deep Drainage from Bare Sediments at a Semiarid Site", *Vadose Zone Journal*, Vol. 4, No. 1, p. 9.
- Gee, G.W., M. Oostrom, M.D. Freshley, M.L. Rockhold, and J.M. Zachara, 2007, "Hanford Site Vadose Zone Studies: An Overview", *Vadose Zone Journal*, Vol. 6, No. 4, pp. 899-905.
- Gelhar, L.W., C. Welty, and K.R. Rehfeldt, 1992, "A Critical Review of Data on Field-scale Dispersion in Aquifers", *Water Resources Research*, Vol. 28, No. 7, pp. 1955-1974.
- Hajek, B.F., 1966, *Soil Survey Hanford Project in Benton County Washington*, AEC Research and Development Report, Pacific Northwest Laboratory, Richland, Washington.
- Himmelsbach, T., H. Hotzl, and P. Maloszewski, 1998, "Solute Transport Processes in a Highly Permeable Fault Zone of Lindau Fractured Rock Test Site (Germany)", *Ground Water*, Vol. 36, No. 5, pp. 792-800.
- Klein, K.A., 2006, "Contract No. DE-AC06-96RL13200 - Hanford Groundwater Modeling Integration", Letter to R. G. Gallagher. Richland, Washington, U.S. Department of Energy, Richland Operations Office.
- Knudby, C., and J. Carrera. 2006, "On the Use of Apparent Hydraulic Diffusivity as an Indicator of Connectivity", *Journal of Hydrology*, Vol. 329, No. 3-4, pp. 377-389.
- Lavenue, A.M., and P.A. Domenico, 1986, "A Preliminary Assessment of the Regional Dispersivity of Selected Basalt Flows at the Hanford Site, Washington, U.S.A.", *Journal of Hydrology*, Vol. 85, pp. 151-167.
- Lohman, 1972, *Ground-Water Hydraulics*, Geological Survey Professional Paper 708.
- Mas-Pla, J., T.-C.J. Yeh, J.F. McCarthy, and T.M. Williams, 1992, "A Forced Gradient Tracer Experiment in a Coastal Sandy Aquifer, Georgetown site, South Carolina", *Ground Water*, Vol. 30, No. 6, pp. 958-964.

- Mitchell, 1999, *The ESRI Guide to GIS Analysis, Volume 1: Geographic Patterns and Relationships*, Esri Press, Redlands, California.
- National Research Council, 2007, *Models in Environmental Regulatory Decision Making*, National Academy Press, Washington, D.C.
- Newcomb, R. C. and S. G. Brown, 1961, *Evaluation of Bank Storage Along the Columbia River Between Richland and China Bar, Washington*, Geological Survey Water-Supply Paper 1539-I, U.S. Geological Survey, Washington, D.C.
- NLCD 2011, 2015, *Completion of the 2011 National Land Cover Database for the Conterminous United States-Representing a Decade of Land Cover Change Information*, Photogrammetric Engineering and Remote Sensing, Vol. 81, No. 5, pp. 345-354.
- USGS Open File Report 00-92, *MODFLOW-2000, the U.S. Geological Survey Modular Ground-water Model - User Guide to Modularization Concepts and the Ground-Water Flow*, U.S. Geological Survey, Washington, D.C.
- PNL-6403, 1987, *Recharge at the Hanford Site: Status Report*, Pacific Northwest Laboratory, Richland, Washington. Available at: <http://www.osti.gov/bridge/servlets/purl/5539519-iBxaB8/5539519.pdf>.
- PNNL-6415, 2007, *Hanford Site National Environmental Policy Act (NEPA) Characterization*, Rev. 18, Pacific Northwest Laboratory, Richland, Washington. Available at: http://www.pnl.gov/main/publications/external/technical_reports/PNNL-6415Rev18.pdf.
- PNL-6810, 1989, *The Field Lysimeter Test Facility (FLTF) at the Hanford Site: Installation and Initial Tests*, Pacific Northwest Laboratory, Richland, Washington. Available at: <http://www.osti.gov/bridge/servlets/purl/6518216-fj8Lhm/6518216.pdf>.
- PNL-7209, 1990, *Field Lysimeter Test Facility: Second Year (FY 1989) Test Results*, Pacific Northwest Laboratory, Richland, Washington. Available at: <http://www.osti.gov/bridge/servlets/purl/6973885-0GBmG8/6973885.pdf>.
- PNL-10285, 1995, *Estimated Recharge Rates at the Hanford Site*, Pacific Northwest Laboratory, Richland, Washington. Available at: <http://www.osti.gov/energycitations/servlets/purl/10122247-XORHkt/webviewable/10122247.pdf>.
- PNL-10886, 1995, *Development of a Three-Dimensional Ground-Water Model of the Hanford Site Unconfined Aquifer System: FY 1995 Status Report*, Pacific Northwest Laboratory, Richland, Washington. Available at: <http://www.iaea.org/inis/collection/NCLCollectionStore/Public/27/047/27047195.pdf>.
- PNL-10899, 1996, *Strontium-90 Adsorption-Desorption Properties and Sediment Characterization at the 100 N-Area*, Pacific Northwest Laboratory, Richland, Washington. Available at: <http://www.iaea.org/inis/collection/NCLCollectionStore/Public/27/043/27043874.pdf>.
- PNNL-11216, 1997, *STOMP Subsurface Transport Over Multiple Phases: Application Guide*, Pacific Northwest National Laboratory, Richland, Washington. Available at: <http://stomp.pnl.gov/documentation/guides/application.pdf>.

- PNNL-12030, 2000, *STOMP Subsurface Transport Over Multiple Phases: Theory Guide*, Pacific Northwest National Laboratory, Richland, Washington. Available at: <http://stomp.pnl.gov/documentation/guides/theory.pdf>.
- PNNL-13033, 1999, *Recharge Data Package for the Immobilized Low-Activity Waste 2001 Performance Assessment*, Pacific Northwest National Laboratory, Richland, Washington. Available at: http://www.pnl.gov/main/publications/external/technical_reports/13033.pdf.
- PNNL-14702, 2006, *Vadose Zone Hydrogeology Data Package for Hanford Assessments*, Rev. 1, Pacific Northwest National Laboratory, Richland, Washington. Available at: http://www.pnl.gov/main/publications/external/technical_reports/PNNL-14702rev1.pdf.
- PNNL-14744, 2004, *Recharge Data Package for the 2005 Integrated Disposal Facility Performance Assessment*, Pacific Northwest National Laboratory, Richland, Washington. Available at: http://www.pnl.gov/main/publications/external/technical_reports/PNNL-14744.pdf.
- PNNL-14753, 2006, *Groundwater Data Package for Hanford Assessments*, Rev. 1, Pacific Northwest National Laboratory, Richland, Washington. Available at: http://www.pnl.gov/main/publications/external/technical_reports/PNNL-14753Rev1.pdf.
- PNNL-15160, 2005, *Hanford Site Climatological Summary 2004 with Historical Data*, Pacific Northwest National Laboratory, Richland, Washington. Available at: http://www.pnl.gov/main/publications/external/technical_reports/PNNL-15160.pdf.
- PNNL-15782, 2006, *STOMP Subsurface Transport Over Multiple Phases Version 4.0 User's Guide*, Pacific Northwest National Laboratory, Richland, Washington. Available at: <http://stomp.pnl.gov/documentation/guides/userguide.pdf>.
- PNNL-16346, 2007, *Hanford Site Groundwater Monitoring for Fiscal Year 2006*, Pacific Northwest National Laboratory, Richland, Washington. Available at: http://www.pnl.gov/main/publications/external/technical_reports/PNNL-16346.pdf.
- PNNL-16688, 2007, *Recharge Data Package for Hanford Single-Shell Tank Waste Management Areas*, Pacific Northwest National Laboratory, Richland, Washington. Available at: http://www.pnl.gov/main/publications/external/technical_reports/PNNL-16688.pdf.
- PNNL-16894, 2007, *Investigation of the Strontium-90 Contaminant Plume Along the Shoreline of the Columbia River at the 100-N Area of the Hanford Site*, Pacific Northwest National Laboratory, Richland, Washington. Available at: http://www.pnl.gov/main/publications/external/technical_reports/PNNL-16894.pdf.
- PNNL-17674, 2008, *Geochemical Characterization of Chromate Contaminant in the 100 Area Vadose Zone at the Hanford Site*, Pacific Northwest National Laboratory, Richland, Washington. Available at: http://www.pnl.gov/main/publications/external/technical_reports/PNNL-17674.pdf.
- PNNL-17708, 2008, *Three-Dimensional Groundwater Models of the 300 Area at the Hanford Site, Washington State*, Pacific Northwest National Laboratory, Richland, Washington. Available at: http://www.pnl.gov/main/publications/external/technical_reports/PNNL-17708.pdf.

- PNNL-17841, 2008, *Compendium of Data for the Hanford Site (Fiscal Years 2004 to 2008) Applicable to Estimation of Recharge Rates*, Pacific Northwest National Laboratory, Richland, Washington. Available at: http://www.pnl.gov/main/publications/external/technical_reports/PNNL-17841.pdf.
- PNNL-18564, 2009, *Selection and Traceability of Parameters to Support Hanford-Specific RESRAD Analyses: Fiscal Year 2008 Status Report*, Pacific Northwest National Laboratory, Richland, Washington. Available at: http://www.pnl.gov/main/publications/external/technical_reports/PNNL-18564.pdf.
- PNNL-18732, 2009, *Field Test Report: Preliminary Aquifer Test Characterization Results for Well 299-W15-225: Supporting Phase I of the 200-ZP-1 Groundwater Operable Unit Remedial Design*, Pacific Northwest National Laboratory, Richland, Washington. Available at: http://www.pnl.gov/main/publications/external/technical_reports/PNNL-18732.pdf.
- PNNL-19878, 2010, *Development of a High-Resolution Bathymetry Dataset for the Columbia River Through the Hanford Reach*, Pacific Northwest National Laboratory, Richland, Washington. Available at: http://www.pnl.gov/main/publications/external/technical_reports/PNNL-19878.pdf.
- PNNL-21845, 2012, *Investigation of Hexavalent Chromium Flux to Groundwater at the 100-C-7:1 Excavation Site*, Pacific Northwest National Laboratory, Richland, Washington. Available at: http://www.pnnl.gov/main/publications/external/technical_reports/PNNL-21845.pdf.
- Ptak, T., and G. Teutsch, 1994, "Forced and natural gradient tracer tests in a highly heterogeneous porous aquifer: Instrumentation and measurements", *Journal of Hydrology*, Vol. 159, p. 79-104.
- Reimus, P.W., A. Adams, M.J. Haga, A. Humphrey, T. Callahan, I. Anghel, and D. Counce, 1999, *Results and Interpretation of Hydraulic and Tracer Testing in the Prow Pass Tuff at the C-Holes. Yucca Mountain Project Milestone SP32E7M4*, Los Alamos National Laboratory, Los Alamos, New Mexico.
- Rivett, M.O., S. Feenstra, and J.A. Cherry, 1994. , "Transport of a Dissolved-phase Plume from a Residual Solvent Source in a Sand Aquifer", *Journal of Hydrology*, Vol. 159, pp. 27-41.
- Rumbaugh and Rumbaugh, 2011, *Guide to Using Groundwater Vistas Version 6*.
- Schulze-Makuch, D., 2005, "Longitudinal Dispersivity Data and Implications for Scaling Behavior", *Ground Water*, Vol. 43, No. 3, pp. 443-456.
- SGW-39305, 2008, *Technical Evaluation of the Interaction of Groundwater with the Columbia River at the U.S. Department of Energy Hanford Site, 100-D Area*, Rev. 0, Fluor Hanford, Inc., Richland, Washington. Available at: <http://www5.hanford.gov/arpir/?content=findpage&AKey=0812290631>.
- SGW-40781, 2012, *100-HR-3 Remedial Process Optimization Modeling Data Package*, Rev. 2, CH2M HILL Plateau Remediation Company, Richland, Washington. Available at: <https://pdw.hanford.gov/arpir/index.cfm/viewDoc?accession=1211191621>.
- SGW-44022, 2010, *Geohydrologic Data Package in Support of 100-BC-5 Modeling*, Rev. 1, CH2M HILL Plateau Remediation Company, Richland, Washington. Available at: <https://pdw.hanford.gov/arpir/index.cfm/viewDoc?accession=0087246>.

- SGW-46279, 2010, *Conceptual Framework and Numerical Implementation of 100 Areas Groundwater Flow and Transport Model*, Rev. 2, CH2M Hill Plateau Remediation Company, Richland, Washington. Available at:
<http://pdw.hanford.gov/arpir/index.cfm/viewDoc?accession=0087245>.
- SERDP-99-1, *MT3DMS: A Modular Three-Dimensional Multispecies Transport Model for Simulation of Advection, Dispersion, and Chemical Reactions of Contaminants in Groundwater Systems; Documentation and User's Guide*, US Army Corps of Engineers, Engineer Research and Development Center, Washington, D.C. Available at:
<https://hydro.geo.iaea.org/mt3d/mt3dmanual.pdf>.
- S-N/99205-084, 2006, *Well ER-6-1 Tracer Test Analysis: Yucca Flat, Nevada Test Site, Nye County, Nevada*, Rev. 0, Stoller-Navarro Joint Venture (SNJV), Las Vegas, Nevada. Available at:
<https://www.osti.gov/servlets/purl/892034>.
- S-N/99205-096, 2007, *Phase I Contaminant Transport Parameters for the Groundwater Flow and Contaminant Transport Model of Corrective Action Unit 97: Yucca Flat/Climax Mine, Nevada Test Site, Nye County, Nevada*, Rev. 0, Stoller-Navarro Joint Venture (SNJV), Las Vegas, Nevada. Available at: https://inis.iaea.org/search/search.aspx?orig_q=RN:39106132.
- Suthersan, S., C.E. Divine, and S.T. Potter, 2009, "Remediating Large Plumes: Overcoming the Scale Challenge", *Ground Water Monitoring & Remediation*, Vol. 29, No. 1, pp. 45-50.
- Suthersan, S.S., S. Potter, and M. Schnobrich, 2013, "Groundwater Restoration: Large-Scale Benefits of Small-Scale Processes", *Groundwater Monitoring & Remediation*, Vol. 33, No 3.
- van der Kamp, G., L.D. Luba, J.A. Cherry, and H. Maathuis, 1994, "Field study of a long and very narrow contaminant plume", *Ground Water*, Vol. 32, No. 6, p. 1008-1016.
- WCH-380, 2010, *Field Summary Report for Remedial Investigation of Hanford Site Releases to the Columbia River, Hanford Site, Washington: Collection of Surface Water, Pore Water, and Sediment Samples for Characterization of Groundwater Upwelling*, Rev. 1, Washington Closure Hanford, LLC, Richland, Washington. Available at:
http://www.osti.gov/bridge/product.biblio.jsp?osti_id=1017505.
- WHC-SD-EN-DP-090, 1994, *Borehole Data Package for the 100-K Area Groundwater Wells for CY 1994*, Rev. 0, Westinghouse Hanford Company, Richland, Washington. Available at:
<http://www5.hanford.gov/arpir/?content=findpage&AKey=D196047730>.
- WHC-SD-ER-TI-003, 1991, *Geology and Hydrology of the Hanford Site: A Standardized Text for Use in Westinghouse Hanford Company Documents and Reports*, Westinghouse Hanford Company, Richland, Washington.
- WHC-SA-0740-FP, 1989, *Sedimentology and Stratigraphy of the Miocene Pliocene Ringold Formation, Hanford Site, South Central Washington*, Westinghouse Hanford Company, Richland, Washington.

Appendix A

Priest Rapids to K-Gauge Correlation

Summary

Accurate water elevations along the Columbia River are needed to develop the boundary conditions used in the Hanford 100 Areas Groundwater Flow and Transport Models. Elevation data has been collected at various times and locations, but continuous monitoring data in the model domain and during modeled time periods is not available. In order to obtain this information, a set of regression equations were developed using data from the United States Geological Survey (USGS) Priest Rapids Dam Station-12472800 to estimate and fill in data gaps. Because the 100-K Groundwater Flow and Transport Model (GWFTM) uses a 5-day and monthly stress periods, the equations that were developed use daily mean elevation data.

Regression Analysis – Input Data

Hanford 100 Area gage data was obtained from the CH2M HILL Plateau Remediation Company's (CHPRC) AWLN by request from INTERA staff. The data was reported in NAVD88-meter and was generally collected in 1-hour increments. Each gage has a different recorded time span, with an overall range from 1/1/2004 through 7/31/2014. 15-minute stage data from 1/1/2004 through 12/31/2015 for USGS gage #12472800 was then downloaded from the USGS' Instantaneous Data Archive (USGS, 2015a) and National Water Information System: Web Interface (USGS, 2015b). Then end of 2015 was selected because the model simulation only went through this period, and because some data past this date was still marked as "Provisional" by the USGS when this analysis started. USGS gage #12472800 stage data was then converted into a water surface elevation in NAVD88-meter using the following equation: where, S is the recorded "Stage" value, 390 is the datum of the gage in NAVD 1929-Feet, 3.49 converts the NAVD 1929 elevation to NAVD 88 (NOAA, 2015), and 3.2808 converts the elevation from feet to meters.

$$WSE(m) = \frac{(S + 390 + 3.49)ft}{3.2808 \frac{ft}{m}}$$

Figure A.1 shows the location of the Hanford 100 Area gages, USGS #12472800, and the extent of the 100-K GWFTM. Regression equations were developed for the Hanford 100 Area B, K, N, and D gages which are in close proximity to the model boundary.

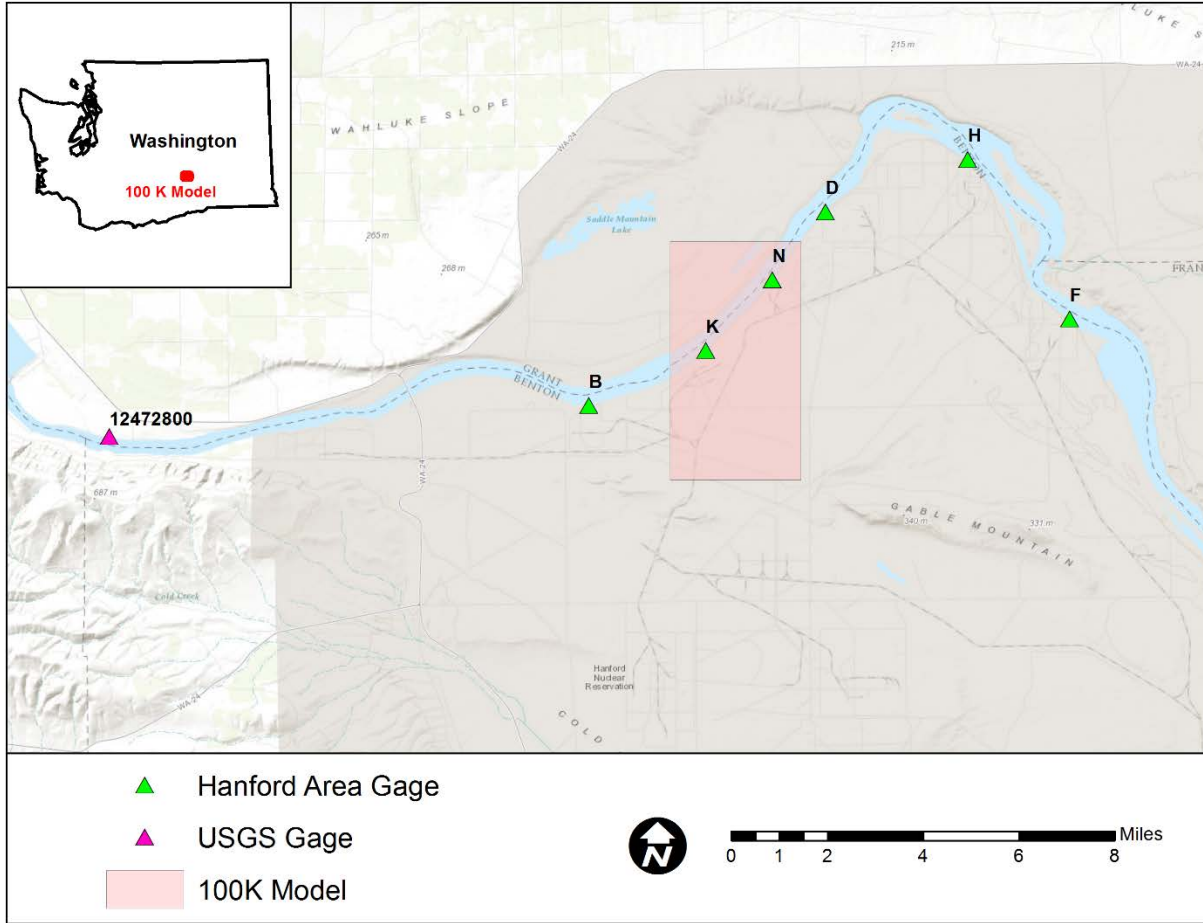


Figure A.1. Elevation Gages near the 100K Modeling Domain

Figure A.2 presents the raw data collected at each of these sites. The B, D, and N gages all started continuous sampling at the beginning of 2004, but the K gage record does not start until 2008. Daily mean values were then calculated from each of the gages using a custom Python script called “100Kdata.py”. This was accomplished using a special Python library called “Pandas”, which can calculate several statistics based on different time windows (e.g., day, week, month, and year). Separate output files for each gage were then produced that had four columns of data: 1) Year, 2) Month, 3) Day, 4) Number of Measurements, and 5) Mean Elevation. Calculated daily mean elevations are shown in Figure A.3.

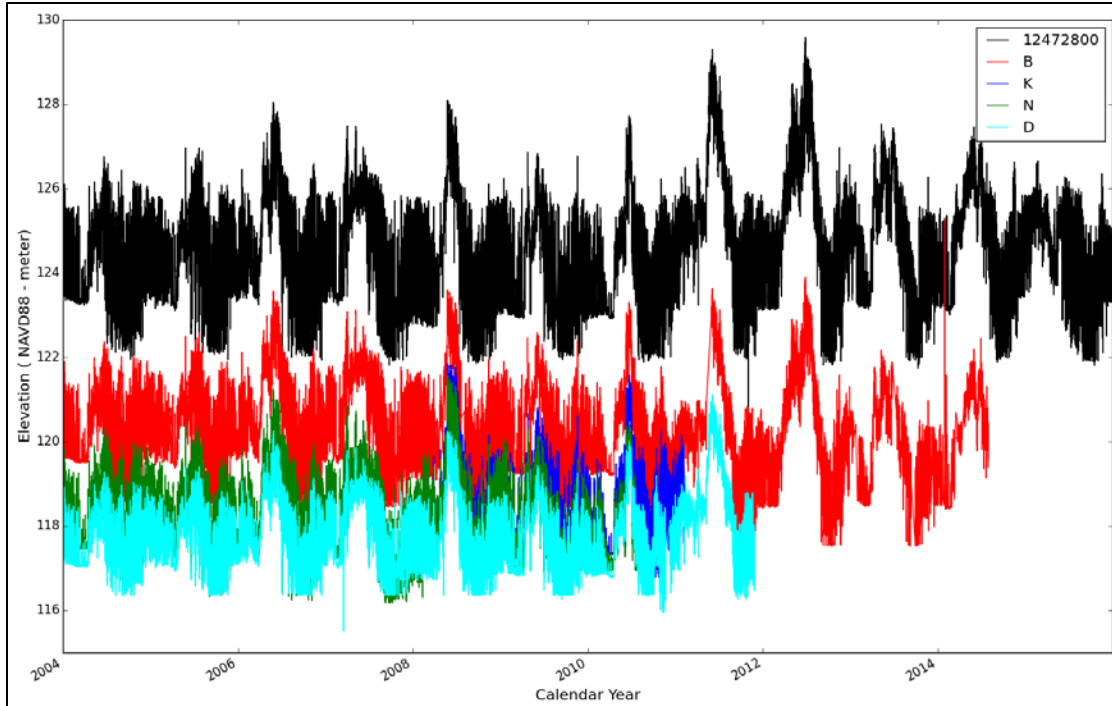


Figure A.2. Raw Elevation Data for Gauges in the 100-K GWFTM Vicinity

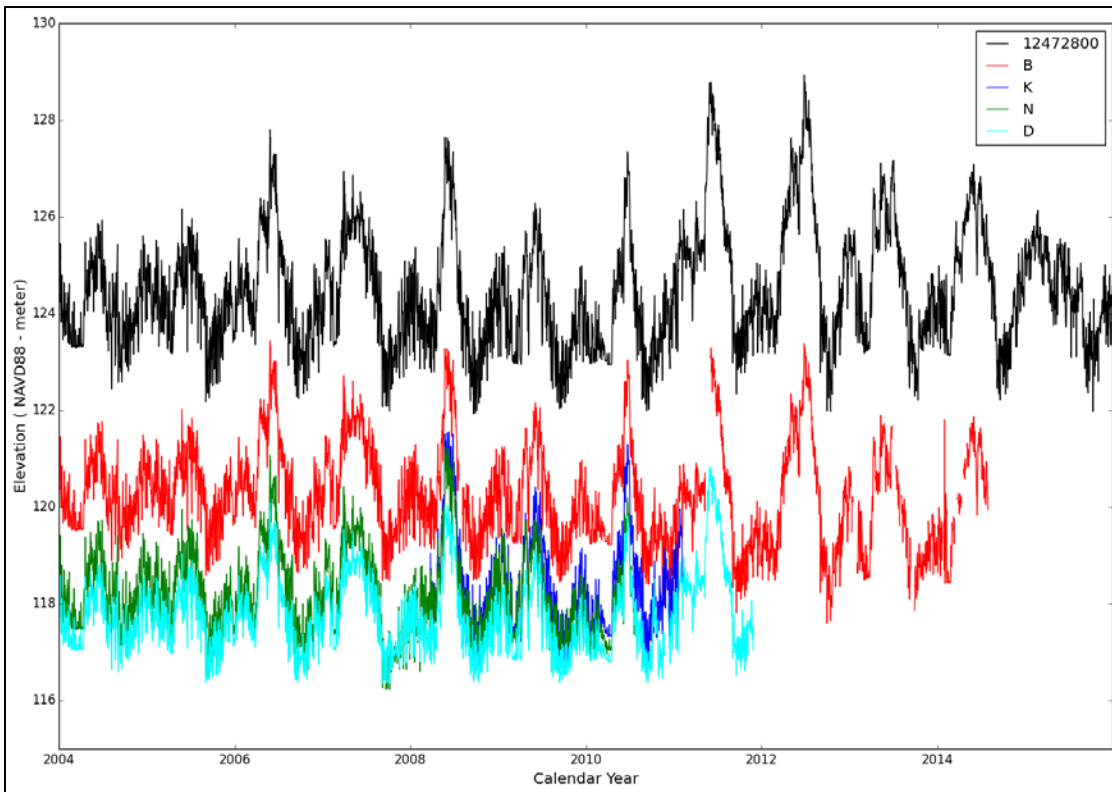
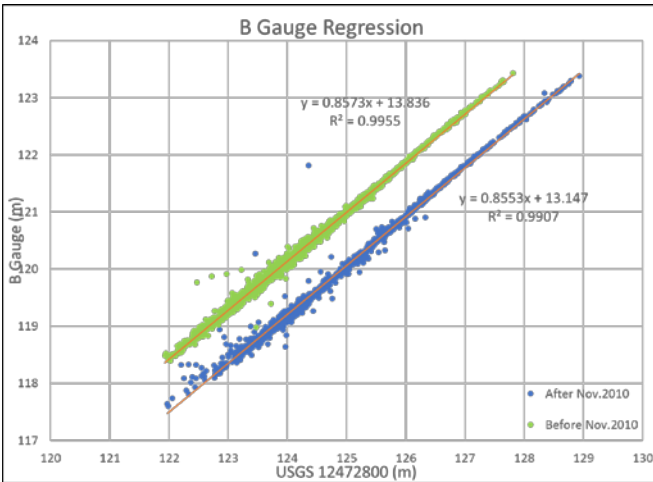


Figure A.3. Mean Daily Elevation Data for Gauges in the 100-K GWFTM Vicinity

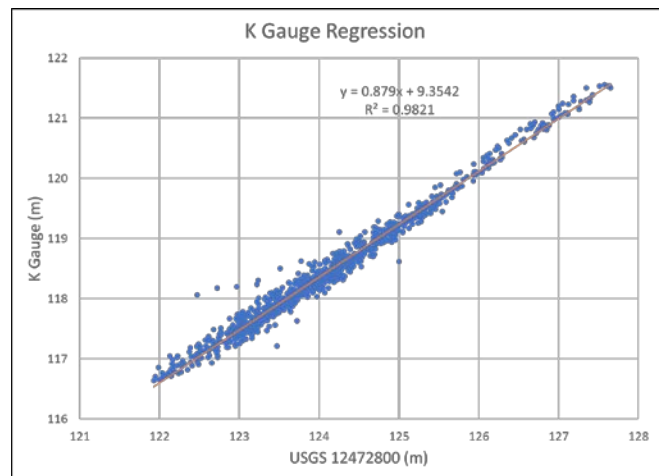
Regression Analysis - Results

Linear regression models were created in MS Excel for each of the Hanford 100 Area gauges using the mean monthly data shown in Figure A.3 with USGS gauge #12472800 data as the independent variable. Figure A.4 shows the result of this analysis and the model equations that were developed.

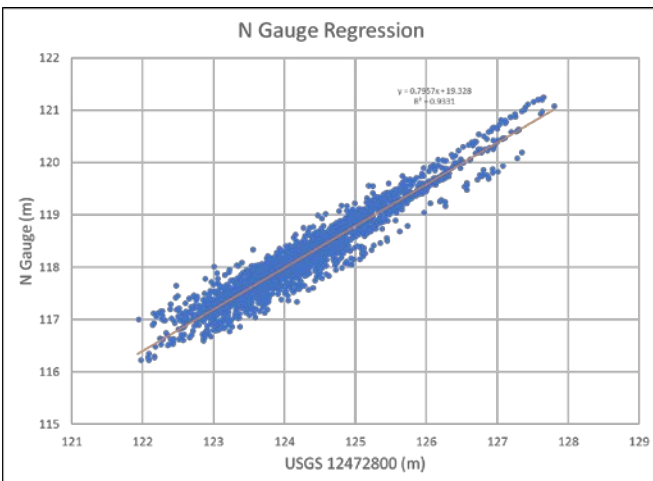
A)



B)



C)



D)

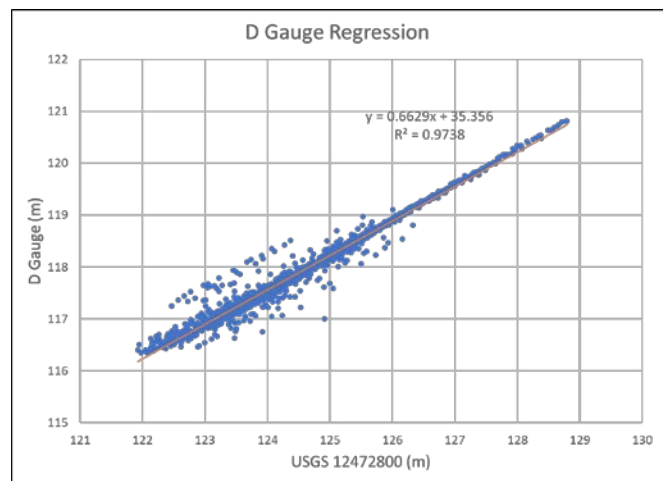


Figure A.4. Regression Models for Hanford 100 Area Gauges in the 100-K GWFTM Vicinity

A previous memo by Furnans (2015) showed that there was a clear difference between the elevation reported before and after November 1st, 2010 for the B gauge. In his memo, Dr. Furnans does not give a definitive answer to explain this difference, but he does suggest that, “B-River water surface elevations recorded after 2010-11-01 are likely to be referenced to the NGVD29 vertical datum rather than to the reported NAVD88 datum.” While the difference between the NGVD29 and NAVD88 datum is approximately 1.06 meters there appears to be a shift of 0.96 meters when comparing data before and after the shift date. These values are only different by 0.1 meters, but there is no way of definitively saying that this is the reason for the shift. This shift could also easily be explained due to a sudden

movement at the gauge. For this analysis, data after the shift was not included in the regression analysis, and no attempt to correct the data after this date was made. Table A.1 presents the final regression equations that were developed for this analysis. Residual time series for each regression equation are presented in Figure A.5.

Table A.1. Regression Equation Results and Location Information

Gauge	Northing	Easting	River Mile	Regression Equation	R ²
B	145,242.2	564,832.3	384.1	$y = 0.8573x + 13.836$	0.996
K	147,084.3	568,758.2	381.5	$y = 0.879x + 9.354$	0.982
N	149,457.1	570,988.7	379.5	$y = 0.7957x + 19.328$	0.933
D	151,738.4	572,778.4	377.7	$y = 0.6629x + 35.356$	0.986

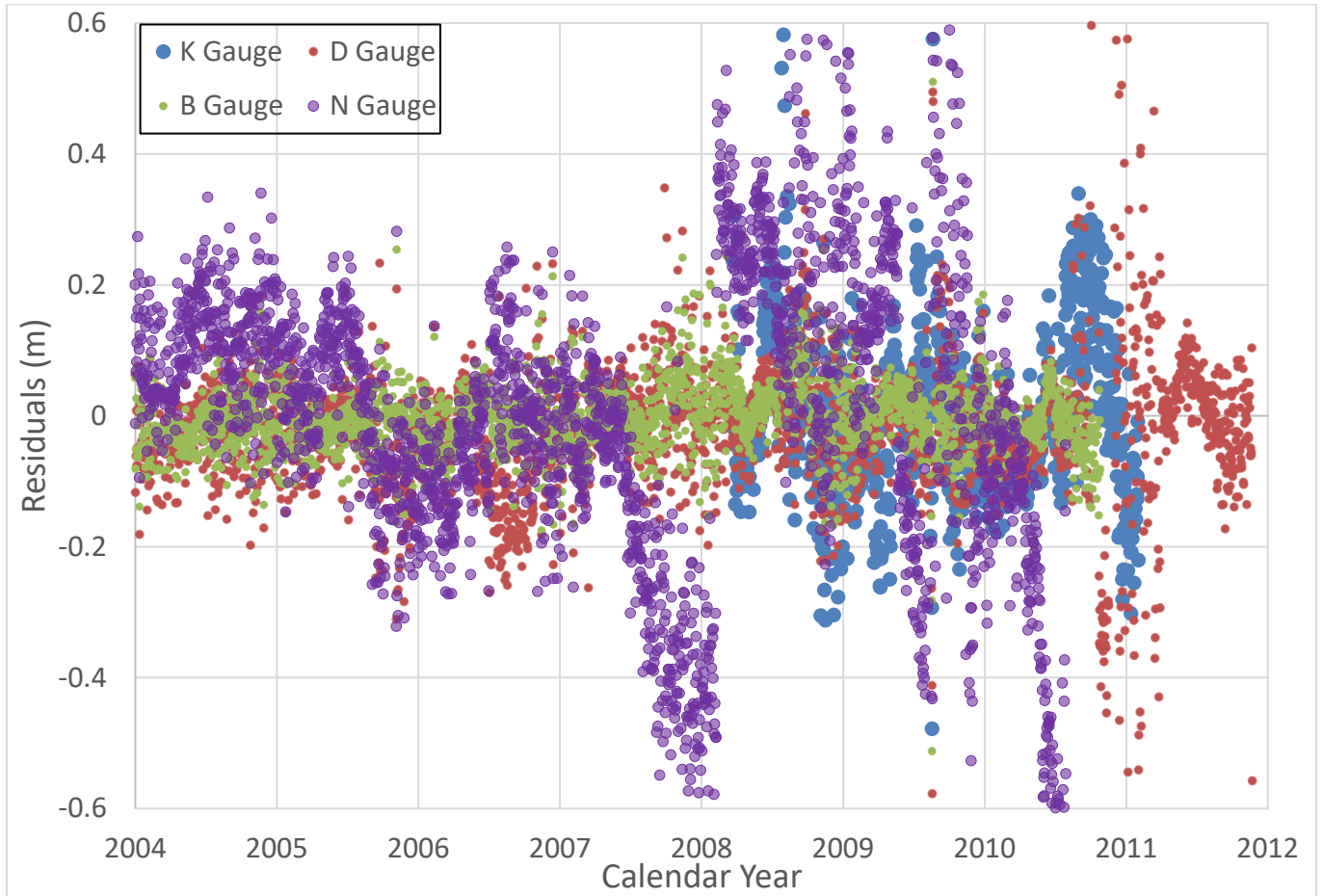


Figure A.5. Residual Time Series for Regression Equations

The Hanford 100 Area N Gauge was not used to develop any data for the 100-K GWFTM because there appears to be a correlation between the residuals over time, starting in the beginning of 2007. According to Helsel and Hirsch (2002), additional terms need to be added to the equation to account for any trends in the data. This gage location, however, was not critical to the overall analysis because the K Gage is located just downstream of the model boundary and the water surface slope changes very little between the D and K Gages.

References

CH2MHILL, 2014. *Columbia River Stage Correlation for the Hanford Area*, ECF-HANFORD-13-0028. CH2M Hill Plateau Remediation Company. Richland, Washington.

CH2MHILL, 2015, Automated Water Level Network, Hanford Virtual Library. CH2M Hill Plateau Remediation Company, Richland, Washington.

Furnans, J., 2015, "B-River Gauge Regression Analysis & Report", Memo to G. Ruskauff. September 24, 2015.

Helsel, D.R. and R. M. Hirsch, 2002. *Statistical Methods in Water Resources Techniques of Water Resources Investigations*, Book 4, Chapter A3. U.S. Geological Survey. 522 pages

NOAA, 2015. VERTCON, Accessed September 9, 2015 at URL http://alt.ngs.noaa.gov/cgi-bin/vertcon/vert_con.prl.

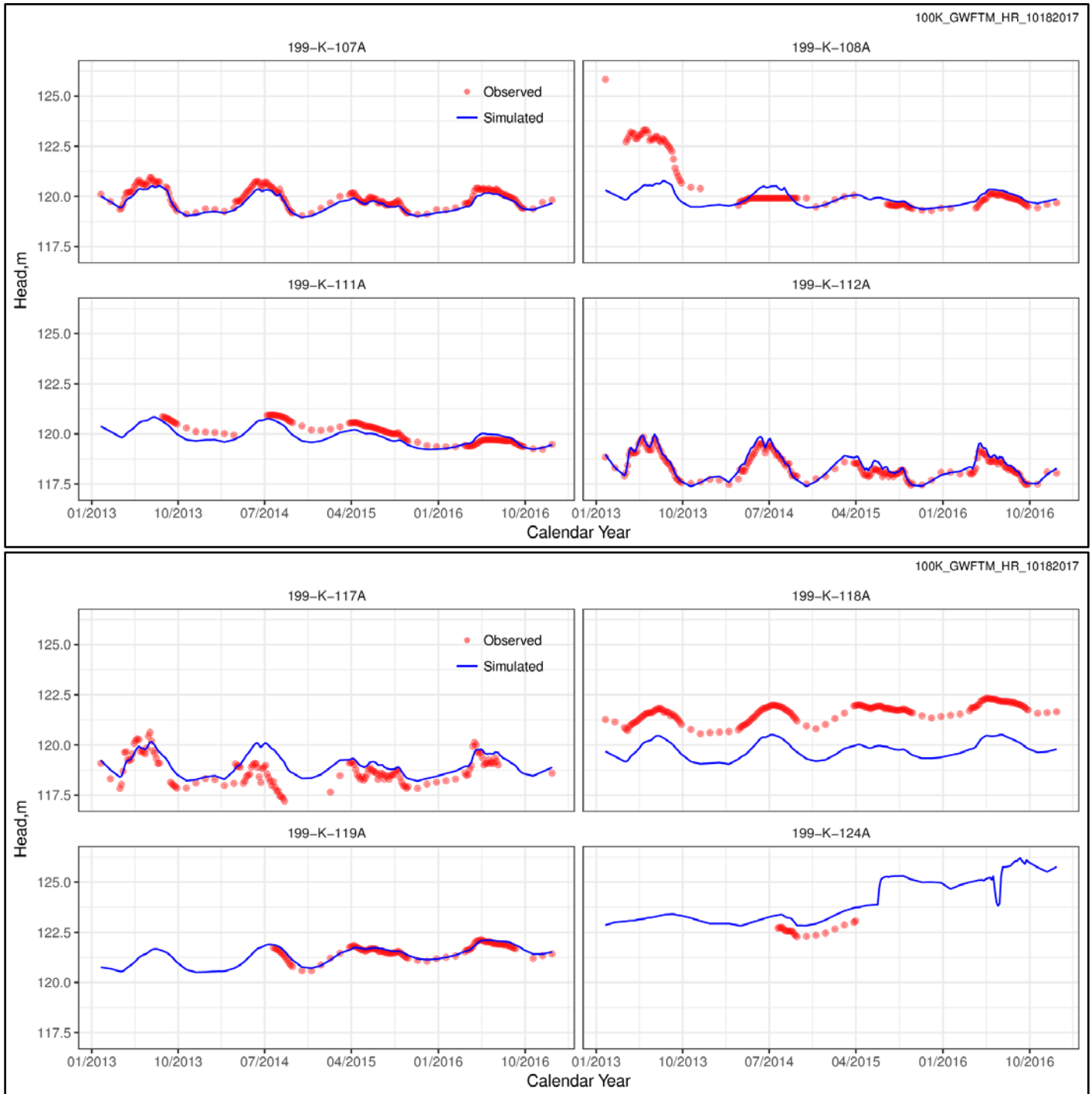
USGS, 2016a, Instantaneous Data Archive data available on the World Wide Web, accessed April 2016 at URL http://ida.water.usgs.gov/ida/available_records.cfm?sn=12472800.

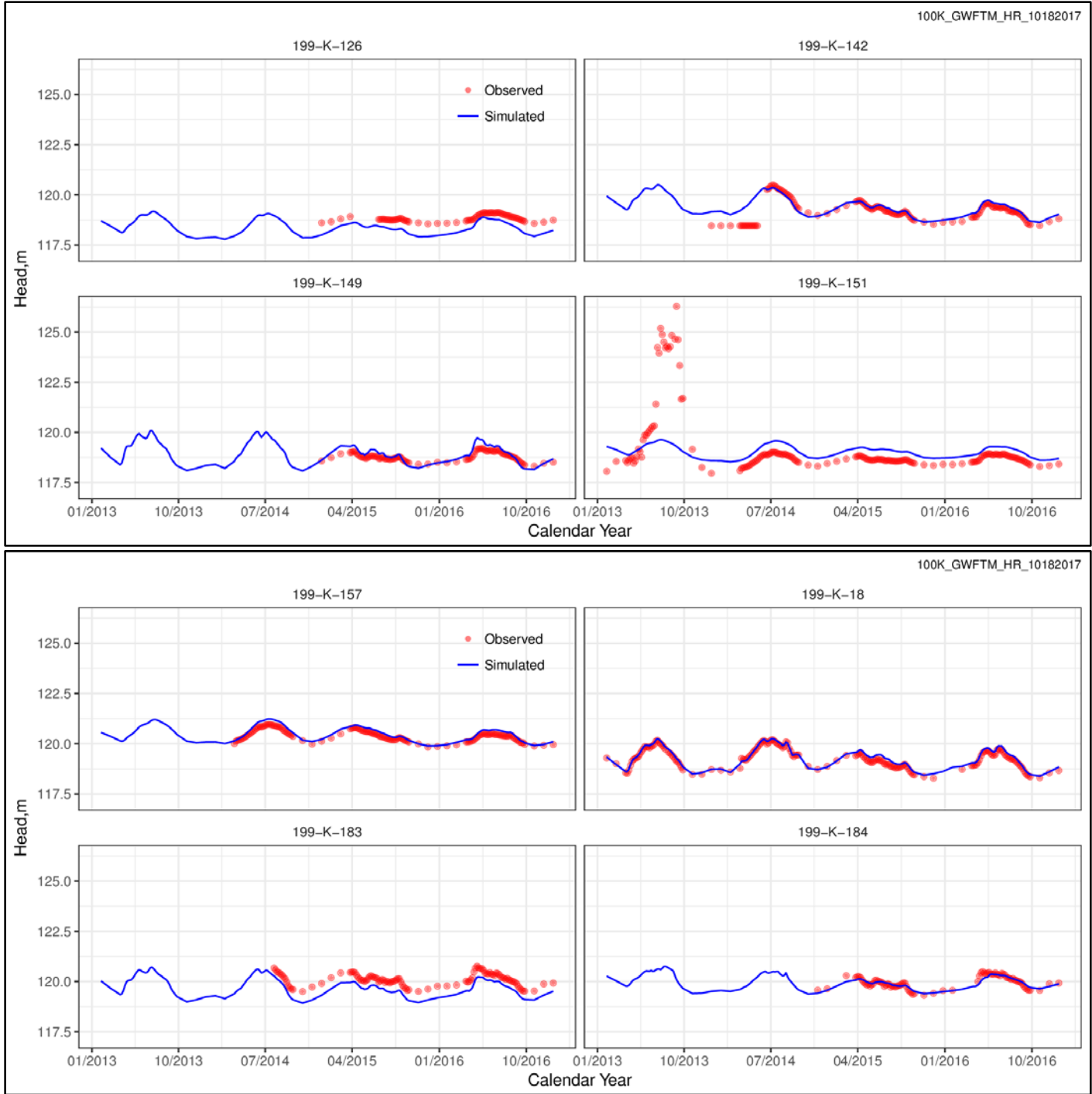
USGS, 2016b, National Water Information System data available on the World Wide Web (USGS Water Data for the Nation), accessed April 2016 at URL http://waterdata.usgs.gov/nwis/uv/?site_no=12472800&agency_cd=USGS.

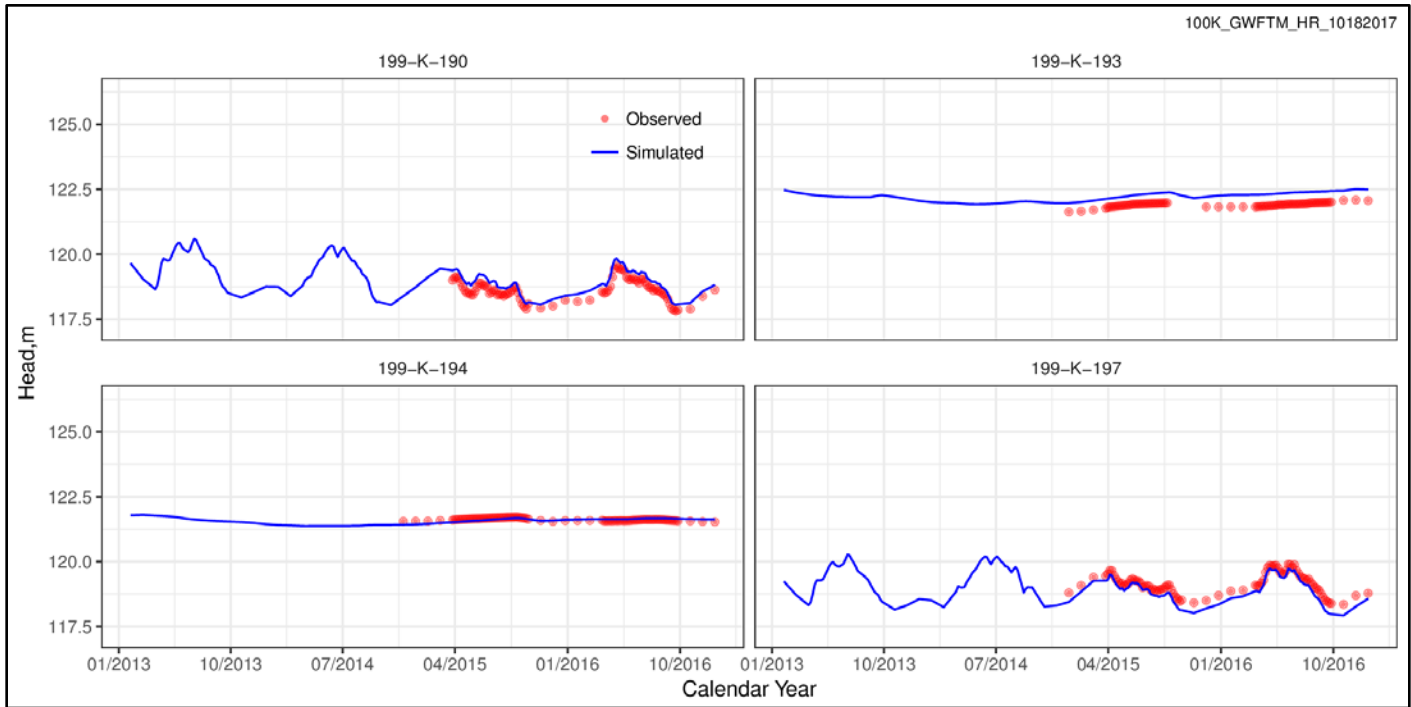
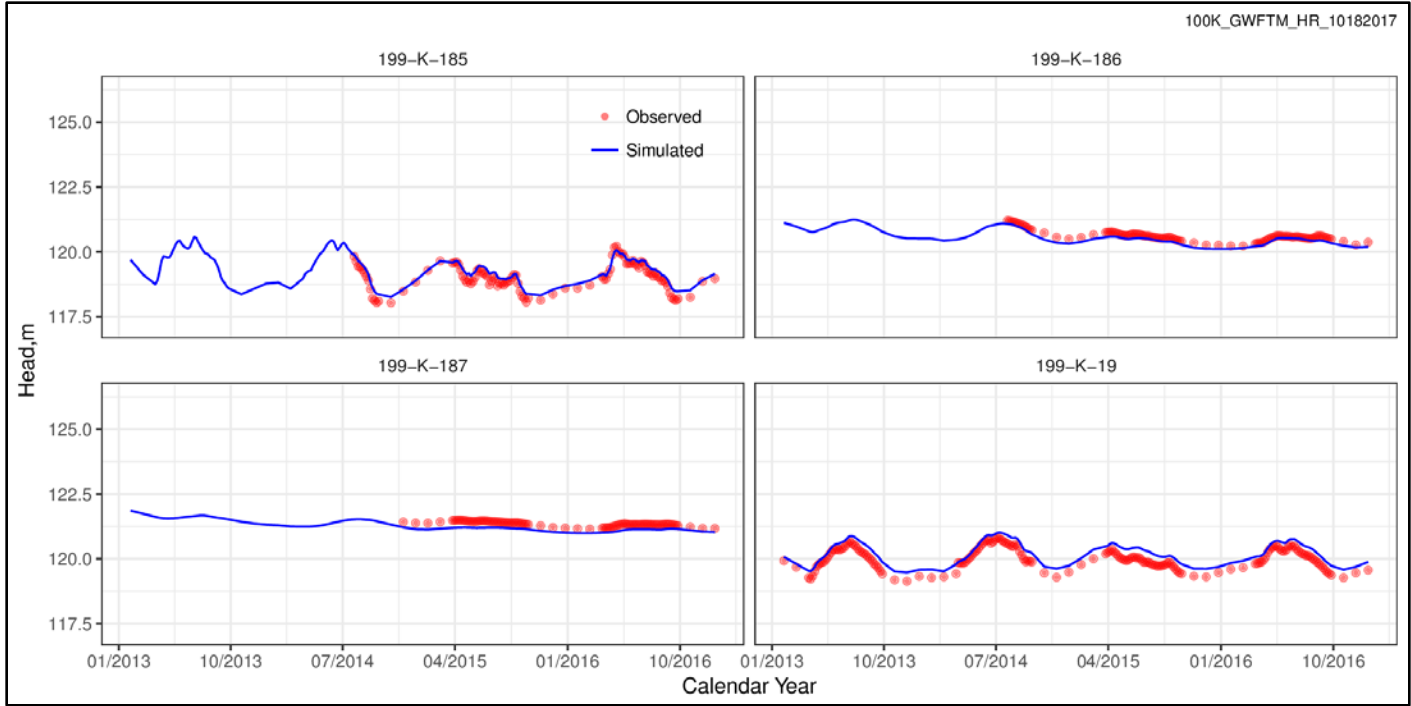
Appendix B

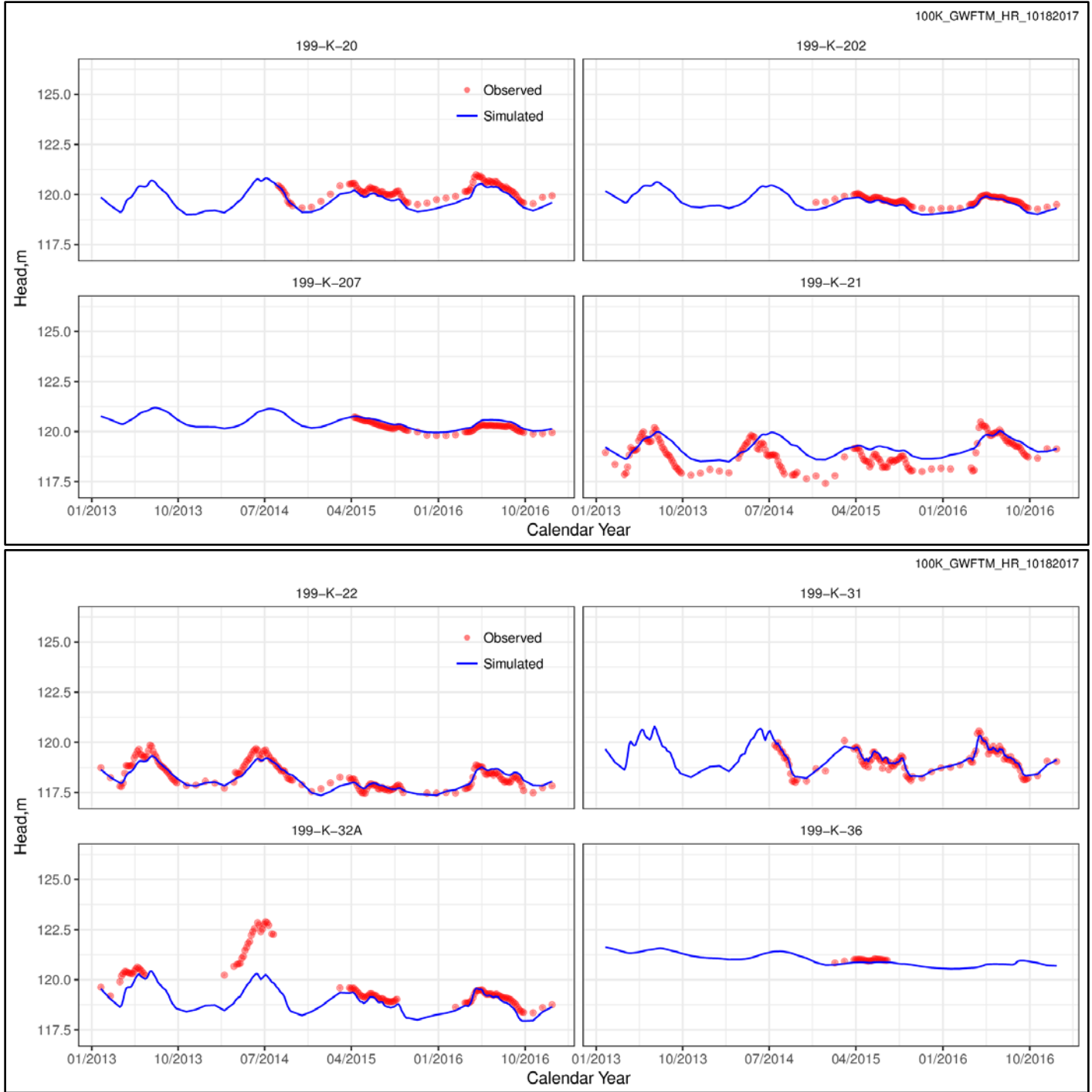
Observed Data and Simulated Hydrographs

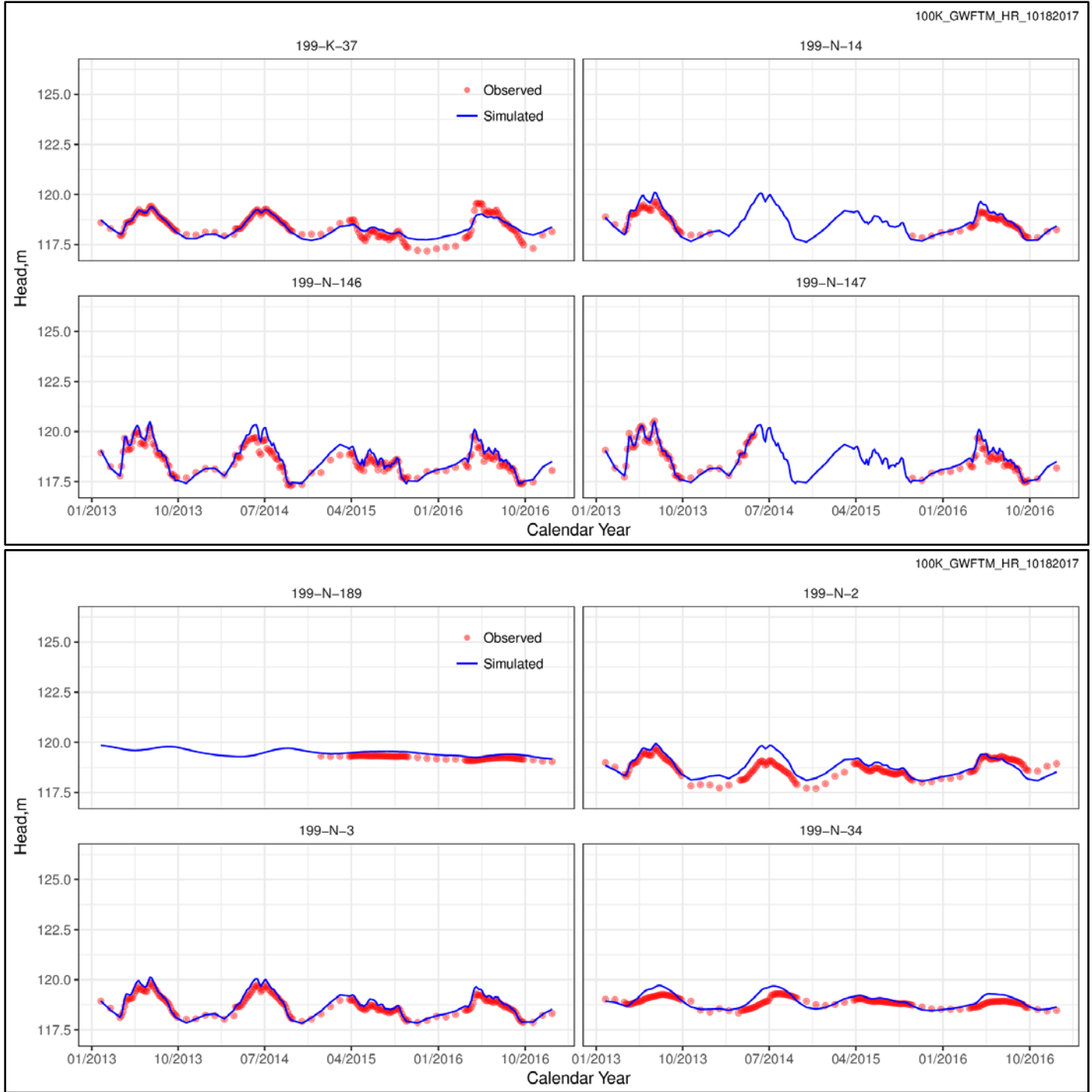
Observed vs Simulated Hydrographs for AWLN Wells:

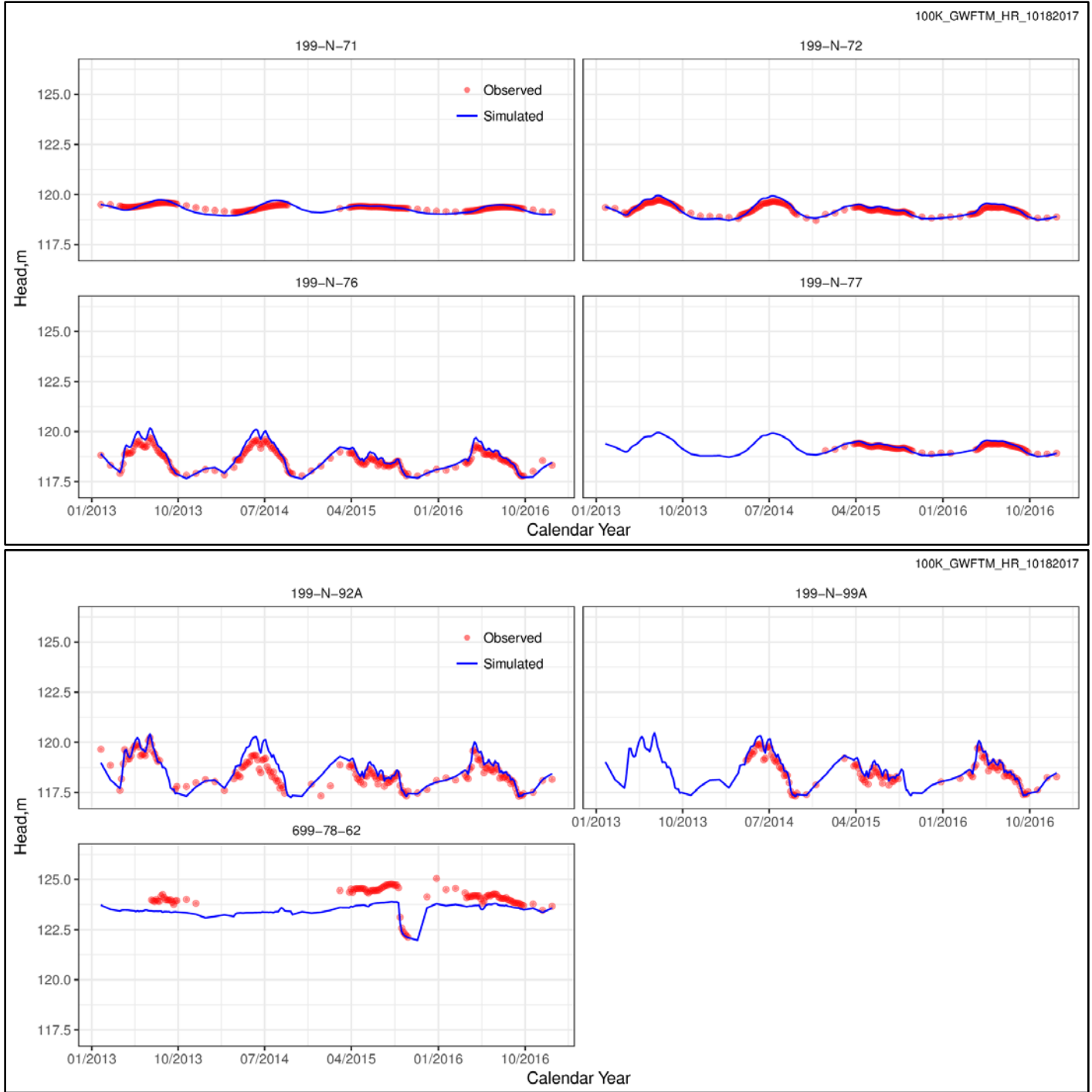












Observed vs Simulated Hydrographs for Manual Measurement Wells:

